Metabolic and Mechanistic Exploration of a Novel Programmable Genotoxicant against Prostate Cancer

By

Charles Ingalls Morton IV

S.B., Chemical Engineering (1997)
Massachusetts Institute of Technology

Submitted to the Department of Biological Engineering in Partial Fulfillment of the Requirements for the Degree of

Doctor of Philosophy in Molecular Systems Pharmacology and Toxicology

at the

Massachusetts Institute of Technology

June 2009

Signature of Author: _____
Department of Biological Engineering
May 21, 2009

Certified by: _____
John M. Essigmann
William and Betsy Leitch Professor of Chemistry and Toxicology
Thesis Supervisor

Accepted by: _____
Alan J. Grodzinsky
Professor of Electrical, Mechanical, and Biological Engineering
Chair, Course XX Graduate Program Committee

This doctoral thesis has been examined by a committee of the Department of Biological Engineering as follows:

Steven R. Tannenbaum _____
Underwood-Prescott Professor of Toxicology and Chemistry
Chair

John M. Essigmann _____
William and Betsy Leitch Professor of Chemistry and Toxicology
Thesis Supervisor

Robert G. Croy _____
Research Scientist in Biological Engineering
Principal Investigator

Douglas A. Lauffenburger _____
Whitaker Professor of Biological Engineering, Chemical Engineering, and Biology
Director, MIT Department of Biological Engineering

Metabolic and Mechanistic Exploration of a Novel Programmable Genotoxicant against Prostate Cancer

by
Charles Ingalls Morton IV

Submitted to the Department of Biological Engineering on May 20, 2009 in Partial Fulfillment of the Requirements for the Degree of Doctor of Philosophy in Molecular and Systems Toxicology and Pharmacology

Molecular design of novel pharmaceutical agents depends on a mechanistic paradigm. A library of compounds was designed to mimic some features of cisplatin that are believed to be in part responsible for its success as a chemotherapeutic agent against testicular cancer. The new compounds are designed to utilize proteins such as steroid receptors that are abnormally expressed in cancers to enhance toxicity and specificity. The synthetic phase of this project successfully produced a compound, 11β, that when tested against cancer cell lines demonstrated remarkable potency, including the induction of apoptosis in normally apoptosis-resistant prostate cancer lines. This drug candidate, comprising an aniline mustard tethered to a steroid moiety, is intended to form covalent adducts with DNA that, through association with the androgen receptor over-expressed in some prostate cancers, are likely to be shielded from repair, generating lethal crosslinks. Moreover, the titration of androgen receptor away from its normal function as a transcription factor may further inhibit tumor growth.

While the mechanistic features of 11β are still under investigation, the potent anti-cancer activity warrants consideration of its possible clinical use, specifically against hormone-refractory, metastatic prostate cancer, for which current therapeutic options are extremely limited. One important step toward that goal involves characterizing the pharmacokinetics of the compound, including: a) understanding the rate of hydrolytic decomposition, b) evaluating the metabolic conversion by intracellular enzymes to active or inactive derivatives, and c) exploring the potential for contraindications between this drug candidate and other medications a prostate cancer patient may be taking concurrently.

Herein are described the experiments that elucidate the pharmacokinetics of 11β, showing that the drug candidate is a) subject to hydrolysis at rates that depend on the presence of plasma protein; b) extensively metabolized by the cytochromes P450 to products demonstrating reduced capacity for forming covalent adducts with DNA; and c) a potent inhibitor of the metabolism of known substrates of the 2D6 and 3A isoforms of cytochrome P450.

Thesis Supervisor: John M. Essigmann
Title: William and Betsy Leitch Professor of Chemistry and Toxicology

ACKNOWLEDGEMENTS:

I have been blessed with the opportunity to work with and learn from a phenomenal series of teachers, colleagues, and peers, each going above and beyond the call of duty to help me realize my goals and achieve more than I thought possible. I will try to acknowledge them here in a vaguely chronological fashion reflective of an educational path that was tortuous for me and frequently torturous for those brave souls charged with having me in their classrooms.

Naomi Hamachi masterfully allowed me to explore anything and everything that piqued my interest for four years, preparing me intellectually for Al Gunther and Betsy Ferris, who so thoroughly cultivated my love of math and science that it became mission-critical for me not just to learn what they were teaching but to impress them in the process.

Thanks to the efforts of Jane Faller and Yasuko Morihara, I had the opportunity to go to the Chadwick School, where Nadine Juton and Dr. Terry Andrews helped me discover the art of communication and the craft of writing, where David Badger and Andy Williamson patiently taught me calculus while managing my ego, and where Dr. Jim Spalding encouraged a fledgling engineer to embrace the rigor of problem solving and the history of scientific exploration.

At MIT, it wasn't until I had Prof. Linda Griffith for Transport Phenomena that I was convinced that chemical engineering was for me, and her expertise in teaching that material led me to seek out the new biomedical engineering minor—shoving those extra six classes into my last three undergraduate semesters was not exactly a recipe for healthy sleep patterns, but I would not be where I am today without having been introduced to the research side of medicine.

I got my first taste of research on the frontier of a field from Dr. Guillermo Ameer while working in Prof. Robert Langer's lab, and when the Division of Bioengineering and Environmental Health came into existence, it represented a gathering of all of my favorite professors from my undergraduate years, including Professors Griffith and Langer as well Prof. Douglas Lauffenburger, Prof. Pete Dedon, and, of course, Prof. John Essigmann.

I have been privileged to know Prof. Essigmann as a teacher, housemaster, and advisor, and I must thank him and his family for their generosity and patience. It is no secret that I have tried to follow in John's footsteps in every way possible—from working at Arthur D. Little to coming to MIT for grad school to trying to emulate his ability to pull double-duty running a lab and managing hundreds of undergrads in a dorm by adding volleyball coaching to my research duties. I cannot express in words my debt of gratitude to John for allowing me to pursue a novel approach to the work going on in his lab and for redefining my project's scope into something manageable.

Tremendous thanks go to my committee members: Prof. Steven Tannenbaum and Dr. Robert Croy provided extensive guidance in experimental design and protocol troubleshooting and were incredibly patient with my lack of an analytical chemistry

background. Prof. Lauffenburger was a singular motivational presence and absolutely the embodiment of all of the intellectual creativity essential to the crossover between biology and engineering, a mindset that inspires us all to pursue aggressively the most difficult problems we can formulate.

Further thanks go to Prof. Tannenbaum for generously offering access to his lab's personnel and equipment. Drs. Pete Wishnok, Peter Slade, Rosa Liberman, and Paul Skipper were invaluable to my introduction and immediate head-first plunge into all of the different types of mass spectrometry. Dr. Wishnok merits special thanks for being an incredibly enthusiastic and patient mentor—I inadvertently caused more catastrophic system failures on the ESI–TOF and QQQ than either of us thought possible. Throughout each incident, Pete was the consummate teacher, taking the opportunity to share with me the maintenance and inner workings of the devices, speaking passionately about everything from mass spectrometry to guitar- and banjo-playing.

Professors Bevin Engelward and William Thilly were crucial sources of information and guidance, each demonstrating the cheerful alacrity that defines our department's commitment to both broad creativity and attention to detail.

To Drs. Can Ozbal, Bill LaMarr, and Michelle Romm of BioTrove, without whose generosity I would be missing a chapter's worth of data, I offer my deepest thanks. To Dr. Nate Tedford, Ryan Littrell, and Dr. Afshin Beheshti, your help with protocol development was vital to my moving forward.

I offer my heartfelt gratitude to the members of the Essigmann lab past and present, especially Drs. Jim Delaney, Peter Rye, and Shawn Hillier, for teaching me how to actually do these experiments, and for taking the time to teach an engineer how to operate in a science lab. I offer thanks and wish the best of luck to expert former UROP and soon-to-be graduate student Jason Bouhenguel, who made intellectual contributions well beyond expectations and is on his way to a brilliant career.

Drs. Hector Hernandez and Kyle Proffitt have been essential to my being able to finish this project, as sources of stimulating intellectual discussions and debates as well as the unconditional moral support that bridged some of the abysmal pitfalls I encountered along the way.

I must thank Paul Dill for being the big brother I never had and for teaching me that the pursuits of happiness and excellence are parallel paths. It has been a great honor and source of personal pride for me to remain involved with MIT Volleyball beyond my days as a player. The opportunity to learn how to be an educator in another context while working with Samantha Lampert and scores of uniquely talented student-athletes over the last decade has led directly to many of my life's most poignant experiences.

To Matt Landry, thank you for being a tremendous friend and a quality human being, opening your family's doors to me, always reading the situation to know exactly when I needed a break, beer, booking, or all three. To Matt Doyle, thank you for delivering the

single deadliest one-two wiffle combo of knuckling happy-face and rising chin-music while pretending that I was not one of your clients (in the past four years) even though the next DSM volume projects to have an entire heading concerning everything that happened on L Street. To Chris Carbone, who injected a love of sports and a competitive streak into my formative years, thank you for convincing me that I could be an athlete despite my entirely inauspicious forays into high school basketball. To Sean Mullan, thank you for editing drafts and offering your feedback while we discussed the finer points of the inadequacies of conventional hockey statistics.

To my brothers, seeing you growing into young adults and pursuing your interests with such dedication is a source of extreme motivation and pride for me, and while I have spent an inordinate length of time 3,000 miles away, I have always been amused at how similar we are despite our having found our respective paths nearly independently.

To my dad, who demonstrated the earliest understanding of what my personality would entail by letting me raid his briefcase for mechanical pencils and graph paper and teaching me algebra when I was four while we played cribbage, I offer my thanks and appreciation that our mutual interests have evolved to include ecology, road trips, and fine ales from microbreweries near and far. This thesis did not reach the length of the report you wrote on the 105 interchange, but…I tried.

To Dr. Lauren Frick, representing the maximum Venn diagram overlap in the circles of my existence, from MIT Volleyball to the Essigmann Lab to BioTrove, thank you for being an editor, motivator, critic, nutritionist, painter, cat advocate, remodeling and interior design consultant, physical therapy client, entertainment planner, and best friend. I could not have done any of this without your help, support, guidance, and encouragement.

Finally, I would like to honor my mom, who grew up in a place and time that saw little encouragement offered to black women with the intellectual acumen to pursue careers in science. I've walked past the Infinite Corridor display honoring Dr. Shirley Ann Jackson thousands of times, and each time it catches my eye I think of where your curiosity and creativity would have taken you with even half the opportunities I was handed over the years. Your commitment to prioritizing our family over career advancement commensurate with your ability is indescribable, and I will consider myself successful beyond all expectations if I am even half the scientist you would be today had you been given the kind of access to resources and support that you made sure I never went without. Thank you for nurturing my interests in music and languages that balance my scientific endeavors; I am the person I am today because you have always encouraged me to embrace knowledge and seek the connections between seemingly disparate concepts and ideas.

TABLE OF CONTENTS

ABBREVIATIONS

11βCl_2	11β–dichloro
11βClOMe	11β–monochloro–monomethoxy
11β$(OMe)_2$	11β–dimethoxy
11βClOH	11β–monochloro–monohydroxy
11β$(OH)_2$	11β–dihydroxy
11β-MOR	11β–morpholino
11β-DHP	11β–2,3-dihydropyrrole
AFB_1	aflatoxin B_1
AR	androgen receptor
AR-LBD	androgen receptor ligand binding domain
CH_3CN/ACN	acetonitrile
CHL	chlorambucil
CYP/P450	cytochrome P450
ddH_2O	distilled, deionized water
DAD	diode array detector
DDI	drug-drug interaction
DMSO	dimethylsulfoxide
DNA	deoxyribonucleic acid
EDTA	ethylenediaminetetraacetic acid
ER	estrogen receptor
ESI-TOF	electrospray ionization-time of flight
EtOAc	ethyl acetate
HPLC	high pressure liquid chromatography
LC	liquid chromatography
MeOH	methanol
MEL	melphalan
milogP	molecular inspiration logP partition coefficient
mtDNA	mitochondrial DNA
NADPH	nicotinamide adenine dinucleotide phosphate
nDNA	nuclear DNA
NH_4OAc	ammonium acetate
NMR	nuclear magnetic resonance
PBS	phosphate-buffered saline
QQQ	triple quadrupole mass spectrometer
QSAR	quantitative structure-activity relationship
TNE	tris-sodium chloride-EDTA buffer

LIST OF FIGURES

LIST OF TABLES

Chapter 1: Introduction to the Design, Efficacy, and Pharmacology of 11β-dichloro, a Programmable Genotoxicant against Human Prostate Cancer

Prostate Cancer

Among the leading killers of men in the United States, adenocarcinoma of the prostate is a peculiar disease, originating in a non-essential gland whose function is only partially understood, and frequently progressing so slowly as to make "watchful waiting" a primary strategy upon diagnosis[1]. In 2008, over 185,000 new cases were diagnosed, making prostate cancer the most common cancer in men[2]. Prostate cancer is second only to lung cancer in mortality, causing 10% (>28,000) of all cancer deaths in men[2].

The prostate gland, normally about the size of a golf ball, surrounds the urethra at the base of the bladder, and serves to nourish sperm with a variety of micronutrients and proteins[3]. The transient gelatinous consistency of human semen is created by semenogelin I[4] and degraded by human seminal proteinase[5], also known as prostate-specific antigen (PSA)[6]. Over the last two decades, screening for PSA levels in the blood of men over the age of fifty has become standard practice in diagnostic oncology since the initial discovery[7] of a strong correlation between prostate tumor volume and circulating PSA levels. The increased frequency and reliability of this test has improved the rate of detection of neoplasia, made more precise the distinction between neoplasia and benign prostate hyperplasia (BPE), and lowered the average stage at which cancer is diagnosed, as evidenced by the downturn from peak incidence (>300,000) and death (40,000) rates attributed to prostate cancer in 1996[8]. Before PSA screening, patients would not likely be diagnosed with prostate cancer until the presentation of clinical symptoms or detection of nodules by digital rectal examination (DRE).

A positive (>4 ng/mL) PSA screen will provoke a DRE to explore the peripheral zone of the gland where tumors are more likely to occur followed by a multifocal biopsy to assess the degree of uniformity and differentiation of the prostatic epithelia. Based on the histology, the patient will be given a Gleason score between two and ten, calculated by summing the Gleason grades describing the levels of differentiation observed in the two largest areas of the tissue sample. A Gleason grade of 1 represents uniform, closely-packed, well-differentiated glands, while a Gleason grade of 5 indicates a complete loss of organ morphology[9]. A combined Gleason score of 9 or 10 or a single Gleason grade of 5 indicate the poorest prognosis for patient survival[10], likely describing tumors that have already metastasized or will soon metastasize to distant foci, most commonly bone

and lymph nodes. While elevated PSA levels are correlated with an increase in prostate size, the distinction between BPE and prostate cancer, as well as the assessment of the aggressiveness of a tumor, may be more accurately characterized by the rate of increase rather than the absolute levels of PSA in plasma[11]. The trio of Gleason score, kinetics of PSA expression, and tumor stage combine to characterize the risk stratification of the disease and guide the selection of a therapeutic course[12].

Detection preceding metastasis allows a full slate of targeted treatment options, including androgen ablation achieved chemically or through bilateral orchiectomy, radical prostatectomy, or radiation therapy. Typically, if the tumor has not penetrated the prostatic capsule, surgical resection of the gland is preferred[13]. If instead tumor cells have progressed to the point of being able to infiltrate neighboring tissues, external beam radiation[14], brachytherapy[15], and/or intensity-modulated radiation[16,17] may target the diseased prostate and surrounding invasions[18]. Once a prostate tumor has metastasized, however, systemically-delivered drugs are the only remaining treatment strategy.

Prostate cancer is one of several human cancers arising in tissues dependent on steroid hormones for cell cycle regulation. The regulation of the distribution and function of steroids is holistic and inherently tissue-specific. While all of these hormones are derived from cholesterol[19], sharing common synthetic machinery across diverse tissue types, the signal transduction pathways actuated by each individual steroid are tightly controlled by glandular feedback mechanisms to maintain healthy adult homeostasis. Gonadotropin-releasing hormone (GnRH) secreted by the hypothalamus promotes the release of follicle-stimulating hormone (FSH) and luteinizing hormone (LH) from the anterior pituitary. FSH and LH in turn incite the testicles to produce testosterone, which, once released into the blood stream, is sufficiently hydrophobic to cross the blood-brain barrier and repress the further production and release of GnRH, FSH, and LH[20,21]. Circulating testosterone diffuses into prostate epithelia and is converted by 5α-reductase type II in the smooth endoplasmic reticulum to dihydrotestosterone (DHT)[22,23], which, with seven-fold higher affinity for the androgen receptor (AR)[24], is the primary ligand associated with signal transduction[25]. Once bound to ligand, androgen receptor dissociates from chaperone heat shock proteins Hsp90 and Hsp70[26] and forms a homodimer[27,28] phosphorylated by various kinases. Phosphorylated homodimer

translocates to the nucleus to promote gene transcription through binding to cognate sequences in the genomic DNA known as androgen-response elements (AREs)[29]. This AR-mediated gene transcription is the primary growth-promoting impetus in prostate tissue; the goal of anti-androgen therapy is either to remove steroids completely through physical or chemical castration, or to compete directly with AR binding sites to squelch the signal and disrupt cell cycling (Figure 1-1).

Since the majority of prostate tumors demonstrate a high level of AR expression, and the signaling effects of the androgen receptor bound to its ligand can promote the further growth of the cancerous cells, androgen ablation will always be preferred to comparatively invasive or toxic therapy options. Extended treatment with anti-androgens, however, eventually provokes progression to androgen-independent tumors that can be effectively attacked only by administration of cytotoxicants. To confound matters, a negative PSA screen may miss the presence of an already-androgen-insensitive tumor, as PSA expression depends on AR-promoted transcription. A combination of PSA screening and DRE is now believed to most reliably detect prostate cancer[30].

Acquisition of androgen-insensitivity may occur through one or more of several mechanisms: mutation, leading to dysregulation of the ligand-receptor binding specificity[31]; adaptation, caused by up-regulation of the growth-promoting signaling cascade through changes in gene expression[32]; or selection, in which pre-existing androgen-independent cancer stem cells undergo clonal expansion even in the absence of hormone signal, replacing their dying androgen-dependent counterparts during a period of tumor macrostasis (or regression)[33]. No matter which mechanism is responsible for the progression, once it occurs, prognosis is at its nadir, with the only remaining therapeutic window being the differential between the division rates of cancerous and healthy tissue. Rapidly-dividing tumor cells cannot withstand the antineoplastic agents that block DNA replication, while most healthy adult tissue is not actively dividing and can therefore sustain and repair DNA damage. The adult tissue that is not static is susceptible to the slate of side effects that limit therapy.

The most common chemical agents used to treat PC include the anti-androgens, comprising steroidal (cyproterone acetate) and non-steroidal (bicalutamide, flutamide) direct AR competitors (Figure 1-2a) as well as the hormone regulation disruptors

leuprolide and ketoconazole (Figure 1-2b); the anti-mitotic microtubule inhibitors estramustine phosphate and docetaxel (Figure 1-2c); and the DNA replication inhibitors, including the topoisomerase inhibitor mitoxantrone (Figure 1-2d). The progression of prostate disease from early-stage, androgen-dependent neoplasia to invasive, androgen-independent metastatic cancer necessitates a commensurate evolution of treatment strategies (Figure 1-3).

There exists an opportunity to widen the therapeutic window through the clever design of toxicants that exploit the phenotypic aspects of prostate cancer. The growth signaling associated with the normal function and trafficking of the androgen receptor is mediated by its promotion of the transcription of genes that lead to progression through the cell cycle. Diversion of the receptor from its function as a transcription factor should slow the rate of division, but in cancers that have achieved androgen-independence, this functionality is lost. However, the continued presence of a high level of androgen receptor, even in distant metastatic foci[34], suggests that a drug candidate whose toxicity is facilitated or enhanced by interaction with the receptor should kill selectively those tumor cells—regardless of metastatic milieu—that arose from prostate tissue.

Cisplatin and Testicular Cancer

One of the brightest success stories in the centuries-old fight against human cancers comes from the mechanism of toxicity of *cis*-diamminedichloroplatinum(II) (cisplatin), a bifunctional, platinum-containing DNA-damaging agent central to the 93% cure rate for testicular cancer[35]. Unlike its non-cytotoxic and therapeutically ineffective trans isomer, cisplatin is capable of coordinating adjacent purines at the N7 position of each base. The resulting kink in the DNA backbone is bound with strong affinity ($K_D \sim 60$ pM)[36] by the human upstream binding factor (hUBF), a high mobility group (HMG) domain-containing protein associated with the promotion of transcription of ribosomal RNA through recognition of RNA polymerase I. This affinity is comparable ($K_D \sim 18$ pM)[36] to the association between hUBF and the cognate response element upstream of the gene encoding ribosomal DNA. While there are many mechanisms that have been proposed for cisplatin, the data on protein binding[37] suggested two novel ones (Figure 1-4). First, hUBF or another adduct-binding protein shields the adduct from

nucleotide excision repair[38]. Second, the simple titration of hUBF or other transcription factors away from their normal function as regulators of tumor gene expression contributes to dysregulation of the cell cycle[39].

One branch of the development of next generation anti-cancer drugs seeks to mimic the mechanistic success of cisplatin against testicular cancer in other tissue backgrounds, creating a way either to deliver far less drug while achieving the same toxicity to tumor cells, or to increase the dosage level to kill tumors more effectively while maintaining the same level of side effects as traditional chemotherapy. Conventional alkylating agents, developed from mustard gas, are spectacularly toxic to all dividing tissues, cancerous or healthy. Patients receiving nitrogen mustards hope that the drugs kill their tumors before killing them—the collateral toxicity to normally-renewing tissues, especially myelosuppression[40], is often the limiting factor in clinical settings.

DNA Alkylating Agents

Alkylating agents are most frequently used in combination with other chemotherapeutic agents, delivered as part of empirically-derived regimens that balance tumor-killing efficacy against the side effects suffered by patients. Among these agents are the aniline mustards, including melphalan, used clinically against multiple myeloma[41], and chlorambucil, central to the treatment of chronic lymphocytic leukemia[42] and non-Hodgkin's lymphoma[43]. Mechanistically, attack by the aniline nitrogen on either terminal carbon displaces its chloride leaving group, yielding an electrophilic aziridinium ion. This moiety is susceptible to attack by the nucleophilic sites of biological macromolecules, including several positions on DNA, with N7 of guanine most commonly forming the covalent bond. Held in close proximity to DNA, a second nucleophilic attack can yield a crosslink that, if persistent, can elicit cell cycle arrest and/or cytotoxicity by blocking DNA replication or assaulting genomic structural integrity through creation of a double-strand break. Human cancers treated with alkylating agents can acquire drug resistance, reducing the efficacy of these compounds through the up-regulation of DNA repair pathways[44] or metabolic detoxification machinery[45-48]. Again, whether this proceeds through clonal selection or mutational gain-

of-function, the timeline for a patient following growth of tumors unresponsive to these highly toxic drugs is grim.

Design of Programmable Genotoxicants

Researchers in the drug design field strive to make cancer therapeutics that selectively kill tumor cells while leaving healthy tissue intact. The over-expression of specific proteins in certain cancers has provided a plan of attack: compounds toxic in the presence of a steroid receptor more abundant in cancerous tissue than in non-diseased cells should be more effective chemotherapeutic agents than drugs whose toxicity is independent of receptor expression. The abundance of androgen receptor in prostate tissue suggests that a compound whose toxicity requires—or is at least enhanced by—interaction with the receptor would make a useful agent in achieving selectivity. Cytotoxic agents linked to steroid moieties, such as estramustine and prednimustine[49], have been developed with the goal of achieving selective delivery, hormone antagonism, or stability enhancement, but the deleterious interaction between a transcription factor and a site of DNA damage in the mechanism of cisplatin represented a novel pharmaceutical design strategy.

The Essigmann Laboratory, recognizing this opportunity for innovation in the treatment of several kinds of cancer, has taken a combinatorial approach to the design of these programmable genotoxicants, seeking to optimize through chemistry the potency of the alkylating agents, stability of the linkers, and affinity to target receptors of the ligand analogs. This library comprises aniline mustards and platinum centers[50] as alkylating "warheads," a series of solubility-enhancing linkers of various functionalities and lengths designed to optimize the interaction between the receptor and the DNA adduct[51], and ligands for the androgen[52] and estrogen[53,54] receptors to combat prostate, breast, and ovarian cancers (Figure 1-5). The efficacy of cisplatin arises from its multiple mechanisms and their inherent cooperation: titration of growth factor away from its signaling cascade also shields toxic DNA lesions from repair. The programmable genotoxicants designed in the Essigmann Laboratory are designed to achieve a similar multi-functionality[55].

The leading candidate against prostate cancer from this library is an 11β-substituted estra $\Delta^{4(5),9(10)}$-3-one linked to an N,N-*bis*-(2-chloroethyl)-aniline by a linker containing a carbamate synthetic handle and a solubility-enhancing secondary amine, known as 11β-dichloro[†] and abbreviated in this report as 11β. Two control compounds with derivative versions of the nitrogen mustard were synthesized as well: 11β-dimethoxy, incapable of any DNA alkylation, and 11β-monochloro–monomethoxy (monochloro), capable of forming a covalent adduct with DNA but lacking the second chloroethyl arm necessary for the formation of DNA crosslinks. The relative binding affinity (RBA) of 11β-dichloro and 11β-dimethoxy for the AR in comparison with the standard reference synthetic androgen methyltrienolone (R1881) has been measured as 11% and 18%, respectively (Figure 1-6)[52]. A sixteen-base-pair DNA oligomer containing a covalent 11β adduct was shown to have an RBA of 0.22%[52], suggesting that a sufficient adduct load may disrupt the native AR-promoted transcriptional program.

Preliminary *in vitro* and *in vivo* treatments have been performed, demonstrating the potent toxicity of 11β against several cell lines derived from metastatic prostate cancer, including the androgen-dependent LNCaP line[56], as well as moderate toxicity against the AR-expressing but androgen-independent PC3 and DU-145 lines[57] (Figure 1-7). Promisingly, the growth of tumors arising from LNCaP xenografts implanted subcutaneously in a mouse model[52] was strikingly inhibited by daily administration of 11β with minimal toxicity to the host (Figure 1-8), thus provoking the need to confirm the mechanism of toxicity and explore the pharmacokinetic behavior of the drug candidate.

Clinical Pharmacology

The practice of drug design characterizes **a**bsorption, **d**istribution, **m**etabolism, **e**xcretion, and **tox**icology (ADME/Tox) in order to determine the fitness of a drug candidate for progression from bench-top screening to clinical trials. Of primary concern is the relationship between dosage and exposure, which depends strongly on the ability of the body to clear xenobiotic chemicals from its circulation. Clinicians monitor plasma

[†] 2-(6-((8S,11S,13S,14S,17S)-17-Hydroxy-13-methyl-3-oxo-2,3,6,7,8,11,12,13,14,15,16,17 dodecahydro-1H-cyclopenta[a]phenanthren-11-yl)hexylamino)ethyl 3-(4-(bis(2-chloroethyl)amino)phenyl)propylcarbamate

concentration of a drug (or its metabolite biomarker) and derive dosage schedules that maintain most effectively a profile within the therapeutic window of the drug—i.e., abundant enough to achieve a desired outcome but below the toxic threshold.

Hepatic pathways are responsible for the overwhelming majority of drug clearance, shuttling hydrophobic molecules into bile ducts for inclusion in feces, or converting them into more polar species for renal excretion. The biotransformation of xenobiotics to more polar metabolites can also yield a structural chassis onto which solubility-enhancing cofactors can be conjugated, facilitating clearance by either route.

The bulk of these reactions are catalyzed by the cytochromes, a diverse superfamily of redox-capable hemoproteins localized to the endoplasmic reticula and mitochondria of eukaryotes. A subset of this superfamily, the cytochromes P450, comprises the enzymes charged with the bioactivation of drugs necessary to facilitate clearance. These enzymes can be found in almost all epithelia, but are most abundantly expressed in hepatocytes. The P450 family is divided into subgroups based on sequence homology, with expression patterns varying widely at every level of examination: across tissues[58], species[59], and ethnic groups[60,61]. Members of the family are known as isoforms and are identified with an ever-evolving system of nomenclature reflective of the levels of sequence homology. Isoforms are abbreviated as CYP followed by a number representing families sharing at least 40% homology, a letter representing subsets with at least 55% homology, and a second number for an individual gene[62,63]. For example, CYP3A4, the most abundantly-expressed P450 isoform in humans and the enzyme responsible for the vast majority of xenobiotic metabolic transformations, is a member of the CYP3A[64] subset of the CYP3 family[65] of genes localized to chromosome 7[66].

The most common reaction catalyzed by the cytochromes P450 is an oxidation, usually near a site of high electron density on the substrate. This process requires a cycle of the oxidation states of the heme iron (Figure 1-9), with the net effect of reducing molecular oxygen to water and inserting one oxygen atom into the substrate. While the sequence of the conversions and roles of the cofactors are generally conserved, the macrostructure of the enzyme governs its substrate specificity. Substrates that fit into the active site of a given isoform are subject to a diverse array of transformations, including hydroxylation at or near a heteroatom, oxidation of a carbon center, epoxidation of a

carbon-carbon double bond, and even dealkylation. Each of these potential sites of oxidation should directly enhance solubility or enable attachment of a cofactor, effectively increasing renal or fecal clearance and lowering the area under the curve (AUC) achieved by administration of a given dose.

In some cases, however, oxidation activates the compound, generating a reactive intermediate that may have beneficial or deleterious biological activity. The epoxidation of aflatoxin B_1 yields an electrophile capable of forming mutagenic DNA adducts strongly associated with the development of liver cancer (Figure 1-10a)[67,68]. Conversely, the usefulness of cyclophosphamide as an anti-cancer agent depends on oxidation at the 4′ position to enable the ring-opening rearrangement necessary for decomposition into the alkylating agents phosphoramide mustard and acrolein (Figure 1-10b)[69-71]. Furthermore, oxidation by P450 expressed in prostate epithelia has been directly implicated in the generation of DNA-damaging metabolites central to the epidemiological correlation between diets rich in cooked meats and increased incidence of prostate cancer[72].

The molecular structure of a drug candidate can guide the generation of a hypothesis toward determining the P450 isoforms for which it may be a substrate. Comparison with pharmacophores—molecules containing similar structure and/or arrangement of functional groups—yields some clues as to what the metabolic products of a given compound may be. However, it is ultimately necessary to test metabolism empirically by incubating a potential substrate with whole hepatocytes, liver microsomes, or purified P450 enzymes.

Interestingly, the biosynthesis and metabolism of endogenous steroids depend on many of the same enzymes, as the cascade from cholesterol to testosterone, estrogen, and progesterone requires redox chemistry at several steps[19]. Because hormone therapy against prostate cancer includes competitive inhibitors for the androgen receptor, it is important to consider the possibility that these compounds will also be substrates for steroid synthetic machinery. Furthermore, clearance of testosterone also requires hydroxylation by P450, and subtle modifications to the steroid ring system effect dramatic consequences on the affinity of the molecule for the steroid receptors[24].

Cancer therapy frequently involves combinations of drugs in tightly-controlled patterns of administration. Hormone antagonists, cytotoxicants, and the analgesics and

anti-emetics used to mitigate side effects are prescribed together, and it is crucial that their co-administration does not alter the desired pharmacology of each compound. The development of new chemotherapeutic agents must therefore consider the high probability that, if successful, the drug candidates would eventually be administered in combination with other agents. In addition to screening compounds through relevant bioassays for efficacy, pharmacologists must consider drug-drug interactions (DDI) as a potential safety hazard alongside primary toxicity caused by the compound administered alone[73].

Prostate cancer patients may be suffering from a variety of conditions common in the elderly and requiring regular administration of therapeutics. While prostatic is second only to lung in cancer mortality rate in the developed world, cardiovascular, respiratory, and metabolic diseases more frequently cause death and/or require chronic pharmaceutical intervention[74]. High cholesterol dramatically increases the risk of myocardial and cerebral infarction following atherosclerotic plaque growth, making Lipitor (atorvastatin[75], metabolized by CYP3A4[76]), the most commonly-prescribed medicine in the United States in 2007. Also metabolized by CYP3A4 are the anti-inflammatory corticosteroid fluticasone[77] and the β2-adrenergic receptor agonist salmeterol[78], which are combined to treat chronic obstructive pulmonary disease as Advair, ranked third on the most-prescribed list. Avandia (rosiglitazone, metabolized by CYP2C8[79]), which inhibits insulin expression by promoting the expression of peroxisome proliferator-activated receptor gamma[80], is the top prescription for countering insulin resistance in patients with type 2 diabetes mellitus.

Before even considering multiple disease states interfering with prostate cancer treatment, it is important to note that the erectile and urinary dysfunctions[81] caused by prostate cancer surgery and radiation treatment frequently provoke the prescription of the cGMP-phosphodiesterase inhibitor Viagra (sildenafil, metabolized[82] by CYP3A4 and CYP2C9), which effects localized vasodilation through the release of nitric oxide[83], and Flomax (tamsulosin, metabolized[84] by CYP3A4 and CYP2D6), which lowers bladder pressure through inhibition of the α_{1a}-adrenorecptor in prostate tissue. The non-steroidal anti-inflammatory drug diclofenac, which reduces pain by inhibiting the arachidonic acid cascade necessary for the synthesis of prostaglandin[85], holds the distinction of being a

standard anti-arthritis medication, commonly-prescribed in the maintenance of pain associated with prostate cancer bone metastases, and widely-accepted as a standard probe for the assessment of metabolism by CYP2C8[86].

The variable expression of P450 across species and individuals limits the power of data generated from animal trials when predicting the behavior of a drug candidate in humans. The DDI potential in a multi-drug treatment regimen may be of great concern in one patient but inconsequential in another due to both genetically-determined expression levels and allelic variants of the isoforms. Advances in genetic screening and bioinformatics are personalizing the practice of medicine in all specialties, and over the last few decades, pharmacologists have not only classified the metabolic machinery responsible for the transformation of existing drugs, but also added the characterization of the metabolic profile of a drug candidate to the pre-clinical checklist.

Specific Aims

The promising activity of 11β against prostate cancer cells *in vitro* and LNCaP xenografts *in vivo* prompted systematic study of the pharmacokinetic and pharmacodynamic properties of the drug candidate. The analysis of stability to hydrolysis and the identification of hydrolytic decomposition products of 11β in various aqueous systems are discussed in Chapter 2, serving as a necessary prelude to an examination of the metabolic profile of the drug candidate as described in Chapter 3. Metabolic exploration of 11β comprised qualitative and quantitative assessments of the extent of conversion, spectrum of daughter compounds, and identity of P450 isoforms catalyzing the transformations. Incubation of radio- or unlabeled compound with various preparations of liver microsomes allowed separation and characterization of metabolites by a combination of analytical techniques, including high-pressure liquid chromatography, electrospray ionization–time of flight, triple quadrupole, and accelerator mass spectrometry, and high-throughput DDI screening. Finally, preliminary examination of the effects of formulation and delivery route on the organ-level bioavailability of 11β as well as subcellular transport, distribution phenomena, and non-specific binding of the drug candidate *in vitro* are reported in Chapter 4.

Figure 1-1: The Hypothalamus–Pituitary–Gonadal axis regulates circulating testosterone levels and is a target for therapeutic intervention

Testosterone homeostasis is maintained via a negative feedback loop comprising the hypothalamus, anterior pituitary, and testes. Circulating testosterone diffuses into the prostate, where it is converted to dihydrotestosterone (DHT) by 5α-reductase. DHT binds the cytoplasmic androgen receptor (AR), provoking its dissociation from chaperone proteins. The AR is then phosphorylated, after which it dimerizes and translocates to the nucleus to stimulate gene expression and cell division. Leuprolide inhibits the production of follicle stimulating hormone and luteinizing hormone, while ketoconazole inhibits testosterone production. Cytotoxicants and radiation can directly target a prostate tumor. The AR competitors bicalutamide and flutamide can saturate ligand binding domains, locking them into conformations that prevent the completion of the signal transduction pathway.

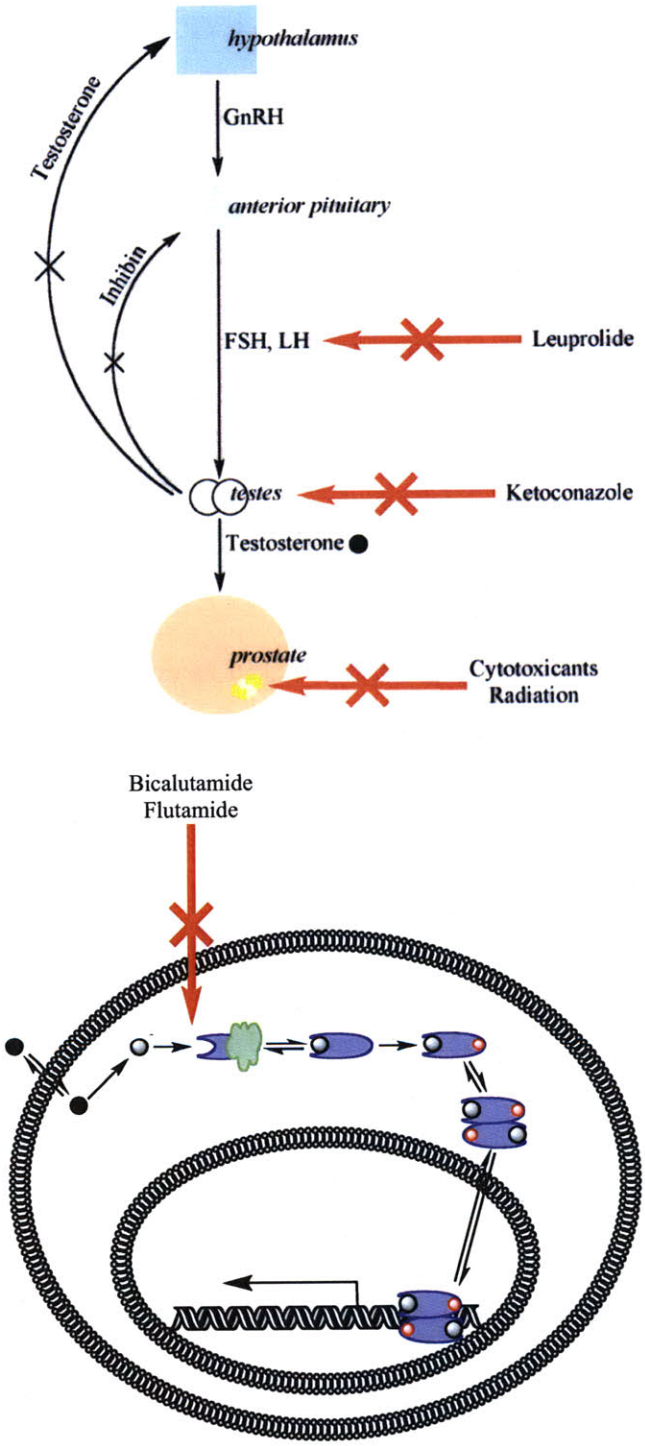

Figure 1-2: Several classes of drugs are used in concert against prostate cancer

a) Androgen receptor competitors

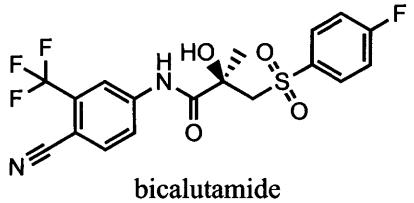

bicalutamide

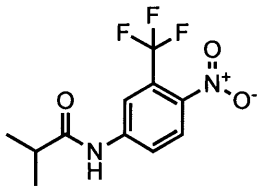

flutamide

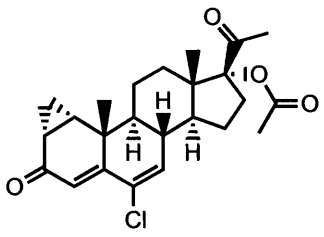

cyproterone acetate

b) Systemic hormone regulation antagonists

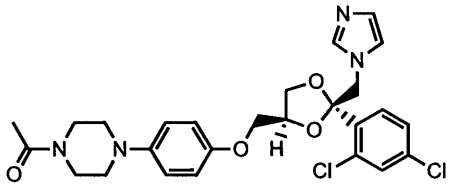

ketoconazole

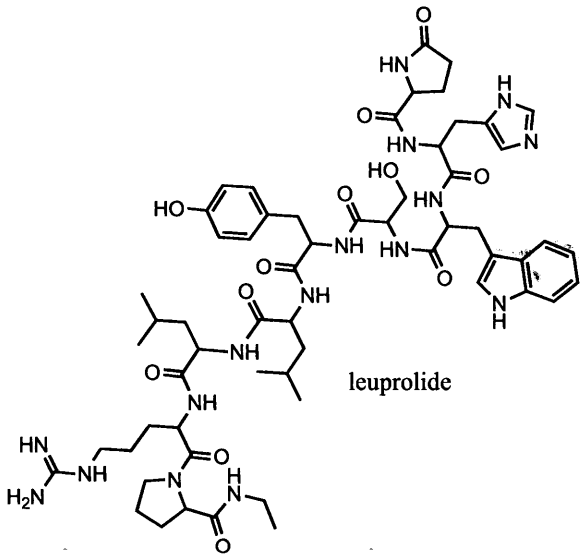

leuprolide

Figure 1-2: Several classes of drugs are used in concert against prostate cancer

c) Microtubule inhibitors

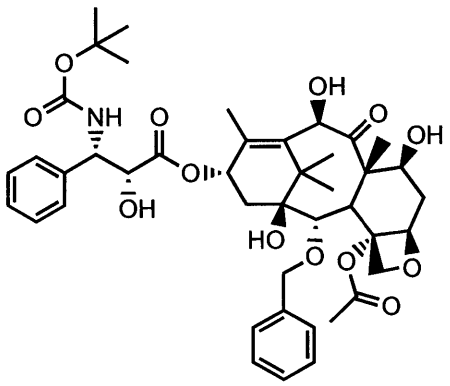

docetaxel

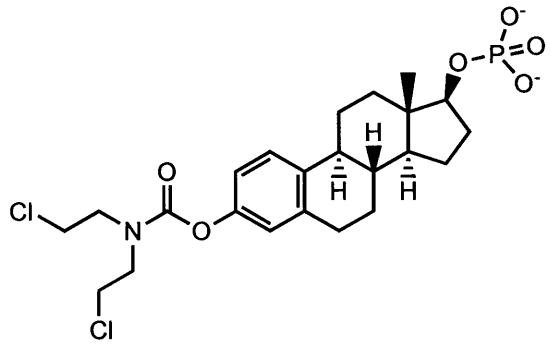

estramustine phosphate

d) Topoisomerase inhibitor

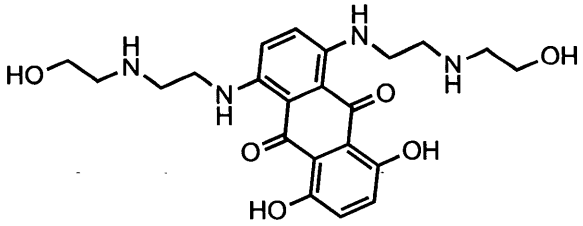

mitoxantrone

Figure 1-3: Treatment options strongly depend on the stage of progression of prostate cancer

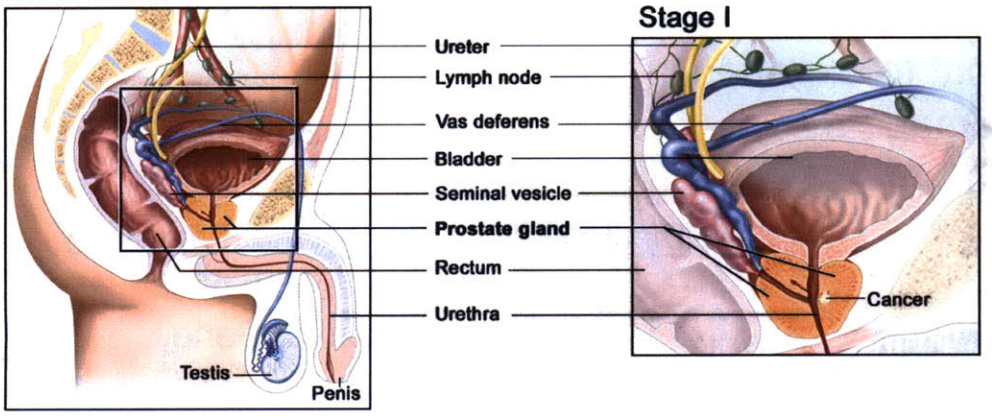

If detected at Stage I†, prostate cancer is localized and may be treated through targeted radiation or implantation of radioactive material (brachytherapy) to kill the tumor, with radical prostatectomy an option but not a requirement. Follow-up treatment involves simply monitoring PSA levels and velocity to detect any abnormal re-growth.

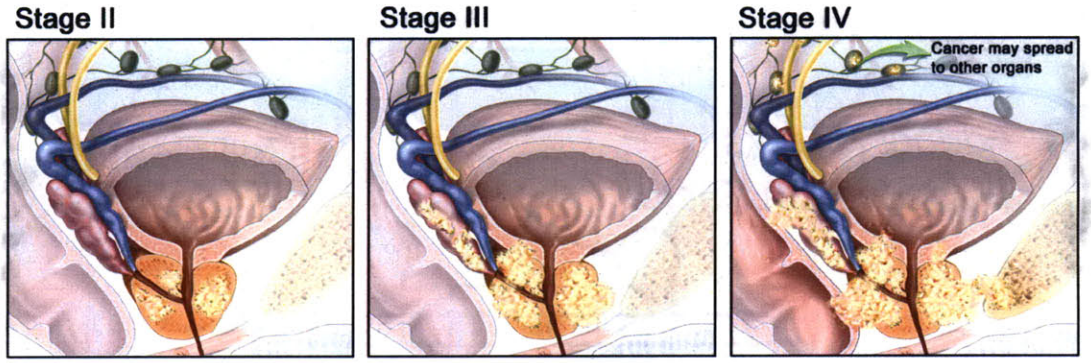

Multiple foci contained within the prostate capsule constitute Stage II cancer, for which surgical resection and targeted radiation treatment are prescribed. Should the tumor infiltrate the local surrounding organs (Stage III), surgery and radiation are not sufficient to kill all of the cancerous tissue. In this case, chemical androgen blockade will be added to the treatment to mitigate the growth of hormone-responsive tissue. Once the cancer has reached Stage IV, spreading to the bladder, rectum, bone, and/or lymph nodes, systemic administration of anti-androgens and cytotoxicants are the only option for treatment, and are palliative at best, given that the tumor will inevitably progress to androgen independence and acquire resistance to cytotoxic agents. The design of 11β is based on creating an alternative to the chemotherapeutic agents that demonstrate toxicity to all dividing tissues, in hopes that the androgen-independent metastases that still express high levels of androgen receptor experience enhanced toxicity compared to healthy tissue.

† National Cancer Institute, retrieved from www.dana-farber.org April 30, 2009.

Figure 1-4: The bifunctional drug cisplatin is central to the 93% cure rate of testicular cancer

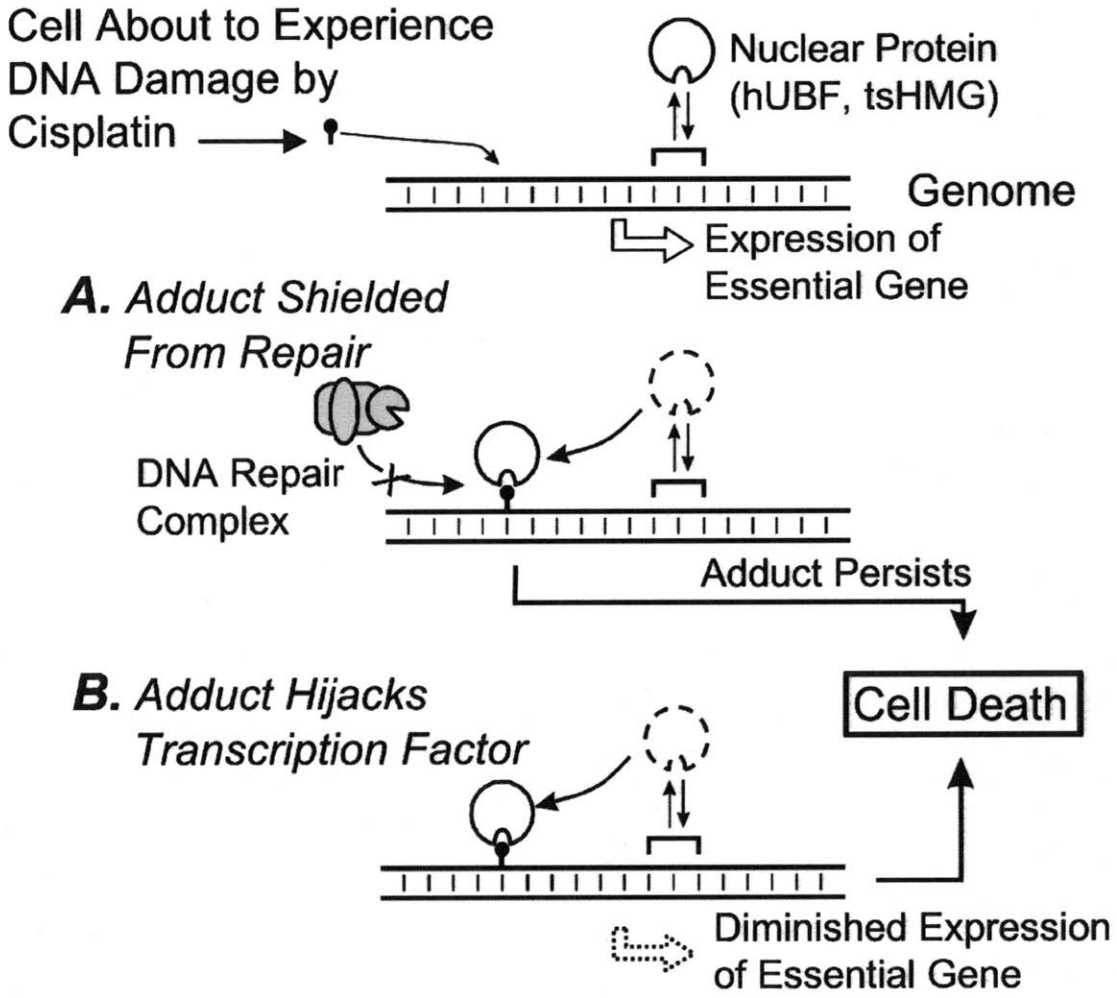

Cisplatin forms DNA adducts and crosslinks, creating a kink in the DNA structure that is recognized with very high affinity ($K_D \sim 60$ pM) by the human upstream binding factor (hUBF), which normally promotes the transcription of ribosomal RNA. This receptor–adduct interaction can **A)** shield the adduct from repair, or **B)** hijack hUBF away from its native function. Either mechanism eventually leads to cell death.[36,37,87]

Figure 1-5: A library of programmable genotoxicants has been created against cancers expressing steroid receptors

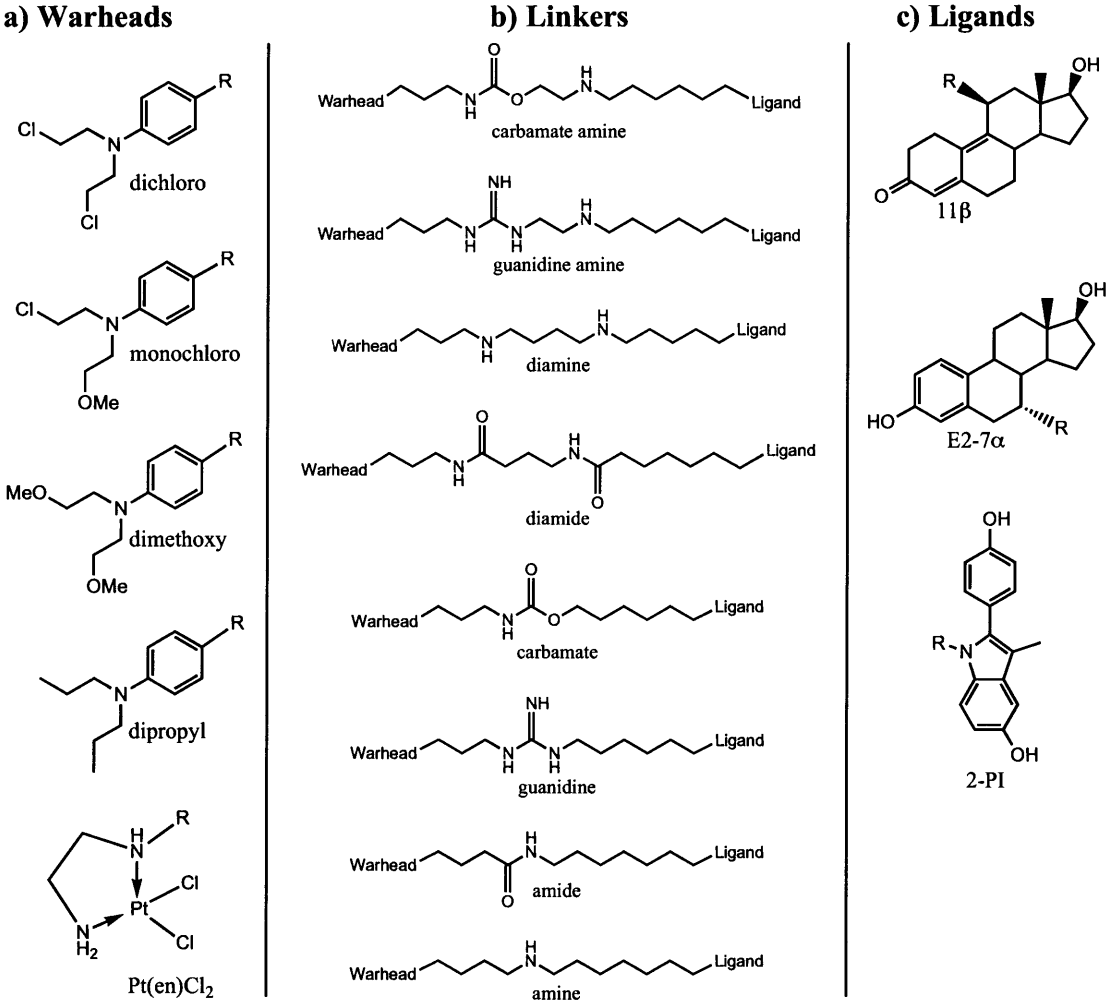

The Essigmann Laboratory has developed the technology to design and assemble programmable genotoxicants against human cancers. A DNA-damaging warhead from column A can be tethered by a linker featuring variable length and functionality from column B to a ligand for a target receptor in column C. The work described in this report concerns the aniline mustard tethered to the 11β position of an androgen receptor ligand based on RU-486 by a carbamate amine linker, and is referred to as 11β-dichloro, shown below.

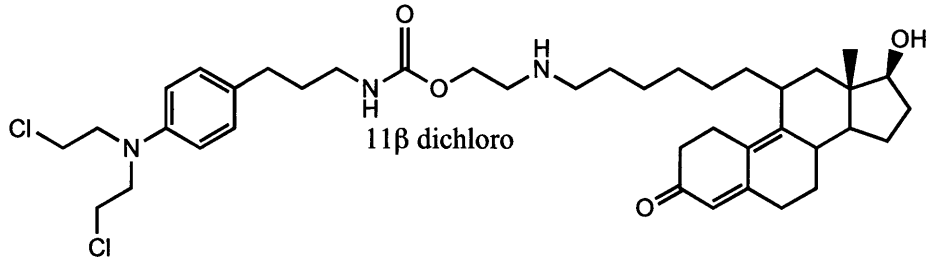

Figure 1-6: The 11β compounds show affinity for the androgen receptor comparable to the synthetic androgen R1881

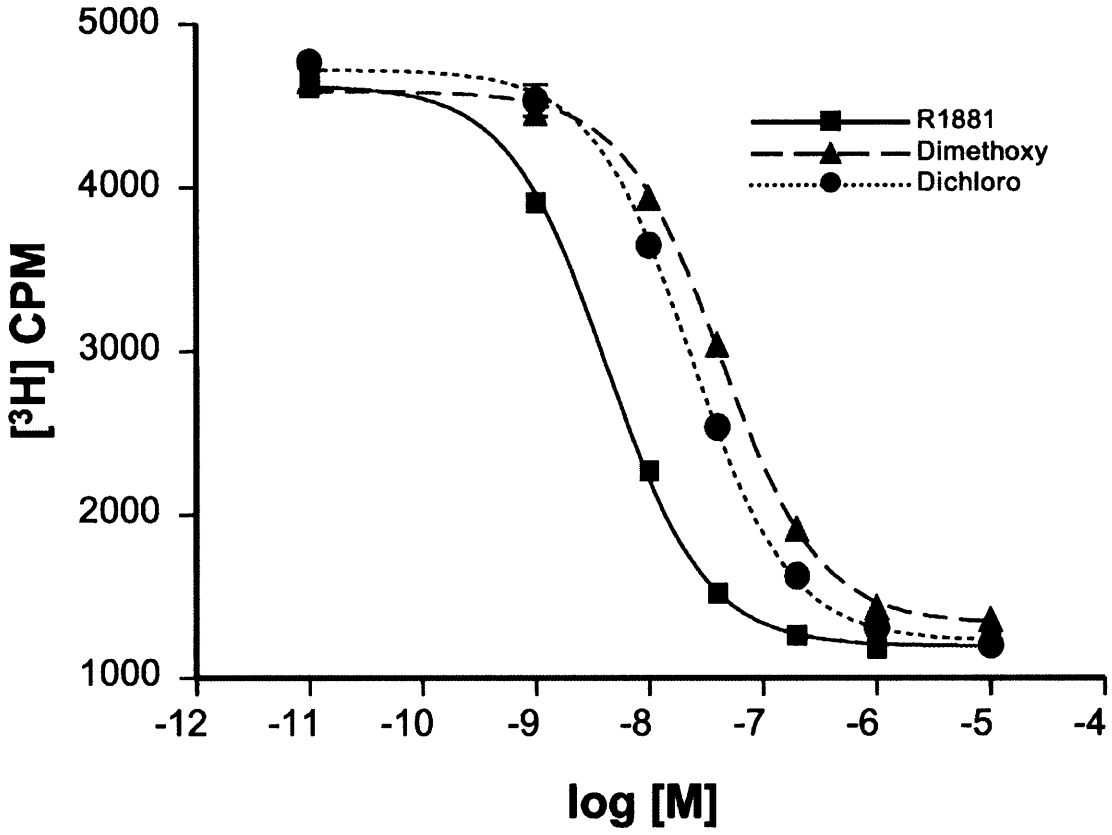

In LNCaP cell extract, 11β-dichloro (11%) and 11β-dimethoxy (18%) were shown to effectively compete away the binding of the reference compound ^{3}H-R1881, indicating affinity for the androgen receptor on the order of magnitude of the native androgen testosterone (19%[24], not shown). Adapted from Marquis et al. (2005)[52].

Figure 1-7: Toxicity of 11β to prostate cancer cell lines *in vitro* exceeds that of the aniline mustard chlorambucil

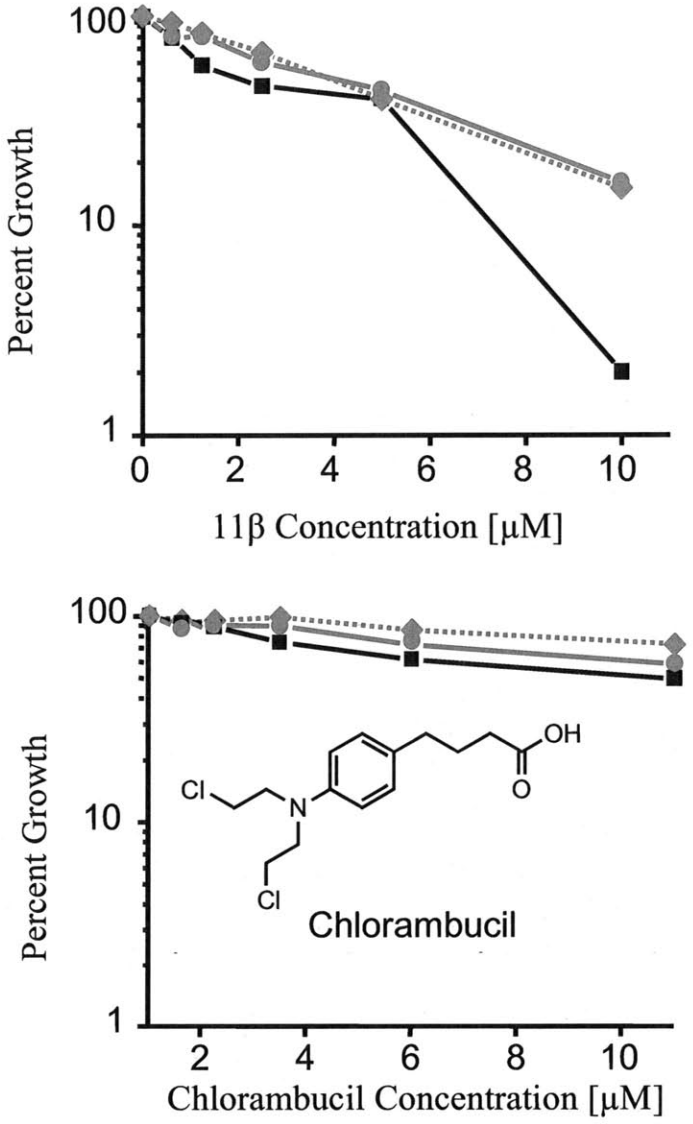

11β elicited markedly more toxicity than chlorambucil against prostate cancer cell lines *in vitro*. The AR-dependent LNCaP cell line (squares) showed significantly higher sensitivity to 11β than the AR-independent cell lines DU-145 (diamonds) and PC-3 (circles). Figure courtesy of Shawn Hillier.

Figure 1-8: 11β inhibits LNCaP xenograft tumors and is well-tolerated by the host

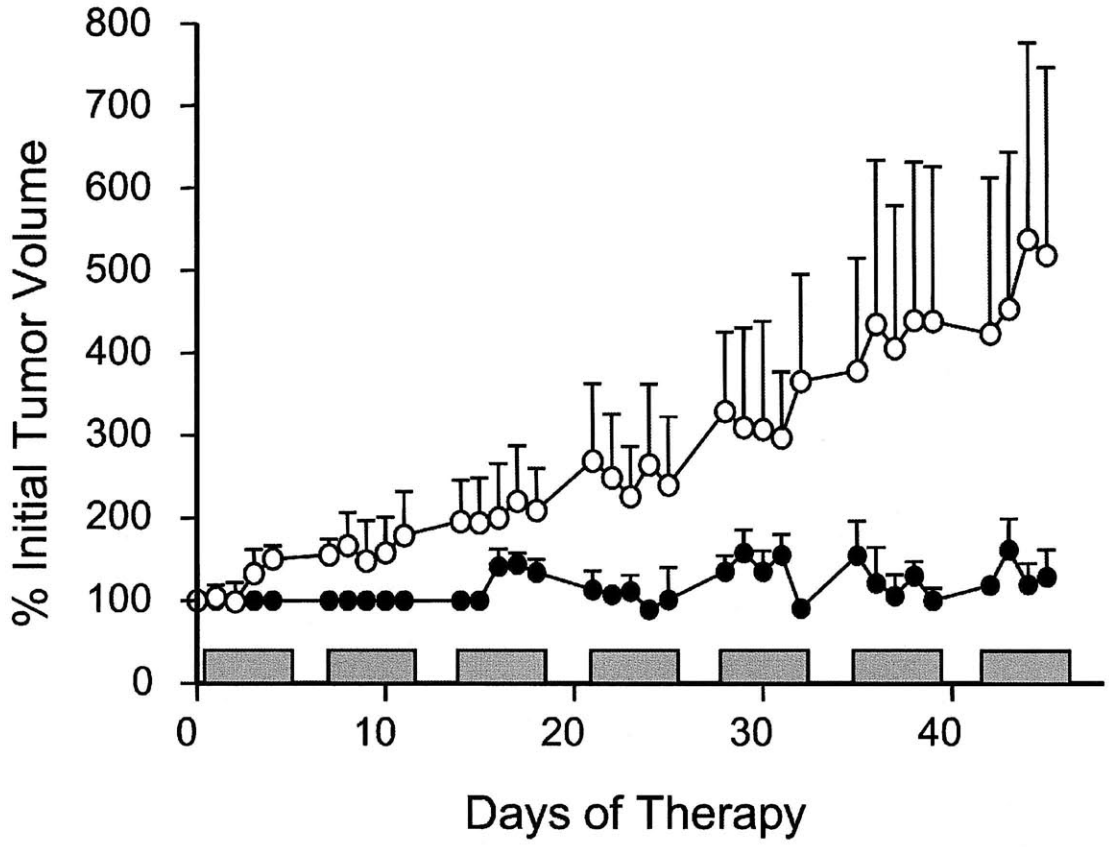

Subcutaneous LNCaP xenograft tumors were implanted into mice treated with either vehicle (open circles) or vehicle with 11β (filled circles). The mice receiving 11β showed neither tumor growth nor peripheral toxicity from the treatment. Adapted from Marquis et al. (2005).[52]

Figure 1-9: Cytochrome P450 catalyzes xenobiotic oxidations through a cycling of the oxidation states of heme iron

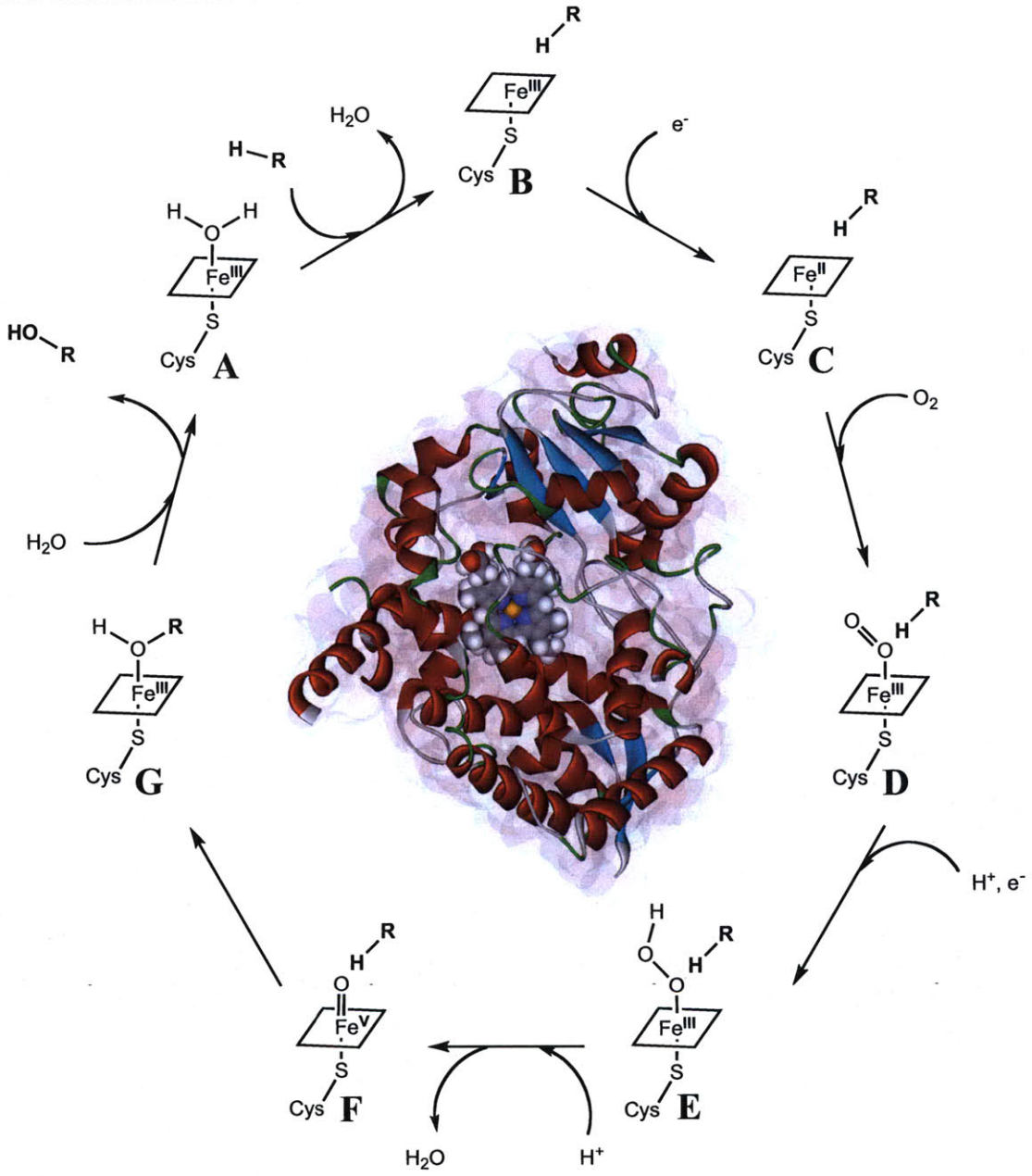

Substrate R-H diffuses into the active site of P450, displacing water from ferrous heme iron [**A**->**B**]. NADPH supplies an electron to reduce iron to its ferric form [**C**] before being oxidized [**D**]. A proton and an electron from NADPH reduce the active site to peroxo-iron [**E**]. Water is generated as the iron temporarily takes a +5 oxidation state [**F**] before the R-H bond of the substrate binds the oxygen [**G**] and restores iron to its initial state. Water displaces the oxidized product. Crystal structure of CYP3A4[88] shown with heme group exposed at center. Redox cycle figure adapted from Casarett & Doull's Toxicology[89].

Figure 1-10: Aflatoxin B_1 and cyclophosphamide are activated by P450 with divergent consequences

a) Aflatoxin B_1 (AFB_1) is epoxidized by P450 to AFB_1-8,9-oxide, which forms a mutagenic lesion at N7 of guanine. Figure adapted from Smela et al. 2002[90].

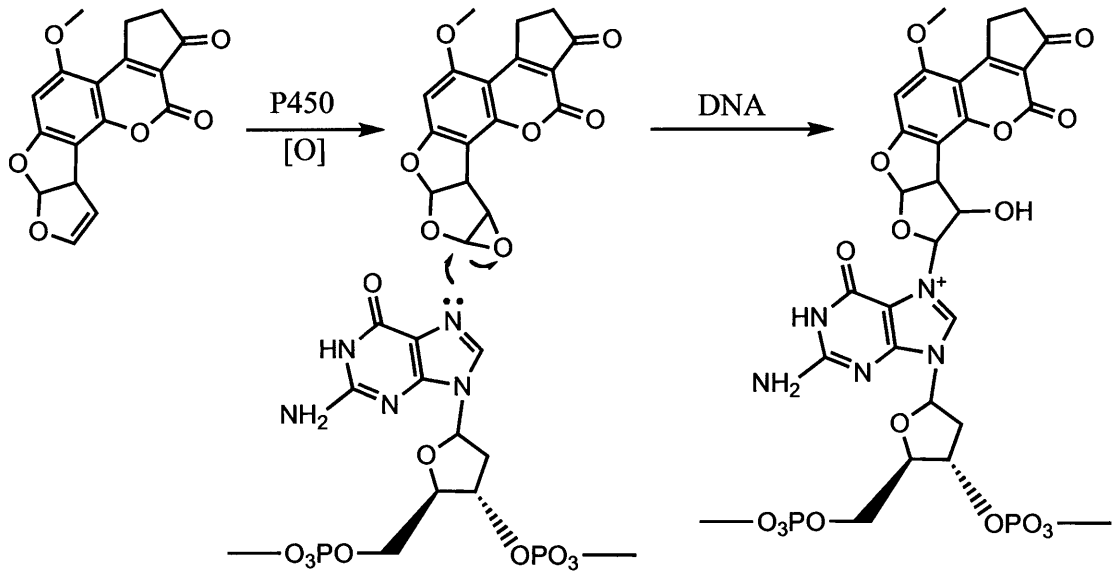

b) The pro-drug cyclophosphamide is activated by P450 to 4′-hydroxycyclophosphamide. This rearranges to aldophosphamide, which decomposes into phosphoramide mustard and acrolein, both capable of forming covalent adducts with DNA[70].

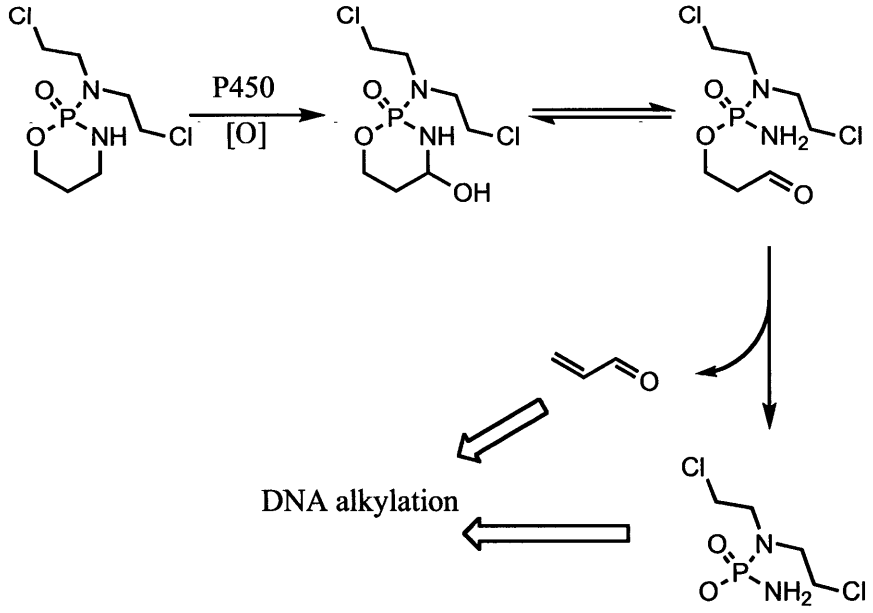

References

1. Albertsen, P.C., Hanley, J.A. & Fine, J. 20-year outcomes following conservative management of clinically localized prostate cancer. *JAMA* **293**, 2095-2101(2005).
2. Jemal, A. et al. Cancer statistics, 2008. *CA Cancer J Clin* **58**, 71-96(2008).
3. Utleg, A.G. et al. Proteomic analysis of human prostasomes. *Prostate* **56**, 150-161(2003).
4. Lilja, H., Abrahamsson, P.A. & Lundwall, A. Semenogelin, the predominant protein in human semen. Primary structure and identification of closely related proteins in the male accessory sex glands and on the spermatozoa. *J. Biol. Chem* **264**, 1894-1900(1989).
5. Robert, M. et al. Characterization of prostate-specific antigen proteolytic activity on its major physiological substrate, the sperm motility inhibitor precursor/semenogelin I. *Biochemistry* **36**, 3811-3819(1997).
6. Waheed, A. et al. Human seminal proteinase and prostate-specific antigen are the same protein. *J. Biosci* **33**, 195-207(2008).
7. Stamey, T.A. et al. Prostate-specific antigen as a serum marker for adenocarcinoma of the prostate. *N. Engl. J. Med* **317**, 909-916(1987).
8. McDavid, K. et al. Prostate cancer incidence and mortality rates and trends in the United States and Canada. *Public Health Rep* **119**, 174-186(2004).
9. Gleason, D.F. Classification of prostatic carcinomas. *Cancer Chemother Rep* **50**, 125-128(1966).
10. Gleason, D.F. Histologic grade, clinical stage, and patient age in prostate cancer. *NCI Monogr* 15-18(1988).
11. Punglia, R.S. et al. Prostate-specific antigen velocity and the detection of gleason score 7 to 10 prostate cancer. *Cancer* **110**, 1973-1978(2007).
12. Yoon, J.H. et al. Predictive factor analysis as the basis for the clinical utility of percent positive prostate biopsies in patients with intermediate-risk prostate cancer. *Urology* **60**, 454-457(2002).
13. Han, M. et al. Isolated local recurrence is rare after radical prostatectomy in men with Gleason 7 prostate cancer and positive surgical margins: therapeutic implications. *J. Urol* **165**, 864-866(2001).
14. D'Amico, A.V. et al. Equivalent biochemical failure-free survival after external beam radiation therapy or radical prostatectomy in patients with a pretreatment prostate specific antigen of > 4-20 ng/ml. *Int. J. Radiat. Oncol. Biol. Phys* **37**, 1053-1058(1997).
15. Zelefsky, M.J. et al. Comparison of the 5-year outcome and morbidity of three-dimensional conformal radiotherapy versus transperineal permanent iodine-125 implantation for early-stage prostatic cancer. *J. Clin. Oncol* **17**, 517-522(1999).
16. Zelefsky, M.J. et al. Incidence of late rectal and urinary toxicities after three-dimensional conformal radiotherapy and intensity-modulated radiotherapy for localized prostate cancer. *Int. J. Radiat. Oncol. Biol. Phys* **70**, 1124-1129(2008).
17. Zelefsky, M.J. et al. Combined brachytherapy with external beam radiotherapy for localized prostate cancer: reduced morbidity with an intraoperative brachytherapy planning technique and supplemental intensity-modulated radiation therapy. *Brachytherapy* **7**, 1-6(2008).

18. Stokes, S.H. Comparison of biochemical disease-free survival of patients with localized carcinoma of the prostate undergoing radical prostatectomy, transperineal ultrasound-guided radioactive seed implantation, or definitive external beam irradiation. *Int. J. Radiat. Oncol. Biol. Phys* **47**, 129-136(2000).
19. Miller, W.L. Androgen biosynthesis from cholesterol to DHEA. *Mol. Cell. Endocrinol* **198**, 7-14(2002).
20. Mohler, J.L. et al. The androgen axis in recurrent prostate cancer. *Clin Cancer Res* **10**, 440-8(2004).
21. Romeo, R.D. et al. Stress History and Pubertal Development Interact to Shape Hypothalamic-Pituitary-Adrenal Axis Plasticity. *Endocrinology* **147**, 1664-1674(2006).
22. Bruchovsky, N. & Wilson, J.D. The Conversion of Testosterone to 5agr-Androstan-17{beta}-ol-3-one by Rat Prostate in Vivo and in Vitro. *J. Biol. Chem.* **243**, 2012-2021(1968).
23. Bruchovsky, N. & Wilson, J.D. The Intranuclear Binding of Testosterone and 5agr-Androstan-17{beta}-ol-3-one by Rat Prostate. *J. Biol. Chem.* **243**, 5953-5960(1968).
24. Fang, H. et al. Study of 202 natural, synthetic, and environmental chemicals for binding to the androgen receptor. *Chem. Res. Toxicol* **16**, 1338-1358(2003).
25. Fang, S., Anderson, K.M. & Liao, S. Receptor Proteins for Androgens. On the role of specific proteins in selective retention of 17beta-hydroxy-5alpha-androstan-3-one by rat ventral prostate in vivo and in vitro. *J. Biol. Chem.* **244**, 6584-6595(1969).
26. Pratt, W.B. & Toft, D.O. Steroid receptor interactions with heat shock protein and immunophilin chaperones. *Endocr. Rev* **18**, 306-360(1997).
27. Wong, C.I. et al. Steroid requirement for androgen receptor dimerization and DNA binding. Modulation by intramolecular interactions between the NH2-terminal and steroid-binding domains. *J. Biol. Chem* **268**, 19004-19012(1993).
28. Nemoto, T. et al. Dimerization characteristics of the DNA- and steroid-binding domains of the androgen receptor. *J. Steroid Biochem. Mol. Biol* **50**, 225-233(1994).
29. Shaffer, P.L. et al. Structural basis of androgen receptor binding to selective androgen response elements. *Proc. Natl. Acad. Sci. U.S.A* **101**, 4758-4763(2004).
30. Hudson, M.A., Bahnson, R.R. & Catalona, W.J. Clinical use of prostate specific antigen in patients with prostate cancer. *J Urol* **142**, 1011-7(1989).
31. Tilley, W.D. et al. Mutations in the androgen receptor gene are associated with progression of human prostate cancer to androgen independence. *Clin. Cancer Res* **2**, 277-285(1996).
32. Koivisto, P. et al. Androgen receptor gene amplification: a possible molecular mechanism for androgen deprivation therapy failure in prostate cancer. *Cancer Res* **57**, 314-319(1997).
33. Stapleton, A.M. et al. Primary human prostate cancer cells harboring p53 mutations are clonally expanded in metastases. *Clin. Cancer Res* **3**, 1389-1397(1997).
34. Hobisch, A. et al. Distant metastases from prostatic carcinoma express androgen receptor protein. *Cancer Res* **55**, 3068-3072(1995).
35. Einhorn, L.H. Curing metastatic testicular cancer. *Proc. Natl. Acad. Sci. U.S.A* **99**, 4592-4595(2002).

36. Treiber, D.K. et al. Cisplatin-DNA adducts are molecular decoys for the ribosomal RNA transcription factor hUBF (human upstream binding factor). *Proc. Natl. Acad. Sci. U.S.A* **91**, 5672-5676(1994).
37. Kartalou, M. & Essigmann, J.M. Recognition of cisplatin adducts by cellular proteins. *Mutat. Res* **478**, 1-21(2001).
38. Huang, J.C. et al. HMG-domain proteins specifically inhibit the repair of the major DNA adduct of the anticancer drug cisplatin by human excision nuclease. *Proc. Natl. Acad. Sci. U.S.A* **91**, 10394-10398(1994).
39. Zhai, X. et al. Cisplatin-DNA Adducts Inhibit Ribosomal RNA Synthesis by Hijacking the Transcription Factor Human Upstream Binding Factor. *Biochemistry* **37**, 16307-16315(1998).
40. Lyman, G.H. Chemotherapy dose intensity and quality cancer care. *Oncology (Williston Park, N.Y.)* **20**, 16-25(2006).
41. Falco, P. et al. Melphalan and its role in the management of patients with multiple myeloma. *Expert Rev Anticancer Ther* **7**, 945-957(2007).
42. Kay, N.E., Rai, K.R. & O'Brien, S. Chronic lymphocytic leukemia: current and emerging treatment approaches. *Clin Adv Hematol Oncol* **4**, 1-10; quiz 11-12(2006).
43. Fisher, R.I. & Oken, M.M. Clinical practice guidelines: non-Hodgkin's lymphomas. *Cleve Clin J Med* **62 Suppl 1**, SI6-42, quiz SI43-45(1995).
44. Panasci, L. et al. Chlorambucil drug resistance in chronic lymphocytic leukemia: the emerging role of DNA repair. *Clin. Cancer Res* **7**, 454-461(2001).
45. Colvin, O.M. et al. Role of glutathione in cellular resistance to alkylating agents. *Adv. Enzyme Regul* **33**, 19-26(1993).
46. Gamcsik, M.P. et al. Mechanisms of resistance to the toxicity of cyclophosphamide. *Curr. Pharm. Des* **5**, 587-605(1999).
47. Hall, A.G. & Tilby, M.J. Mechanisms of action of, and modes of resistance to, alkylating agents used in the treatment of haematological malignancies. *Blood Rev* **6**, 163-173(1992).
48. Kartalou, M. & Essigmann, J.M. Mechanisms of resistance to cisplatin. *Mutation Research/Fundamental and Molecular Mechanisms of Mutagenesis* **478**, 23-43(2001).
49. Mittelman, A., Catane, R. & Murphy, G.P. New steroidal alkylating agents in advanced stage D carcinoma of the prostate. *Cancer Treat Rep* **61**, 307-310(1977).
50. Kim, E. et al. A bifunctional platinum(II) antitumor agent that forms DNA adducts with affinity for the estrogen receptor. *J Inorg Biochem* **103**, 256-61(2009).
51. Sharma, U. et al. Design, synthesis, and evaluation of estradiol-linked genotoxicants as anti-cancer agents. *Bioorg Med Chem Lett* **14**, 3829-33(2004).
52. Marquis, J.C. et al. Disruption of gene expression and induction of apoptosis in prostate cancer cells by a DNA-damaging agent tethered to an androgen receptor ligand. *Chem. Biol* **12**, 779-787(2005).
53. Mitra, K. et al. A rationally designed genotoxin that selectively destroys estrogen receptor-positive breast cancer cells. *J Am Chem Soc* **124**, 1862-3(2002).
54. Rink, S. et al. Synthesis and biological activity of DNA damaging agents that form decoy binding sites for the estrogen receptor. *Proc Natl Acad Sci U S A.* **93**, 15063–15068(1996).

55. Essigmann, J.M. et al. Design of DNA damaging agents that hijack transcription factors and block DNA repair. *Adv Exp Med Biol* **500**, 301-13(2001).
56. Horoszewicz, J.S. et al. LNCaP model of human prostatic carcinoma. *Cancer Res* **43**, 1809-1818(1983).
57. Alimirah, F. et al. DU-145 and PC-3 human prostate cancer cell lines express androgen receptor: implications for the androgen receptor functions and regulation. *FEBS Lett* **580**, 2294-2300(2006).
58. Seliskar, M. & Rozman, D. Mammalian cytochromes P450--importance of tissue specificity. *Biochim. Biophys. Acta* **1770**, 458-466(2007).
59. Graham, M.J. & Lake, B.G. Induction of drug metabolism: species differences and toxicological relevance. *Toxicology* **254**, 184-191(2008).
60. Johnson, J.A. Predictability of the effects of race or ethnicity on pharmacokinetics of drugs. *Int J Clin Pharmacol Ther* **38**, 53-60(2000).
61. Inoue, S. et al. Prediction of in vivo drug clearance from in vitro data. II: potential inter-ethnic differences. *Xenobiotica* **36**, 499-513(2006).
62. Nelson, D.R. Cytochrome P450 nomenclature, 2004. *Methods Mol. Biol* **320**, 1-10(2006).
63. Nelson, D.R. et al. Comparison of cytochrome P450 (CYP) genes from the mouse and human genomes, including nomenclature recommendations for genes, pseudogenes and alternative-splice variants. *Pharmacogenetics* **14**, 1-18(2004).
64. Finta, C. & Zaphiropoulos, P.G. The human cytochrome P450 3A locus. Gene evolution by capture of downstream exons. *Gene* **260**, 13-23(2000).
65. McArthur, A. et al. Phylogenetic Analysis of the Cytochrome P450 3 (CYP3) Gene Family. *Journal of Molecular Evolution* **57**, 200-211(2003).
66. Hillier, L.W. et al. The DNA sequence of human chromosome 7. *Nature* **424**, 157-164(2003).
67. Essigmann, J.M. et al. Structural identification of the major DNA adduct formed by aflatoxin B1 in vitro. *Proc. Natl. Acad. Sci. U.S.A* **74**, 1870-1874(1977).
68. Croy, R.G. et al. Identification of the principal aflatoxin B1-DNA adduct formed in vivo in rat liver. *Proc. Natl. Acad. Sci. U.S.A* **75**, 1745-1749(1978).
69. Hill, D.L., Laster, W.R. & Struck, R.F. Enzymatic metabolism of cyclophosphamide and nicotine and production of a toxic cyclophosphamide metabolite. *Cancer Res* **32**, 658-665(1972).
70. Low, J.E., Borch, R.F. & Sladek, N.E. Conversion of 4-hydroperoxycyclophosphamide and 4-hydroxycyclophosphamide to phosphoramide mustard and acrolein mediated by bifunctional catalysis. *Cancer Res* **42**, 830-837(1982).
71. Colvin, M. et al. Alkylating properties of phosphoramide mustard. *Cancer Res* **36**, 1121-6(1976).
72. Williams, J.A. et al. Metabolic activation of carcinogens and expression of various cytochromes P450 in human prostate tissue. *Carcinogenesis* **21**, 1683-1689(2000).
73. Lazarou, J., Pomeranz, B.H. & Corey, P.N. Incidence of adverse drug reactions in hospitalized patients: a meta-analysis of prospective studies. *JAMA* **279**, 1200-1205(1998).
74. WHO | World health report 2002 statistical annex. at <http://www.who.int/whr/2002/annex/en/index.html>

75. Bakker-Arkema, R.G. et al. Efficacy and safety of a new HMG-CoA reductase inhibitor, atorvastatin, in patients with hypertriglyceridemia. *JAMA* **275**, 128-133(1996).
76. Jacobson, T.A. Comparative pharmacokinetic interaction profiles of pravastatin, simvastatin, and atorvastatin when coadministered with cytochrome P450 inhibitors. *Am. J. Cardiol* **94**, 1140-1146(2004).
77. Pearce, R.E., Leeder, J.S. & Kearns, G.L. Biotransformation of fluticasone: in vitro characterization. *Drug Metab. Dispos* **34**, 1035-1040(2006).
78. Manchee, G.R. et al. The aliphatic oxidation of salmeterol to alpha-hydroxysalmeterol in human liver microsomes is catalyzed by CYP3A. *Drug Metab. Dispos* **24**, 555-559(1996).
79. Baldwin, S.J., Clarke, S.E. & Chenery, R.J. Characterization of the cytochrome P450 enzymes involved in the in vitro metabolism of rosiglitazone. *Br J Clin Pharmacol* **48**, 424-432(1999).
80. Schinner, S. et al. Inhibition of human insulin gene transcription by peroxisome proliferator-activated receptor gamma and thiazolidinedione oral antidiabetic drugs. *Br. J. Pharmacol* (2009).doi:10.1111/j.1476-5381.2009.00208.x
81. Stanford, J.L. et al. Urinary and sexual function after radical prostatectomy for clinically localized prostate cancer: the Prostate Cancer Outcomes Study. *JAMA* **283**, 354-360(2000).
82. Warrington, J.S. et al. In vitro biotransformation of sildenafil (Viagra): identification of human cytochromes and potential drug interactions. *Drug Metab. Dispos* **28**, 392-397(2000).
83. Webb, D.J. et al. Sildenafil citrate and blood-pressure-lowering drugs: results of drug interaction studies with an organic nitrate and a calcium antagonist. *Am. J. Cardiol* **83**, 21C-28C(1999).
84. Kamimura, H. et al. Identification of cytochrome P450 isozymes involved in metabolism of the alpha1-adrenoceptor blocker tamsulosin in human liver microsomes. *Xenobiotica* **28**, 909-922(1998).
85. Ku, E.C. et al. Effect of diclofenac sodium on the arachidonic acid cascade. *Am. J. Med* **80**, 18-23(1986).
86. Walsky, R.L. & Obach, R.S. Validated assays for human cytochrome P450 activities. *Drug Metab. Dispos* **32**, 647-660(2004).
87. Zhai, X. et al. Cisplatin-DNA adducts inhibit ribosomal RNA synthesis by hijacking the transcription factor human upstream binding factor. *Biochemistry* **37**, 16307-16315(1998).
88. Williams, P.A. et al. Crystal structures of human cytochrome P450 3A4 bound to metyrapone and progesterone. *Science* **305**, 683-686(2004).
89. Casarett, L.J., Klaassen, C.D. & Doull, J. *Casarett and Doull's Toxicology: The Basic Science of Poisons*. 174(McGraw Hill, New York: 2001).
90. Smela, M.E. et al. The aflatoxin B(1) formamidopyrimidine adduct plays a major role in causing the types of mutations observed in human hepatocellular carcinoma. *Proc. Natl. Acad. Sci. U.S.A* **99**, 6655-6660(2002).

Chapter 2: Kinetics and Product Spectrum of the Hydrolysis of 11β-dichloro

Introduction

Nitrogen, and in particular, aniline mustards are an integral part of the chemotherapeutic regimens of many human cancers. These agents are frequently used in combination with other compounds[1,2]. The high non-specific toxicity of these alkylating agents, affecting both tumor and healthy cells, makes it very important to monitor and control the exposure patterns of patients. As with any drug, calibration of the treatment schedule depends on precise characterization of the stability of the compound both *in vitro* and *in vivo*. The nitrogen mustards undergo an intramolecular ring-closing to form an electrophilic aziridinium ion known to react covalently with nucleophilic loci of DNA, with the N7 position of guanine being a primary site of adduction (Figure 2-1)[3]. Subsequently, the bifunctional mustard can generate a second electrophile through an analogous aziridinium formation, yielding a reactive species held in close proximity to DNA, thus potentiating a second hit on DNA via an intra-molecular reaction. This second aziridinium ring can generate an intra- or interstrand crosslink with DNA, the latter leading to potentially lethal double-strand breaks upon the processive failure of replication machinery[4-7].

The target sites on DNA are not the only nucleophiles that can attack the electrophilic sites generated by a nitrogen mustard. In any aqueous system, the aziridinium ion can be hydrolyzed by water, yielding a comparatively innocuous hydroxyethyl byproduct lacking the leaving group necessary to re-form the aziridinium electrophile (Figure 2-2). The kinetics of this process, independent of any enzymatic conversion, represent the baseline rate of inactivation of these compounds. Singly-hydrolyzed mustards can still form mono-adducts with DNA, but these lesions, as well as intrastrand crosslinks, are removed through nucleotide excision repair[8]. Both chloroethyl arms must be intact in order to form the more deleterious interstrand crosslink.

A novel bifunctional aniline mustard tethered to a steroid moiety has been synthesized and shown to kill selectively LNCaP prostate cancer cells *in vivo* and *in vitro*. This compound, 11β-dichloro[†] (11β), has been shown to generate DNA adducts and disrupt gene expression normally promoted by the androgen receptor (AR)[9,10],

[†] 2-(6-((8S,11S,13S,14S,17S)-17-hydroxy-13-methyl-3-oxo-2,3,6,7,8,11,12,13,14,15,16,17 dodecahydro-1H-cyclopenta[a]phenanthren-11-yl)hexylamino)ethyl 3-(4-(bis(2-chloroethyl)amino)phenyl)propylcarbamate

leading to cell cycle arrest and apoptosis. The working hypothesis governing the mechanism of toxicity of 11β involves a combination of two distinct pathways, each dependent on and the high levels of androgen receptor expression in prostate cancer. DNA adducts formed by 11β may be shielded from nucleotide excision repair by interaction with the androgen receptor, causing persistent damage. The affinity of 11β and 11β–DNA adducts to the androgen receptor may also hijack the ability of AR to promote gene transcription necessary for cell division. These two pathways may work in concert to elicit a more potent toxic response than a co-administration of DNA alkylating agents and AR inhibitors as separate molecular entities. Like all aniline mustards, 11β is susceptible to hydrolytic decomposition. In addition, any xenobiotic agent is subject to metabolic transformation. A combination of hydrolytic and metabolic pathways may transform 11β into any number of daughter species, each potentially demonstrating DNA adduction and AR binding capabilities distinct from the parent compound.

Before studying the enzymatic metabolism of 11β, it was necessary to determine the baseline inactivation level of the compound through hydrolysis, such that the spectrum of daughter species produced after introduction of 11β into a biological system could be parsed into those arising through simple hydrolysis and those resulting from enzymatic conversion. Assuming enzymatic conversion was only relevant in a biological system, the difference in compositions between the spectra of 11β and daughter compounds arising from a system including metabolic machinery and one without defined the contribution of that metabolic machinery to the total conversion of 11β to its products.

Clinically-used alkylating agents include several drugs whose reactive electrophiles result from the formation of aziridinium rings, for example, the nitrogen mustards mechlorethamine, cyclophosphamide, and ifosfamide; and the aniline mustards chlorambucil and melphalan (Figure 2-3). While cyclophosphamide and ifosfamide are pro-drugs requiring enzymatic activation, all of these compounds generate electrophiles through nucleophilic attack by the nitrogen lone pair on the terminal carbon of the chloroethyl arm. Displacement of the leaving group is slowed by increasing local concentration of free chloride, which is naturally present at ~100mM in plasma, thus rendering the rate of formation of the aziridinium and, consequently, the propensity for

covalent attachment to cellular nucleophiles, strongly compartment-specific[11,12]. Ideally, the aziridinium species would not form until the agent has diffused or been transported to the vicinity of its target nucleophile—i.e., DNA in the nucleus. It is reasonable to expect that a given dose of compound would yield a level of DNA damage proportional to the extent to which intact chloroethyl arms or aziridinium ions reach the nucleus.

In work described in this chapter, the rates of hydrolysis of clinically-used compounds were compared to 11β and related species to assess the timescale within which presence in an aqueous system would lead to the deactivation of the mustard arms of 11β. The aniline mustards chlorambucil and melphalan were expected to behave most like 11β, with alkyl chains *para* to the mustard substituent of a phenyl ring. The published half-lives for the decomposition of the dichloro forms of these alkylating agents are summarized in Table 2-1.

A combination of chromatographic and mass spectrometric techniques was used to measure qualitatively the identities of the daughter species and quantitatively the disappearance of 11β-dichloro over time. The stability of 11β was assessed in a variety of relevant aqueous systems: distilled and deionized water (ddH_2O), phosphate-buffered saline (PBS), tissue culture media, and the *in vitro* metabolism reaction buffer system without microsomes. The information gleaned from these experiments provided a backdrop for and facilitated careful qualitative and quantitative analyses of the enzymatic metabolism of 11β as described in Chapter 3. These data also help develop a more chemically-rigorous understanding of the results of *in vitro* toxicity experiments whose timescales were significantly longer than the half-life of 11β in tissue culture media.

Materials & Methods

Qualitative hydrolysis of 11β in water and phosphate-buffered saline: In order to determine the identities of 11β hydrolysis products and optimize the conditions for their detection by mass spectrometry, 1μL of a 20 mM stock of 11β in DMSO was dissolved in 1mL of either ddH_2O (RICCA Chemical, Fort Worth, TX) or Dulbecco's PBS (Invitrogen, Carlsbad, CA) pre-warmed to 37°C. Samples were vortexed to mix and placed in a 37°C water bath to initiate the reaction. At times 0, 0.5, 1, 1.5, 2, 4, 6, 12, 24, and 48 hours after initiation, a 50 μL aliquot was taken and stored at -80°C before separation by liquid chromatography (LC) and analysis by electrospray ionization–time of flight mass spectrometry (ESI-TOF).

Optimization of chromatography and spectrometry conditions: Solutions comprising 1 μM each of 11β-dichloro, 11β-monochloro–monomethoxy, and 11β-dimethoxy (Figure 2-4) were prepared in solvents with various ddH_2O:acetonitrile ratios. These three-compound samples were used to measure the resolution with which the chromatography method developed by Hillier et al.[9] would separate 11β from its hydrolysis products. Samples were injected with a 1200 Series LC system into a Sorbax XDB-C18 (2.1x50mm, 5μm pore size) column upstream of a 1200 Series diode array detector in tandem with a 1200 Series ESI-TOF mass spectrometer (all Agilent Technologies, Santa Clara, CA) in the Mass Spectrometry lab of the MIT Department of Biological Engineering. Liquid chromatography was performed at a total flow rate of 0.2 mL/min, with aqueous mobile phase "A" containing 0.25% acetic acid in distilled, deionized water prepared in-house and organic mobile phase "B" containing 0.25% acetic acid in methanol. The method program comprised 2 minutes at 50% B followed by a 20-minute ramp to 100% B, a 5-minute hold at 100% B, a 5-minute ramp back down to 50% B, and a 3-minute hold at 50% B to re-equilibrate the column. Mass spectrometry was performed in positive ion mode with source conditions ranging from 300–325°C heated capillary, 7–15 L/min drying gas (N_2, AirGas, Salem, MA), 15–30 psig nebulizer pressure, and 3000–4500 V needle voltage. Peaks were identified with the Agilent Analyst QS software package.

LC–ESI-TOF detection and m/z identification of 11β hydrolysis products: Aliquots of samples were diluted to 25% acetonitrile for a 1 μM sample concentration in order to provide approximately ten picomoles of total material (parent + daughters) per injection. Liquid chromatography and diode array settings were as described in the previous section, with mass spectrometry source conditions optimized to 325°C heated capillary, 12 L/min drying gas, 25 psig nebulizer pressure, and 4000 V needle voltage. In the samples containing PBS, sample flow was diverted to waste downstream of the diode array for the first two minutes of each method, preventing salts from entering the mass spectrometer. Peaks were identified with the Agilent Analyst QS software package, with the mass-to-charge ratio (m/z) of the monoisotopic peak associated with a given compound used for ion extraction.

Quantitative hydrolysis of 11β in water: Before attempting to characterize the decomposition of 11β in the complex aqueous systems of interest, preliminary experiments were performed in ddH_2O in order to optimize operating conditions for mass spectrometry. Quantitation was achieved through tracking the disappearance of the fragment associated with the steroid half of the parent compound with a Series 6410 triple quadrupole (QQQ) mass spectrometer (Agilent) in the Tannenbaum Laboratory of the MIT Department of Biological Engineering.

A 5 μL aliquot of a 0.2 mM solution of 11β in acetonitrile was diluted into 995 μL of ddH_2O for an initial concentration of 1 μM. The solution was vortexed and 200 μL were immediately withdrawn and transferred to storage at -20°C. The remaining reaction volume was placed in a 37°C water bath to start the incubation. At 2, 4, 8, and 24 hours after introduction to the water bath, a 200 μL sample was withdrawn, transferred to a fresh Eppendorf tube, and stored at -20°C for later processing. Before analysis, 2 μL of a 0.5 mM solution of 11β-dimethoxy in acetonitrile were added to the defrosted 200 μL sample as an internal standard.

Quantitative hydrolysis of 11β in tissue culture media: A 5 μL aliquot of a 2 mM solution of 11β in acetonitrile was dissolved into LNCaP media, comprising RPMI 1640

supplemented with 10% fetal bovine serum (Hyclone, Salt Lake City, UT), 1 mM sodium pyruvate (Invitrogen), 2.5 g/L glucose, and 10 mM HEPES (Invitrogen) to a final volume of 1 mL for an initial 11β concentration of 10 μM. This solution was vortexed and a 200 μL aliquot was immediately transferred to a fresh tube, where it was quickly mixed with 200 μL ice cold acetonitrile containing 0.1% formic acid and 0.5 μM 11β dimethoxy as an internal standard, vortexed, and spun for 30 minutes at 18,000 g in a microcentrifuge kept at 4°C. A 300 μL aliquot of supernatant was added to 700 μL ddH_2O to bring the total organic solvent content down to 15%. The 1 mL was then loaded onto a C18 SepPak (Waters, Milford, MA) equilibrated with a 2 mL wash of 10% methanol after initial wetting with 2 mL acetonitrile. The sample was washed with 2 mL of 10% methanol to remove remaining salts and hydrophilic macromolecules and then eluted with 2 mL of 100% methanol. Eluates were stored at -20°C until immediately before analysis.

Quantitative hydrolysis of 11β in microsomal metabolism system: Five microliters of a 0.5 mM solution of 11β in acetonitrile, 50 μL of NADPH Regeneration System A and 10 μL of NADPH Regeneration System B (BD Biosciences, San Jose, CA) were added to 935 μL of 0.1 M potassium phosphate buffer at pH 7.4, representing the *in vitro* metabolism machinery without microsomes. Phosphate buffer and NADPH regeneration system solutions were pre-warmed to 37°C. Final system component concentrations were 2.5 μM 11β, 1.25 mM $NADP^+$, 3.3 mM glucose-6-phosphate, 0.4 U/mL glucose-6-phosphate dehydrogenase, 50 μM sodium citrate, and 3.3 mM magnesium chloride. The initial solution was vortexed and a 200 μL aliquot was immediately transferred to a fresh tube, where it was quickly mixed with 200 μL ice cold acetonitrile containing 0.1% formic acid and 0.5 μM 11β-dimethoxy as an internal standard, vortexed, and spun for 30 minutes at 18,000 g in a microcentrifuge kept at 4°C. The remaining reaction volume was placed in a 37°C water bath. At 2, 4, 8, and 24 hours after initiation, the system was quickly removed from the water bath, vortexed to ensure uniformity, and a 200 μL aliquot was removed, transferred to a new tube, and quenched and centrifuged in the same manner as the initial sample. A 300 μL aliquot of the supernatant from each sample was mixed with 700 μL cold ddH_2O to bring the total organic content down to 15%. The

1 mL was then loaded onto a C18 SepPak previously equilibrated to 10% methanol after wetting with 100% acetonitrile. The sample was washed with 2 mL of 10% methanol to remove the remaining salts and hydrophilic reaction components and then eluted with 2 mL of 100% methanol. Eluates were stored at -20°C until immediately before analysis.

QQQ detection of 11β and its hydrolysis products *in vitro*:

Hydrolysis in ddH_2O. Analyses of hydrolysis experiments were performed on the Agilent Series 6410 QQQ operating in positive ion mode with source conditions 325°C heated capillary, 12 L/min drying gas, 25 psig nebulizer pressure, and 4000 V needle voltage. Samples were delivered as bolus injections with a carrier mobile phase of 0.25% acetic acid in methanol at 4 μL/min. Multiple reaction monitoring (MRM) mode was used to track abundance of each species after optimization of fragmentor voltage and collision energy for 11β, its hydrolyzed daughter compounds, and the internal standard (Table 2-2). Abundance traces were smoothed and integrated in Agilent Qualitative Analysis, with areas under the curve for each of the test species divided by that of the internal standard from the same injection to normalize for the variable efficiency of the workup. Normalized AUCs for parent compound were fit as one-phase exponential decay processes in Prism 5 (GraphPad Software, La Jolla, CA).

Hydrolysis in tissue culture media and microsomal buffer system. Analyses of hydrolysis experiments in these systems were performed as above but using a carrier mobile phase of 80% acetonitrile and 0.1% formic acid flowing at 4 μL/min. Multiple reaction monitoring mode was again used to track abundance of each species after re-optimizing fragmentor voltage and collision energy for the new mobile phase conditions. Abundance traces were smoothed and integrated in Agilent Qualitative Analysis, with areas under the curve for each of the test species divided by that of the internal standard from the same injection to normalize for the variable efficiency of the workup. Normalized AUCs for parent compound were fit as one-phase exponential decay processes in Prism 5.

Results

Optimization of chromatography and spectrometry conditions: Chromatography performance was very sensitive to composition of the sample, with 25% acetonitrile eventually giving the most reproducible separation. Dimethoxy (m/z 708), monochloro–monomethoxy (712), and dichloro (716) came off the column at 11.4, 13.6, and 14.5 minutes, respectively (Figure 2-5). Identities were corroborated by the characteristic chlorine isotope patterns. The 11β family of compounds, rich with heteroatoms and already protonated at the linker secondary amine, gave robust signals with electrospray conditions at 325°C, 12 L/min drying gas, 25 psig, and 4000 V capillary voltage.

LC–ESI-TOF identification of hydrolysis products: Stability of 11β was tracked qualitatively by ESI-TOF as disappearance of the ion with m/z 716. Chromatography conditions were more than sufficient to separate dichloro from its primary hydrolysis products 11β N,N-2-chloroethyl,2-hydroxyethyl (monohydroxyl, m/z 698), and 11β N,N-*bis*-2-hydroxyethyl (dihydroxyl). Singly-hydrolyzed compound eluted at 11.5 minutes (inconveniently on top of the dimethoxy internal standard). Doubly-hydrolyzed compound eluted far earlier at 4.9 minutes (Figure 2-6). The strong effect of the presence of a chlorine atom on the elution time with these chromatography conditions was useful for establishing the identities of the compounds in each peak. Elution times and m/z values for all observed species are summarized in Table 2-3.

Interestingly, in searching for the dihydroxyl compound, ion extraction revealed both the expected dihydroxyl species and a peak with m/z 680 and an isotope pattern indicating one chlorine atom (Figure 2-7). This species co-eluted with a peak showing monoisotopic m/z 340, 0.5 mass unit isotope spacing and significantly more abundance than the singly protonated compound, and as such was classified as the aziridinium intermediate with either a +2 charge state (340, aziridinium ion and protonated linker amine) or +1 (680, aziridinium ion, neutral linker). The aziridinium ion was not expected to be more than a transient intermediate in the hydrolysis cascade; its separation and detection by LC–ESI-TOF was surprising.

A peak with m/z 778 and one chlorine eluted two minutes earlier than parent (12.7 minutes) in the PBS preparations but not the ddH_2O ones, indicating a displacement of chlorine by phosphate to yield a monochloro–monophosphate product (Figure 2-8). Surprisingly, the corresponding monohydroxyl–monophosphate species (m/z 760) eluted earlier than the dihydroxyl, opposite the relationship between the monohydroxyl– and monochloro–monophosphate species. A doubly-phosphorolyzed compound with putative m/z 840 was not observed.

Also intriguing were two species with m/z 662 and 644, neither containing a chlorine atom, eluting at 8.6 and 7.7 minutes, respectively. The compound with m/z 662 suggested the formation of a second aziridinium ion after earlier hydrolysis of the other chloroethyl arm. The dominant m/z for such a species—with positive charges at both the linker amine and the aziridinium ion—should have been at 331, but none was detected. Instead, it is proposed that the monovalent species with mass 662 arises from an intramolecular attack, with the hydroxyethyl oxygen displacing the remaining chlorine to generate a morpholinyl moiety. This molecule could then undergo further decomposition through dehydration and rearrangement to a dihydropyrrole (m/z 644). While the unsaturated carbon–carbon bond in the latter would conjugate with the nitrogen lone pair and phenyl π-orbitals of the aniline group, the abundance of this species was not sufficiently above background signal to observe a change in the absorbance spectrum. Structures for these additional hydrolysis products are shown in Figure 2-9. Dehydration in the ionization source was ruled out by the distinct elution times of the two species.

QQQ quantitation of 11β hydrolysis: Stability of 11β was measured through disappearance of the parent compound. The formic acid in the mobile phases used with the media and microsomal system experiments made the doubly-charged compound (m/z 358.9) more abundant than the singly-charged version (716.4) that had dominated in both the ESI-TOF experiments and the quantitative hydrolysis experiment in ddH_2O. In all systems, collision conditions were optimized to break the molecule at the carbamate, likely yielding a fragment (416.3) that would subsequently dehydrate to the target species with (398.3), representing the unmodified steroid half of the molecule protonated at the linker amine (Figure 2-10). Normalization to the dimethoxy internal standard (354.9 ->

398.3 or 708.4 -> 398.3) controlled for the variance in the separation workup, with the assumption that dimethoxy and dichloro in a given sample would adsorb to and desorb from the SepPak columns with equal efficiency.

Quantitative hydrolysis in ddH_2O and media gave half-lives for dichloro of 0.40 and 3.03 hours, respectively (Figure 2-11). Decomposition of the compound in the microsomal metabolism system proceeded with nearly identical kinetics as in ddH_2O with a half-life of 0.42 hours.

Discussion

Separation and mass spectrometry of 11β control species: The incremental decomposition steps of the mustard arms of 11β expected through hydrolysis represent only very slight changes to the overall molecular structure. As such, it was necessary to confirm whether chromatography conditions originally derived by Hillier et al.[9] would be sufficient to separate the hydrolysis products with acceptable resolution. The compounds 11β-monochloro and 11β-dimethoxy had been synthesized previously as controls to assess the roles DNA adduction and crosslinking play in the toxicity of the dichloro compound[10]. The subtle changes to the substitutions on the aniline nitrogen of these analogs were seen as a suitable model for testing separation conditions.

While the performance of the chromatography was encouraging, there were obvious differences in the propensities for each of the compounds to be detected by the ESI-TOF: the peaks shown in Figure 2-4 arose from equal concentrations of the three components in the original mixture, which was prepared from pure stocks. As a result, the analyses by ESI-TOF were considered qualitative only, valuable for identifying compounds and optimizing conditions for their analysis, but not useful for quantifying relative abundances of species in a mixture. Furthermore, since many of the hydrolysis and metabolism experiments required multiple separations to isolate compounds from complex media, quantitative mass spectrometric data could only be obtained through inclusion of 11β-dimethoxy as an internal standard.

Product spectrum: The half-life of 11β due to hydrolysis was expected to be strongly dependent on solvent conditions, with the decomposition rate of the mustard chloroethyl arms fastest in water and decreasing in systems containing biological macromolecules onto which 11β can adsorb. In order to quantify the stability of 11β in all of the preparations relevant to the scope of this study, it was necessary to measure the rate of hydrolysis of 11β in tissue culture media and the phosphate buffer containing NADPH regeneration machinery used in microsomal metabolism systems. While rates were expected to differ, the product spectrum was expected to be essentially the same in all systems, comprising dichloro, monohydroxyl, and dihydroxyl.

The abundance of the dichloro species fell over time with first-order kinetics, yielding a transient presence of monohydroxyl that was observed to decompose further into several products. In qualitative experiments with water and phosphate-buffered saline, 11β decomposed rapidly, with an apparent half-life of approximately three hours in each. However, these experiments were performed with quantities of 11β well beyond those that are soluble in purely aqueous solutions. Instead, it is believed that the vast majority of the 11β introduced into those systems was in suspension, with some material diffusing into the bulk solution to replace hydrolyzed compound. The precision of the ESI-TOF enabled the observation of additional daughter species, including phosphorolyzed compound, intramolecular decomposition of the monochloro-monohydroxyl to a morpholinyl group, and dehydration of the morpholinyl to a dihydropyrrole. Rearrangements of bifunctional nitrogen mustards have been previously reported as mechanisms for the conversion of the active mustard metabolites of cyclophosphamide and ifosfamide to oxaza- and diazaphospholidines[13].

Kinetics of 11β hydrolysis: The presence of fetal bovine serum in tissue culture media ostensibly allowed adsorption of the hydrophobic 11β onto albumin, protecting it from the bulk solution and consequently increasing its stability. The ramifications of these data on the design of new *in vitro* and *in vivo* experiments and the interpretation of existing data are crucial. At the end of a two-hour treatment of 11β in tissue culture media, only 63% of the compound will have avoided at least one hydrolytic decomposition. The AUC of such treatments must therefore be scaled to account for the stability of the compound, especially when comparing treatment protocols that involve exposures of different lengths. Analogous studies of the rate of hydrolysis of melphalan in cell culture media have shown the compound to be significantly less resistant to hydrolysis than 11β, with a reported half-life of 1.1 hours[14]. It is reasonable to conclude that the hydrophobic steroid moiety of 11β increases its adsorption to albumin in the media, extending the half-life of the mustard arms to 3.03 hours. In fact, melphalan and chlorambucil derivatives have been synthesized through conjugation to various functional groups to improve stability in hopes of increasing toxicity[15,16].

The DNA-damaging ability of 11β is central to the mechanism of toxicity implicated in its design. The ability of the compound to alkylate DNA and subsequently form crosslinks is strongly dependent on the kinetics of hydrolysis of the mustard moiety. The number of opportunities for the aziridinium ion to form and to be hydrolyzed by a nucleophile other than the N7 of guanine is immense—collateral covalent adduction of proteins and RNA is extremely likely. Furthermore, detoxification of the aziridinium ion by glutathione has been shown to be a primary means of deactivation of several alkylating agents, including chlorambucil and melphalan[17-22]. The hydrophobic steroid moiety distinguishes 11β from chlorambucil and melphalan, however, as its bulk transport characteristics should change the residence times in the series of compartments 11β must pass through before reaching nuclear DNA.

Fundamentally, introduction of 11β into any aqueous medium at physiological temperature and pH will involve a rate of decomposition of the drug that will change the system behavior from a single reaction of interest to a time-dependent array of analogous mechanisms comprising 11β and all of its daughter species. In the case of DNA adduction, if only crosslinks are considered important for toxicity, the rate of hydrolysis of the first chloroethyl arm is of primary importance: only the parent compound is active, and the tracking of its disappearance over time is sufficient to derive the AUC. However, if monoadducts can cause toxicity, or if the interaction between the drug and target steroid receptors exerts a biological effect independent of the status of the mustard, then the dynamics of all 11β species are relevant. Based on the dramatic differences in elution times of the 11β compounds caused by very slight changes to the molecule, it is reasonable to expect that the distribution of 11β molecules in a complex biological system would be strongly dependent on, at the very least, the number of chlorine atoms still present. If there are compartment-specific mechanisms of dysregulation of cellular function, the partitioning of 11β and all of its daughter compounds will necessarily influence its effectiveness as a drug.

QQQ as a quantitative analytical tool: The mass spectrometry conditions derived in the quantitation of hydrolysis were essential in enabling the design of experiments to determine the locations of metabolic modifications to 11β (Chapter 3) and the effects of

plasma protein and chloride ion concentration on uptake and stability (Chapter 4). However, the individual ionization constants for 11β and its daughter species are different, so quantitation is limited to tracking the disappearance of parent rather than generating data from which to rate constants for conversions to specific products could be derived.

Future directions: The kinetics of deactivation of 11β through hydrolysis will have a strong effect on the eventual design of a delivery system and choice of administration route. If alkylation damage is the most important of the many potential cellular processes 11β could disrupt, protection of the chlorine leaving groups is of primary concern in maximizing the compound's efficacy. Alternatively, should ligand–receptor interactions elicit the most desirable responses, the hydrolysis of the mustard arms may increase bioavailability through reducing hydrophobicity. Most likely, multiple biochemical mechanisms are in play, and parsing the effects of hydrolysis on each would be necessary to evaluate the opportunity to tailor both drug redesign and clinical dosage regimens to maximize selective toxicity.

Quantitation of the hydrolysis of 11β *in situ* through nuclear magnetic resonance (NMR) would obviate the need for protocol steps that may confound results[17]. If aqueous systems can inactivate half of the compound in less than thirty minutes, there is an inevitable loss of precision when measuring the dose-response relationships between 11β and its putative macromolecular targets in assays of longer duration. Furthermore, analysis by NMR could confirm the identities of the proposed morpholinyl and dihydropyrrole derivatives.

Figure 2-1: Formation of an adduct at the N7 position of guanine

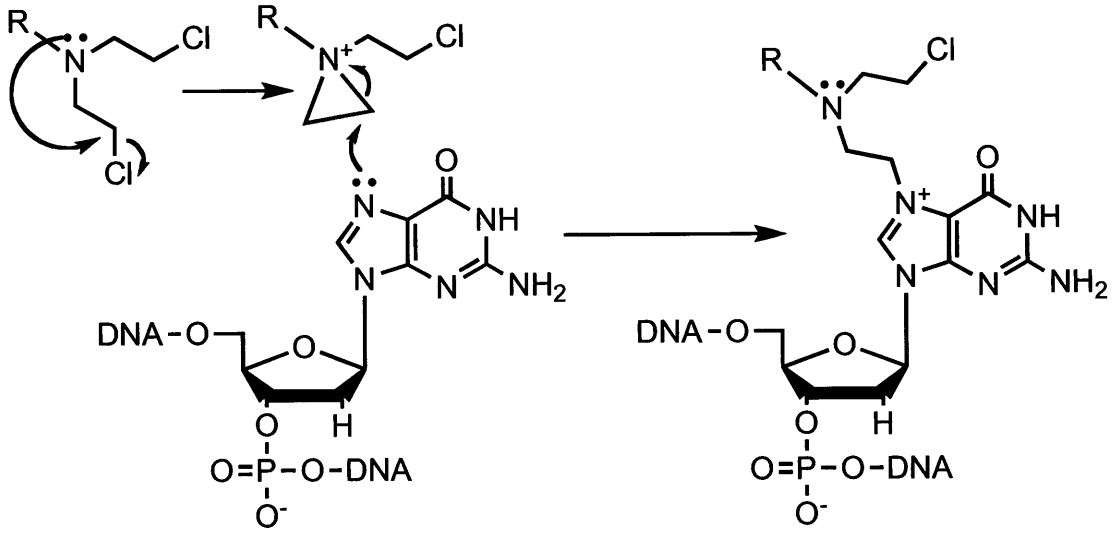

The lone pair on the N7 position of either purine can attack the electrophilic aziridinium formed by the nitrogen mustard's intramolecular ring closing. The resulting species can form intra- or interstrand crosslinks with a second nucleophilic site.

Figure 2-2: Mechanism of hydrolysis of 11β

The lone pair on the aniline nitrogen of 11β dichloro attacks the beta carbon to displace the chloride leaving group, leaving a highly-electrophilic aziridinium ion. A hydroxyl anion attacks the positively-charged, constrained ring to yield a hydroxyethyl group unable to regenerate the electrophile necessary for DNA adduction. The process can repeat on the remaining chloroethyl arm to yield a dihydroxyl product.

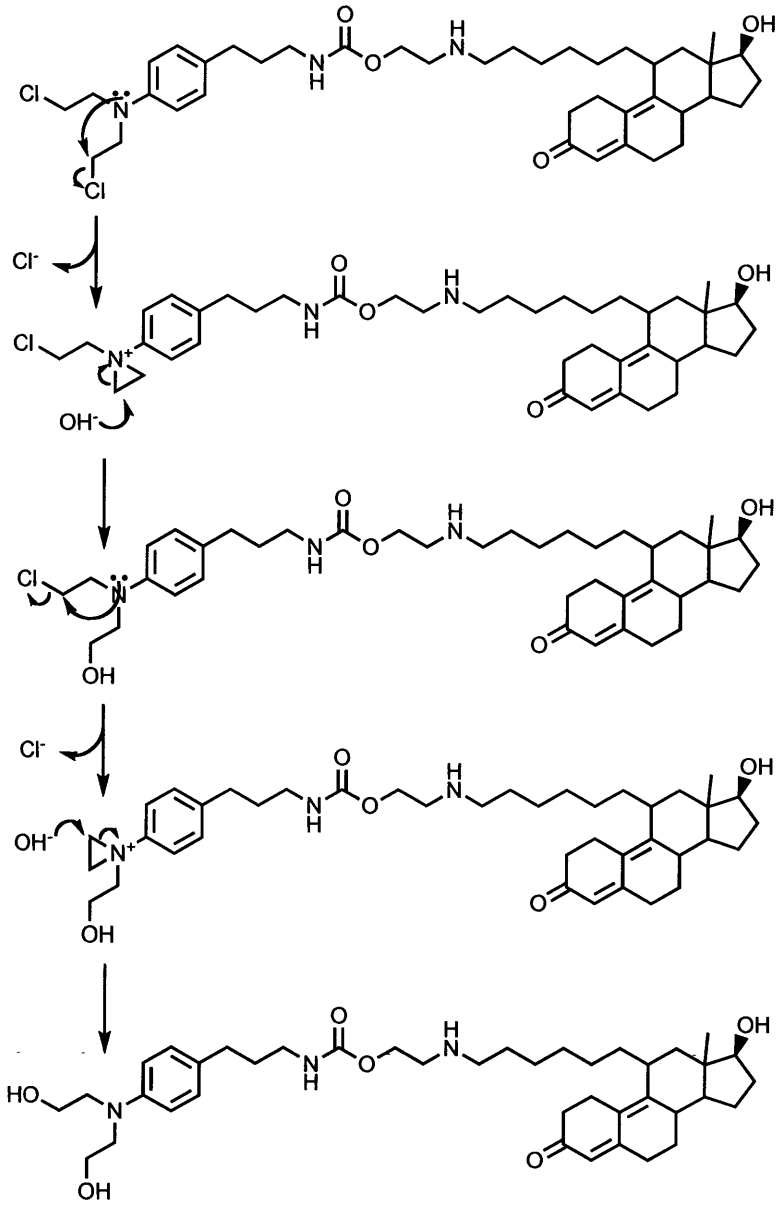

Figure 2-3: Clinically-used nitrogen and aniline mustards

Mechlorethamine

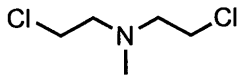

Ifosfamide

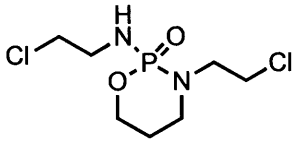

Cyclophosphamide

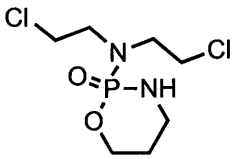

Chlorambucil

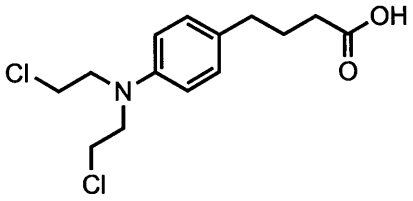

Melphalan

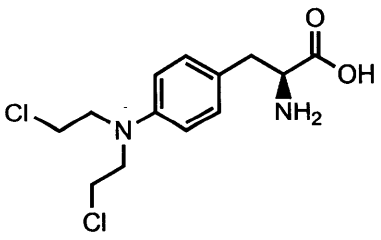

Figure 2-4: 11β and its related species

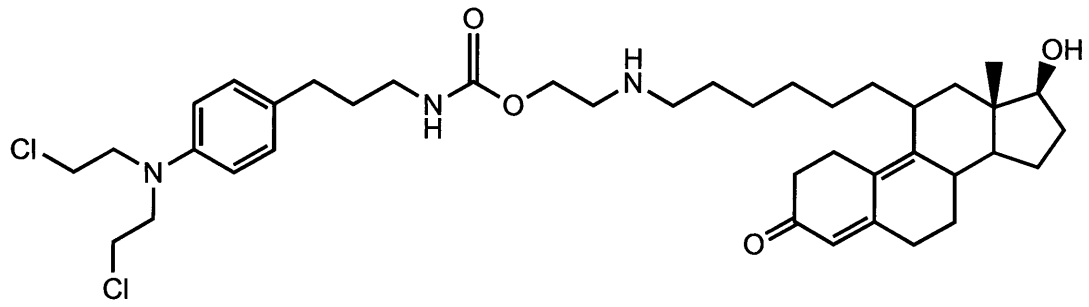

Dichloro: Molecular Weight 716.8

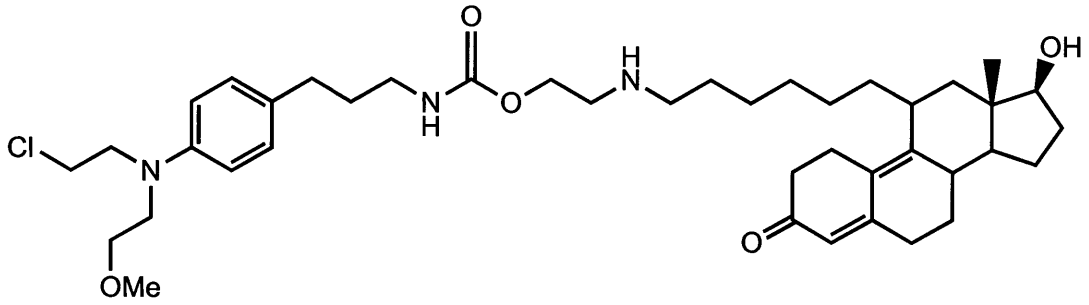

Monochloro–monomethoxy: Molecular Weight 712.4

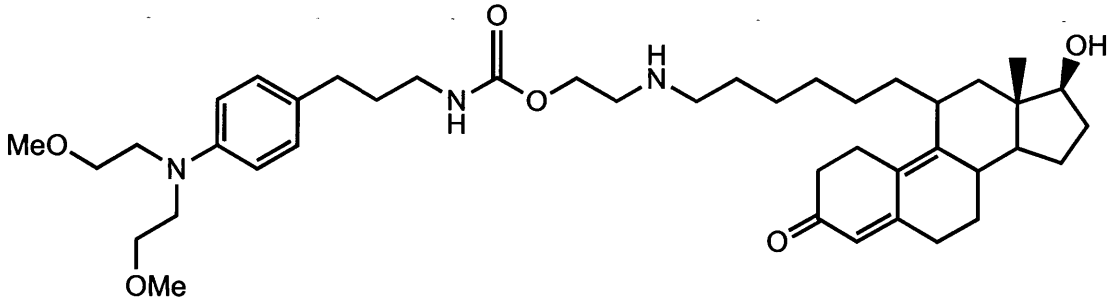

Dimethoxy: Molecular Weight 708.0

Figure 2-5: Separation and identification of three 11β compounds by LC-ESI-TOF

a) Dimethoxy

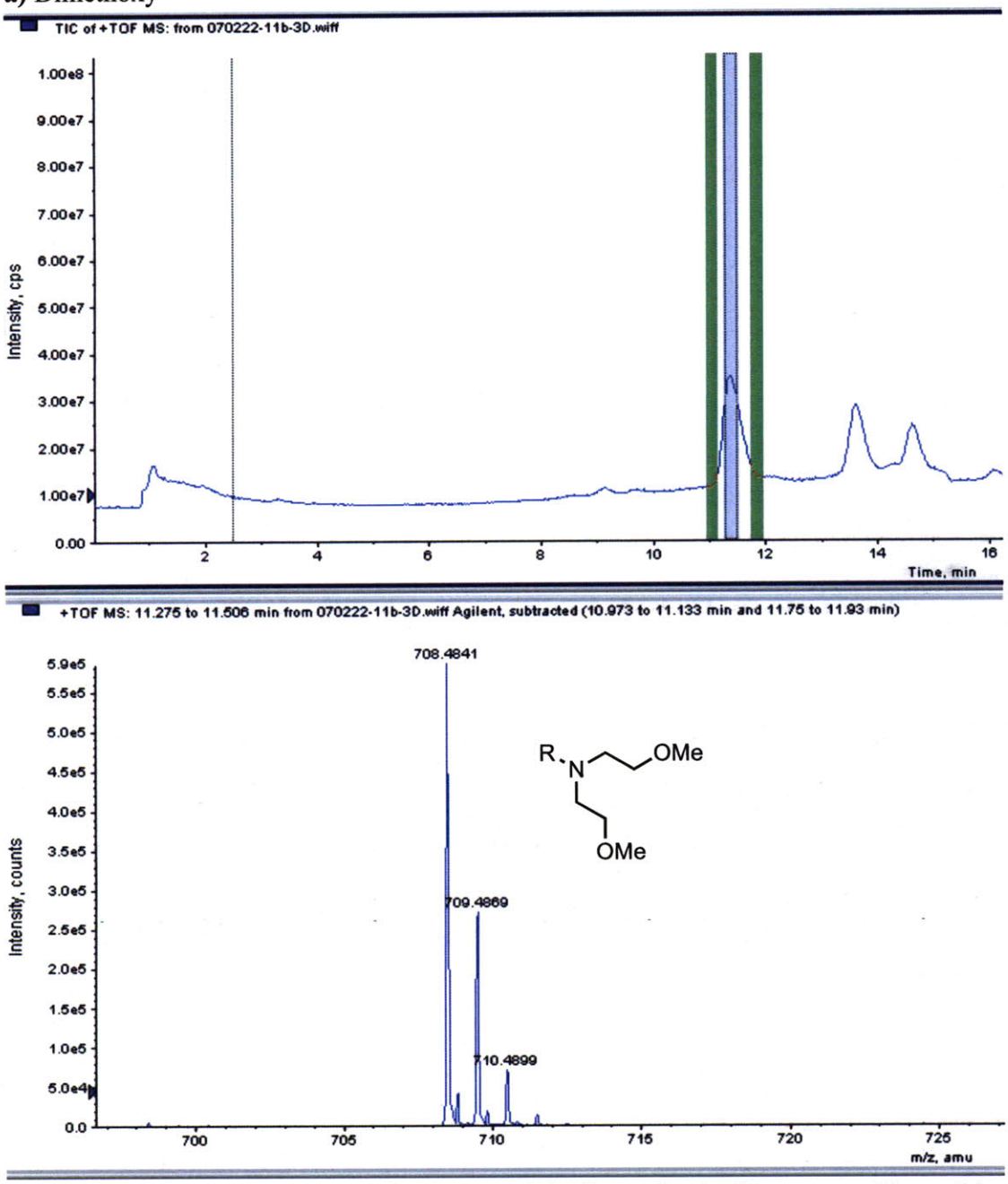

Dimethoxy 11β (m/z 708, no chlorines) was originally synthesized as a control incapable of forming covalent adducts with DNA but likely to have similar biodistribution and receptor affinity character to the dichloro compound[10]. Dimethoxy was stable to hydrolysis and easily separated from its dichloro and monochloro analogs, allowing its use as an internal standard for quantitative experiments done on the triple quadrupole mass spectrometer.

Figure 2-5: Separation and identification of three 11β compounds by LC-ESI-TOF

b) Monochloro–monomethoxy

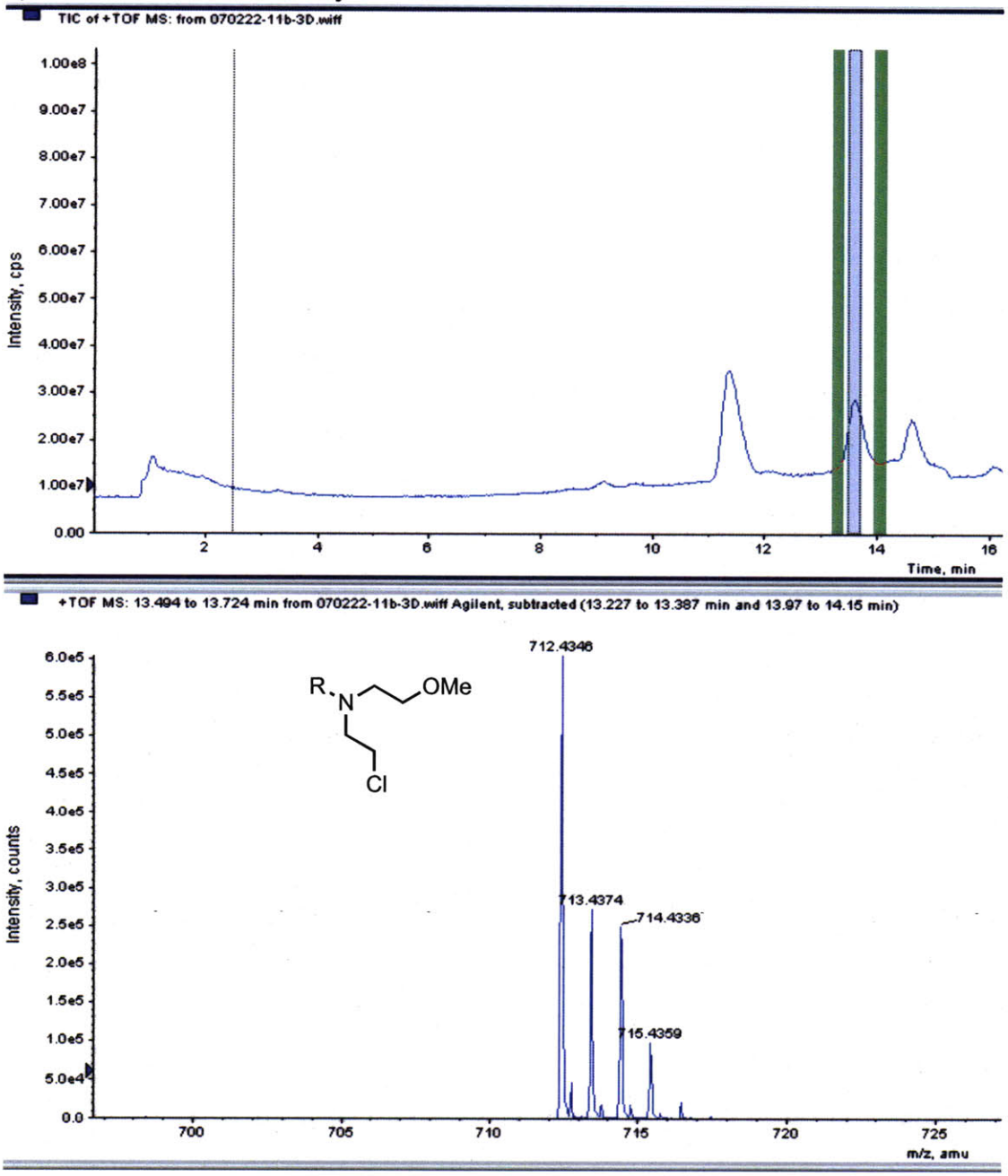

Monochloro–monomethoxy 11β had been synthesized previously as a control molecule incapable of forming DNA crosslinks. Chromatography conditions were sufficient to separate it (elution time 13.6 minutes) from the dichloro species (14.5). Isotope pattern suggesting C_{40} and Cl_1 confirmed its identity, enabling rapid classification of hydrolysis products with the same signature.

Figure 2-5: Separation and identification of three 11β compounds by LC-ESI-TOF

c) Dichloro

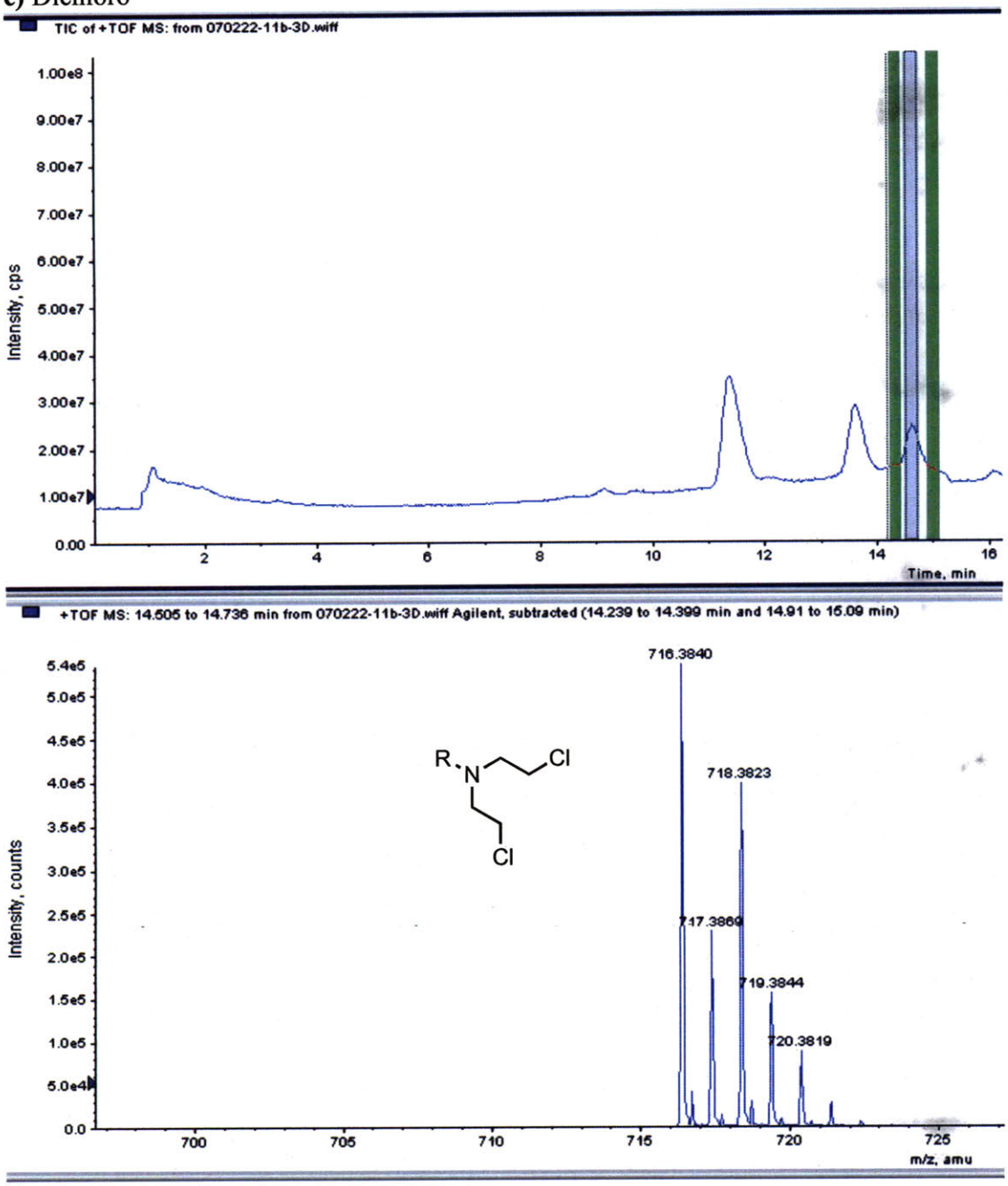

The two-chlorine signature was essential in confirming the identity of 11β as well as that of its metabolic products described in Chapter 3.

Figure 2-6: Separation and identification of primary 11β hydrolysis products

a) Total ion chromatogram (m/z 100–1000)

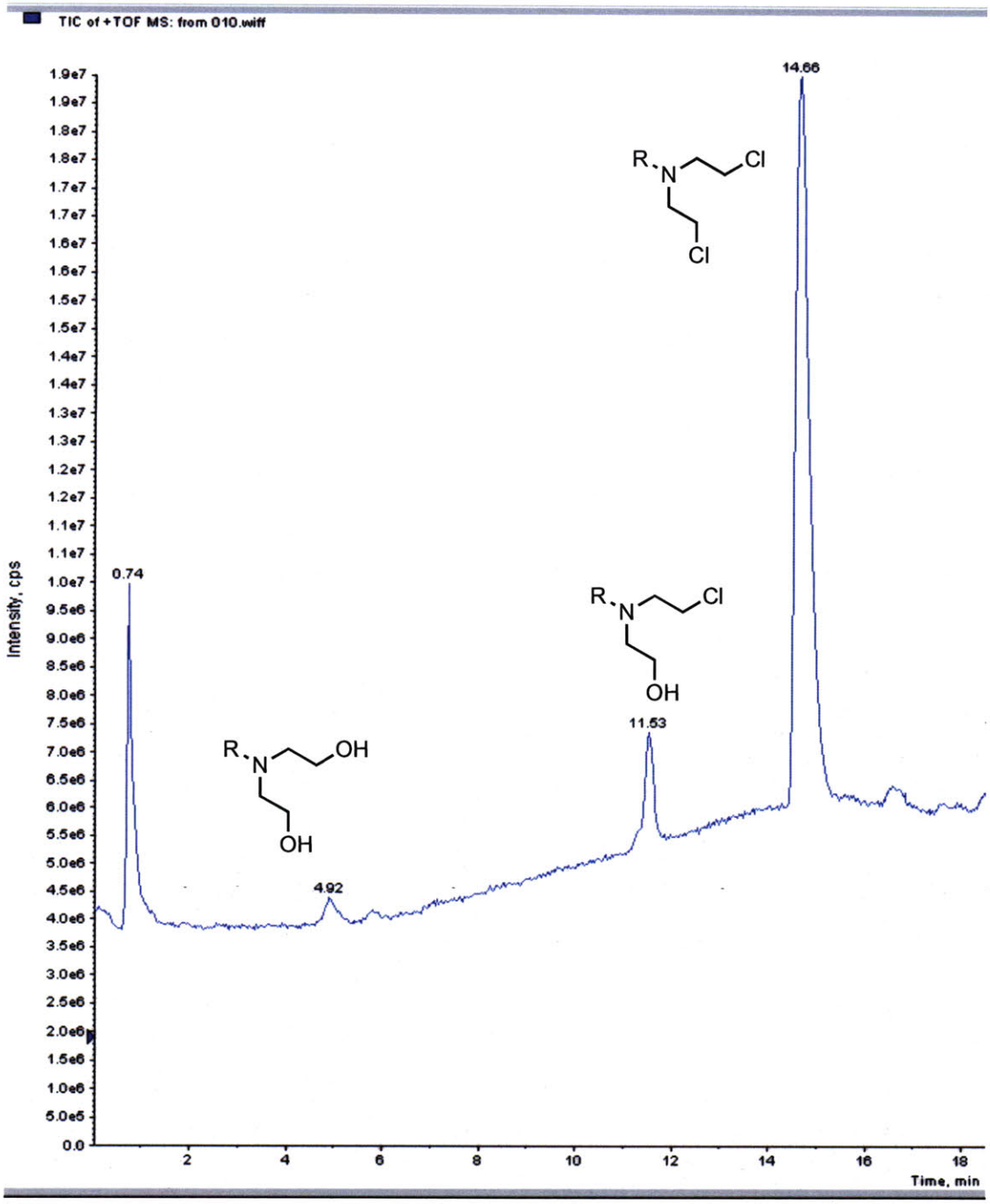

The 50–100% methanol gradient provided excellent separation of 11β from its primary hydrolysis products 11β-monohydroxyl (elution at 11.5 minutes) and 11β-dihydroxyl (4.9 minutes).

Figure 2-6: Separation and identification of primary 11β hydrolysis products

b) Mass spectrum of 11β-monohydroxyl

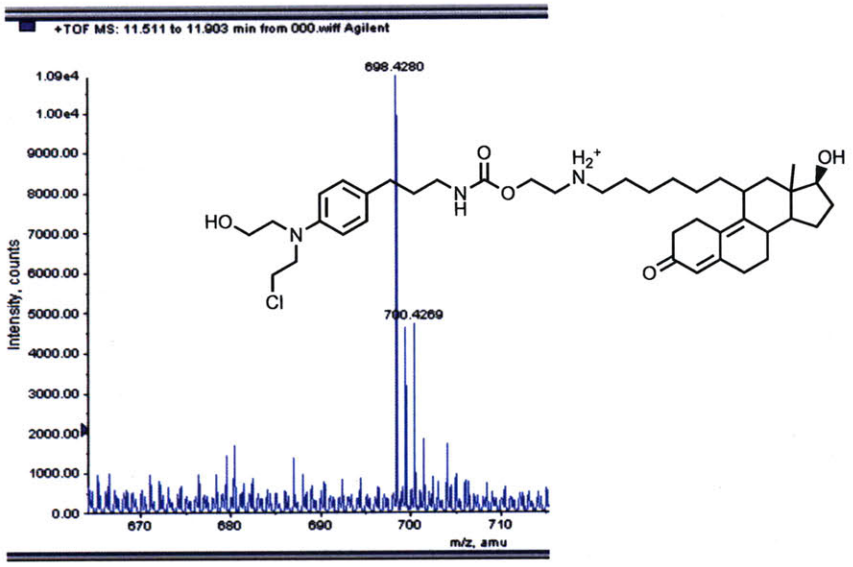

c) Mass spectrum of 11β-dihydroxyl

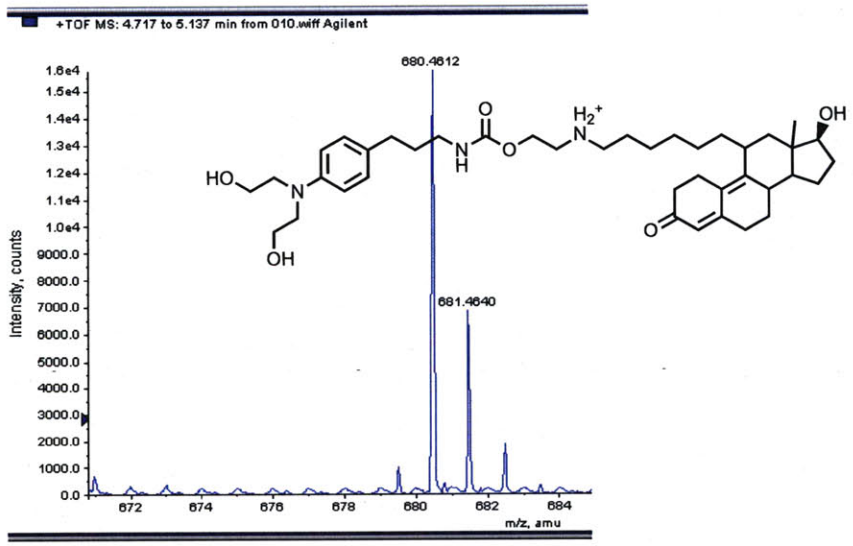

Mass spectra of primary hydrolysis products of 11β show isotope patterns consistent with their composition: b) 11β-monohydroxyl has an m+2 peak with abundance relative to the monoisotopic 698 consistent with the presence of one ^{37}Cl atom, while c) 11β-dihydroxyl (monoisotopic m/z 680) shows a sparse m+2 signal resulting only from the presence of two ^{13}C atoms.

Figure 2-7: Mass spectrum of an intact aziridinium intermediate

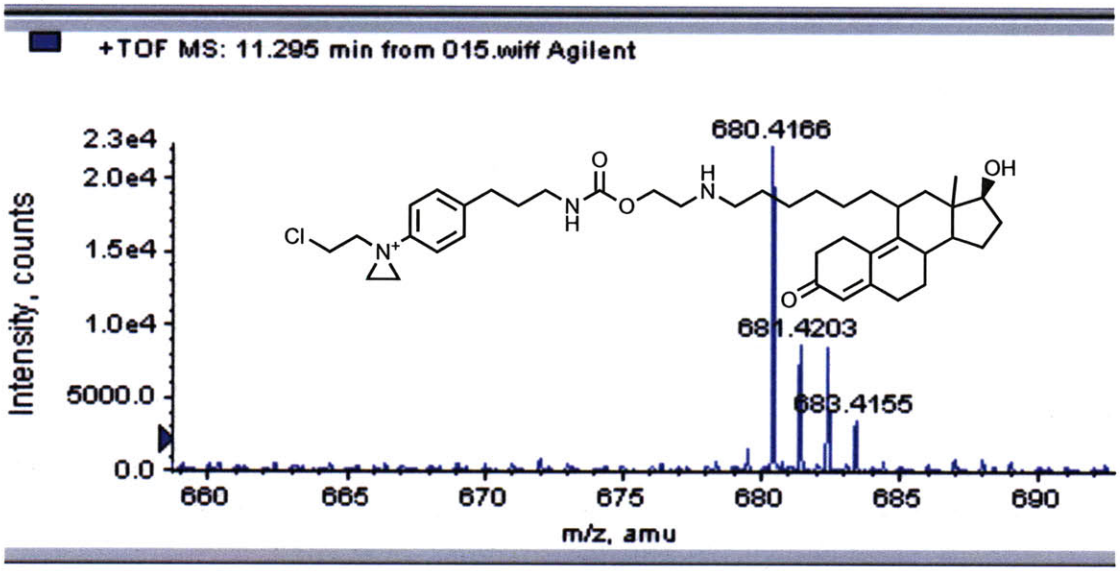

Though sparse, the aziridinium ion was detected by ESI-TOF during an ion extraction at m/z 680 to isolate doubly-hydrolyzed 11β. This species, still containing a chlorine atom, eluted six minutes later than the dihydroxyl compound with the same monoisotopic mass; the difference in prominence of the signals at 682 (see Figure 2-5c) confirmed their respective identities.

Figure 2-8: Mass spectra of phosphorolyzed 11β species

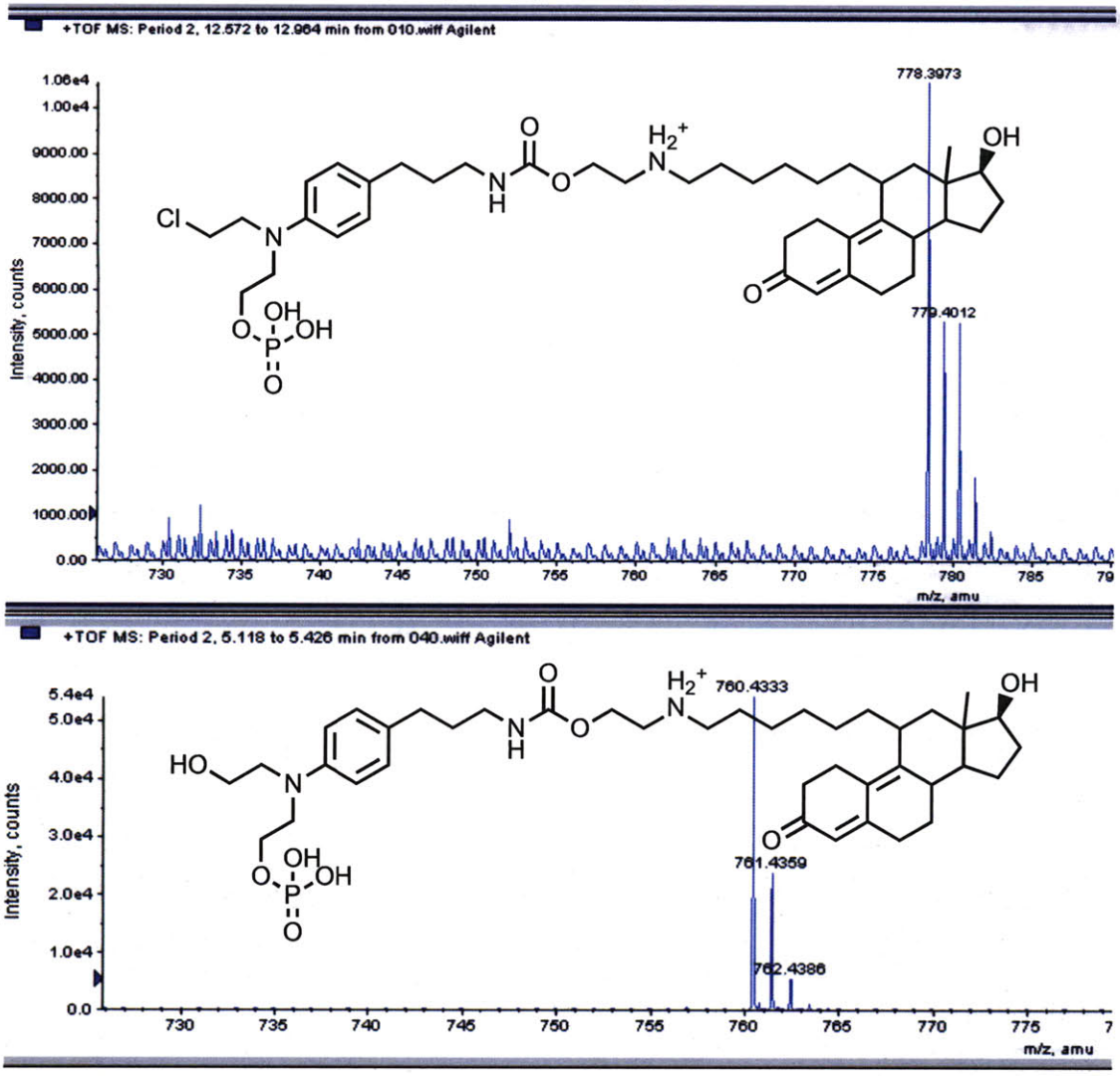

Buffer inorganic phosphate ion executed a nucleophilic attack on the aziridinium ion to generate a phosphorolyzed species (top, 778). The second chloroethyl arm subsequently hydrolyzed to yield m/z 760.

Figure 2-9: Mass spectra of secondary hydrolysis products

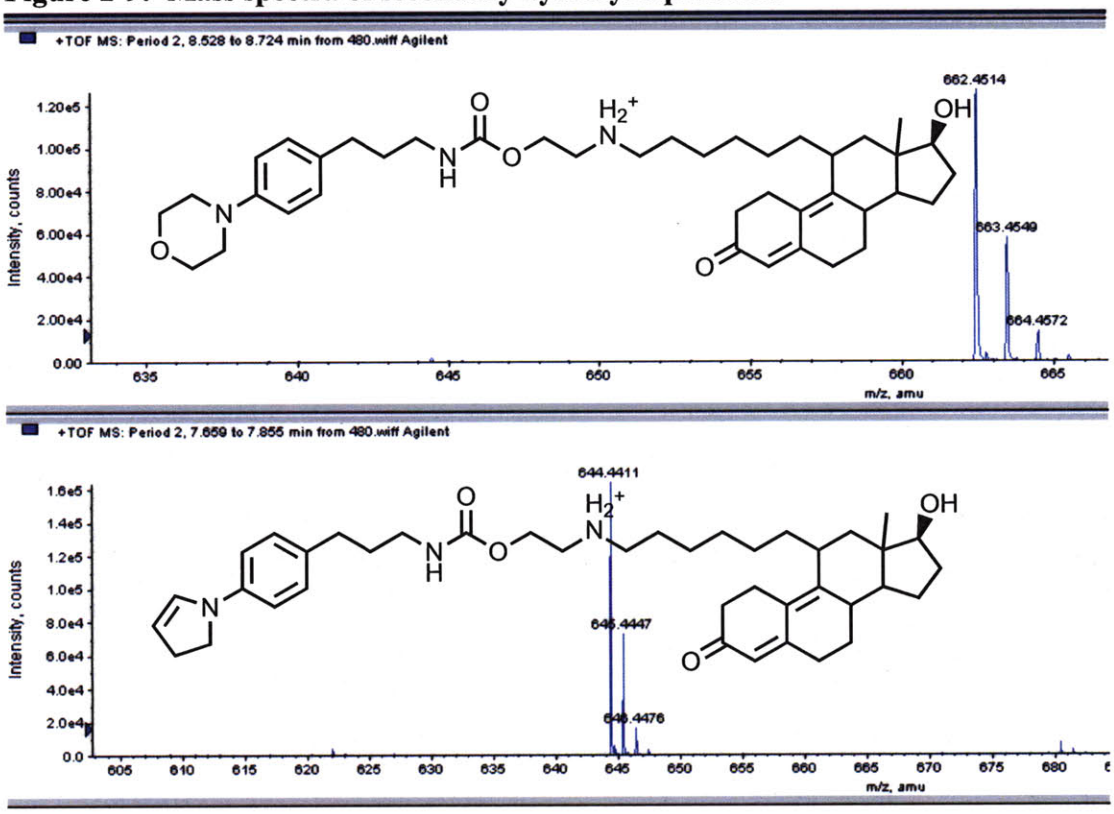

Species without chlorine atoms were detected and tentatively assigned structures associated with an intramolecular attack of the second chloroethyl arm by its already-hydrolyzed counterpart. The morpholinyl species (m/z 662, top) could likely rearrange and dehydrate to a dihydropyrrole (644).

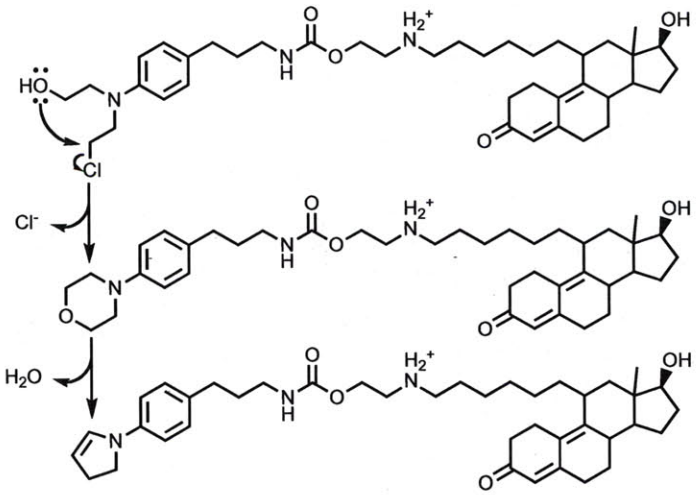

Figure 2-10: Fragmentation of 11β for detection by QQQ

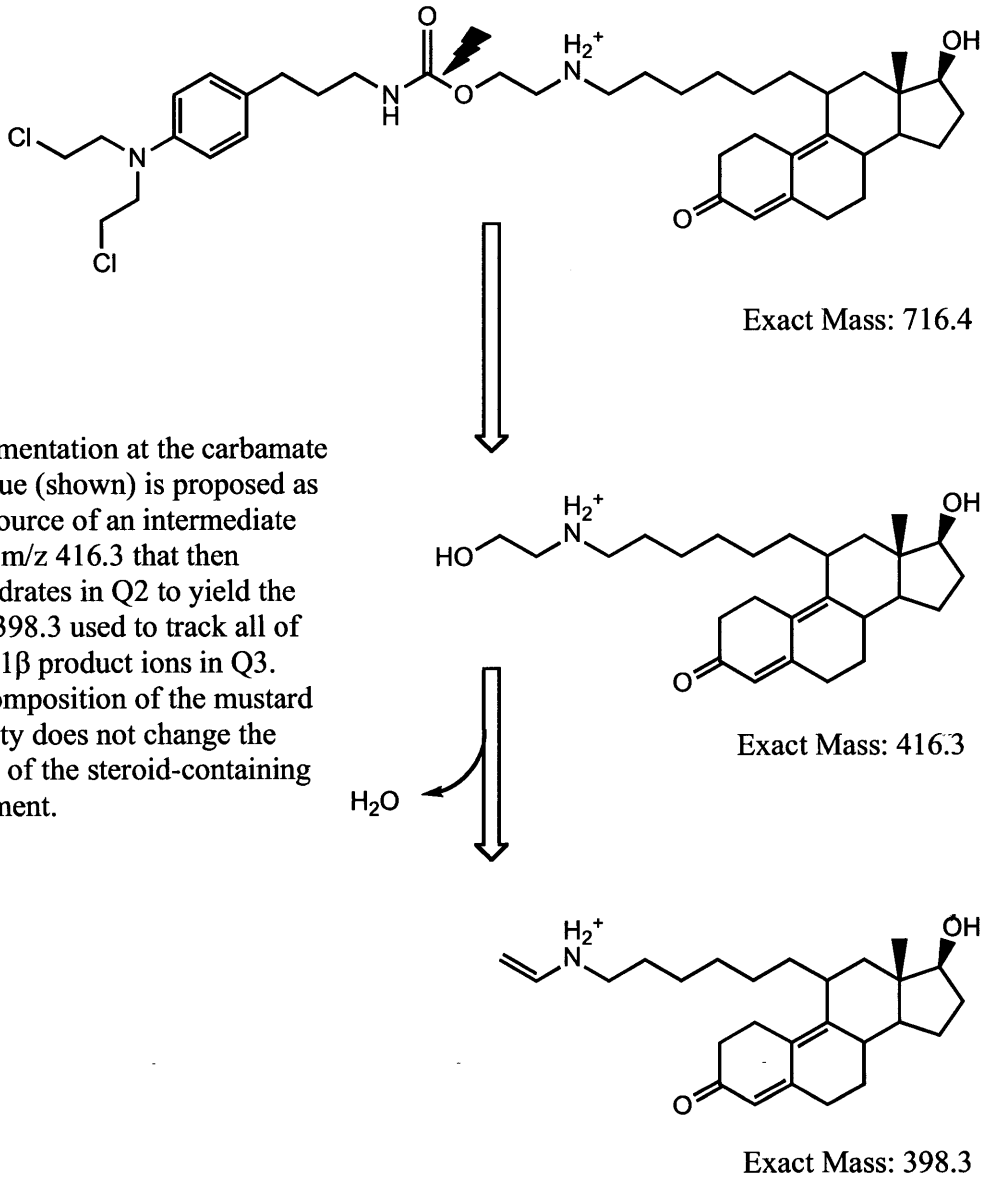

Fragmentation at the carbamate residue (shown) is proposed as the source of an intermediate with m/z 416.3 that then dehydrates in Q2 to yield the m/z 398.3 used to track all of the 11β product ions in Q3. Decomposition of the mustard moiety does not change the mass of the steroid-containing fragment.

Figure 2-11: Decomposition of 11β as tracked by QQQ

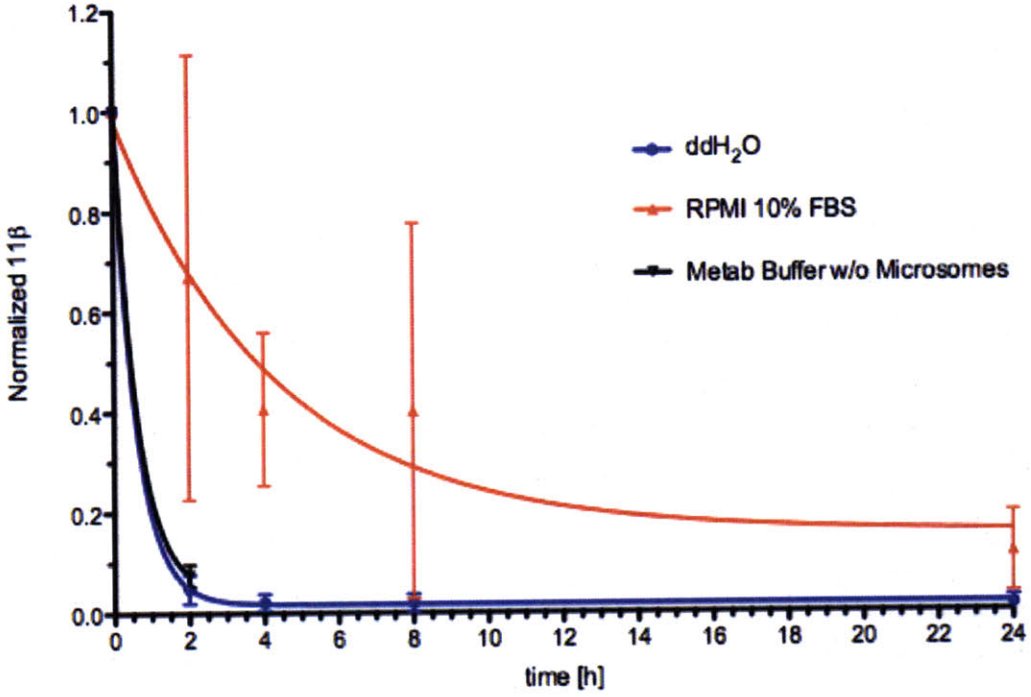

11β rapidly decomposed in water and the microsomal buffer system with both half-lives under 30 minutes (ddH_2O $t_{1/2}$ = 0.40 h, R^2=0.999, microsomal buffer system $t_{1/2}$ = 0.42 h, R^2=0.999). In tissue culture media supplemented with 10% FBS, 11β was more stable, with $t_{1/2}$ = 3.03 h, R^2=0.613. Error bars represent mean ± standard deviation, with n=3 for all time points.

Table 2-1: Hydrolysis rates of clinically-used alkylating agents

Compound	Cancers	$t_{1/2}$ [hours]
Mechlorethamine	Hodgkin's lymphoma, lung	<0.1[23]
Ifosfamide mustard	Lung, cervix, testicle, Ewing's sarcoma, neuroblastoma	0.9*[13]
Cyclophosphamide mustard	Lymphoma, myeloma, acute and chronic leukemias, neuroblastoma, retinoblastoma, breast, ovary	0.33*[24]
Chlorambucil	Chronic lymphatic leukemia, lymphoma	0.26[11]
Melphalan	Multiple myeloma, ovary	0.68–0.74**[25,12,26]

*The pro-drugs cyclophosphamide and ifosfamide decompose into their respective mustards following enzymatic activation[27-29].
**Reported as k_{cat} [min^{-1}].

Table 2-2: Fragmentation and collision conditions for detection of 11β species by triple quadrupole mass spectrometry

11β Species (dominant charge state)	Transition Q1->Q3	Fragmentation Voltage	Collision Energy
Dichloro (+1)	716.4 -> 398.3	135	35
Dichloro (+2)	358.9 -> 398.3	110	13
Dimethoxy (+1)	716.4 -> 398.3	135	35
Dimethoxy (+2)	354.9 -> 398.3	110	17
Monochloro–monohydroxyl (+2)	349.9 -> 398.3	110	13
Dihydroxyl (+2)	340.9 -> 398.3	110	13

Table 2-3: Elution times and mass-to-charge ratios for 11β hydrolysis products

Compound	Monoisotopic m/z	Elution time [min]
11β dichloro (parent)	716	14.5
Monochloro–monophosphate	778	12.7
Monochloro–monohydroxyl	698	11.5
Aziridinium ion	680	11.3
Morpholinyl	662	8.6
Dihydropyrrole	644	7.7
Monohydroxyl–monophosphate	760	5.3
Dihydroxyl	680	4.9

References

1. DeVita, V.T., Young, R.C. & Canellos, G.P. Combination versus single agent chemotherapy: a review of the basis for selection of drug treatment of cancer. *Cancer* **35**, 98-110(1975).
2. Goodman, L.S. et al. Landmark article Sept. 21, 1946: Nitrogen mustard therapy. Use of methyl-bis(beta-chloroethyl)amine hydrochloride and tris(beta-chloroethyl)amine hydrochloride for Hodgkin's disease, lymphosarcoma, leukemia and certain allied and miscellaneous disorders. By Louis S. Goodman, Maxwell M. Wintrobe, William Dameshek, Morton J. Goodman, Alfred Gilman and Margaret T. McLennan. *JAMA* **251**, 2255-2261(1984).
3. Mattes, W.B., Hartley, J.A. & Kohn, K.W. DNA sequence selectivity of guanine-N7 alkylation by nitrogen mustards. *Nucleic Acids Res* **14**, 2971-2987(1986).
4. Rink, S.M. et al. Covalent structure of a nitrogen mustard-induced DNA interstrand cross-link: an N7-to-N7 linkage of deoxyguanosine residues at the duplex sequence 5'-d(GNC). *Journal of the American Chemical Society* **115**, 2551-2557(1993).
5. De Silva, I.U. et al. Defining the roles of nucleotide excision repair and recombination in the repair of DNA interstrand cross-links in mammalian cells. *Mol Cell Biol* **20**, 7980-90(2000).
6. Hansson, J. et al. Formation and removal of DNA cross-links induced by melphalan and nitrogen mustard in relation to drug-induced cytotoxicity in human melanoma cells. *Cancer Res* **47**, 2631-2637(1987).
7. Frankfurt, O.S. Inhibition of DNA repair and the enhancement of cytotoxicity of alkylating agents. *Int J Cancer* **48**, 916-23(1991).
8. Lawley, P.D. & Phillips, D.H. DNA adducts from chemotherapeutic agents. *Mutat Res* **355**, 13-40(1996).
9. Hillier, S.M. et al. DNA adducts formed by a novel antitumor agent 11β-dichloro in vitro and in vivo. *Mol. Cancer Ther* **5**, 977-984(2006).
10. Marquis, J.C. et al. Disruption of gene expression and induction of apoptosis in prostate cancer cells by a DNA-damaging agent tethered to an androgen receptor ligand. *Chem. Biol* **12**, 779-787(2005).
11. Chatterji, D.C., Yeager, R.L. & Gallelli, J.F. Kinetics of chlorambucil hydrolysis using high-pressure liquid chromatography. *J Pharm Sci* **71**, 50-4(1982).
12. Chang, S.Y., Evans, T.L. & Alberts, D.S. The stability of melphalan in the presence of chloride ion. *J PHARM PHA* **31**, 853-4(1979).
13. Springer, J.B. et al. 1,3- vs 1,5-intramolecular alkylation reactions in isophosphoramide and phosphoramide mustards. *Chem. Res. Toxicol* **17**, 1217-1226(2004).
14. Bosanquet, A.G. & Bird, M.C. Degradation of melphalan in vitro: rationale for the use of continuous exposure in chemosensitivity assays. *Cancer Chemother Pharmacol* **21**, 211-5(1988).
15. Urbaniak, M.D. et al. Design and synthesis of a nitrogen mustard derivative stabilized by apo-neocarzinostatin. *J. Med. Chem* **47**, 4710-4715(2004).
16. Vijayaraghavan, S. et al. Enhanced hydrolytic stability and water solubility of an aromatic nitrogen mustard by conjugation with molecular umbrellas. *Bioconjug. Chem* **14**, 667-671(2003).

17. Gamcsik, M.P., Hamill, T.G. & Colvin, M. NMR studies of the conjugation of mechlorethamine with glutathione. *J Med Chem* **33**, 1009-14(1990).
18. Colvin, O.M. et al. Role of glutathione in cellular resistance to alkylating agents. *Adv. Enzyme Regul* **33**, 19-26(1993).
19. Gamcsik, M.P., Millis, K.K. & Hamill, T.G. Kinetics of the conjugation of aniline mustards with glutathione and thiosulfate. *Chem. Biol. Interact* **105**, 35-52(1997).
20. Gamcsik, M.P. et al. Mechanisms of resistance to the toxicity of cyclophosphamide. *Curr. Pharm. Des* **5**, 587-605(1999).
21. Guenthner, T., Whalen, R. & Jevtovic-Todorovic, V. Direct measurement of melphalan conjugation with glutathione: studies with human melanoma cells and mammalian liver. *J Pharmacol Exp Ther* **260**, 1331-1336(1992).
22. O'Brien, M.L. & Tew, K.D. Glutathione and related enzymes in multidrug resistance. *European Journal of Cancer* **32**, 967-978(1996).
23. Lemire, S.W., Ashley, D.L. & Calafat, A.M. Quantitative determination of the hydrolysis products of nitrogen mustards in human urine by liquid chromatography-electrospray ionization tandem mass spectrometry. *J Anal Toxicol* **27**, 1-6(2003).
24. Hemminki, K. et al. Kinetics of hydrolysis in vitro of nornitrogen mustard, a metabolite of phosphoramide mustard and cyclophosphamide. *Arch Toxicol* **61**, 126-30(1987).
25. Bolton, M.G. et al. Kinetic analysis of the reaction of melphalan with water, phosphate, and glutathione. *Drug Metab Dispos* **21**, 986-96(1993).
26. Stout, S.A. & Riley, C.M. The hydrolysis of l-phenylalanine mustard (melphalan). *International Journal of Pharmaceutics* **24**, 193-208(1985).
27. Borch, R.F. & Getman, K.M. Base-catalyzed hydrolysis of 4-hydroperoxycyclophosphamide: evidence for iminocyclophosphamide as an intermediate. *J Med Chem* **27**, 485-90(1984).
28. Low, J.E., Borch, R.F. & Sladek, N.E. Conversion of 4-hydroperoxycyclophosphamide and 4-hydroxycyclophosphamide to phosphoramide mustard and acrolein mediated by bifunctional catalysis. *Cancer Res* **42**, 830-837(1982).
29. Ludeman, S.M. The chemistry of the metabolites of cyclophosphamide. *Curr Pharm Des* **5**, 627-43(1999).

Chapter 3: Exploration of the Kinetics, Product Spectrum, and Enzyme-Specificity of the Metabolic Transformations of 11β

Introduction

Metabolism of xenobiotics

The path from drug candidate to viable therapeutic agent begins with efficacy: a compound must elicit a desirable biological response even to be considered for further development. Once the potency has been characterized, the evolution of a therapy depends on the pharmacokinetics and pharmacodynamics of a system. In order to assess safety, derive treatment schedules, and choose delivery routes, researchers must quantify the dose–response relationship *in vivo*. Of primary concern are the rates of clearance and metabolic transformations of a given compound. These reactions, comprising simple hydrolysis, redox chemistry, and conjugation to cofactors, are critical for understanding both activation and deactivation pathways associated with a compound.

The cytochromes P450, named for their distinct absorbance pattern at 450 nm when bound to carbon monoxide, are a diverse family of heme-containing monooxygenases expressed in the endoplasmic reticula of several tissues, with hepatic activity implicated in catalyzing transformations of both xenobiotics and endogenous agents[1]. Substrate specificity for isoforms of P450 is strongly dependent on the structures of the enzymes. As a result, compounds with thermodynamically-favorable sites for modification may escape reaction due to an inability to access the active site. Oxidations, comprising the majority of the reactions catalyzed by P450, can facilitate clearance by directly increasing the hydrophilicity of a compound or by providing a scaffold for conjugation to a solubility-enhancing cofactor. The rate and extent of these reactions strongly influence the exposure associated with a given dose of a compound.

Preliminary study of the metabolism of any drug candidate begins with analysis of its pharmacophores: compounds with similar molecular structure or shared moieties. Containing both an aniline mustard and a steroid ring system, 11β is rich with potential sites of modification (Figure 3-1). As such, the underlying hypothesis guiding the work described in this chapter was that 11β[†] would be a substrate for those P450 isoforms responsible for metabolism of chlorambucil or testosterone.

[†] 2-(6-((8S,11S,13S,14S,17S)-17-Hydroxy-13-methyl-3-oxo-2,3,6,7,8,11,12,13,14,15,16,17 dodecahydro-1H-cyclopenta[a]phenanthren-11-yl)hexylamino)ethyl 3-(4-(bis(2-chloroethyl)amino)phenyl)propylcarbamate

Metabolism of chlorambucil

The bifunctional aniline mustard 4-[4-*bis*(2-chloroethyl)aminophenyl]butyric acid (chlorambucil) features five heteroatoms and a phenyl ring, suggesting the possibility of N-dealkylation, epoxidation of the phenyl ring, or oxidation near the carboxyl group. Chlorambucil has been shown to undergo β-oxidation catalyzed by P450 followed by dehydration to generate 4-[4-bis(2-chloroethyl)aminophenyl]but-3-enoic acid, which is further processed into phenylacetic acid mustard (PAAM, Figure 3-2)[2]. PAAM is significantly more toxic to normal tissues than the parent drug, ostensibly due to increased bioavailability associated with improved solubility. However, this higher toxicity narrows its therapeutic window[3]. Both parent chlorambucil and PAAM can undergo N-dechloroethylation, rendering them incapable of forming DNA crosslinks and presumably non-toxic[4].

Metabolism of testosterone

The primary regulatory signaling cascade in the maintenance of prostate morphology involves the interaction between dihydrotestosterone (DHT) and the androgen receptor (AR)[5-10]. Circulating testosterone readily diffuses into prostate tissue where it is converted via reaction with 5α-reductase to DHT, which has a seven-fold higher affinity for the AR than the parent hormone[11]. Testosterone is also susceptible to oxidation by P450 from either face and at several loci: hydroxyl groups can be added at positions 1β, 2α/β, 6α/β, 7α, 11β, 15α/β, and 16α/β, and the 17-hydroxyl group can be oxidized to yield androstenedione (Figure 3-3)[12-14]. The regio- and stereoselectivity of testosterone hydroxylation by P450 has been extensively studied[12,15,16].

Subtle changes in the structure of testosterone can strikingly affect its affinity for the androgen receptor[11]. As such, the development of a drug candidate relying on mimicking that ligand-receptor interaction depends on adequate characterization of the degree to which metabolism of the parent compound changes its patterns of interaction with the target protein. Preliminary studies of relative binding affinity between the AR and 11β compounds as well as an oligonucleotide containing an 11β adduct have been

performed[17]. The dichloro parent shows a relative binding affinity (RBA) to AR of 11% when compared to R1881, a synthetic androgen compound often used as a benchmark, with roughly five times the affinity to the AR as testosterone (19.3%)[11]. Interestingly, the dimethoxy analog is an even better ligand with an RBA of 18%, suggesting that both ends of the molecule play a role in receptor binding. While this effect could be an artifact of differential solubility between the two compounds altering their distribution in the whole-cell extracts used in the binding assays, the pattern nonetheless demonstrates the sensitivity of the interaction to small structural modifications.

Multiple sites on 11β may be substrates for any number of isoforms of P450, and the resulting modifications may enhance or impede the performance of 11β as a drug candidate. Deleterious modifications analogous to those to which chlorambucil is susceptible could arise from dechloroethylation of the mustard to reduce DNA crosslinking potential, while hydroxylation of the steroid could enhance or sabotage the receptor interactions on which the premise of selective toxicity is based.

In vitro metabolism by liver microsomes

Nearly all xenobiotic agents reaching the bloodstream will eventually undergo metabolic processing by the liver. Depending on the delivery route, these compounds may be rapidly absorbed by the portal system before entering systemic circulation, as in the case of adsorption through the gut wall following oral administration, or they may diffuse into the liver after achieving systemic bioavailability through intravenous or intramuscular injection. The array of drugs and their metabolites resulting from first-pass metabolism by hepatic enzymes is primarily due to interactions with various isoforms of P450[18]. These metabolic reactions strongly influence the clearance rate of the active compound and consequently, the design of the therapeutic regimen. Measuring the relationship between the administration of a given dose and the time course of the resultant plasma concentration depends on isolation of a drug and its metabolites from blood. Before clinical trials, tissue fractions are invaluable for metabolic analysis to characterize the product spectrum and offer predictive power as to what the extent and rate of conversion will be *in vivo*. Furthermore, the identification and characterization of

metabolites and other biomarkers is essential to the design of the analytical procedures necessary to measure the dose–exposure relationship.

Sequential differential centrifugations can be used to separate complete cytosolic (S9) and endoplasmic reticulum (microsomal) fractions from homogenized whole liver tissue. The resulting preparations demonstrate concentrated metabolic activity and are central to the *in vitro* study of xenobiotic transformations and conjugations. Historically, microsomes derived from animal livers have been a valuable tool for pre-clinical assessment of the metabolic potential of a drug candidate. However, the correlation between the hepatic drug metabolism characteristics of humans and that of animal models is variable[19]. Initial probes of the metabolism of a drug candidate may be performed with an animal model, such as rat liver microsomes, with the caveat that the activity profile may be divergent from that of an analogous experiment performed with human material. The availability of pooled human liver microsomes from organ donors enables the study of metabolism caused by enzymatic machinery extracted from the species whose disease states the drugs are actually designed to treat, rather than a model species from which the information gleaned may not represent the relevant clinical metabolic profile. The Essigmann Laboratory has used mice as a host for testing the effectiveness of 11β in treating LNCaP xenograft tumors. As such, this necessitated study of murine metabolism in addition to rat and human models. In the work described in this chapter, a combination of preparations was used, including commercially-obtained pooled human, male rat, and female rat liver microsomes; as well as male and female mouse liver microsomes prepared in-house.

In work described in this chapter, quantitative levels of conversion were tracked by using high-pressure liquid chromatography to separate the metabolites of radiolabeled 11β. Following the quantitative experiments, unlabeled 11β was incubated in analogous microsomal preparations for qualitative metabolite analysis by liquid chromatography and electrospray ionization-time of flight mass spectrometry (LC–ESI-TOF). The diversity of products observed in both series of experiments provoked follow-up studies using triple quadrupole mass spectrometry (QQQ) in an attempt to identify the locations of metabolic modifications.

Drug-drug interactions

Cancer therapy frequently involves the sequential or concurrent administration of multiple drugs. It is critical to understand the metabolic pathways associated with the transformations of each drug in order to avoid dangerous drug-drug interactions (DDI)[20]. Should multiple drugs require the same metabolic machinery for activation or clearance, or if one drug induces or inhibits the expression of an isoform of P450 responsible for the metabolism of another compound, the pharmacokinetics of the treatment may deviate substantially from those observed during clinical trials in which the drug candidate is administered alone. This pathway interference could lead to a higher or lower exposure for a given compound, potentially rendering it toxic, if it persists in plasma long enough for consecutive doses to overlap, or inactive, if its clearance is enhanced or bioavailability impeded. The incidence of adverse drug reactions leading to patient death may very well be high enough to rival the fatality rates of cancer[21], thus necessitating thorough analysis of metabolic profiles in drug development.

Approximately 75% of all xenobiotic metabolism is catalyzed by the cytochromes P450, with CYPs 1A2, 2B6, 2C8, 2C9, 2C19, 2D6, 2E1, and 3A(4/5) responsible for over 95% of those reactions[22,23]. Understanding the behavior of a given drug candidate with respect to this P450 subset is an essential part of the screening process of drug development. Demonstration that a given compound does not show inhibitory activity toward these key isoforms *in vitro* can obviate the need for costlier *in vivo* assays. Conversely, if that compound is shown to possess strong activity toward an isoform crucial to a given disease state, it can be shelved or redesigned at the molecular level in order to balance efficacy with safety[24]. Comparisons of the results *in vitro* and *in vivo* DDI studies have shown sufficient correlations to confirm the predictive power of the *in vitro* work[20].

Several strategies are commonly employed to screen drug candidates for metabolic activity. Monoclonal antibodies against specific isoforms of P450 have proven useful in parsing the relative contributions of individual isoforms to the composite metabolic profile of a substrate with multiple labile sites[25]. The desire for high-

throughput compound screening has provoked the development of fluorogenic assays that eliminate the need for time-intensive separations downstream of the reaction[26]. Cocktails of substrates have been used both to inhibit multiple P450 isoforms in the same microsomal preparation and track the conversions of multiple probes via liquid chromatography and mass spectrometry (LC–MS)[27-30]. The industrial pursuit of new therapeutic agents has made the need for rapid screening of vast compound libraries a critical cost-management task. As such, standard assays have been developed to determine whether a compound is likely to fail in the developmental process due to DDI arising from specific P450 isoform induction or inhibition[24].

In order to determine whether 11β is a substrate for or inhibitor of five of these isoforms, *in vitro* incubations with a series of human, mouse, or rat liver microsomes were performed, taking advantage of a high-throughput automated mass spectrometry technology developed at BioTrove (Woburn, MA). The speed and precision of this technique enabled rapid analysis, yielding inhibition data for CYP isoforms 1A2, 2C8, 2C9, 2D6, and 3A(4/5).

Isoform-product correlation

With some preliminary information as to which P450 substrates were relevant to the metabolism of 11β, attempts were made to further characterize the catalysis by investigating the correlation between isoform activity and product spectra. Incubations of 11β containing high enough concentrations of probes to selectively inactivate subsets of P450 isoforms were performed to determine whether the products observed in earlier experiments could be attributed to specific isoforms of P450. The high sensitivity of the QQQ enabled detection of trace levels of products and obviated the need for chromatographic separation of the mixture before analysis. Because several metabolite species had been identified previously through work done on the ESI-TOF, the mass-to-charge ratios (m/z) of major metabolites were known, allowing the conditions for their detection by MS-MS to be derived quickly.

Materials & Methods

Materials: Pooled human liver microsomes (HLM) and male rat liver microsomes (RLM), each containing 20 mg/mL total protein in 250 mM sucrose, were obtained from BD Biosciences (Woburn, MA), defrosted and distributed into 50-100 µL aliquots, flash frozen in liquid nitrogen, and stored at -80°C until use. NADPH regeneration components, also from BD Biosciences, came in two preparations: Solution A (20X), comprising 25 mM $NADP^+$, 66 mM glucose-6-phosphate, and 66 mM $MgCl_2$ in H_2O; and Solution B (100X), comprising 40 U/mL glucose-6-phosphate dehydrogenase in 5 mM sodium citrate. Mouse liver microsomes and S9 fractions were prepared in-house. The NADPH regeneration systems were similarly defrosted and separated into aliquots before flash freezing and storage at -20°C until use. A 0.1 M potassium phosphate buffer at pH 7.4 was prepared weekly in 100 mL volumes and stored in a tightly-sealed brown bottle shielded from light at 4°C. The buffer pH was adjusted each morning that metabolism incubations were performed and unused volumes were discarded at the conclusion of each session.

Preparation of mouse liver microsomes and S9 fractions: Five male and six female four- to six-week-old NIH Swiss Webster mice weighing 25–35 g each were purchased from Charles River Laboratories (Wilmington, MA). Mice were sacrificed by cervical dislocation and eviscerated. Livers were perfused through the hepatic portal vein or abdominal aorta with 1.15% KCl in 0.05 M Tris at pH 7.4 (KCl/Tris) and immediately resected, washed in ice-cold Dulbecco's phosphate-buffered saline (PBS), and stored on ice in a Petri dish. Tissue masses were 9–10 g from either gender. Once all livers from a gender were harvested, they were minced to ~5 mm x 5 mm sections with a razorblade. Minced liver was then added to four volumes of ice cold KCl/Tris buffer in a 50 mL tube. The solution was transferred to a 50 mL volume Dounce homogenizer and processed until uniform (~12 strokes). Ligaments and connective tissue were decanted off. Homogenate was transferred to two centrifuge tubes and spun at 9,000 g (10,000 rpm) in a Ti50:1 rotor at under vacuum at 4°C for 30 minutes. Supernatants below the lipid layer were transferred to new centrifuge tubes, with ten 1 mL aliquots of these S9 fractions

saved on dry ice. A 50 μL aliquot of the homogenized S9 fraction from each gender was saved for later protein content quantification. The remaining supernatants were spun at 100,000 g (28,000 rpm) in an Sw40 swinging bucket rotor under vacuum at 4°C for 60 minutes. The supernatants and lipid layers were removed by Pasteur pipet and discarded. The red, gelatinous pellets were transferred by spatula to a small, pre-chilled homogenizer already containing 2 mL KCl/Tris buffer. An additional 500 μL of buffer was used to wash residual microsomal material from the centrifuge tubes. The solutions were combined and homogenized with 10–12 strokes. A 50 μL aliquot from each gender was saved for later protein content quantification. The homogenized microsomes were transferred in 200–250 μL aliquots to fresh tubes and immediately frozen on dry ice. Frozen microsomes and S9 fractions were stored at -80°C until needed. Protein concentrations were determined by the Bradford dye binding assay (Bio-Rad Laboratories, Hercules, CA).

Metabolism of radiolabeled 11β by liver microsomes: Incubations of ^{14}C 11β with liver microsomes followed the generalized protocol described below, with substrate and enzyme concentrations, reaction times, and cofactor inclusion or exclusion varied to test for NADPH dependence, kinetics of conversion, activity of protein, and species and gender specificity. Aliquots of liver fractions and Solutions A and B were quickly defrosted in a 37°C water bath and transferred to ice. Potassium phosphate buffer was pre-warmed to 37°C in a 25 mL glass Erlenmeyer flask. Microsomes were added to buffer to desired final protein concentration. Subsequently, Solution B (100X) and 11β (200X) were added and mixed by swirling. Reactions were initiated by addition of Solution A (20X) and again mixed by swirling. A small aliquot (5–20 μL) of the complete reaction system was withdrawn for scintillation counting. Flasks were covered with parafilm needle-punctured to allow oxygen exchange and secured in a rotating water bath maintained at 37°C, situated to an immersion depth sufficient to ensure temperature uniformity in the reaction volume during vigorous mixing. Incubations lacking NADPH machinery were pre-warmed to 37°C and initiated by addition of 11β.

At time points of interest, samples were withdrawn from the flask and mixed with an equal volume of ice-cold ethyl acetate in a glass sample vial. This mixture was shaken

vigorously to quench the reaction, dissociate the microsomes, and separate 11β and its daughter compounds into the organic phase, and allowed to settle on ice for fifteen minutes. After a second shake and settle, the vial was spun for five minutes at 1,000 g and 4°C in a swinging bucket centrifuge to enhance the phase separation. A small aliquot of the organic phase was taken for scintillation counting, with the rest carefully withdrawn with a Pasteur pipet to avoid disrupting the interface layer and transferred to a fresh glass vial. A small amount (~1 g) of sodium sulfate powder was added to absorb residual water from the organic fraction, which was shaken and left to settle on ice. After fifteen minutes, the vial was shaken and the organic–salt slurry was filtered through a Pasteur pipet with a cotton plug into a 10 mL pear-shaped glass flask. This flask was immersed to the liquid level of its contents in a stationary water bath over mild heat. A gentle stream of filtered air was blown into the flask to speed evaporation of solvent. While the first ethyl acetate-sodium sulfate system equilibrated, a second equal volume of ethyl acetate was added to the remaining aqueous fraction, vigorously remixed, and centrifuged identically to the first. The organic layer of this extraction step was similarly dehydrated over sodium sulfate and added to the pear-shaped flask through the cotton plug. An aliquot of the remaining aqueous phase was taken for scintillation counting of water-soluble metabolism products. After complete evaporation of the ethyl acetate, the material was redissolved in 100% methanol and a small aliquot was taken for scintillation counting to quantify total recovery and ensure sufficient activity for detection. Recovery rates were consistently >60%. Samples were stored at -80°C until immediately before analysis. All aliquots for activity quantification were mixed with Hionic-Fluor scintillation fluid (Perkin-Elmer, Waltham, MA) and counted with a Beckman LS1801 liquid scintillation counter (Beckman-Coulter, Fullerton, CA).

Quantification of ^{14}C 11β species by HPLC–UV–Radio: Reconstituted samples were separated by reversed-phase HPLC and analyzed with a Series 330 Photodiode Array (PDA) detector (Varian) in tandem with a Flow Scintillation Analyzer Model 150TR (Packard Biosciences, Meriden, CT) radiochemical detector.

Chromatography Method 1 was a modified version of a program originally developed by Hillier et al.[31], using ddH_2O with 10% acetonitrile and 10 mM sodium

acetate as mobile phase "A" and 100% methanol as mobile phase "B." A Sorbax XDB-C18 column (4.6x250 mm, 5 μM pore size; Agilent, Santa Clara, CA) was used with a total mobile phase flow rate of 1 mL/min. This method comprised 2 minutes at 0% B, followed by a 20-minute ramp to 100% B, a 5-minute hold at 100% B, a 5-minute ramp back down to 0% B, and a 3-minute hold at 0% B to re-equilibrate the column. Immediately upstream of the radiochemical detector, Ultima-Flo M scintillation fluid (Perkin-Elmer) was introduced at a flow rate of 2.5 mL/min.

Previous HPLC separations of 11β used a ramp from 50–100% B over the same twenty-minute interval, with 11β usually eluting at or around 95% B. Given the uncertainty as to the degree to which metabolites of 11β would be less hydrophobic, and therefore elute earlier, it was necessary to adjust the initial conditions to 0% B in order to allow all species to be retained on the stationary phase.

Chromatography Method 2, used for the mouse liver microsomal time course, bypassed the PDA, going straight from column to radiochemical detector to reduce void volume, and replaced the mobile phases with those used for LC-MS: 0.25% acetic acid in ddH_2O prepared in-house for solvent A; 0.25% acetic acid in methanol for solvent B. A Sorbax XDB-C18 column (2.1x50 mm, 5 μM pore size) was again used with a total solvent flow rate of 0.4 mL/min. This method began with a 2.5-minute hold at 25% B followed by a 2.5-minute ramp to 45% B, a 20-minute ramp to 75% B, a 5-minute hold at 75% B, a 5-minute ramp back down to 25% B, and a 5-minute hold at 25% B. Scintillation fluid was added at a rate of 1 mL/min. This method was designed following the observation that in experiments with unlabeled compound, separated and analyzed by LC–ESI-TOF as described below, 70% methanol was sufficient to elute 11β from the C18 columns—the apparent need to reach 100% B on the tandem UV-radiochemical detector apparatus was an artifact of the large void volume between the column outlet and the radio detector.

All radio-chromatograms were smoothed with a 6^{th}-order, 25-point Savitzky-Golay algorithm and integrated in Prism 5 (GraphPad Software, La Jolla, CA) to determine areas under the curve for separated peaks. Time course experiments were modeled in Prism 5 as first-order kinetics.

Preparation of metabolites for identification by mass spectrometry: Incubations of unlabeled 11β were performed with human, rat, and mouse liver microsomes for separation and analysis by LC–ESI-TOF. Reactions were prepared with the same reagents and procedures as those used for the experiments with labeled compound but with 1mL final reaction volumes. Instead of ethyl acetate extractions, samples at time points of interest were quenched by addition of 500 μL of ice-cold acetonitrile, vortexed, and placed on ice for thirty minutes. Samples were then spun in a microcentrifuge at 18,000 g and 4°C. Supernatants were withdrawn into 10 mL syringes already containing 6 mL cold ddH_2O (RICCA) to reduce total organic content to approximately 7%. This mixture was passed twice through a C18 SepPak (Waters) previously wetted with 100% acetonitrile and equilibrated to 10% methanol. Loaded columns were washed with 1 mL ddH_2O to remove any lingering salts, and then slowly eluted with two 2.5 mL volumes of 100% methanol. The eluates were evaporated over mild heat and filtered air, and reconstituted in 25% acetonitrile to match initial conditions for chromatography method 3 described below. Samples were stored at -80°C when immediate analysis was not feasible.

Detection and identification of 11β metabolites by LC–MS: Samples were injected with a 1200 Series LC system into a Sorbax XDB-C18 (2.1x50 mm, 5 μm pore size) column upstream of a 1200 Series diode array detector in tandem with a 1200 Series ESI-TOF mass spectrometer (all Agilent Technologies, Santa Clara, CA) in the Mass Spectrometry Laboratory of the MIT Department of Biological Engineering. Liquid chromatography was performed at a total flow rate of 0.2 mL/min using Method 2 described above. Mass spectrometry was performed in positive ion mode with source conditions previously optimized at 325°C heated capillary, 12 L/min drying gas (N_2, AirGas, Salem, MA), 25 psig nebulizer pressure, and 4000 V needle voltage. Peaks were identified with the Agilent Analyst QS software package.

DDI Screen of 11β against five P450 substrates: Incubations for each of four microsomal preparations (pooled human, male mouse, female mouse, and male rat) were prepared in a 96-well format, all including 0.5 mg/mL microsomal protein and NADPH

regeneration machinery in the same concentrations as the larger-scale metabolism experiments but with 50 μL total reaction volumes. The isoform-probe pairs used are summarized in Figure 3-4. For each preparation, triplicate analyses of eight 1:10 serial dilutions of 11β (ranging from 100 mM to 10 pM) were performed. Reactions were initiated with addition of Solution A and incubated at 37°C for thirty minutes. Reactions were quenched with 50 μL of ice-cold acetonitrile containing 0.1% formic acid and 200 nM bupivacaine as an internal standard, and stored on dry ice until analysis. Measurement of the levels of probe products was performed with a RapidFire high-throughput injection system (BioTrove, Woburn, MA) coupled to an Agilent Series 6410 triple quadrupole mass spectrometer. Each 10 μL sample was withdrawn from its well, desalted on a C4 microcolumn cartridge with water : formic acid (FA) : trifluoroacetic acid (TFA) (99.9% : 0.09% : 0.01%), and back-eluted with acetonitrile : FA : TFA (99.9% : 0.09% : 0.01%) into the QQQ source. Multiple reaction monitoring (MRM) mode with source conditions 350°C heated capillary, 13 L/min drying gas, 60 psig nebulizer pressure, and 4000 V needle voltage was used to measure species abundance. Transition conditions for the probe metabolites are summarized in Table 3-1. Cycle time between injections was 6–8 seconds, allowing the processing of plates in a matter of minutes. Integration of the MRM peak intensities was performed at BioTrove using the proprietary RapidFire Integrator Software. These data were modeled as enzyme inhibition processes in Prism 5 to extract an IC_{50} from the inflection point of the probe abundance vs. competitor concentration curve for each isoform.

QQQ identification of modification location by fragmentation analysis: Analysis by triple quadrupole mass spectrometry was performed on the Agilent Series 6410 QQQ operating in positive ion mode with source conditions 325°C heated capillary, 12 L/min drying gas, 25 psig nebulizer pressure, and 4000 V needle voltage. Samples were delivered as bolus injections with a carrier mobile phase of 0.25% acetic acid in methanol at 4 μL/min. Based on the spectrum of products seen in previous analyses performed on the ESI-TOF, a method to distinguish structurally the metabolites with identical mass-to-charge ratios but distinct elution times was devised (Figure 3-5). A set of transitions were derived and tested to try to determine on which side of the carbamate fragmentation

site a metabolic reaction had occurred. MRM mode was used to track abundance of each species after optimization of fragmentor voltage and collision energy for 11β, its metabolites, and 11β-dimethoxy as an internal standard (Table 3-2). Abundance traces were smoothed and integrated in Agilent Qualitative Analysis, with areas under the curve for each of the test species divided by that of the internal standard from the same injection to normalize for the variable efficiency of the workup.

Isoform elimination screen: In order to determine whether certain P450 isoforms were responsible for the generation of specific metabolites or subsets of the metabolites of 11β, a set of elimination assays were performed containing high (≥10 K_m) concentrations of probes in various combinations, each designed to leave only one of the major isoforms active. Values for K_m of the individual probes were taken from Walsky and Obach (2004)[24]. Based on the results of the DDI screen, tacrine (CYP1A2) was omitted from the preparations, replaced with mephenytoin for CYP2C19. Reaction volumes were each 0.5 mL, containing 0.5 mg/mL pooled HLM and all cofactors as previously described.

Incubations lasted thirty minutes and included 1 μM 11β with: 1) no microsomes; 2) no inhibitors; 3–7) five mixtures, each containing all but one of the inhibitor set; and 8) all five inhibitors. Reactions were initiated with addition of Solution A and quenched with an equal volume ice-cold acetonitrile containing 0.1% formic acid and 0.5 μM 11β-dimethoxy as an internal standard. Separations were performed as described previously, with material loaded onto C18 SepPaks, washed with ddH_2O, and eluted with 100% methanol. The high sensitivity of the QQQ obviated the need for sample concentration, instead allowing 1 μL bolus injections of each sample, with a 4 μL/min carrier phase of 0.1% formic acid in methanol. Abundance curves were smoothed, integrated, and normalized to internal standard. AUCs were compared across the individual preparations to assess the presence, if any, of isoform-specific patterns.

Results

P450 catalysis depends on NADPH. Incubations with rat or human liver microsomes showed minimal conversion of parent compound after thirty minutes, with 11β 93% intact in both pooled HLM (Figure 3-6) and male RLM preparations (Figure 3-7). Trace abundance of daughter species eluted only slightly earlier than parent, and as such were considered likely to be singly-hydroxylated, singly-hydrolyzed, or reduced. Even without the addition of NADPH and its regeneration machinery, there was likely a baseline level of cofactors present in the microsomal preparation itself. As such, small levels of conversion were not surprising. The identities of these species would be analyzed in later experiments by mass spectrometry.

Reactions containing human liver microsomes including the NADPH regeneration machinery demonstrated extensive conversion of parent to a vast array of product species at 1 mg/mL microsomal protein. After the thirty-minute incubation period, only 5% of parent was intact, and the overwhelming majority of products eluted upstream of 11β-dichloro, with only trace levels of activity representing species that were more hydrophobic than the parent. Over a dozen species with distinct elution times were observed, but their separation under these chromatography conditions was less than ideal; overlapping peaks complicated quantitation. Rat liver microsomes, on the other hand, were not as active in either extent or diversity: after thirty minutes, >40% of parent was intact, with four distinct peaks comprising the majority of the metabolite spectrum.

Kinetics of conversion

Protein activity: The macromolecular content of microsomes provided a sufficient adsorption surface for 11β, minimizing hydrolysis during half-hour incubations. With the baseline level of inactivation quantified and the dependence of conversion on NADPH confirmed, it was then necessary to determine how much catalysis was occurring per unit protein. The near-complete metabolism of 11β in a 1 mg/mL preparation of human liver microsomes provoked a repeat experiment with 0.5 mg/mL total protein (Figure 3-8) in hopes of determining which were the major metabolites.

The extent to which 11β was shown to be a substrate to human liver microsomes encouraged the in-house production of mouse liver microsomes. In order to conserve material, the reactions with mouse liver microsomes began at 0.5 mg/mL protein. Serial dilutions of protein (all with the same cofactor content as the 1 mg/mL incubations) showed near-complete metabolism of 11β (Figure 3-9) after thirty minutes with as little as 0.25 mg/mL protein, and 0.0625 mg/mL protein was sufficient to metabolize half of the parent compound. A comparison of the mouse liver incubations shows a loss of both product diversity and extent of conversion with declining protein, suggesting that components of the product spectrum arose from multiple hits: after dissociating from the active site of one enzyme, products could undergo further modifications, through either a second P450-catalyzed reaction or a rearrangement facilitated by the original transformation.

Time course of parent disappearance: Male mouse liver microsomes with 0.25 mg/mL total protein demonstrated sufficient activity to catalyze nearly complete metabolism of 11β in thirty minutes. In order to measure the kinetics of conversion, incubations at 0.25 mg/mL were prepared with a 10 mL reaction volume in order to include enough radioactivity for five time points (5, 8, 15, 22, and 30 minutes) without exceeding the solubility limits of parent compound. Transformation of parent was extremely rapid, with 75% conversion achieved within five minutes (Figure 3-10). The disappearance of 11β was modeled as first-order exponential decay with a half-life of 2.1 minutes.

Species-specificity: Significant differences in both extent of conversion and identity of products were observed across the three species analyzed. All were dependent on NADPH for conversion, but human and mouse microsomes demonstrated far greater activity. Apropos the goal of assessing mechanisms for drug candidates against a human disease and the extensive use of mouse models in the Essigmann Laboratory, further exploration of the rat metabolism kinetics was deemed beyond the scope of this work.

Gender-specificity: Male and female mouse liver microsomes showed minimal differences in either extent of conversion or elution times of products (Figure 3-11).

Incubations with 1 mg/mL total protein and NADPH regeneration machinery demonstrated near-complete (>98%) conversion of 11β after thirty minutes.

Product spectrum: A diverse array of metabolites was observed through analysis by ESI-TOF, comprising oxidations, N-dealkylation, and dehydrations (Figure 3-12). At least four different species showing dichloro isotope patterns and with monoisotopic m/z 732 (+16 from parent) were observed with distinct elution times, suggesting hydroxyl group additions at separate loci. Twice-hydroxylated 11β was also observed with m/z 748. Dehydration (-18) of these putative hydroxylation products was also detected, with dichloro species appearing at 714 (dehydrated 732) and 712 (twice-dehydrated 748). The N-deschloroethyl 11β species with m/z 654 and one chlorine was one of the most abundant metabolites. This N-deschloroethyl daughter compound could undergo subsequent hydroxylation to m/z 670. Interestingly, there were as many distinct m/z 670 peaks as there were m/z 732 peaks, indicating that severing of the chloroethyl arm resulted from a separate P450 encounter than the addition of hydroxyl groups, and that the variety of loci on which hydroxyl groups could be added was just as broad after N-dealkylation as before. The spectrum of metabolites was broadest in the incubations with human liver microsomes (Table 3-3). Both male and female mouse liver microsomes generated product spectra that were subsets of the slate of metabolites observed in the human preparations, with females demonstrating slightly less conversion to the N-deschloroethyl 11β than males.

Drug-drug interaction potential

Results of the DDI screens are shown in Figure 3-13 and detailed in Table 3-4.

CYP2C8. 11β was shown to be a potent inhibitor of the metabolism of amodiaquine to desethylamodiaquine in microsomes from male rats and both genders of mice, with sub-micromolar IC_{50} values in mice and an IC_{50} of <5 μM in rats. However, 11β was ineffective at preventing the metabolism of amodiaquine when incubated with human liver microsomes.

CYP2C9. Diclofenac was extensively oxidized to 4'-hydroxydiclofenac in all microsomal preparations except for male mice, where ~2 μM 11β was sufficient to inhibit half of the conversion.

CYP2D6. The O-demethylation of dextromethorphan to dextrorphan was impeded by the presence of 11β in all systems, with 50% inhibition occurring at concentrations as under 0.5 μM in male mouse microsomal systems.

CYP1A2. Conversion of tacrine to 1-hydroxytacrine was rapid in all tissue preparations. No amount of 11β effected any change on the rate of tacrine metabolism, such that the IC_{50} curve fits for human and mouse microsomes would not converge.

CYP3A. Hydroxylation at the 6β position of testosterone proceeded readily in all tissues except for those derived from male rat livers. Pooled human liver microsomes were the most sensitive to 11β, where the IC_{50} was calculated as 1.25 μM. Both mouse genders showed 50% inhibition at micromolar concentrations of 11β as well.

Isoform elimination screen: Very few correlations could be extracted from the incubations of 11β with various competitor cocktails. In all cases, detection focused on the steroid side of the carbamate, assuming the formic acid carrier phase would keep the secondary amine protonated and guarantee detection in Q3. Fragments from the mustard side of the molecule were not observed. Results are summarized in Table 3-5. In all preparations, the most abundant products were those with monoisotopic m/z 714, 712, or 654, indicating that oxidations (or hydroxylations followed by dehydrations) and N-dealkylation were the major mechanisms. Interestingly, the location of the hydroxylations was more prominent on the mustard side of the carbamate, with transitions 357->398 and 366->398 dominating the intensity of the spectra of products with modifications on the steroid side of the carbamate.

Discussion

Extent of metabolism: 11β was metabolized extensively and rapidly by human and mouse liver microsomes yet only modestly by rat liver microsomes. All conversions were dependent on the presence of NADPH; half-hour incubations in either human or rat microsomes lacking NADPH left more than 90% of the parent compound intact, in contrast with the previously shown rapid decomposition of 11β in the metabolism solution lacking microsomes. The protective effect of a macromolecular compartment onto which 11β could adsorb to escape hydrolysis was pronounced. Gender had minimal effect on metabolism, which may not be of immediate importance in view of prostate cancer, but would be important to characterize should 11β prove promising against cancers outside the prostate.

Product spectrum of 11β: The complexity of 11β as a potentially multifunctional drug candidate necessarily increases the number of transformation events it may experience between administration and clearance. With high lipophilicity, nine heteroatoms, an aromatic ring, and a conjugated carbonyl, few loci on the molecule are not putative substrate sites for modification by P450. The comparison of 11β to its constituent pharmacophores chlorambucil and testosterone led to the hypothesis that many reactions would occur, which was confirmed by the diverse array of derivative species observed in experiments with both radiolabeled and cold material. Additive and subtractive transformations were observed in all regions of the molecule. Hydrolytic degradation and enzymatic catabolism of the mustard arms generates a series of derivates incapable of DNA crosslinking. Oxidations of at least four distinct loci as well as multiple oxidations on the same molecule give a group of products easily separable by HPLC and likely possessing different affinities for the AR. Furthermore, the detection of products that had undergone both oxidation and mustard decomposition indicates that there is, in effect, a combinatorial array of products arising from metabolism with P450.

The metabolic reactions catalyzed showed only a few consistent signatures: +16, from addition of an oxygen; -2, from oxidation of a single bond to a double bond; -18, dehydration; and -62, N-dechloroethylation. Combinations of these transformations

generate an array of putative products, several of which were observed (Figure 3-14). Hydrolysis was not a significant source of decomposition given the timescale and composition of these experiments. However, it is reasonable to expect that the timescale of hydrolysis would be relevant during an *in vivo* treatment. As such, each of the additive metabolic products would also yield a set of corresponding hydrolyzed analogs, such that the 716->698->680->662->644 sequence observed in the sequential hydrolysis of the chloroethyl arms described in Chapter 2 would manifest as 732->714->696->678->660 or 748->730->712->694->676, representing the incremental hydrolytic mustard decompositions on singly- and doubly-oxidized species, respectively. Even though the replacement of a chlorine atom with a hydroxyl group has the same net change in mass as dehydration (-18), the loss of chlorine isotope character associated with the former transformation allows the distinction between the two by mass spectrometry. In all species, the most common transformation was to m/z 732, indicating hydroxylation of 11β but persistence of intact dichloro mustard capable of forming DNA crosslinks

The atomic composition of a daughter species can be derived from the mass-to-charge ratio and isotope pattern of its spectrum. The change in molecular weight from parent compound indicates the series of reaction or reactions that gave rise to that particular molecule. However, the ability to pinpoint the locations of the modifications depends on more advanced techniques. Preliminary attempts to glean some structural understanding from the mass spectra were made based on the consistency of the conditions used in the QQQ to fragment 11β and its derivatives at the carbamate linker, sending the steroid half of the molecule into Q3 for detection. If a particular metabolite contained a moiety that changed the m/z of the Q3 fragment, the location of the modification could at least be assigned to the steroid half of the molecule. If, on the other hand, an 11β derivative yielded a Q3 of 398.3, identical to parent, then any modifications must have occurred on the mustard half of the molecule. Samples of MRM spectra illustrating this behavior are shown in Figure 3-15. Analysis of fragmentation patterns suggested that more modification was occurring on the mustard half of the molecule than on the steroid half, which was surprising in light of the original hypothesis that the steroid ring system would be the main target of oxidation.

Drug-drug interaction screen: Tracking N-dealkylation in amodiaquine, O-demethylation of dextromethorphan, and hydroxylation of testosterone and the phenyl ring in diclofenac, the DDI screens confirmed that 11β would likely compete for the binding sites of several important isoforms of P450. 11β demonstrated such negligible interaction with CYP1A2 that tacrine was omitted from the isoform elimination screen, replaced instead by S-mephenytoin, the standard substrate for CYP2C19. Because both *in vivo* and *in vitro* toxicity studies performed with 11β involve drug treatments up to 10 μM in media or plasma, IC_{50} levels below this level were considered noteworthy. The abundance of deschloroethyl 11β in the *in vitro* metabolism assays analyzed by ESI-TOF and the degree to which 11β inhibited the formation of desethylamodiaquine and dextrorphan suggest that CYP2C8 and CYP2D6 may be important isoforms in the deactivation of the DNA crosslinking ability of the compound. Similarly, the marked inhibition of the formation 6β-hydroxytestosterone indicates that CYP3A4 may catalyze any or all of the hydroxylation products of 11β that were observed.

Isoform-product specificity: Little correlation was observed between the product spectra and the elimination of specific isoforms. This result can be interpreted in several ways: a) 11β is a substrate for other isoforms not inhibited by the cocktail and the level of background conversion rendered parsing of the contributions of the individual isoforms impossible; b) 11β is a substrate for all of the isoforms tested and the sets of loci at which the individual isoforms can catalyze a reaction are overlapping; c) the limited structural information available was not sufficient to distinguish distinct modification locations on products with the same m/z signal; or d) inhibition was so extensive that the signals observed were below the noise threshold for quantitative analysis.

Future directions: The relative insolubility of 11β in aqueous systems and the scarcity of radiolabeled material presented limitations as to the design of *in vitro* experiments that quantify conversion, but are even more profound when contemplating *in vivo* metabolic exploration. The rapid conversion of 11β to its daughter species in the presence of microsomes demonstrates the existence of a vast combinatorial array of products with different solubilities, AR affinities, and DNA binding capabilities. As such, it is

reasonable to expect that individual members of the spectrum of 11β species arising in that system may have distinct levels of cytotoxic activity.

In order to more precisely characterize the location and disposition of the observed metabolic transformations, it would be necessary to use nuclear magnetic resonance (NMR) or ion trap mass spectrometry (MS^n). For NMR, a larger amount of material and more elaborate purification schemes would be essential in assuring interpretable spectra. In contrast to metabolic studies on commercially-available compounds, the limited supplies of radiolabeled 11β for quantitative *in vivo* studies and unlabeled 11β for NMR and/or mass spectrometry force significant constraints on experimental design. Ion trap mass spectrometry in tandem with more effective chromatography would help elucidate the locations of hydroxylations, as sequential fragmentations of species with the same m/z but separate elution times could help solve the structures of the metabolites.

Finally, the potential for metabolites maintaining bifunctional DNA alkylation ability to create DNA adducts with m/z signatures distinct from those previously analyzed must be explored. It is consistent with the hypothesis governing the design of the compound that modifications to the steroid ring will alter receptor affinity, which may affect the kinetics of both repair of lesions and formation of crosslinks. Quantitative adduction studies by accelerator mass spectrometry (AMS)[31] do not distinguish adducts based on the molecular weight of the alkylating species. Monoadducts and crosslinks derived from both 11β and its metabolic derivatives may be generating the ^{14}C signals measured in those experiments. While it would be impractical to attempt to synthesize hypothetical 11β derivatives in order to generate standards for comparison, the sophistication of the mass spectrometric techniques available in the Tannenbaum Laboratory would certainly enable the detection of adducts generated by 11β metabolites.

Figure 3-1: Putative modification loci on 11β

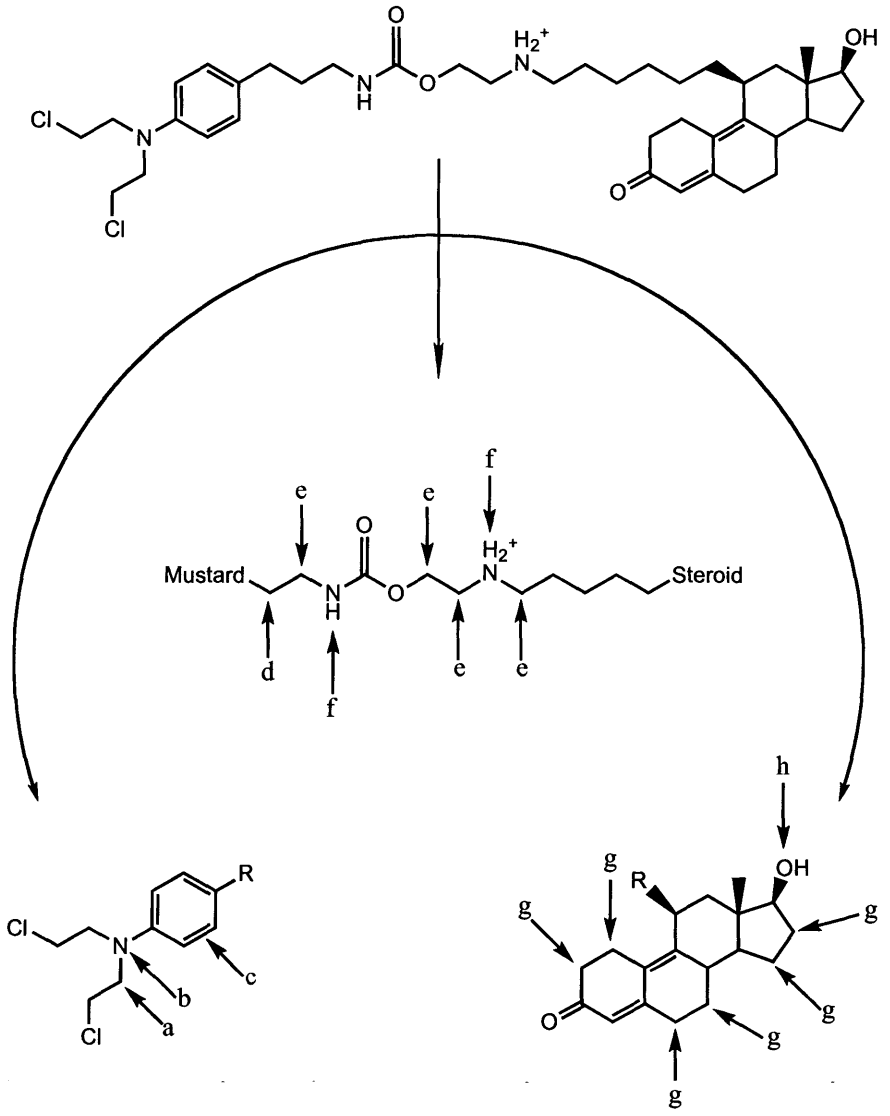

Dichloro 11β, comprising an aniline mustard, linker with carbamate and secondary amine, and steroid ring, is susceptible to numerous modifications by P450. On the mustard, 11β may be a substrate for a) oxidation alpha to nitrogen leading to dealkylation; b) oxidation of the nitrogen; c) epoxidation of the phenyl ring. The linker may experience d) β-oxidation similar to that seen in chlorambucil metabolism; e) oxidation alpha to heteroatoms; f) oxidation of nitrogens. Steroid metabolism catalyzed by P450 has been observed at g) the 1, 2, 6, 7, 15, and 16 positions, most of which can be attacked on either face; and h) oxidation of the 17-hydroxyl group to a ketone. It was assumed that hydroxylation at the 11 position observed by Choi et al.[13] would be sterically hindered by the attached linker. Oxidations on the steroid system leading to extensions of the conjugated 3-keto group were expected in hopes of altering the UV absorption spectrum of the molecule.

Figure 3-2: Chlorambucil metabolism

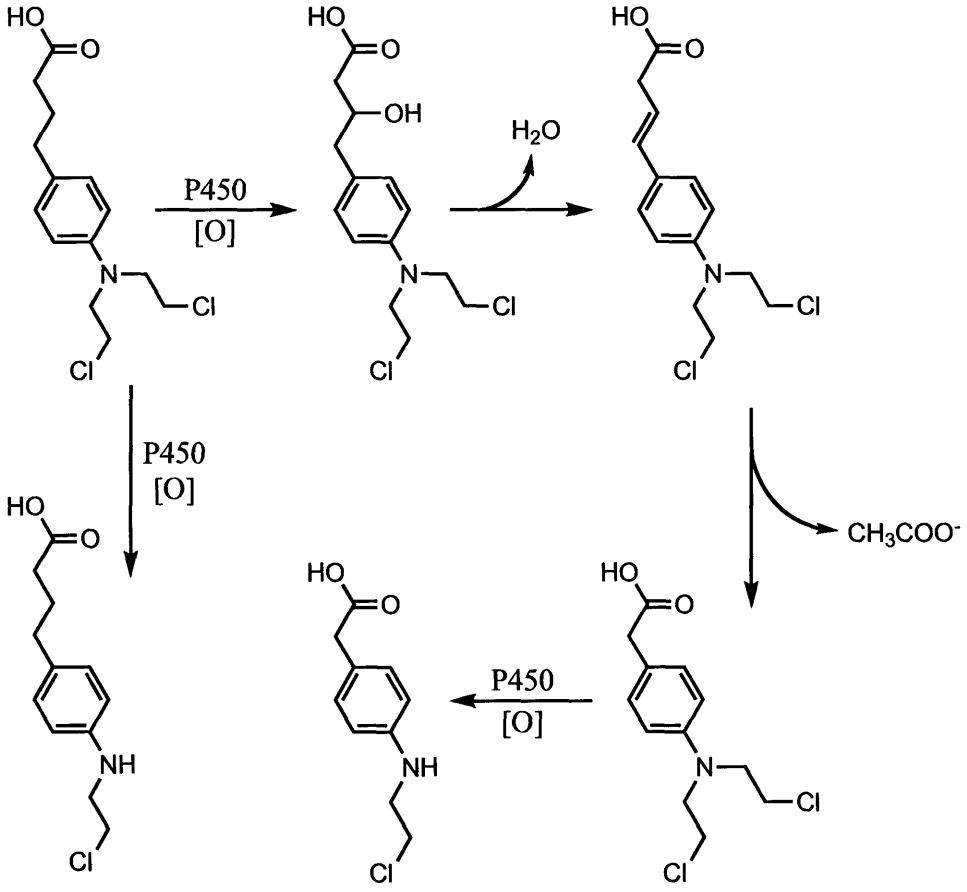

Chlorambucil (top left) undergoes P450-catalyzed 11β-oxidation and dehydration to 4-[4-bis(2-chloroethyl)aminophenyl]but-3-enoic acid. This intermediate decomposes to phenylacetic acid mustard (PAAM, bottom right). Both chlorambucil and PAAM are subject to N-dechloroethylation to their corresponding monofunctional products. Adapted from Pettersson-Fernholm et al.[32]

Figure 3-3: Testosterone Metabolism

Testosterone is extensively metabolized by CYP3A4 at several loci. These daughter compounds are easily separated by reversed-phase HPLC[33]. Oxidation of the ring system generally abrogates AR affinity (androstenedione RBA=0.24)[11].

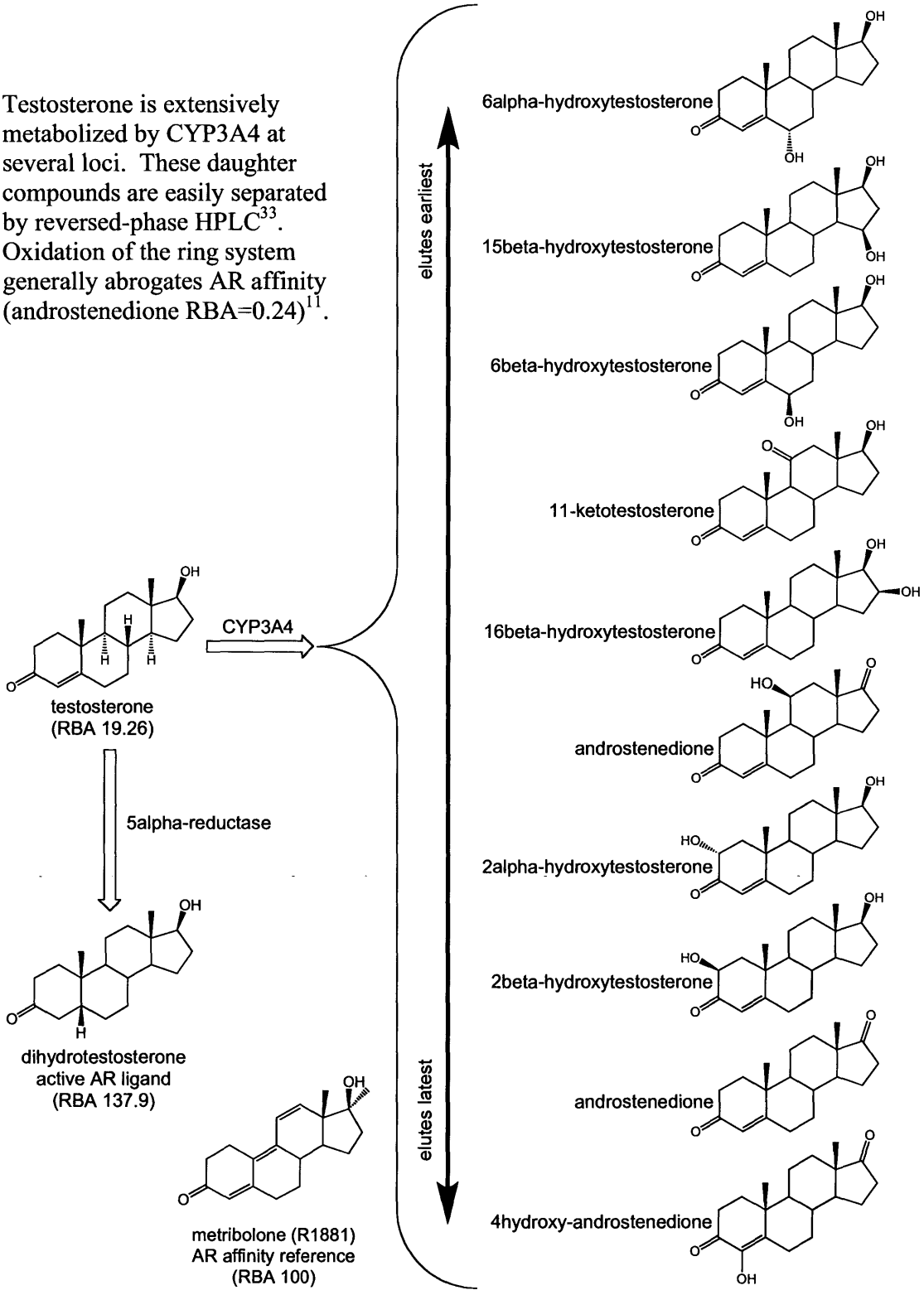

Figure 3-4: DDI probes and their tracked metabolites

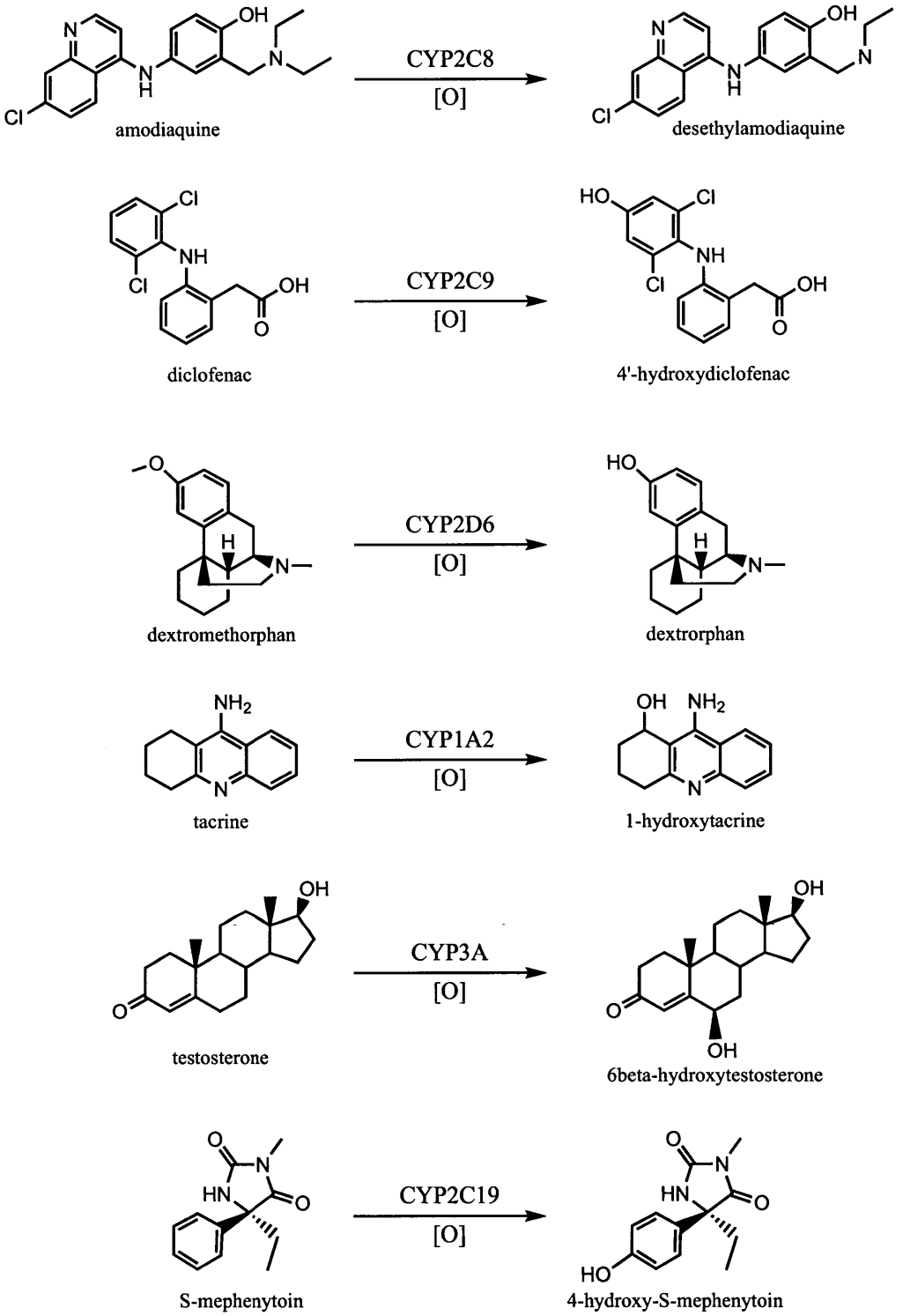

Figure 3-5: 11β metabolite fragmentation patterns

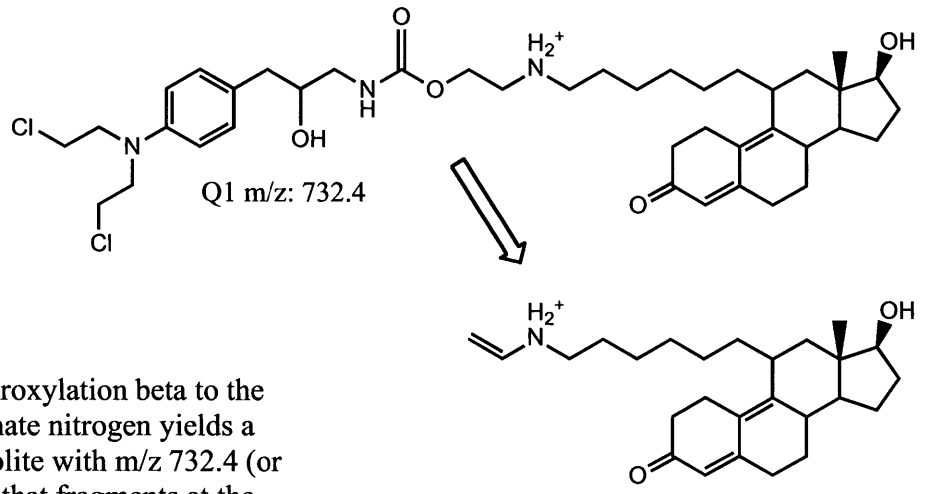

a) Hydroxylation beta to the carbamate nitrogen yields a metabolite with m/z 732.4 (or 366.9) that fragments at the carbamate to yield the steroid half of the molecule with m/z 398.3, identical to unmodified 11β.

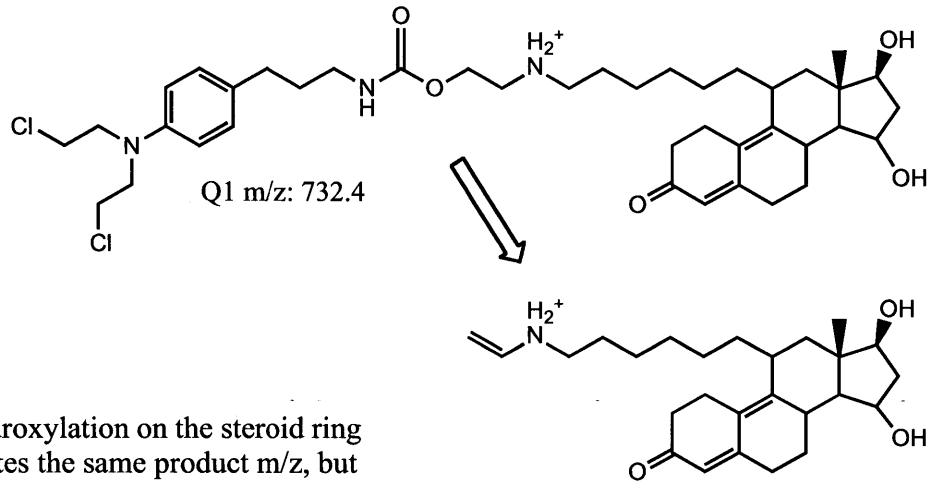

b) Hydroxylation on the steroid ring generates the same product m/z, but fragmentation reveals the location of the metabolic reaction in the Q3 fragment.

Figure 3-5: 11β metabolite fragmentation patterns

c) Metabolites with multiple modifications may yield different Q3 fragments from the same Q1 signal. For example, the species with m/z 748.4 indicates two added oxygen atoms, but may yield fragments with zero (398.3), one (414.3), or two (430.3) oxygens added to the steroid half of the molecule, thus also elucidating the composition of the mustard half.

Q1 m/z: 748.4

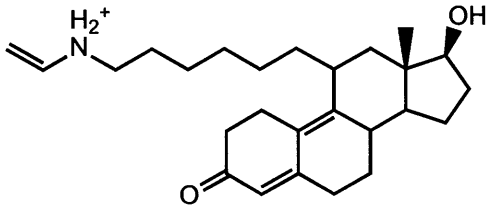

Q3 m/z: 398.3

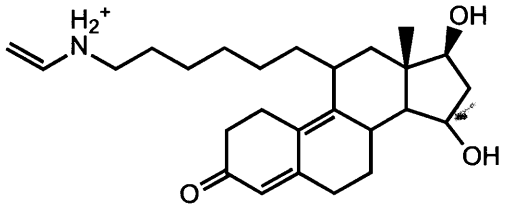

Q3 m/z: 414.3

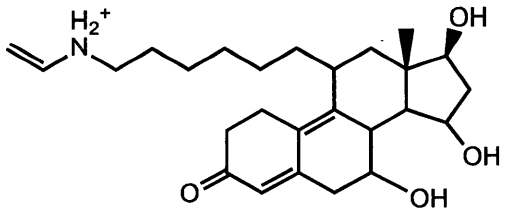

Q3 m/z: 430.3

Figure 3-6: Conversion of 11β in pooled human liver microsomes (1 mg/mL) requires NADPH

a) Incubation with microsomes and no NADPH yielded minimal conversion of parent compound.

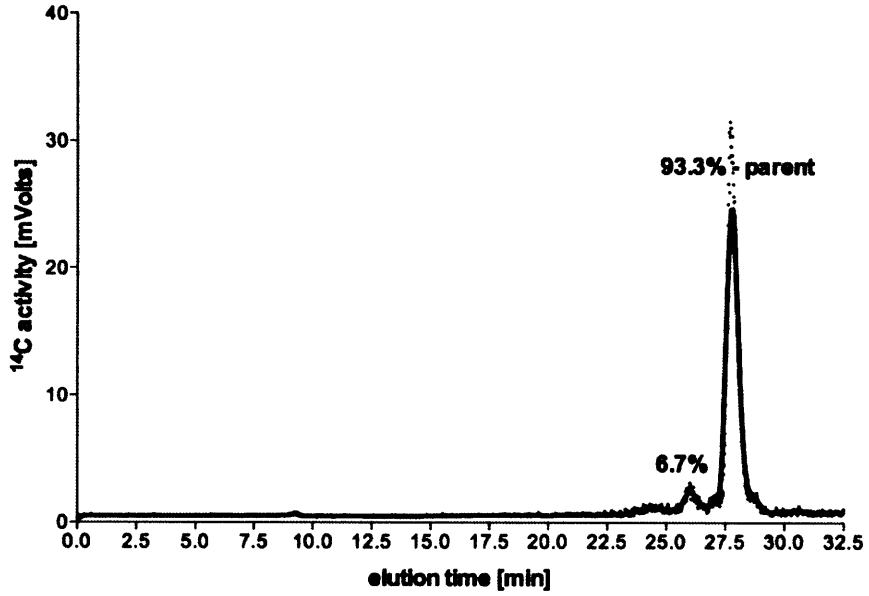

b) With cofactors, the human liver microsomes were potent metabolizers of 11β, achieving ~95% conversion in thirty minutes and generating over a dozen distinct daughter species.

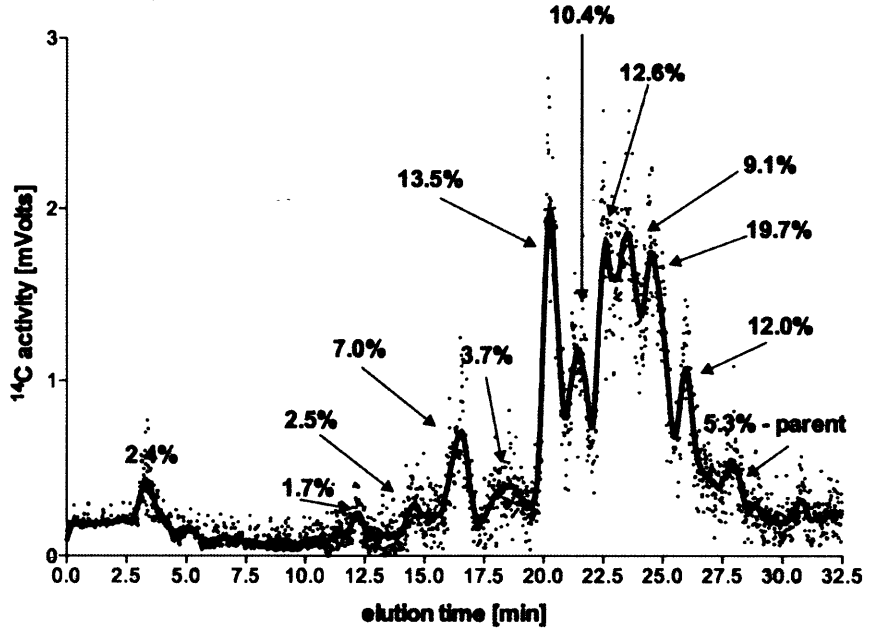

Figure 3-7: Conversion of 11β in male rat liver microsomes (1 mg/mL) depends on the presence of NADPH

a) Without NADPH, minimal product formation is observed after thirty minutes.

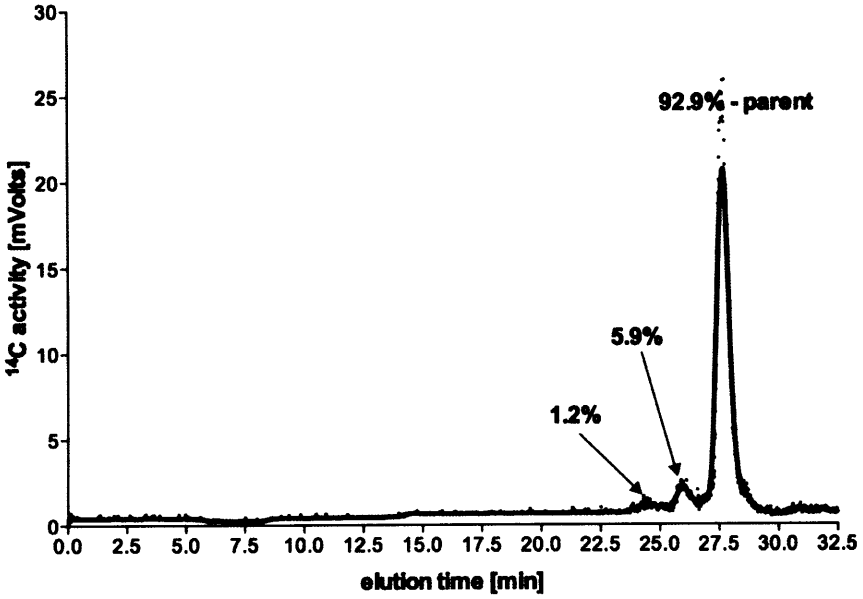

b) Inclusion of NADPH regeneration machinery allows significant metabolite formation, but the diversity of the product spectrum does not compare to that generated by human liver microsomes.

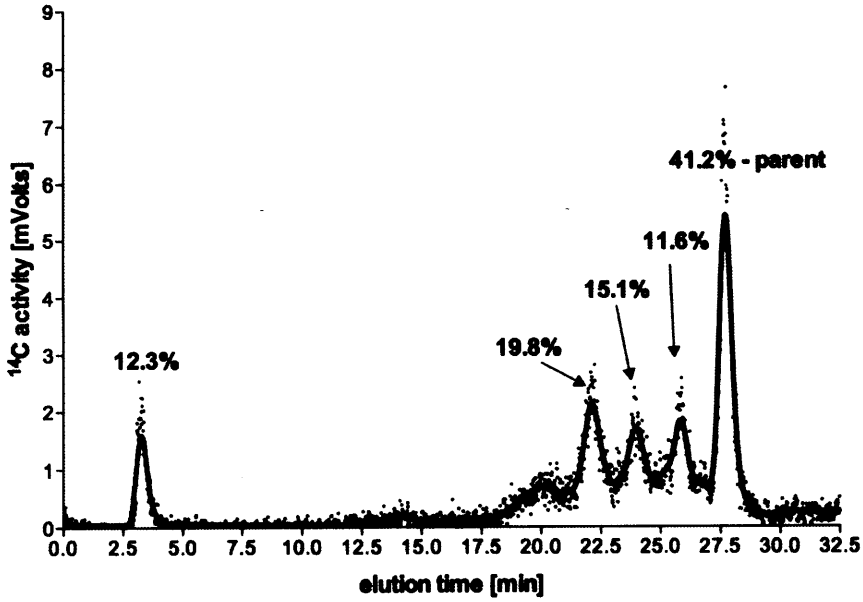

Figure 3-8: Conversion of 11β in pooled human liver microsomes (0.5 mg/mL) with NADPH regeneration system

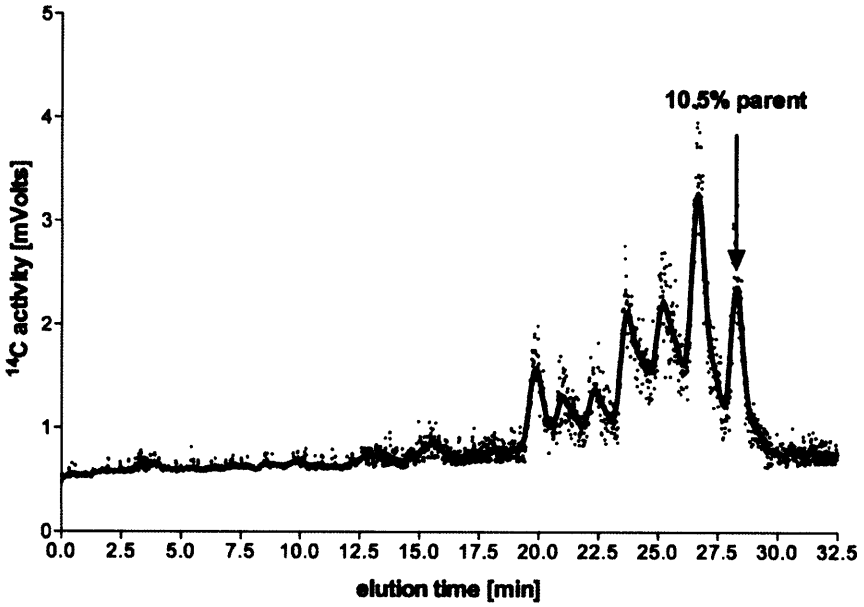

Halving the protein content from the initial reaction conditions reduced both total conversion of 11β and the diversity of the spectrum of products.

Figure 3-9: Reaction of 11β with various amounts of male mouse liver microsomes

a) A protein concentration of 0.5 mg/mL is sufficient to catalyze the conversion of >96% of parent compound

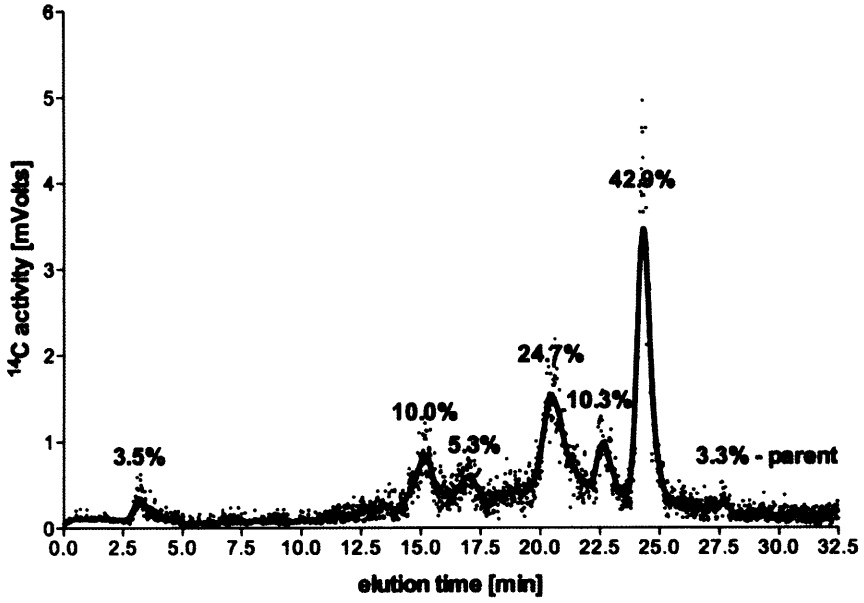

b) Dilution to 0.25 mg/mL shifts product spectrum but does not appreciably the change extent to which 11β is metabolized

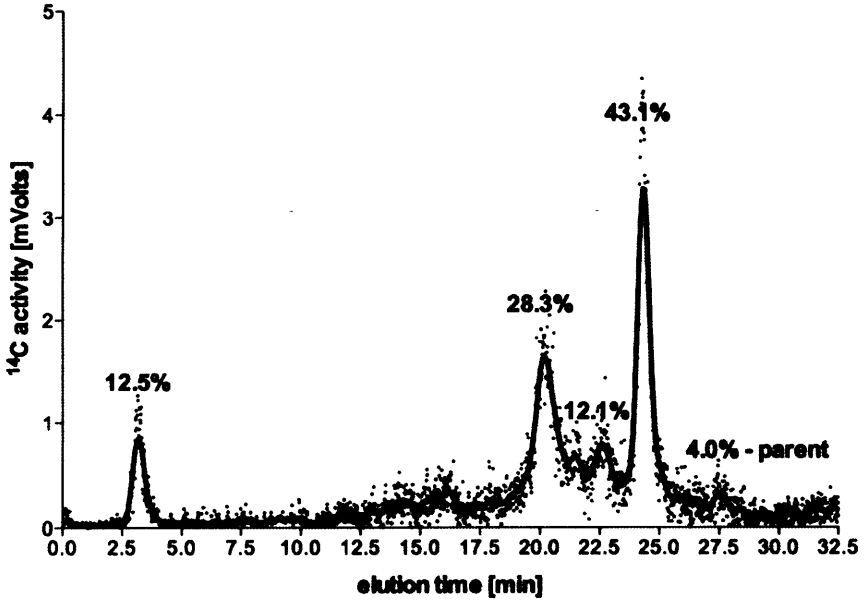

Figure 3-9: Reaction of 11β with various amounts of male mouse liver microsomes

c) At 0.125 mg/mL of protein, three-quarters of the starting material have been metabolized

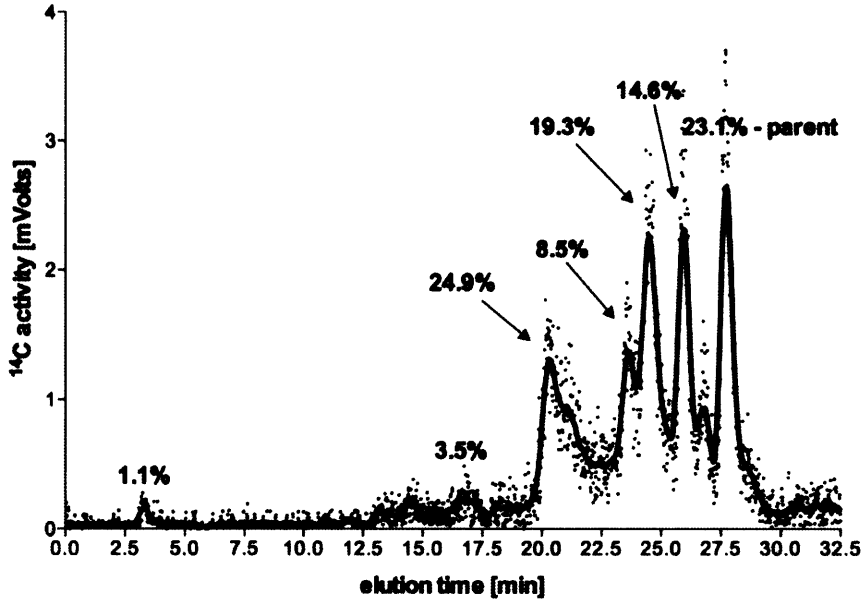

d) A thirty-minute incubation with 0.0625 mg/mL of protein is sufficient to convert nearly half of 11β to products

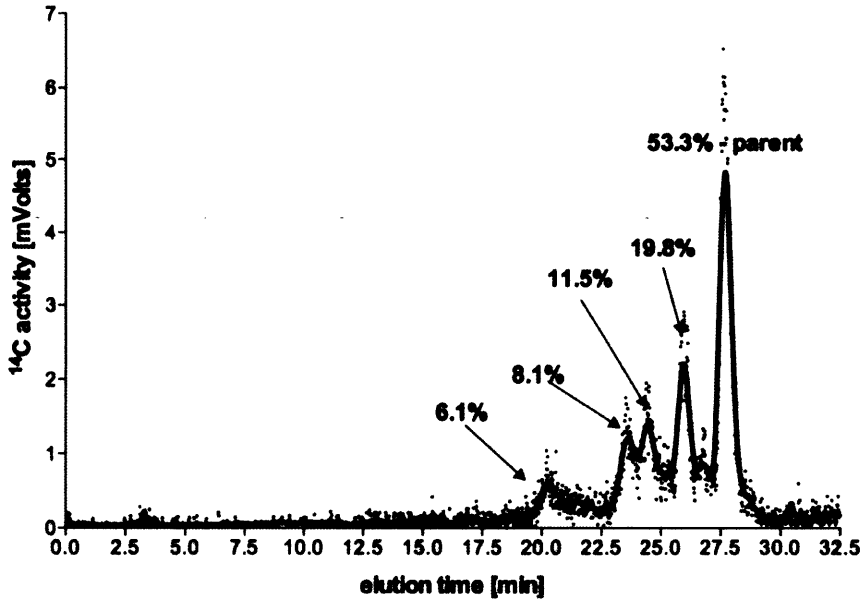

Figure 3-10: Kinetics of 11β conversion in male mouse liver microsomes (0.25 mg/mL with NADPH)

a) 5 minutes after initiation

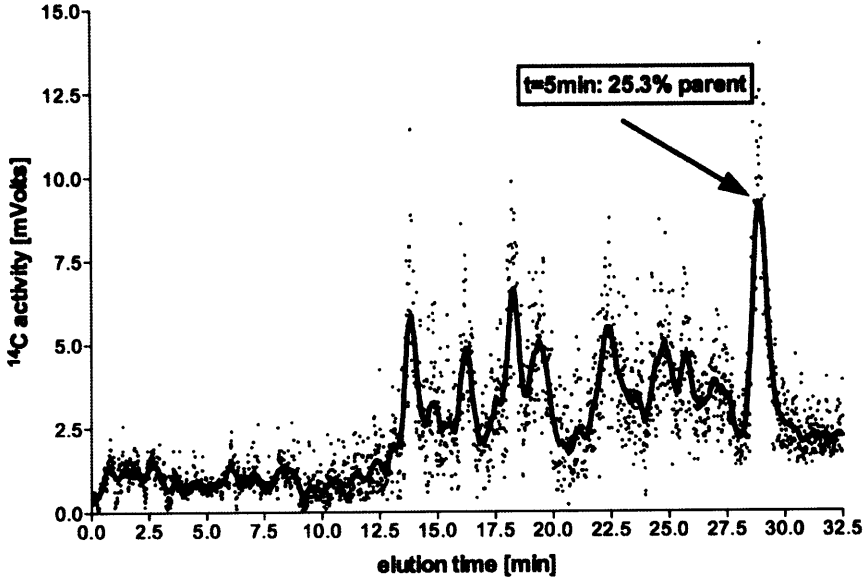

b) 8 minutes

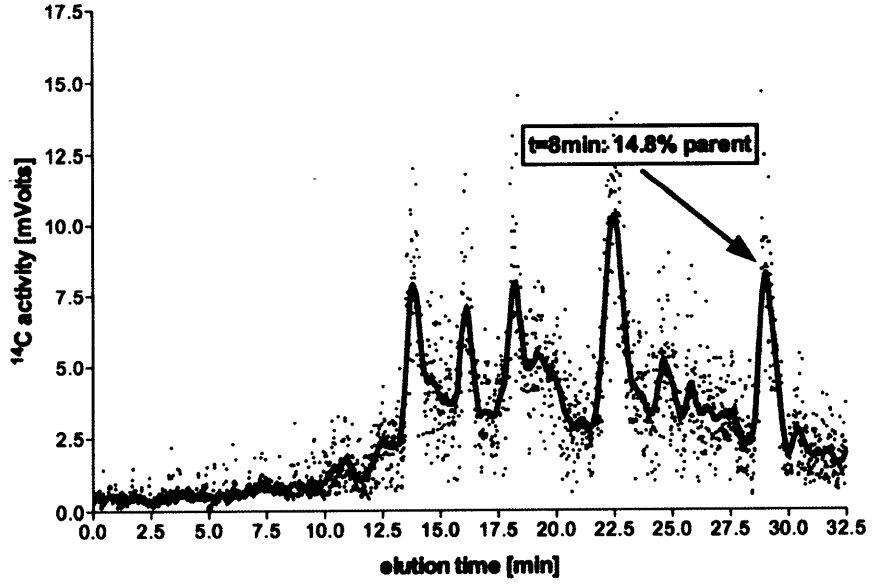

Figure 3-10: Kinetics of 11β conversion in male mouse liver microsomes (0.25 mg/mL with NADPH)

c) 15 minutes

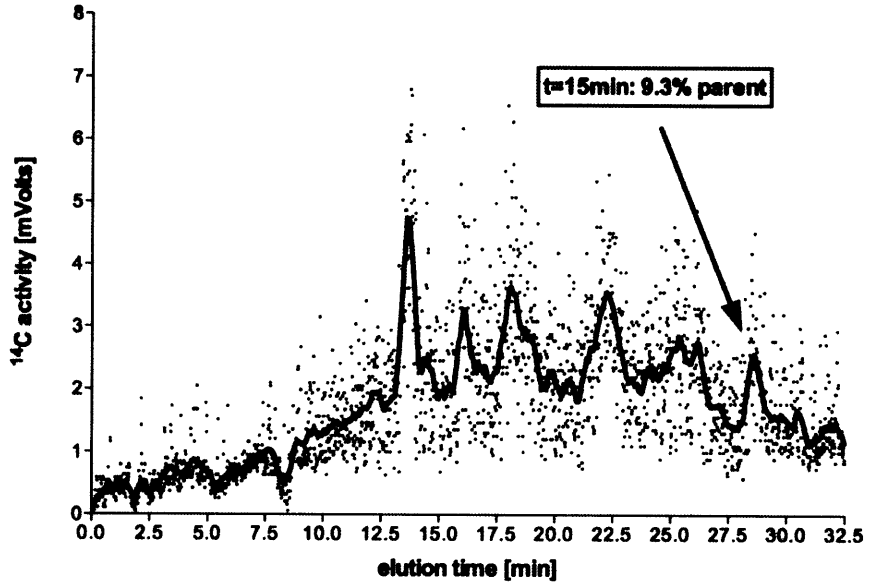

d) 22 minutes

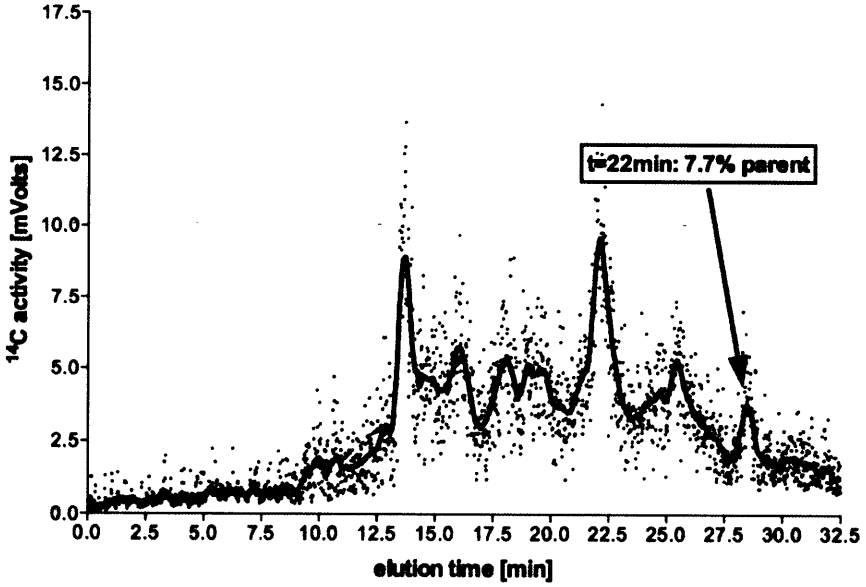

Figure 3-10: Kinetics of 11β conversion in male mouse liver microsomes (0.25 mg/mL with NADPH)

e) 30 minutes

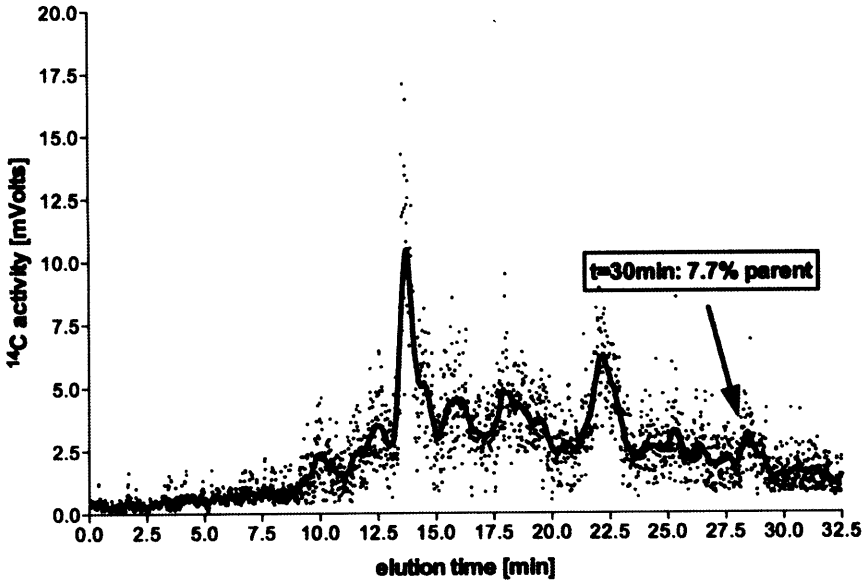

f) Parent disappeared over time with first-order kinetics and a half life of 2.1 minutes.

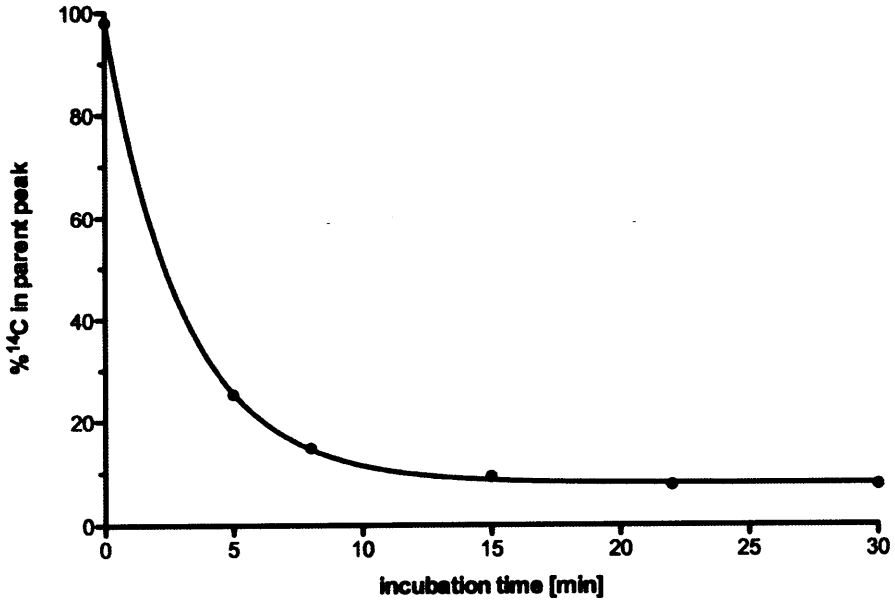

Figure 3-11: Comparison of 11β conversion in male vs. female mouse liver microsomes

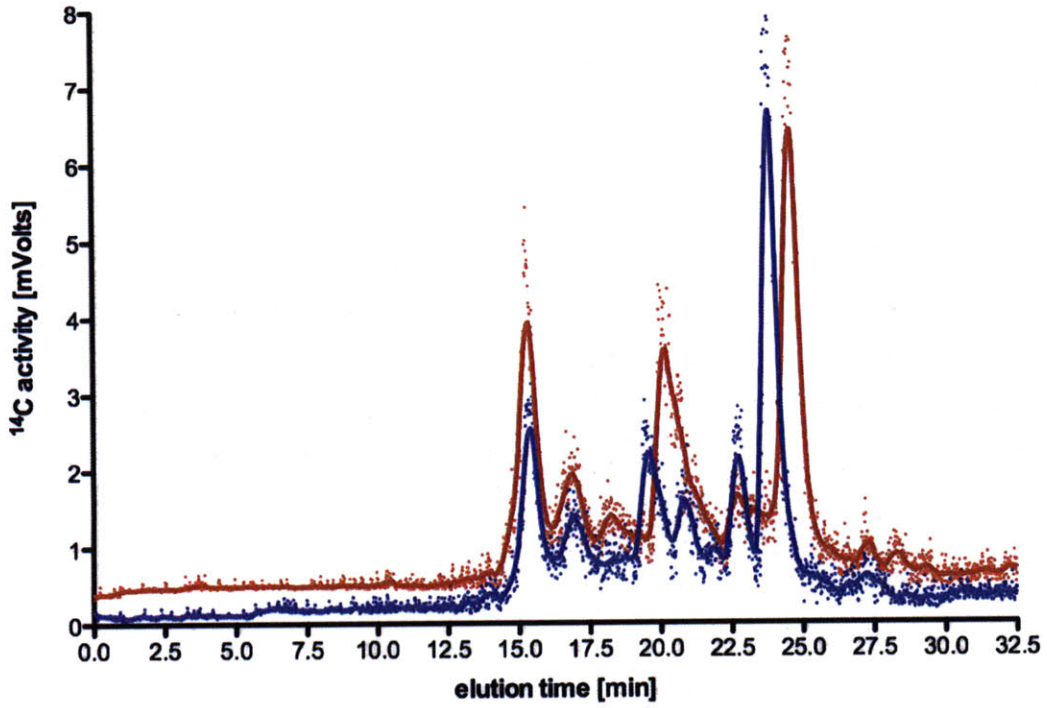

Male (blue) and female (red) mouse liver microsomes prepared in house displayed nearly identical extents of conversion of 11β in thirty minutes at 1 mg/mL total protein, with <2% parent compound remaining in either reaction. Subtle differences in the elution times of the major product eluting at ~24 minutes is likely a single hydroxylation at distinct loci.

Figure 3-12: Extracted ion chromatograms (XIC) of 11β daughter species

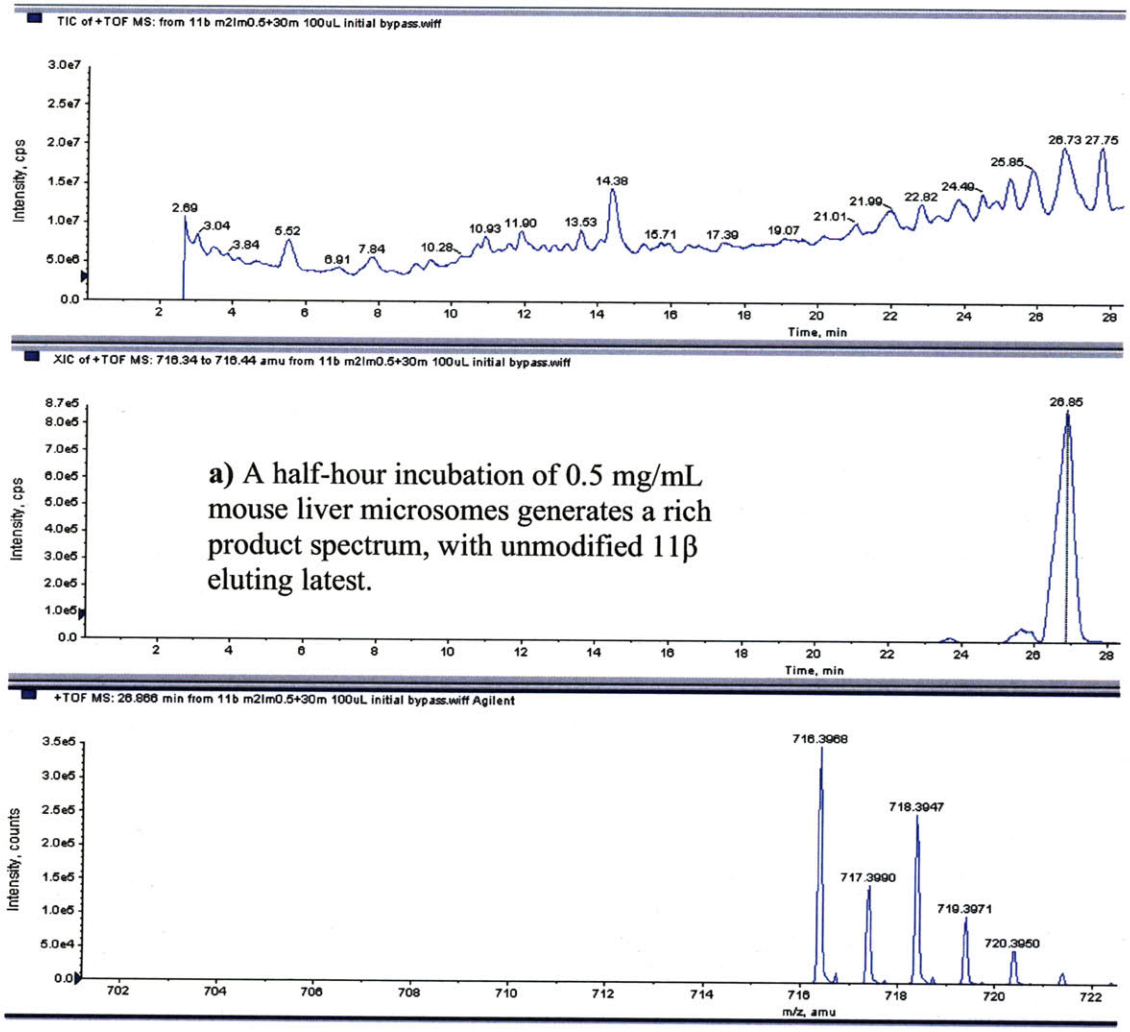

Figure 3-12: Extracted ion chromatograms (XIC) of 11β daughter species

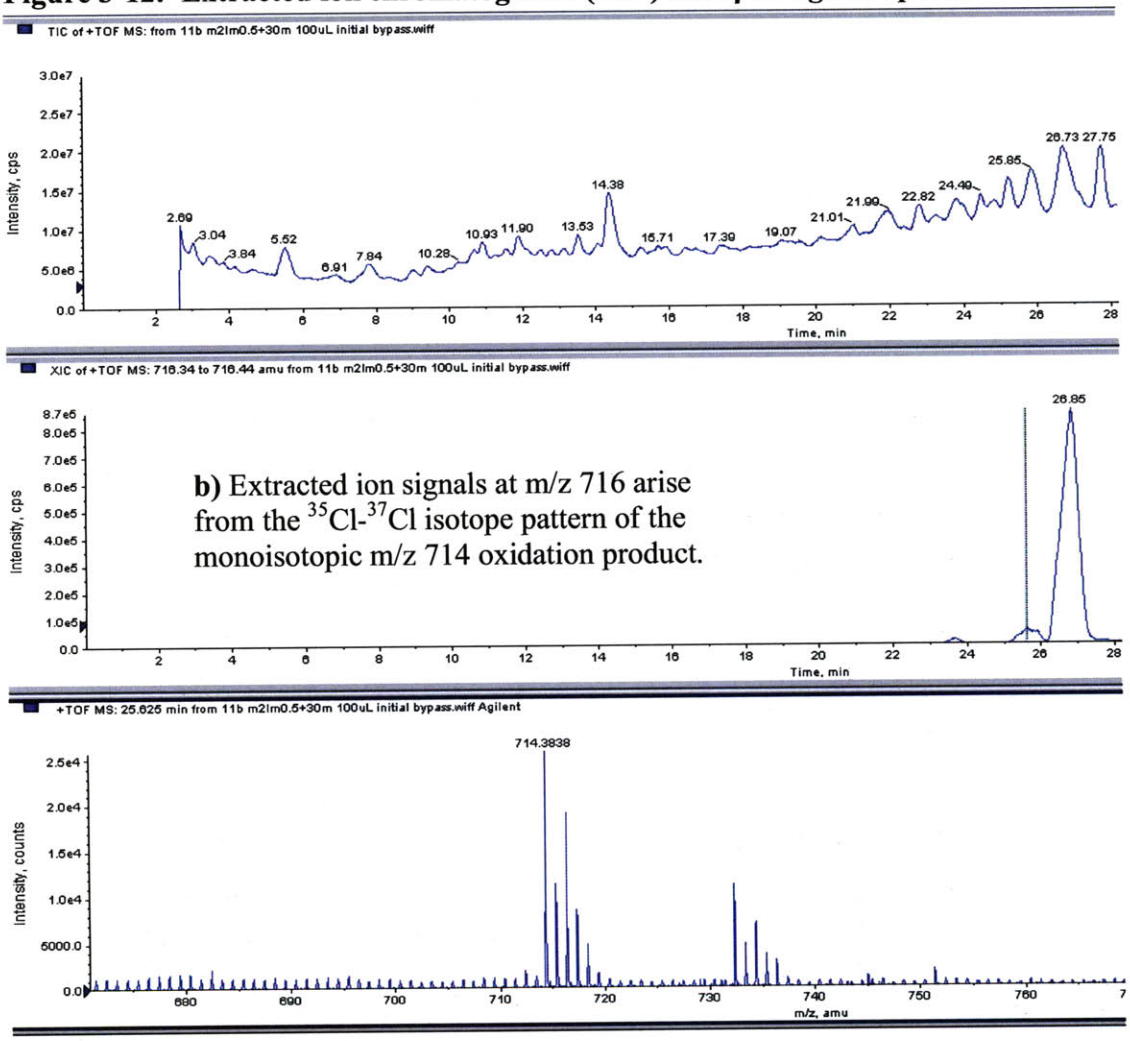

Figure 3-12: Extracted ion chromatograms (XIC) of 11β daughter species

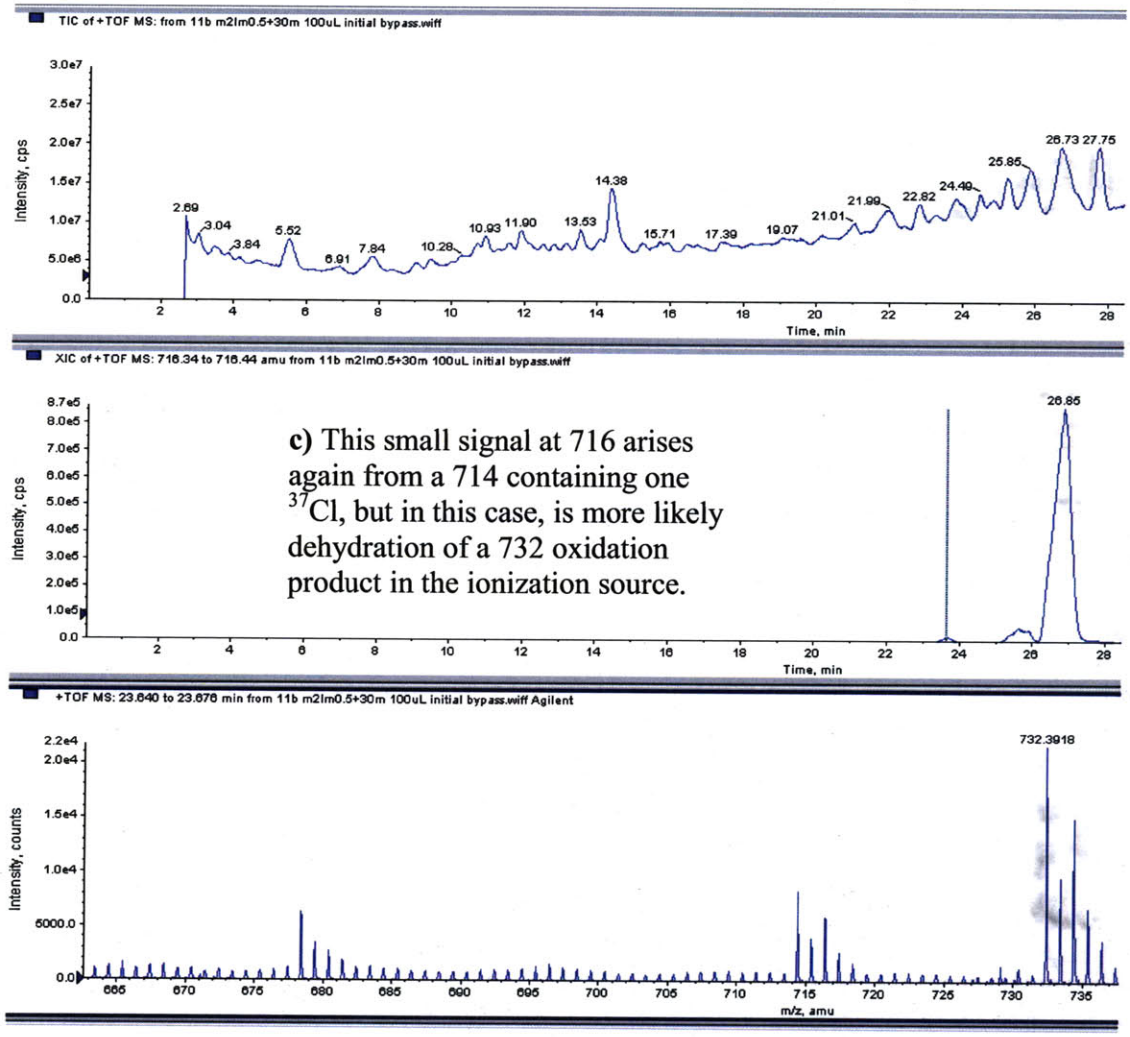

Figure 3-12: Extracted ion chromatograms (XIC) of 11β daughter species

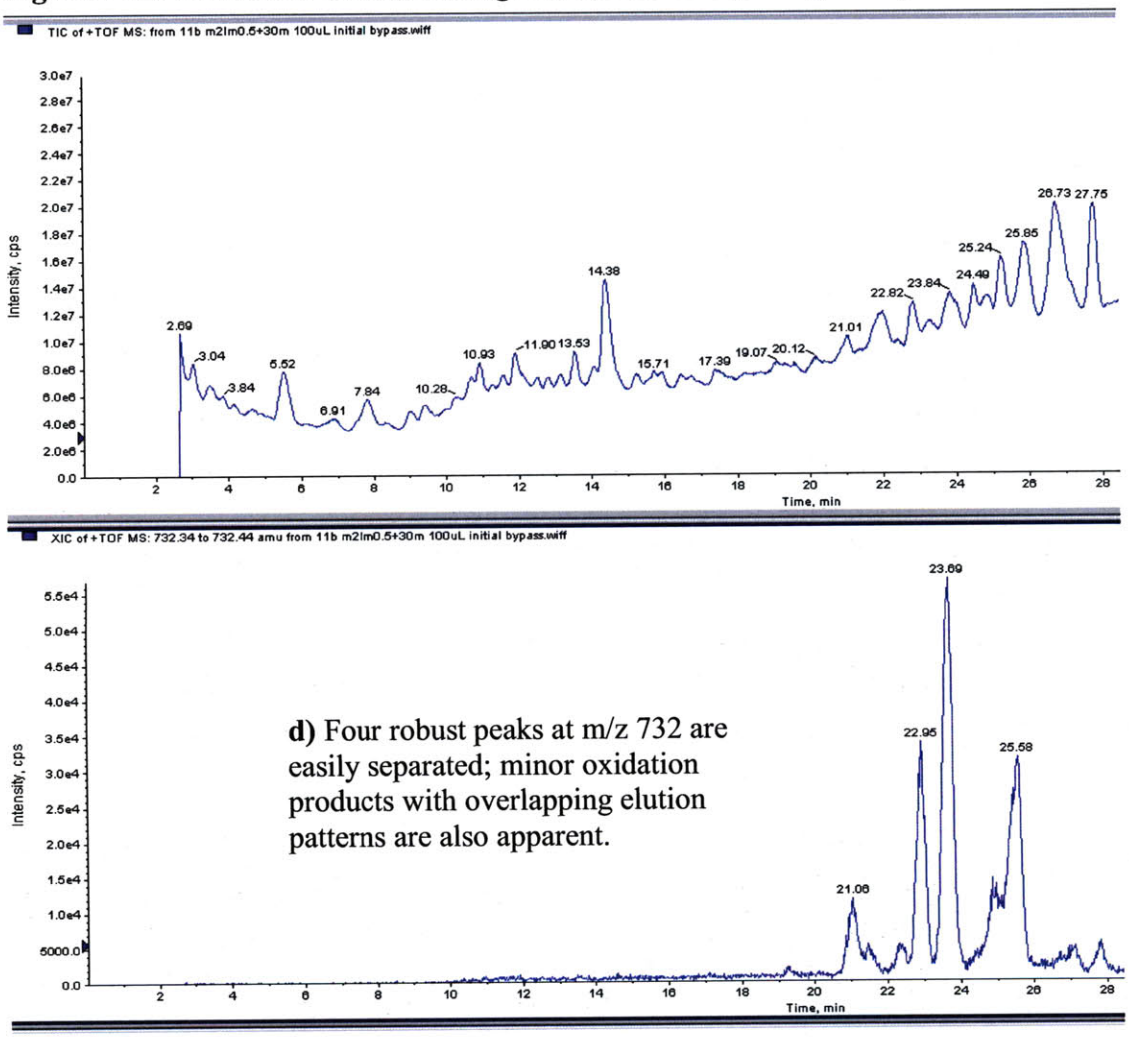

Figure 3-12: Extracted ion chromatograms (XIC) of 11β daughter species

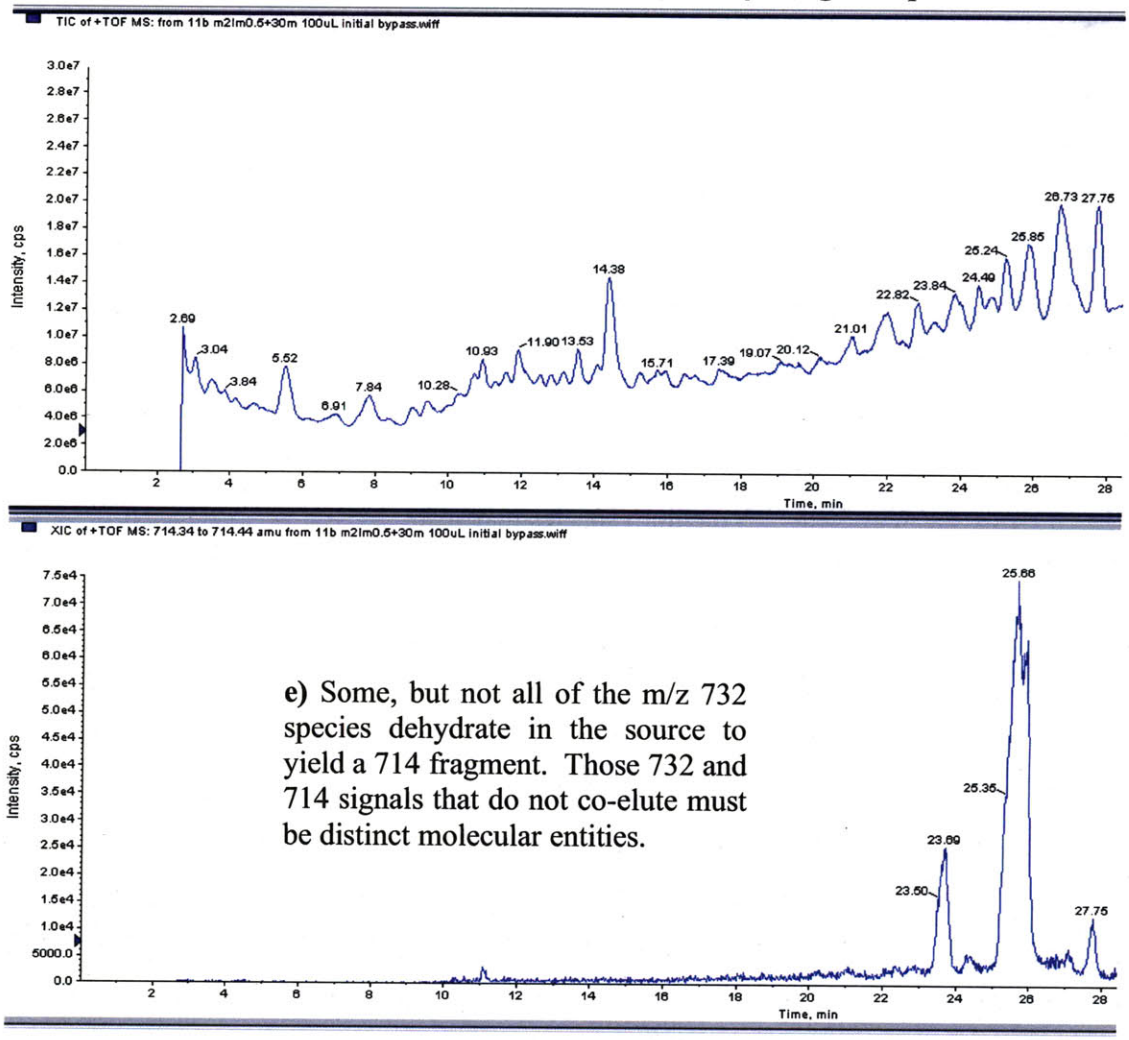

e) Some, but not all of the m/z 732 species dehydrate in the source to yield a 714 fragment. Those 732 and 714 signals that do not co-elute must be distinct molecular entities.

Figure 3-12: Extracted ion chromatograms (XIC) of 11β daughter species

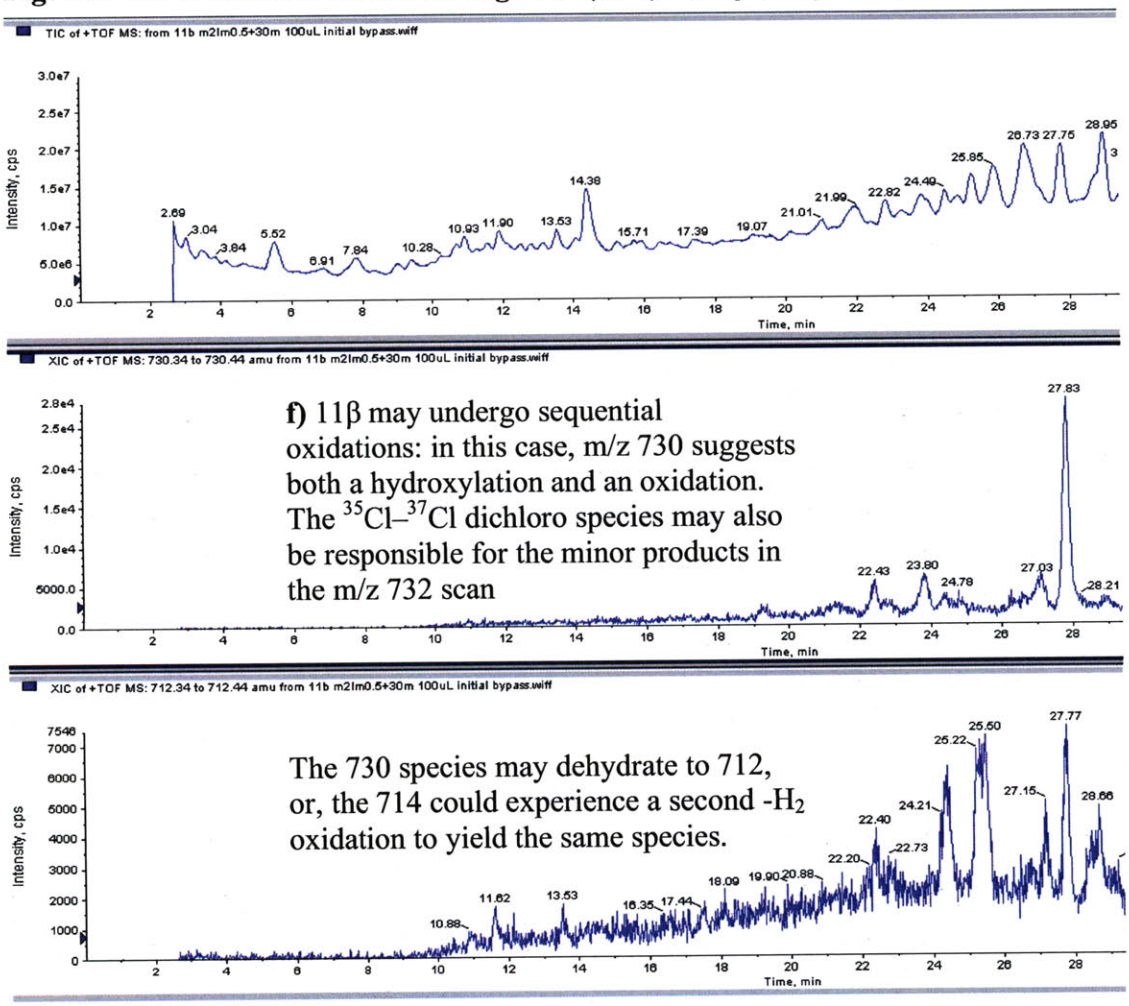

Figure 3-12: Extracted ion chromatograms (XIC) of 11β daughter species

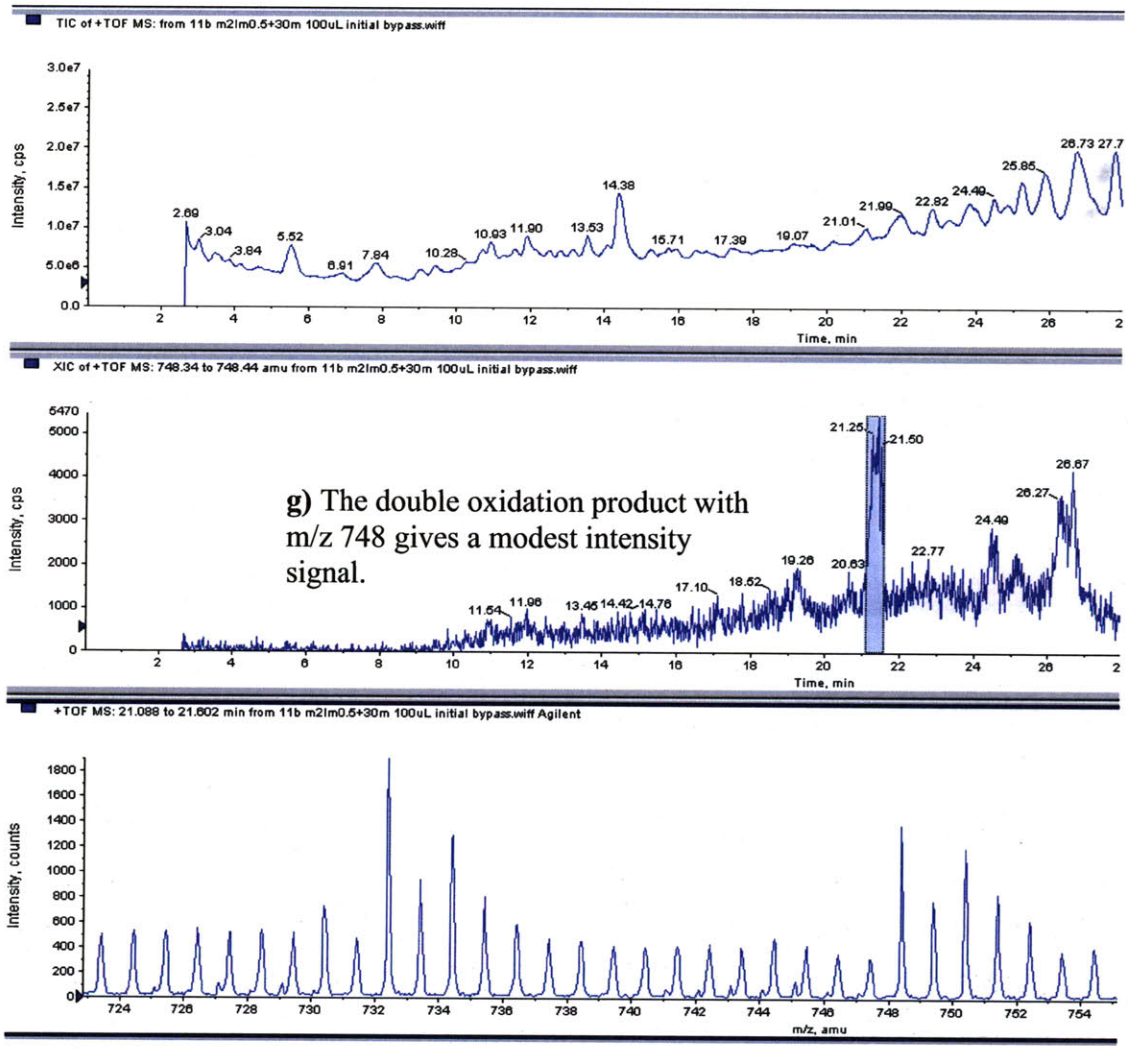

Figure 3-12: Extracted ion chromatograms (XIC) of 11β daughter species

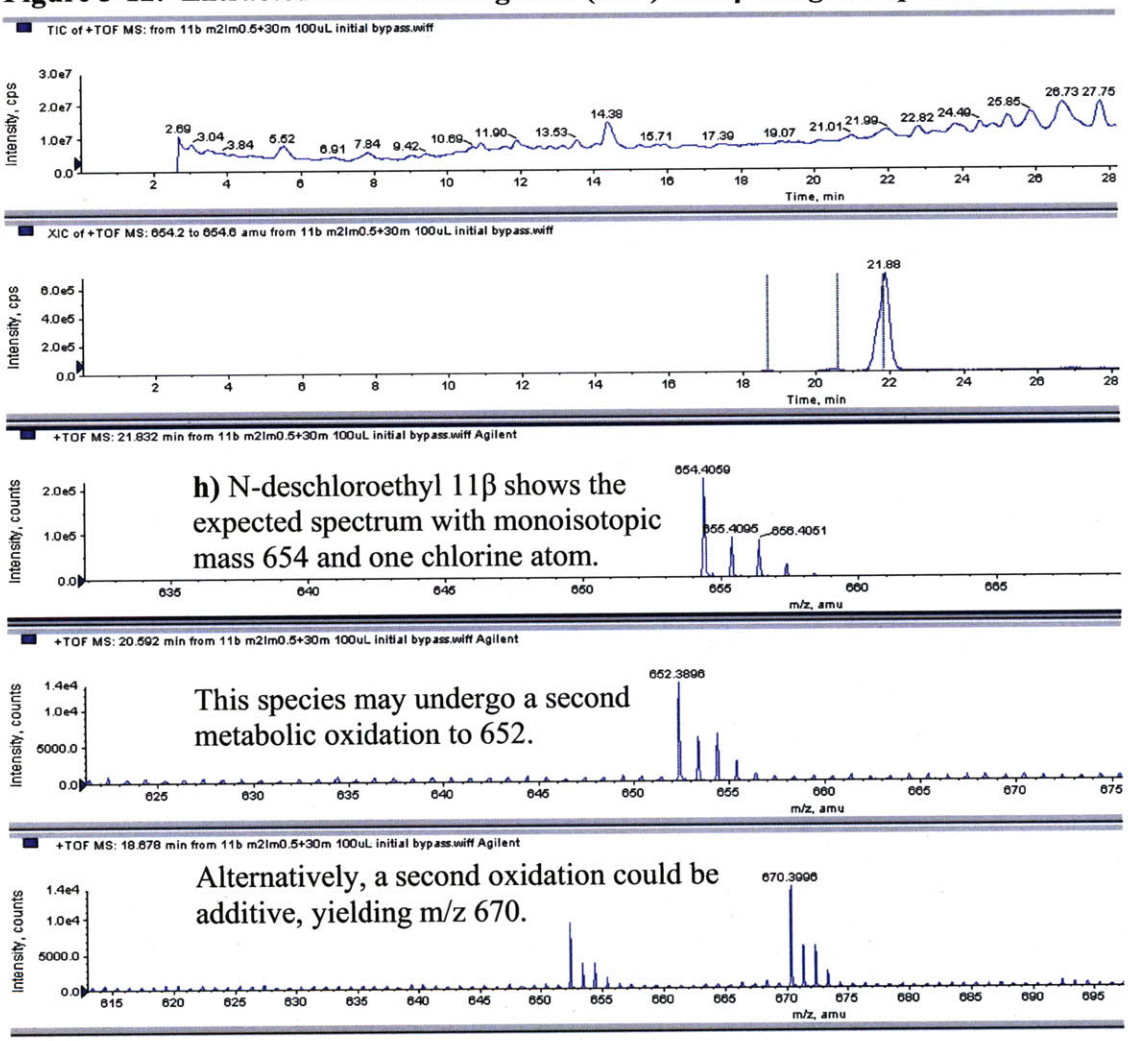

Figure 3-12: Extracted ion chromatograms (XIC) of 11β daughter species

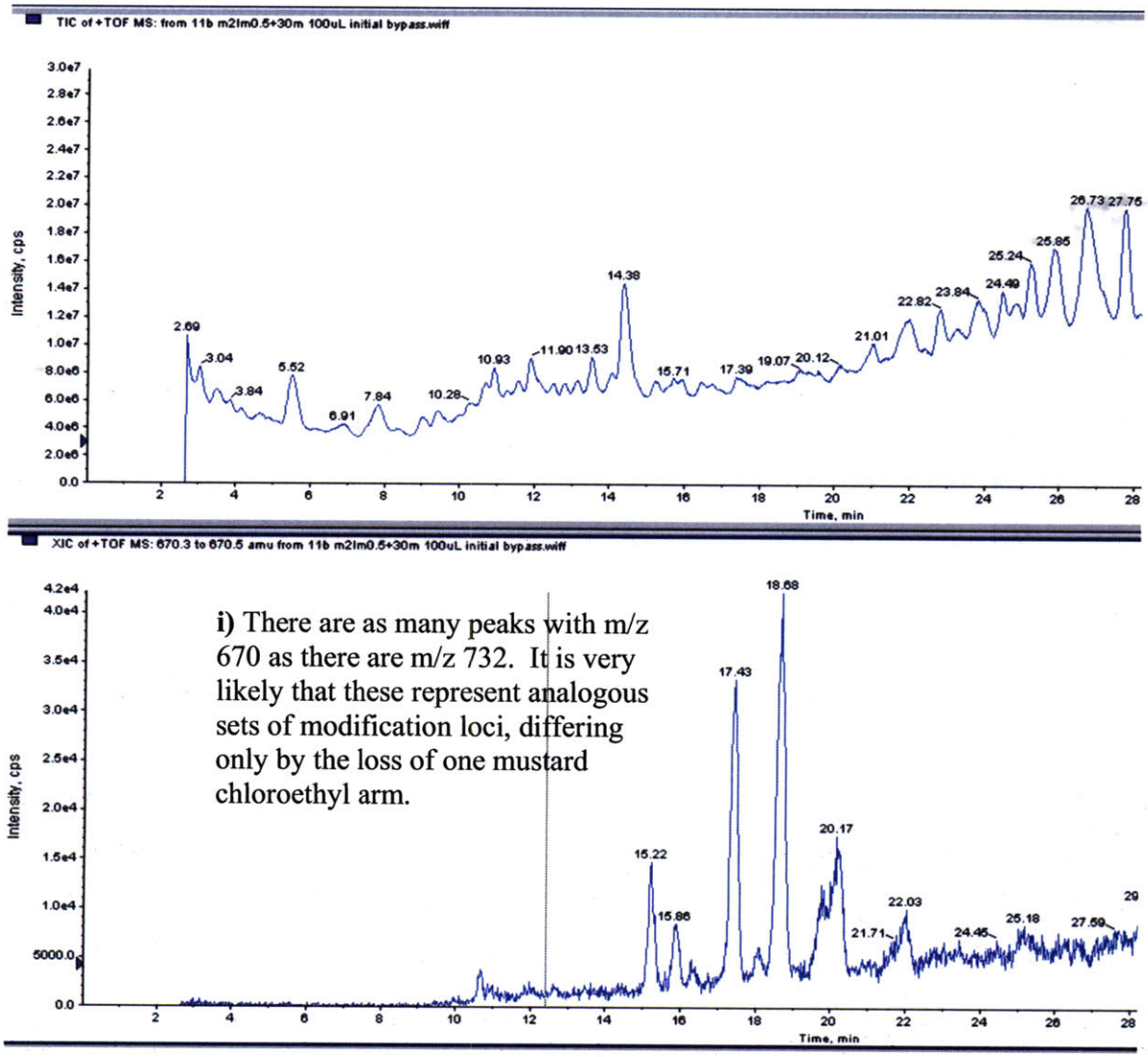

Figure 3-13: Drug-drug interaction screens with pooled human (HLMs), male mouse (mMLMs), female mouse (fMLMs), and male rat (mRLMs) liver microsomes

a) DDI screen with Amodiaquine (CYP2C8)

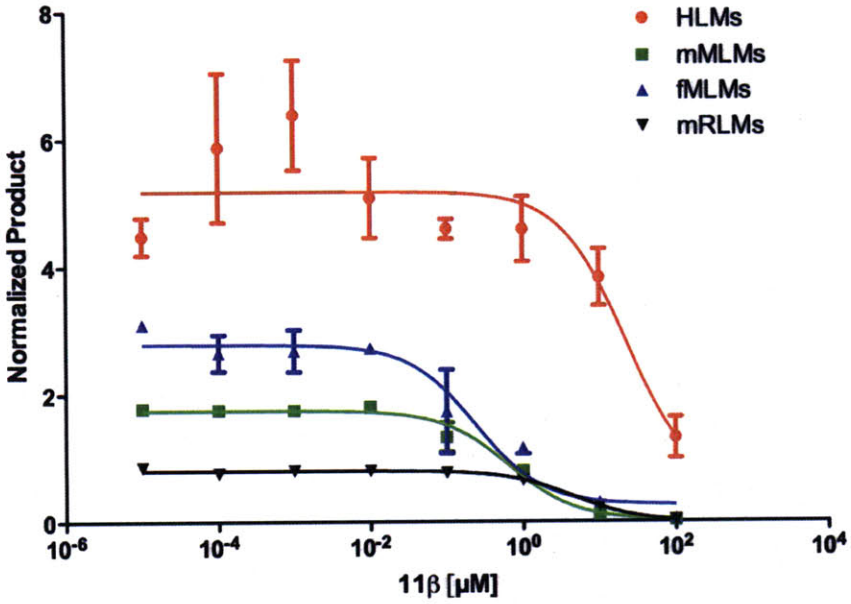

b) DDI screen with Diclofenac (CYP2C9)

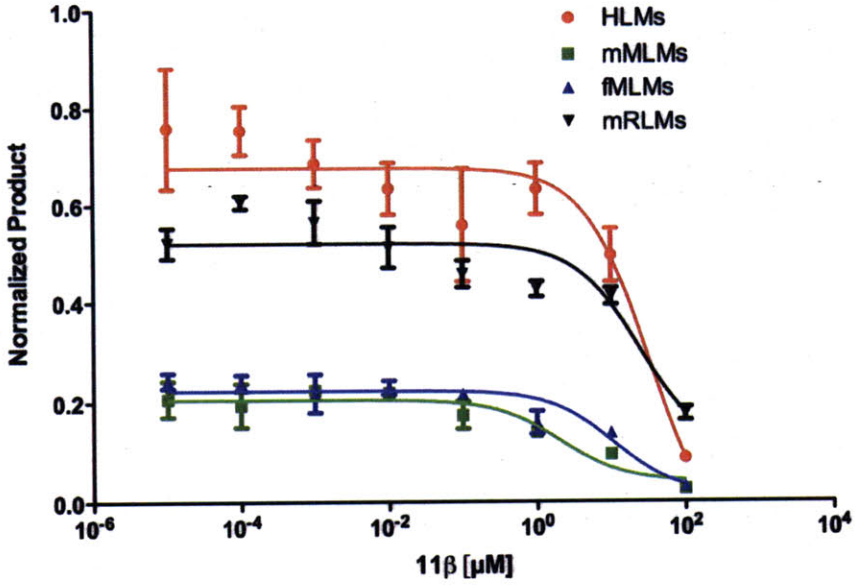

Figure 3-13: Drug-drug interaction screens with pooled human (HLMs), male mouse (mMLMs), female mouse (fMLMs), and male rat (mRLMs) liver microsomes

c) DDI screen with Dextromethorphan (CYP2D6)

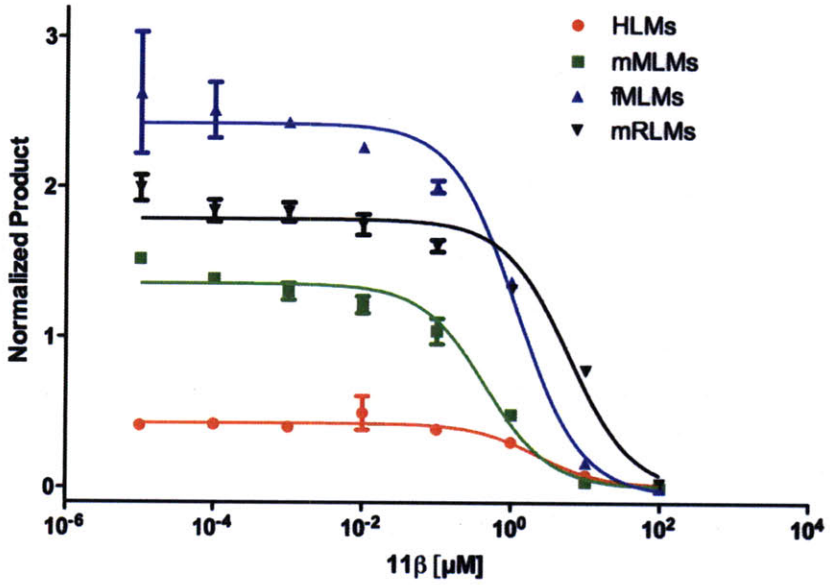

d) DDI screen with Tacrine

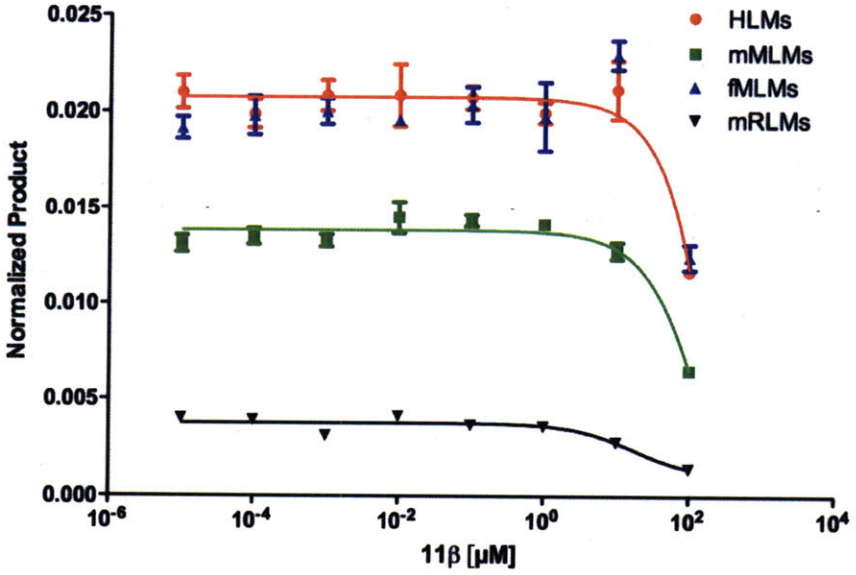

Figure 3-13: Drug-drug interaction screens with pooled human (HLMs), male mouse (mMLMs), female mouse (fMLMs), and male rat (mRLMs) liver microsomes

e) DDI screen with Testosterone (CYP3A)

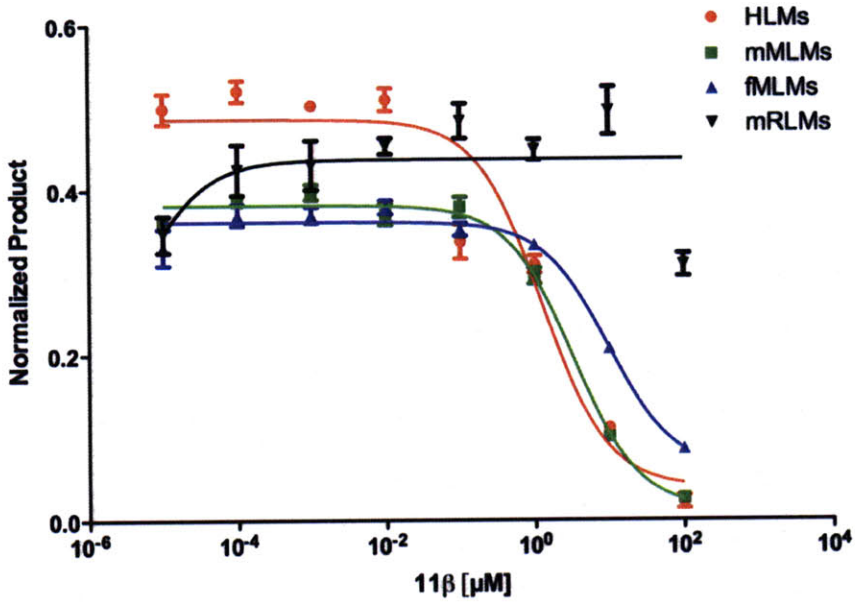

Figure 3-14: Combinatorial family of 11β derivatives

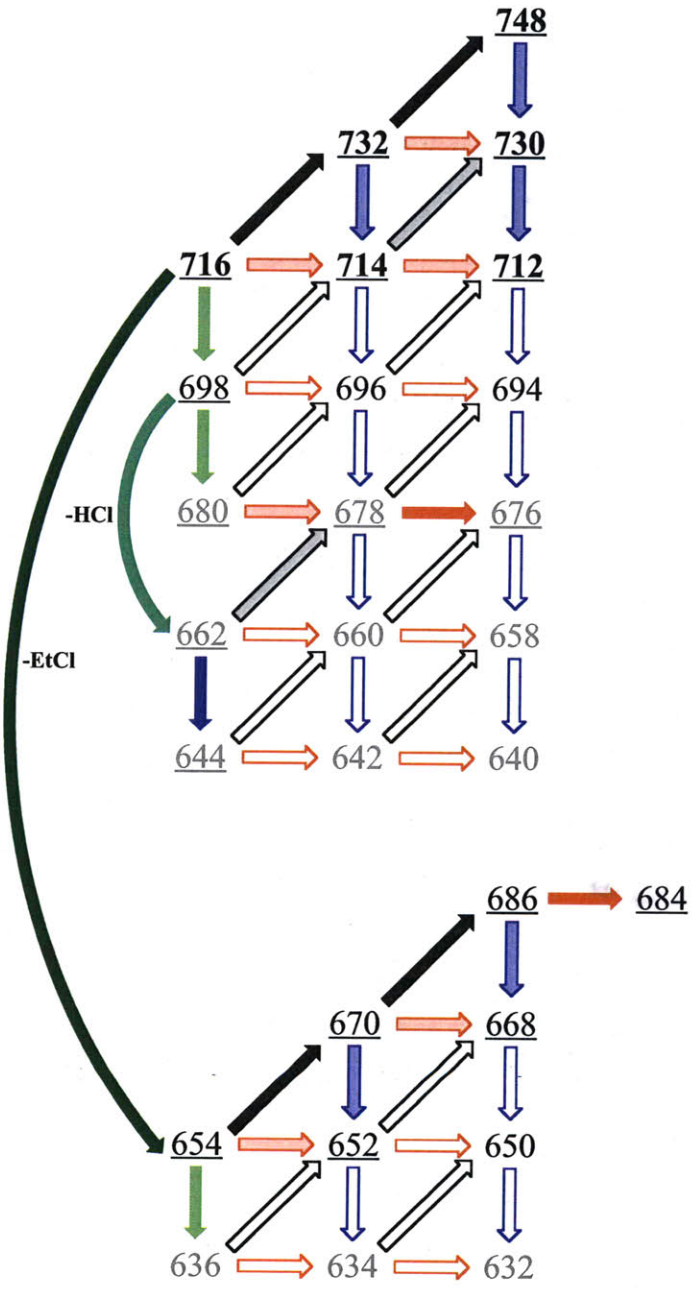

11β is subject to both additive and subtractive modifications by metabolism and hydrolysis. Modular transformations associated with oxidation, dehydration, and decomposition of the chloroethyl arm yield an array of potential products. Underlined m/z values indicate products observed by ESI-TOF after a 30 minute incubation of 11β with human liver microsomes (0.5 mg/mL). Species maintaining two chlorines and the ability to form DNA crosslinks are shown in bold. Normal face type corresponds to products with only one chlorine, still capable of forming DNA monoadducts. Grey labels indicate products without DNA-damaging capability. Solid arrows mark definite transformation paths. Faded arrows represent multiple, indistinguishable paths to the same m/z product. Red arrows indicate oxidation to an alkene or keto group. Black arrows show oxidation by addition of one oxygen atom. Blue arrows represent dehydration. Green arrows indicate the loss of a chlorine through hydrolysis or N-dealkylation.

Figure 3-15: MRM spectra show distinct modification loci on metabolites
a) Product spectra for 11β species maintaining dichloro character were extracted from a set of MRM transitions for a set of Q1 mass-to-charge ratios. Panels, from top to bottom: 1) metabolite with m/z 748 showing both modifications on the mustard side of the carbamate (398), one modification on each side (414), or both modifications on the steroid side (430); 2) metabolite with m/z 732 showing modifications on either side of the fragmentation; 3) metabolite with m/z 730 showing four possible configurations, combining both +O and $-H_2$ oxidations; 4) 11β; 5) metabolite with m/z 714 showing a higher frequency of oxidation occurring on the mustard side of the carbamate (398) than on the steroid side (396); and 6) metabolite with m/z 712 showing no modifications on the steroid half of the molecule.

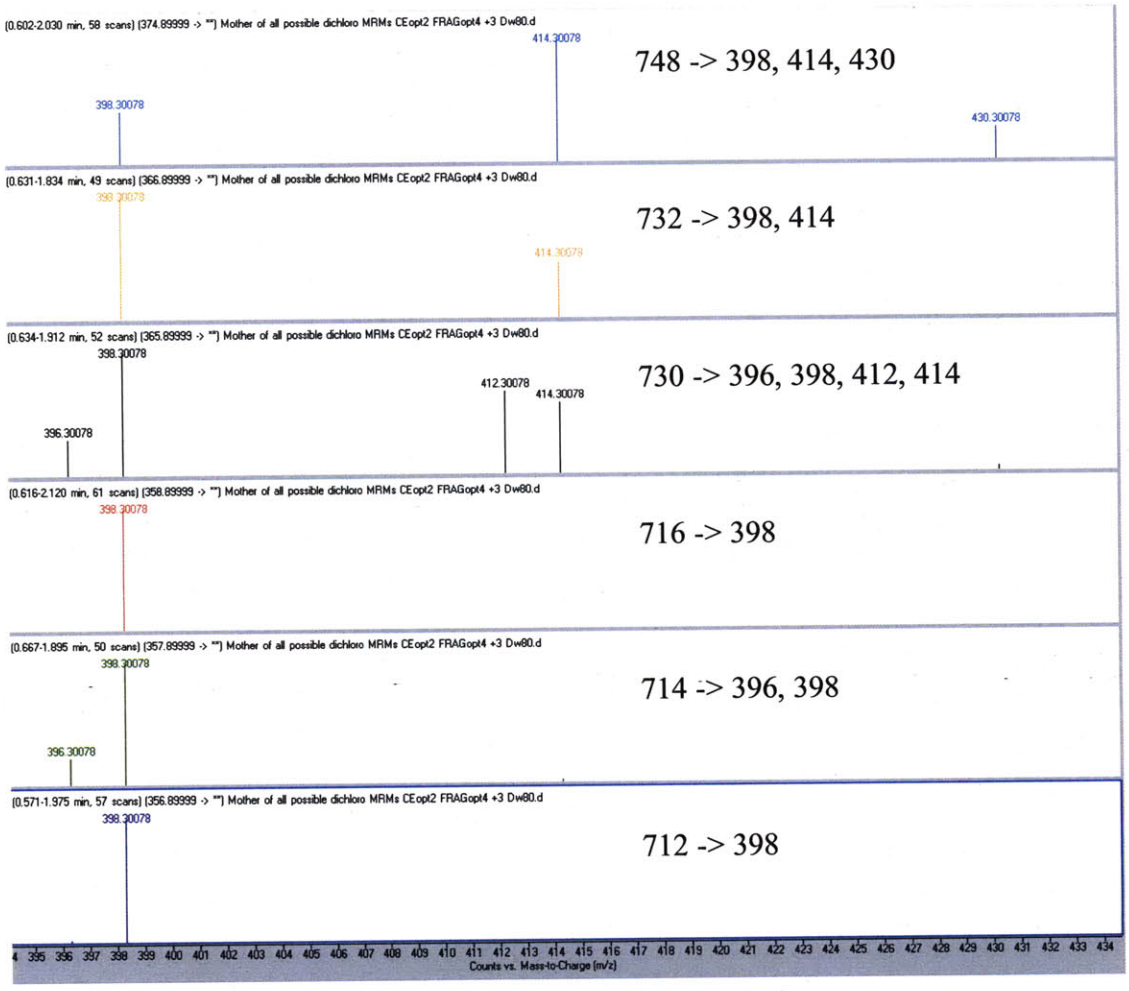

Figure 3-15: MRM spectra show distinct modification loci on metabolites
b) Top panel: N-deschloroethyl hydroxyl 11β is more likely to be oxidized on the steroid side of the carbamate. Middle panel: N-deschloroethyl 11β with steroid system unchanged. Bottom panel: metabolite with m/z 714 showing traces of oxidation on either side of the carbamate (396 or 398) as well as a 414 fragment, indicating a +16 on the steroid side that must be balanced with a -18 on the mustard side.

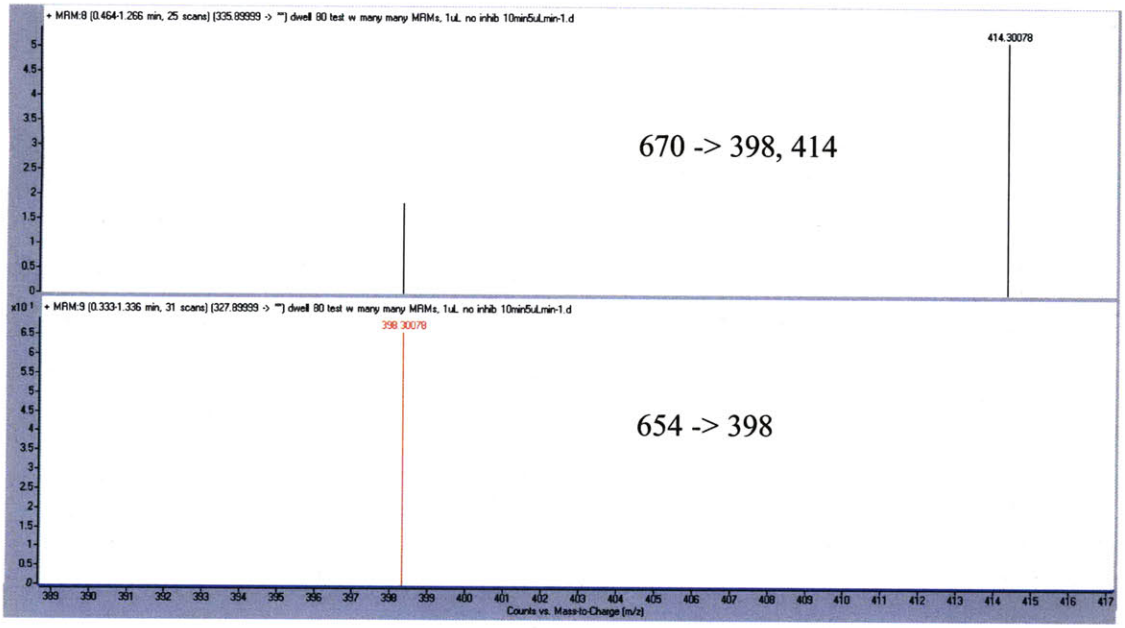

Table 3-1: Reaction and MRM conditions for DDI probes

CYP	Substrate	[μM]	Probe	Transition Q1->Q3	Fragmentation Voltage	Collision Energy
2C8	amodiaquine	15	desethylamodiaquine	328->283	100	20
2C9	diclofenac	15	4'-hydroxydiclofenac	312->230	106	33
2D6	dextromethorphan	5	dextrorphan	258->157	156	41
1A2	tacrine	15	1-hydroxytacrine	215->187	100	40
3A4/5	testosterone	50	6β-hydroxytestosterone	305->269	142	13

Conditions for probe detection were previously optimized for the Agilent 6410 Triple Quadrupole mass spectrometer at BioTrove (Woburn, MA).

Table 3-2: MRM transition conditions for 11β species

m/z (+1)	Description	Modification Zones	Transition Q1->Q3	Fragmentation Voltage	Collision Energy
748	Dihydroxy 11β	+2O M	374->398	110	13
		+O M, +O S	374->414	110	15
732	Hydroxy 11β	+O M	366->398	105	15
		+O S	366->414	125	13
730	748 -H_2O	+O M, -H_2 M	365->398	110	13
		+O S, -H_2 S	365->412	125	13
716	11β dichloro	Parent	358->398	110	13
714	732 –H_2O	-H_2 S	357->396	125	13
		-H_2 M	357->398	130	13
		-H_2O S, +O M	357->414	125	13
712	748 -2H_2O	-2H_2 S	356->394	135	13
		-H_2 M, -H_2 S	356->396	135	13
		-2H_2 M	356->398	115	13
708	11β dimethoxy	Internal Standard	354->398	110	17
670	Hydroxydeschloroethyl 11β	+O M, (-EtCl M)	335->398	115	13
		+O S, (-EtCl M)	335->414	115	13
654	Deschloroethyl 11β	(-EtCl M)	327->398	115	13

Metabolites observed were classified as having modifications on the mustard (M) or steroid (S) side of the Q2 fragmentation at the carbamate (Figure 3-5). All Q1 signals arose from the +2 charge state of the analytes, and all Q3 signals represent the steroid side of the molecule after fragmentation. Separate elution times of {m, m-18} pairs observed by ESI-TOF ruled out dehydration in the Q2. Derivatives of parent 11β with the same Q1 but different Q3 indicate distinct modification loci. Combinations of oxidations (+O or -H_2) and dehydrations (-H_2O) occurring on one or both sides of the fragmentation were examined. Products arising from dealkylation of the mustard nitrogen are annotated as (-EtCl M).

Table 3-3: Relative abundance of the 11β derivatives generated in human and mouse liver microsomes as detected by LC–ESI-TOF

m/z	Pooled human	Male mouse	Female mouse
748	++	++	++
732	++++	++++	++++
730	++	+	+
714	+++	++	+++
712	+++	+	++
698	++	++	++
686	+	-	-
684	+	-	-
680	+	+	+
678	+	-	-
676	+	-	-
670	+++	++	+
662	+	+	+
654	++	++	+
652	+	-	-
644	+	-	-

These data represent thirty minute incubations with NADPH regeneration machinery and 0.5 mg/mL total protein. Mouse liver microsomes from either gender displayed spectra representing roughly equivalent subsets of the product species formed in human preparations, with female mice showing slightly less propensity for N-dealkylation. In both species, the dominant products were multiple single oxidations to m/z 732 at distinct loci as evidenced by chromatographic separation.

Table 3-4: DDI Screen IC_{50} results

Probe (Isoform)	Pooled HLM	Male MLM	Female MLM	Male RLM
Amodiaquine (2C8)	22.6 (3.42–150.) R^2=0.641	**0.644** (0.374–1.11) R^2=0.955	**0.239** (0.0782–0.728) R^2=0.845	**4.45** (2.83–7.01) R^2=0.967
Diclofenac (2C9)	31.8 (5.59–181.) R^2=0.726	**2.06** (0.493–8.56) R^2=0.745	10.8 (3.46–33.8) R^2=0.791	23.3 (5.87–92.5) R^2=0.765
Dextromethorphan (2D6)	**2.25** (0.815–6.190) R^2=0.855	**0.454** (0.285–0.723) R^2=0.968	**1.17** (0.630–2.18) R^2=0.935	**5.86** (3.30–10.4) R^2=0.945
Tacrine (1A2)	N/A	N/A	N/A	17.5 (6.20–49.1) R^2=0.832
Testosterone (3A)	**1.25** (0.640–2.42) R^2=0.926	**3.25** (2.42–4.36) R^2=0.986	**9.62** (6.02–15.4) R^2=0.958	N/A

All IC_{50} values represent 11β [μM], with ranges in parentheses representing the 95% confidence interval. Goodness of fit is reported as R^2. Each dataset comprised 24 points from triplicate biological replicates of the eight serial dilutions of inhibitor. Fields marked N/A indicate a failure of the dataset to converge to a one-site competitive binding curve. Values under 10 μM are shown in bold, indicating an inhibition potential likely to be relevant in the *in vitro* and *in vivo* assays performed in the Essigmann Laboratory.

Table 3-5: Isoform elimination results

Q1->Q3	No microsomes	No inhibitors	2C8	2C9	2D6	3A	2C19	All inhibitors
374.9->398.3	0.39	0.84	0.35	0.44	0.45	0.30	0.28	-
374.9->414.3	-	-	-	-	0.016	-	-	-
366.9->398.3	-	1.9	2.4	2.5	3.5	-	2.8	1.3
366.9->414.3	-	1.1	2.0	2.7	-	-	1.4	2.3
365.9->398.3	-	0.55	0.71	-	-	-	0.59	0.54
358.9->398.3	**180**	**210**	**320**	**390**	**640**	**320**	**290**	**320**
357.9->396.3	-	-	-	-	-	-	0.56	0.74
357.9->398.3	12	16	26	34	37	19	34	42
356.9->398.3	34	46	62	93	130	40	110	110
335.9->398.3	-	0.31	-	-	-	-	-	-
335.9->414.3	-	1.9	-	-	-	-	1.5	-
327.9->398.3	1.5	37	30	43	51	58	48	38

Product spectra after 30 minutes with 0.5 mg/mL human liver microsomes demonstrated significantly less conversion of 11β dichloro (bold) to products than observed in quantitative studies with ^{14}C 11β. The inhibition cocktail consisted of combinations of 20 μM amodiaquine, 40 μM diclofenac, 50 μM dextromethorphan, 500 μM testosterone, and 600 μM mephenytoin as described in Materials and Methods.

References

1. Omura, T. & Sato, R. The carbon monoxide-binding pigment of liver microsomes. I. Evidence for its hemoprotein nature. *J. Biol. Chem* **239**, 2370-2378(1964).
2. McLean, A. et al. The metabolism of chlorambucil. *Biochem. Pharmacol* **29**, 2039-2047(1980).
3. Farmer, P.B. et al. The metabolism of deuterated analogues of chlorambucil by the rat. *Chem. Biol. Interact* **28**, 211-224(1979).
4. Lee, F.Y., Coe, P. & Workman, P. Pharmacokinetic basis for the comparative antitumour activity and toxicity of chlorambucil, phenylacetic acid mustard and beta, beta-difluorochlorambucil (CB 7103) in mice. *Cancer Chemother. Pharmacol* **17**, 21-29(1986).
5. Fang, S., Anderson, K.M. & Liao, S. Receptor Proteins for Androgens. On the role of specific proteins in selective retention of 17beta-hydroxy-5alpha-androstan-3-one by rat ventral prostate in vivo and in vitro. *J. Biol. Chem.* **244**, 6584-6595(1969).
6. Bruchovsky, N. & Wilson, J.D. The Intranuclear Binding of Testosterone and 5agr-Androstan-17{beta}-ol-3-one by Rat Prostate. *J. Biol. Chem.* **243**, 5953-5960(1968).
7. Mainwaring, W.I. & Peterken, B.M. A reconstituted cell-free system for the specific transfer of steroid--receptor complexes into nuclear chromatin isolated from the rat ventral prostate gland. *Biochem. J* **125**, 285-295(1971).
8. Bruchovsky, N. & Wilson, J.D. The Conversion of Testosterone to 5agr-Androstan-17{beta}-ol-3-one by Rat Prostate in Vivo and in Vitro. *J. Biol. Chem.* **243**, 2012-2021(1968).
9. Jung, I. & Baulieu, E.E. Testosterone cytosol "receptor" in the rat levator ani muscle. *Nature New Biol* **237**, 24-26(1972).
10. Baulieu, E.E. & Jung, I. A prostatic cytosol receptor. *Biochem. Biophys. Res. Commun* **38**, 599-606(1970).
11. Fang, H. et al. Study of 202 natural, synthetic, and environmental chemicals for binding to the androgen receptor. *Chem. Res. Toxicol* **16**, 1338-1358(2003).
12. Wood, A.W. et al. Regio- and stereoselective metabolism of two C19 steroids by five highly purified and reconstituted rat hepatic cytochrome P-450 isozymes. *J. Biol. Chem* **258**, 8839-8847(1983).
13. Choi, M.H. et al. Characterization of testosterone 11 beta-hydroxylation catalyzed by human liver microsomal cytochromes P450. *Drug Metab. Dispos* **33**, 714-718(2005).
14. Krauser, J.A. & Guengerich, F.P. Cytochrome P450 3A4-catalyzed testosterone 6beta-hydroxylation stereochemistry, kinetic deuterium isotope effects, and rate-limiting steps. *J. Biol. Chem* **280**, 19496-19506(2005).
15. Waxman, D.J., Ko, A. & Walsh, C. Regioselectivity and stereoselectivity of androgen hydroxylations catalyzed by cytochrome P-450 isozymes purified from phenobarbital-induced rat liver. *J. Biol. Chem* **258**, 11937-11947(1983).
16. Reubi, I. et al. Use of a monoclonal antibody specific for rabbit microsomal cytochrome P-450 3b to characterize the participation of this cytochrome in the microsomal 6 beta- and 16 alpha-hydroxylation of progesterone. *Biochemistry* **23**, 4598-4603(1984).

17. Marquis, J.C. et al. Disruption of gene expression and induction of apoptosis in prostate cancer cells by a DNA-damaging agent tethered to an androgen receptor ligand. *Chem. Biol* **12**, 779-787(2005).
18. Guengerich, F.P. Cytochrome p450 and chemical toxicology. *Chem. Res. Toxicol* **21**, 70-83(2008).
19. Turpeinen, M. et al. Predictive value of animal models for human cytochrome P450 (CYP)-mediated metabolism: a comparative study in vitro. *Xenobiotica* **37**, 1367-1377(2007).
20. Obach, R.S. et al. The utility of in vitro cytochrome P450 inhibition data in the prediction of drug-drug interactions. *J. Pharmacol. Exp. Ther* **316**, 336-348(2006).
21. Lazarou, J., Pomeranz, B.H. & Corey, P.N. Incidence of adverse drug reactions in hospitalized patients: a meta-analysis of prospective studies. *JAMA* **279**, 1200-1205(1998).
22. Wienkers, L.C. & Heath, T.G. Predicting in vivo drug interactions from in vitro drug discovery data. *Nat Rev Drug Discov* **4**, 825-833(2005).
23. Williams, J.A. et al. Drug-drug interactions for UDP-glucuronosyltransferase substrates: a pharmacokinetic explanation for typically observed low exposure (AUCi/AUC) ratios. *Drug Metab. Dispos* **32**, 1201-1208(2004).
24. Walsky, R.L. & Obach, R.S. Validated assays for human cytochrome P450 activities. *Drug Metab. Dispos* **32**, 647-660(2004).
25. Waxman, D.J. et al. Monoclonal antibodies inhibitory to rat hepatic cytochromes P-450: P-450 form specificities and use as probes for cytochrome P-450-dependent steroid hydroxylations. *Mol. Pharmacol* **32**, 615-624(1987).
26. Crespi, C.L. & Stresser, D.M. Fluorometric screening for metabolism-based drug--drug interactions. *J Pharmacol Toxicol Methods* **44**, 325-331(2000).
27. Frye, R.F. et al. Validation of the five-drug "Pittsburgh cocktail" approach for assessment of selective regulation of drug-metabolizing enzymes. *Clin. Pharmacol. Ther* **62**, 365-376(1997).
28. Dierks, E.A. et al. A method for the simultaneous evaluation of the activities of seven major human drug-metabolizing cytochrome P450s using an in vitro cocktail of probe substrates and fast gradient liquid chromatography tandem mass spectrometry. *Drug Metab. Dispos* **29**, 23-29(2001).
29. Floby, E. et al. Use of a cocktail of probe substrates for drug-metabolizing enzymes for the assessment of the metabolic capacity of hepatocyte preparations. *Xenobiotica* **34**, 949-959(2004).
30. Zientek, M. et al. Development of an in vitro drug-drug interaction assay to simultaneously monitor five cytochrome P450 isoforms and performance assessment using drug library compounds. *J Pharmacol Toxicol Methods* **58**, 206-214(2008).
31. Hillier, S.M. et al. DNA adducts formed by a novel antitumor agent 11β-dichloro in vitro and in vivo. *Mol. Cancer Ther* **5**, 977-984(2006).
32. Pettersson-Fernholm, T. et al. Reactions of 4-bis(2-chloroethyl)aminophenylacetic acid (phenylacetic acid mustard) in physiological solutions. *J. Chem. Soc., Perkin Trans. 2* 2183-2187(1999).
33. Usmani, K.A. et al. Inhibition of the Human Liver Microsomal and Human Cytochrome P450 1A2 and 3A4 Metabolism of Estradiol by Deployment-Related and Other Chemicals. *Drug Metab Dispos* **34**, 1606-1614(2006).

Chapter 4: Preliminary Study of the Organismal and Subcellular Biodistribution of 11β and its Metabolites

Introduction

The hydrophobicity, multi-functionality, and reactivity of 11β[†] necessitate a close examination of the patterns of compound distribution into tissue compartments as a function of delivery route. Once in plasma, 11β is likely to be extensively protein-bound, such that the equilibrium between bound and free compound governs the rate of uptake into cells as well as the hydrolytic stability. At the cellular level, the kinetics of hydrolysis and extent of metabolic transformations translate the administration of a single compound into an array of derivatives, each likely to exhibit distinct patterns of distribution into organelles.

With greasy chloroethyl arms on one end, a lipophilic steroid system on the other, and a comparatively water-soluble carbamate and protonated (at physiological pH) secondary amine connecting the two, prediction of the disposition of 11β is beyond intuition. Possessing characteristics of both androgen receptor antagonists and DNA alkylating agents, 11β could be exerting its therapeutic or toxic effects in nearly any organelle of dividing or stationary tissue. While its design and analysis to date have focused on its ability to damage nuclear DNA, better comprehension of the path the compound takes between administration and alkylation of DNA would significantly improve an understanding of the mechanisms relevant to toxicity, as well as guide the evolution of both clinical dosage regimens and next-generation versions of the molecule.

To date, the studies of the mechanistic effects of 11β have not included differentiation between the parent dichloro compound and its hydrolytic and metabolic derivatives. Experiments using radiolabeled material have as a quantitative endpoint either scintillation counting or accelerator mass spectrometry. Whether those counts arise from 11β-dichloro, 11β with singly- or doubly-hydrolyzed mustards, hydroxylated or N-dealkylated 11β, or some combination of modifications is not discernible with the techniques used. However, the degree to which these transformations influence not only the biodistribution of the molecules but also their biological activity is likely very important to both elucidation of the mechanism and design of the therapy in the context of administration route, formulation, and dosage regimen.

[†] 2-(6-((8S,11S,13S,14S,17S)-17-Hydroxy-13-methyl-3-oxo-2,3,6,7,8,11,12,13,14,15,16,17 dodecahydro-1H-cyclopenta[a]phenanthren-11-yl)hexylamino)ethyl 3-(4-(bis(2-chloroethyl)amino)phenyl)propylcarbamate

Organismal Distribution

It is valuable at this point to recapitulate the therapeutic strategy governing the design of these programmable agents. To treat a metastatic cancer whose foci span diverse tissues (bone, bladder, colon, lymph, etc.), systemic bioavailability is preferred, as the disease has outgrown the utility of spatially-targeted treatments. Therefore, it is important to characterize the biodistribution in an animal model with the hopes of extrapolating to a potential human treatment. The correlation between delivery route and organ-level distribution will guide optimization of the formulation of the drug candidate.

In conjunction with the experiments demonstrating toxicity against LNCaP xenografts in a mouse model, biodistribution resulting from the intraperitoneal injections was measured. The 45 mg/kg doses of a ^{14}C-11β preparation with specific activity 1.91 μCi/μmole achieved peak blood levels after fifteen minutes, peak intestinal levels after two hours, peak liver, lung, and kidney levels after four hours, and peak feces levels after six hours[1]. In work described in this chapter, gavage and intraperitoneal delivery routes were compared to determine whether systemic bioavailability could be achieved through oral delivery of 11β suspended in a vegetable oil/DMSO emulsion.

Plasma protein binding

As described in the previous chapters, a diverse array of metabolic and hydrolytic products of 11β was observed, including derivatives of identical m/z but distinct modification locations. The degree to which subtle structural changes were sufficient to alter the elution times of the metabolites from a C18 column suggests that the equilibrium distribution of 11β and its metabolic products in a complex biological system would be necessarily multivariate. Species suffering loss of a chlorine atom through hydrolysis or N-dealkylation demonstrate significantly increased hydrophilicity, and, as such, should be found in a higher ratio of free to bound drug in plasma. As a model for this system, the dynamics between free and bound drug were measured as a function of albumin concentration in an aqueous system. In tandem, to probe further the kinetics of hydrolysis as a function of chloride ion concentration, the albumin-binding experiments were performed at either 116 mM or 4 mM chloride, representing the physiological concentrations of the ion in plasma and cytoplasm, respectively. The sensitivity of triple

quadrupole mass spectrometry allowed the simultaneous tracking of parent 11β-dichloro, the singly-hydrolyzed analog 11β-monochloro-monohydroxyl, and doubly-hydrolyzed compound 11β-dihydroxyl. Based on the differential between the observed half-lives of 11β in aqueous systems with or without protein discussed in Chapter 2, it was expected that the increasing protein concentration would protect parent compound and slow the formation of both hydrolysis products. Similarly, the reaction systems with low chloride were expected to demonstrate the same pattern of hydrolysis in a compressed timescale.

Subcellular distribution

It has been shown that 11β exhibits both agonist and antagonist activity toward AR, provoking translocation of normally-cytoplasmic AR into the nucleus but impeding the transcription and translation of genes when applied in competition with native ligand[†]. It is unclear whether the physical translocation of an 11β-AR complex increases delivery of drug to DNA and results in either enhanced or regio-specific adduct formation. In LNCaP cells, 11β has been shown to form adducts with nuclear DNA[1]. Following treatment of a sufficient dose, LNCaP cells undergo apoptotic programmed death[2]. The hypothesis upon which this project was initiated is that DNA adducts formed by 11β are refractory to nucleotide excision repair if the steroid moiety achieves sufficient interaction with the bulky androgen receptor, leading to enhanced toxicity in cancerous cells with levels of androgen receptor expression higher than those in healthy tissue[3]. The work of Proffitt et al. has cast doubt on the validity of this model. Nevertheless, the drug candidate does cause excessive DNA damage, and inhibiting replication or repair may provoke an apoptotic response mediated by interactions between the nucleus and mitochondria. The signaling cascade ensuing from the breach of the tolerable DNA damage threshold contributes to an apoptotic response[2] but is by no means the only means by which 11β-dichloro could cause cellular dysregulation. As such, it is unclear whether nuclear DNA damage is either the critical event leading to a toxicity response or even an appropriate biomarker for correlating exposure level with the eventual fate of the cell.

[†] Kyle Proffitt, unpublished data.

It is noteworthy that the covalent adducts and crosslinks created by 11β in the DNA of mitochondria, which lack the capacity for nucleotide excision repair[4], may be a more direct and potent trigger of programmed cell death than the analogous species in the nucleus. The hydrophobicity of 11β suggests that the molecule may diffuse easily across organelle membranes. Also, the prevalence of a positively-charged linker amine at physiological pH makes it reasonable to consider the possibility that diffusion across the mitochondrial outer membrane would be energetically favorable[5].

In addition to damage to genomic or mitochondrial DNA, the degree to which the electrophilic aziridinium moiety in activated 11β is attacked by cellular nucleophiles other than DNA must be considered. Furthermore, direct disruption of membrane structure[6] caused by 11β saturation of hydrophobic compartments with limited capacity could trigger apoptosis through ion imbalance and/or depolarization of the mitochondrial membrane[7,8]. In order to ascertain the existence of a pattern of distribution of 11β into specific cellular fractions, sequential separations were performed on cells treated with ^{14}C-11β *in vitro*, and the activities associated with each compartment at different time points resulting from various doses were compared. In separate studies, covalent binding between 11β and protein was explored through incubation with cytochrome c, a small (molecular weight 12,358) protein for which chromatography and mass spectrometry conditions were well-characterized in the Tannenbaum Laboratory[9].

Quantitative structure-activity relationship (QSAR) analysis of 11β species

The array of 11β derivatives resulting from hydrolytic and metabolic transformations will certainly have different interactions with cellular macromolecules based on their individual capacities for formation of covalent adducts and affinities for the androgen receptor. Modifications of the steroid system will undoubtedly affect relative binding affinity[10], which, in the context of antagonism of the AR-promoted signal transduction cascades, may abrogate the previously observed partial agonist/partial antagonist character of the ligand-receptor pair. Metabolic decomposition of the aniline mustard would eliminate the potential for the formation of a DNA crosslink. As discussed in Chapter 3, the elucidation of the structures of 11β metabolites was limited to identifying whether the modification associated with a given mass-to-charge ratio and

fragmentation transition occurred on the mustard or steroid side of the carbamate linkage. However, in work described in this chapter, it was possible to model the expected octanol:water partition coefficient (logP) for the putative metabolites to determine the degree to which the modifications observed would increase or decrease hydrophilicity and, in turn, potentially influence the sequestration of specific metabolites into hydrophilic or hydrophobic compartments of cells.

Materials and Methods

Comparison of 11β bioavailability as a function of delivery route: Female Swiss Webster mice (Taconic, Germantown, NY) aged 8–10 weeks and fasted overnight were treated with either a 30 mg/kg intraperitoneal injection of ^{14}C-11β (specific activity 2.4 μCi/μmole) in a Cremophor EL:ethanol emulsion or a 150 mg/kg gavage delivery of ^{14}C-11β (specific activity 0.5 μCi/μmole) in a vegetable oil:DMSO emulsion. At 0.5, 1, 2, 4, or 6 hours after administration of compound, mice were sacrificed by asphyxiation by 90–100% carbon dioxide. The mice were subsequently dissected and the lungs, liver, kidney, intestines, and feces were collected, with ~100 mg samples of each tissue transferred to pre-weighed 20 mL scintillation vials. Blood (300–500 μL) was collected via cardiac puncture into a syringe containing EDTA to prevent clotting. Organ fractions and a 150 μL aliquot of whole blood were homogenized by a 48-hour incubation with 2 mL Solvable (Packard Biosciences, Meriden, CT) at 60°C. Samples were decolorized by addition of 400 μL hydrogen peroxide over ice and subsequently mixed with 15 mL Hionic-Fluor scintillation fluid (Packard Biosciences) before quantification of radioactivity in an LS1801 Liquid Scintillation Counter (Beckman-Coulter, Fullerton, CA). Whole, unclotted blood was spun for 15 minutes at 1,500 g and 4°C to separate plasma from hematocytes. A 100 μL plasma sample was mixed with an equal volume of ice-cold acetonitrile, vortexed, and spun for two hours at 14,000 g and 4°C. Supernatant was collected and counted for radioactivity as above. Whole blood, and blood fractionated into plasma or blood cells were analyzed to quantify how much ^{14}C was actually in cells, and acetonitrile-extracted plasma supernatant to quantify how much ^{14}C in plasma was covalently attached, rather than simply adsorbed, to plasma protein.

Contribution of plasma protein and free chloride ion to the stability of 11β: In a 96-well format, serial dilutions (1, 0.5, 0.25, and 0 mg/mL bovine serum albumin) were prepared in either ddH_2O supplemented with NaCl for a final chloride concentration of 4 mM or Dulbecco's phosphate-buffered saline (PBS, Invitrogen, Carlsbad, CA) for a final chloride concentration of 116 mM, representing the concentrations of free chloride in mammalian cytoplasm and plasma, respectively. Albumin concentrations were well

below human plasma levels of of 3–5 g/dL[11] but consistent with the ranges used in other *in vitro* experiments. Incubations were initiated by addition of a 1 μL aliquot of 11β in DMSO to bring the final reaction volume to 50 μL and 1 μM 11β in each well, with each albumin-chloride concentration pair prepared in triplicate. Plates were stored in an incubator at 37°C. At times 0, 0.5, 1, 2, 3, 4, 6, and 8 hours following initiation, systems were quenched by addition of 50 μL of ice-cold acetonitrile containing 0.1% formic acid and 0.5 μM 11β-dimethoxy as internal standard. Plates were transferred to storage at -20°C until transport over dry ice. Measurement of the levels of 11β–dichloro, 11β–dimethoxy, 11β–monochloro–monohydroxy, and 11β–dihydroxy species was performed with a RapidFire high-throughput injection system (BioTrove, Woburn, MA) coupled to an Agilent Series 6410 triple quadrupole mass spectrometer. Each 10 μL sample was withdrawn from its well, desalted on a C4 microcolumn cartridge with water : formic acid (FA) : trifluoroacetic acid (TFA) (99.9% : 0.09% : 0.01%), and back-eluted with acetonitrile : FA : TFA (99.9% : 0.09% : 0.01%) into the QQQ source. Multiple reaction monitoring (MRM) mode with source conditions 325°C gas temperature, 12 L/min drying gas, 25 psig nebulizer pressure, and 4000 V needle voltage was used to measure species abundance. Integration of the MRM peak intensities was performed at BioTrove using the proprietary RapidFire Integrator Software. Intensity levels for the compounds of interest were normalized to that of 11β-dimethoxy for each well.

Hydrolysis of 11β in cell culture: PC3-AR1 cells obtained courtesy of Shaoyong Chen (Balk Laboratory, Beth-Israel Deaconess Medical Center, Boston, MA) were grown for 48 hours after an initial seeding of 50,000 cells in each well of a 6-well tissue culture plate in 2 mL RPMI 1640 (Invitrogen) supplemented with 10% fetal bovine serum (FBS, Hyclone, Salt Lake City, UT) and 400 μg/mL G418 (Geneticin, GIBCO). A 200X solution of 11β in DMSO was added to fresh media for a final drug concentration of 5 μM. At initiation, media was aspirated from each well and replaced with 2 mL of the drug-containing preparation. One six-well plate was prepared for each time point. At times 0, 4, 8, and 24 hours after dosing, media was withdrawn to a fresh tube and mixed with ice-cold acetonitrile containing 1 μM 11β-dimethoxy as internal standard. The cells remaining in each well were disrupted with 2 mL of the same 1 μM 11β-dimethoxy in ice

cold acetonitrile, with the resulting solution transferred to a fresh tube. Samples were mixed by vortexing and centrifuged for 30 minutes at 4°C and 18,000 g. Supernatants were diluted with ddH_2O to 15% organic and passed through a C18 SepPak (Waters) previously equilibrated to 10% methanol after an initial wetting with 100% acetonitrile. Samples were eluted with 2 mL 100% methanol and stored at -20°C until immediately prior to mass spectrometry. Quantitation of parent compound and internal standard was achieved through bolus injections of the eluates from the media and cellular compartments into a Series 6410 triple quadrupole mass spectrometer (QQQ, Agilent Technologies, Santa Clara, CA) operating in positive ion mode with source conditions 325°C gas temperature, 12 L/min drying gas (N_2, AirGas, Salem, MA), 25 psig nebulizer pressure, and 4000 V capillary voltage. Abundance traces were smoothed and integrated in Agilent Qualitative Analysis, with areas under the curve for parent 11β-dichloro (m/z 716) divided by that of the internal standard 11β-dimethoxy (m/z 708) from the same injection to normalize for the variable efficiency of the workup. Normalized areas under the curve for parent compound were fit as one-phase exponential decay processes in Prism 5 (GraphPad Software).

Subcellular distribution of 11β *in vitro*: LNCaP cells were obtained from the American Type Culture Collection (Rockville, MD) and grown in 6-well tissue culture plates under LNCaP media, comprising RPMI 1640 (Invitrogen) supplemented with 10% FBS, 1 mM sodium pyruvate (Invitrogen), 2.5 g/L glucose, and 10 mM HEPES (Invitrogen). Cells were seeded at 150,000 per well and allowed to attach and divide for 48 hours under 3 mL media. A 10 mM stock solution of ^{14}C-11β was prepared by dissolving 50 μCi of 11β in 200 μL DMSO for a specific activity of 25 μCi/μmole. At initiation, media was aspirated from each well of six plates, following which cells were washed with 2 mL PBS (Invitrogen). After aspiration of the PBS, cells were immediately delivered 1.5 mL of LNCaP media containing 0, 0.5, 1, 2, 4, or 8 μM 11β with 0.5% DMSO prepared immediately before administration and pre-warmed to 37°C. Except for the zero time point, the plates were stored in an incubator at 37°C under humidified 5% CO_2/atmospheric air, identical to the conditions under which cells grew after seeding. Each 6-well plate contained one well with each dose. At times 0, 20 minutes, 40 minutes,

1 hour, 2 hours, and 4 hours following exposure to compound, one six-well plate was processed for analysis. Media was withdrawn and collected in an Eppendorf tube labeled Fraction A. To lift cells off the plate, a 0.5 mL volume of TrypLE (Invitrogen) was added to each well. The plate was then swirled to ensure complete coverage, and allowed to incubate at 37°C for three minutes, after which 1 mL of fresh media per well was added. All subsequent steps were performed in a 4°C cold room unless otherwise noted, and all separated fractions were stored immediately at 4°C. The resulting 1.5 mL system of media and detached cells was transferred to an Eppendorf tube and centrifuged for 20 minutes at 1,000 g. Supernatants were collected and labeled Fraction B. The pellet was resuspended in a hypotonic pH 7.4 aqueous solution with 250 mM sucrose, 10 mM acetic acid, 10 mM triethanolamine, and 1 mM sodium EDTA in a 15 mL tube and allowed to rock gently for 20 minutes. Meanwhile, empty tissue culture wells were washed with 500 µL acetonitrile, which was collected and labeled Fraction D. The swelled cells were then lysed with twelve withdrawals into a 3 mL syringe and expulsions through a 21G 2" needle with the beveled needle tip pressed against the wall of the plastic tube. A 400 µL aliquot of this whole cell lysate was collected and labeled Fraction C. The remaining 1.1 mL of whole cell lysate was spun at 1,000 g for 15 minutes to pellet nuclei. The post-nuclear supernatant (PNS) was collected and a 10 µL aliquot was examined with a hemacytometer to ensure the absence of nuclei. Supernatants with any nuclear contamination were re-centrifuged and re-examined until separation was complete. The PNS was subsequently centrifuged at 5,000 g for 20 minutes to pellet mitochondria and other organelles. This post-mitochondrial supernatant was transferred to a fresh tube labeled Fraction F. Nuclear and mitochondrial pellets were resuspended in 396 µL TNE buffer (50 mM Tris, 100 mM NaCl, 10 mM EDTA, pH 7.6), to which 4 µL of a 0.5 mg/mL solution RNAse A (Qiagen) were added. The resulting solutions were incubated for 90 minutes at 40°C, following which 50 µL of a 5 mg/mL solution of Protease K and 50 µL of 5% sodium dodecyl sulfate in TNE were added to bring the sample volume to 0.5 mL. Samples were subsequently incubated for ninety minutes at 40°C. After cooling to room temperature, 0.5 mL of a phenol:chloroform:isoamyl alcohol (25:24:1) solution was added to each sample, mixed vigorously, and centrifuged for ten minutes at 13,000 g and 4°C. From the aqueous layers, 425 µL (avoiding

disruption of the phase interface) were extracted and mixed with 0.5 mL of a chloroform:isoamyl alcohol (24:1) solution. These solutions were again shaken vigorously and centrifuged for ten minutes at 13,000 g and 4°C, following which 350 µL of the aqueous fraction were transferred to a fresh tube. Next, 35 µL of 3 M sodium acetate and 800 µL of -20°C 100% ethanol were added to each sample, all of which were then stored overnight at -20°C. The organic layers from each extraction step were saved for later scintillation counting, including Fractions E and G, the phenol layers for mitochondrial and nuclear DNA, respectively, and Fractions H and M, the chloroform layers for mitochondrial and nuclear DNA, respectively.

After at least twelve hours at -20°C, the samples were centrifuged for 20 minutes at 18,000 g and 4°C. Supernatants were poured off gently, and 1 mL 70% 4°C ethanol was added to each. Tubes were flicked to re-suspend pellets and samples were centrifuged again for 30 minutes at 18,000 g and 4°C. Supernatants were poured off gently and pellets were dried with the tip of a Kimwipe before being left open at room temperature to air dry completely. Finally, samples were redissolved in 100 µL ddH_2O and stored at -20°C for later quantification by accelerator mass spectrometry (AMS), graciously performed by Rosa Liberman of the Tannenbaum Laboratory.

Purification of DNA was abbreviated from the standard protocol of sequential proteolysis, extraction, RNA digestion, and second extraction in order to minimize the number of protocol steps during which binding and distribution patterns could deviate from those that existed in cells at the time point of interest. Because the genetic material isolated in these steps was never going to be reintroduced into a living system or used for any purpose but AMS, the abbreviated separation protocol was deemed sufficient.

Covalent adduction of 11β to cytochrome c: The protocol for assessing covalent binding between 11β and protein was adapted from Williams et al. 2007[9]. Lyophilized horse heart cytochrome c was purchased from Sigma Chemical (St. Louis, MO), and 98 mg were reconstituted in 968 µL of 100 mM HEPES at pH 7. Binary serial dilutions of 11β in DMSO were prepared, spanning protein:compound ratios from 64:1 to 0.125:1. Reaction volumes of 100 µL containing 8 nmol cytochrome c were incubated at 37°C for 24 hours. Samples were loaded onto a Microcon 3,000 molecular weight cutoff filter

(Millipore, Bedford, MA) and concentrated with sequential centrifugations of ten minutes at 9,000 g followed by two 20-minute spins at 13,000 g, sufficient to concentrate material to ~10 μL. The filter cartridge was inverted over a fresh tube and spun for three minutes to collect the concentrate, which was subsequently brought up in 100 μL of 50 mM ammonium bicarbonate at pH 7. Two 25 μL aliquots of the resulting solution were set aside for digestion by chymotrypsin (1:10, 37°C, 3 hours) or trypsin (1:25, 37°C, 24 hours). Intact protein was extracted with a C18 ZipTip (Millipore) equilibrated to 0.1% trifluoroacetic acid (TFA) in ddH_2O after previous wetting with 100% acetonitrile. Samples were washed with three 10 μL volumes of 0.1% TFA in ddH_2O and eluted with 0.1% TFA in 70% acetonitrile. Samples were separated by reversed phase liquid chromatography on an Agilent Zorbax C18 (2.1 x 50 mm, 5 μM pore size) column with a 50-minute ramp from 5% to 75% B, where aqueous phase A was 0.25% acetic acid in ddH_2O and organic phase B was 0.25% acetic acid in acetonitrile. Chromatography was performed in tandem with an Agilent Series 1200 electrospray ionization–time of flight (ESI–TOF) mass spectrometer with m/z range 200-2000 and source conditions 325°C gas temperature, 10 L/min N_2 drying gas, 15 psig nebulizer pressure, and 3000 V ESI capillary voltage. Chromatograms were analyzed qualitatively with Agilent Analyst QS software, and protein charge envelopes were deconvolved to obtain the mass of the singly-charged species.

Molecular modeling of the putative metabolites of 11β: Hypothetical structures with modifications that may have yielded the transitions observed by QQQ in the experiments described in Chapters 2 and 3 were derived. These included any logical combination of N-dechloroethylation (-62), addition of an oxygen atom (+16), oxidation to an alkene or keto group (-2), and dehydration (-18). Structures were entered into the Molinspiration Interactive logP (milogP) calculator[†] (Molinspiration Cheminformatics, Slovenský Grob, Slovakia) with or without a positive charge on the linker amine. Structures were categorized by m/z and ranked within groups by the deviation of their calculated milogP values from the value calculated for unmodified 11β-dichloro.

[†] Molinspiration Property Calculation Service accessed at www.molinspiration.com.

Results

Organismal distribution: Gavage delivery was evaluated to test the feasibility of oral administration in the event that 11β-dichloro goes into clinical use. Gavage delivery of the vegetable oil emulsion containing 150 mg/kg 11β with specific activity 0.5 μCi/μmole demonstrated significantly higher plasma activity levels than the corresponding intraperitoneal dose of 30 mg/kg with specific activity 2.44 μCi/μmole. Concentration of 11β in blood spiked after one hour and fell off with apparent first-order kinetics over the next several hours. Despite this evident high level of activity in blood, a commensurate uptake of 11β into organs was not observed (Figure 4-1). Organismal biodistribution of 11β into tissues was far more extensive following intraperitoneal delivery despite the absence of a spike in plasma levels upon administration. Separation of whole blood into plasma and cells revealed that approximately 75% of the radioactivity at all time points was associated with the cellular compartment (Figure 4-2).

Plasma protein-binding phenomena: Samples corresponding to time points quenched before a plate was completed and returned to the incubator demonstrated product precipitation and solvent evaporation that obscured the utility of their data. The samples taken after two hours, however, were quenched and immediately frozen, and as such, behaved reliably during downstream analysis. Without reliable data for the zero time point, kinetics could not be derived. After two hours, nearly all the parent material in the 4 mM chloride samples had hydrolyzed (Figure 4-3), while the dichloro species in the 116 mM wells displayed increasing abundance with increasing concentration of albumin.

Hydrolysis of 11β in cell culture: The half-life of 11β-dichloro in the media compartment was calculated to be 3.33 hours, with the 95% confidence interval spanning 4.8–8.0 hours. In the cellular compartment, peak abundance of 11β-dichloro occurred after about six hours and was of the same order of magnitude as the corresponding level in the media compartment (Figure 4-4).

Subcellular distribution: Activity levels for each cellular fraction are summarized in Figure 4-5. Counts for the media Fraction A demonstrated proportionality consistent with the binary dose serial dilutions and minimal degradation over the six-hour incubation. However, these activity levels represent total carbon radionuclide without distinguishing the metabolic and hydrolytic derivatives of 11β. Supernatants from the centrifuged, lysed cells (Fraction B) demonstrated similar proportionality to the initial dose but represented in most cases less than 5% of the total activity measured, indicating that very little material was displaced during trypsinization. Activity in Fraction C, the whole cell lysate, increased over time and measured on average about 10% of the activity left in the corresponding media fractions. Interestingly, acetonitrile washes of the empty tissue culture wells (Fraction D) yielded few counts in the doses from 0.5–2 μM, but yielded levels of activity comparable to the trypsinization supernatant (Fraction B) in the 4 μM and 8 μM doses. Phenol extractions of the post-mitochondrial supernatant (Fraction E) exhibited a level of activity ranging from about 15–30% of the corresponding counts in whole cell lysate. The post-mitochondrial supernatant itself (Fraction F) yielded counts that were roughly twice that observed in Fraction E. Phenol extraction of the nuclear DNA (Fraction G) yielded 15–20% of the activity found in the whole cell lysate. Chloroform extraction organic fractions showed no activity above background. Levels of activity in the nuclear and mitochondrial DNA samples were on the same order of magnitude.

Covalent binding to non-DNA targets: Attempts to characterize the extent of protein binding to cytochrome c were unsuccessful, as no protein charge envelopes corresponding to species with molecular weights of 12,358+653k were observed (Figure 4-6), where k = the number of molecules of 11β per molecule of protein, assuming that covalent adduction would involve the loss of one chlorine through aziridinium formation for -35 and hydrolysis of the other for -18. However, species with m/z 918 and 1120 were present, indicative of a covalent reaction between 11β and one or two molecules of HEPES. Based on this result, the incubations were repeated in aqueous buffer without HEPES, but no protein adduction was detected in this context either. Despite the absence of modified protein, tryptic and chymotryptic digests were performed

and analyzed by mass spectrometry as an exercise in developing familiarity with the equipment and procedures.

Quantitative structure-activity relationship of metabolites: Changes in milogP from parent compound (7.741 – uncharged linker amine, 5.077 – positively charged linker amine) caused by single modifications are ranked as follows: hydroxylation of the carbon beta to the phenyl and linker carbamate, -1.163; hydroxylation of the carbon beta to the linker amine, -1.150; epoxidation of the phenyl, -1.087; hydroxylation of the steroid, -0.916; N-dechloroethylation, -0.891; hydroxylation alpha to the mustard nitrogen, -0.658; oxidation at the 6–7 position of the steroid ring, -0.507; hydroxylation of the carbon alpha to the linker amine, -0.308; hydroxylation of the phenyl ortho to the aniline nitrogen, -0.292; oxidation to 17-keto, -0.186; oxidation at the 11–12 position of the steroid ring, -0.184; oxidation between the phenyl and linker carbamate conjugated to the phenyl aromatic system, +0.029; and oxidation at the 1–2 position of the steroid ring, +0.610, with the differential between charge states of the linker amine being 2.664 for nearly every modification pair. Examples of the combinatorial modifications and their contributions to changes in solubility approximations are shown in Figure 4-7. A complete listing of modifications corresponding to all observed m/z values is provided in Table 4-1.

Discussion

Organismal distribution

Intraperitoneal administration yielded significant absorption of radiolabeled compound into organ tissue, consistent with uptake of the compound through portal circulation. In contrast, gavage delivery of 11β produced a spike in blood concentration with no commensurate diffusion into parenchyma. The vegetable oil preparation, after entering the small intestine, most likely mixes with bile to form an emulsion packaged for circulation as chylomicrons, accounting for the blood concentration and eventual fecal clearance.

The degree to which the measured radioactivity arises from a spectrum of 11β metabolites rather than unmodified parent compound is not sufficiently understood. It is possible that the excreted species, if analyzed for structure, would exhibit modifications from the parent structure that facilitated clearance, while material remaining in systemic circulation may be more likely to have escaped conversion to a daughter compound. The assessment of both absolute toxicity and selectivity of toxicity depends critically on elucidating the distribution fates of both the parent 11β-dichloro and all of its metabolic derivatives.

Plasma protein-binding phenomena

The degree to which the presence of protein protected 11β from hydrolysis in an aqueous system was expected to help calibrate the equilibrium kinetics between free and bound compound. Albumin has been shown to provide at least eleven binding pockets for small-molecule ligands, and has been crystallized in complex with seven long-chain saturated fatty acids[12]. While these are not perfect electronic models for 11β, their size and hydrophobicity are sufficiently comparable to warrant comparison. Unfortunately, the experiment performed to assess the protection of 11β from hydrolysis by albumin and the differential rate of hydrolysis as a function of chloride ion concentration was not adequately optimized to yield kinetic data, though an observation of the most technically reliable time points demonstrated the expected behavior.

The relative toxicities of the metabolites of chlorambucil have also been attributed to plasma protein binding, as the more hydrophilic and toxic phenylacetic acid mustard metabolite was measured in plasma as 3.2% free drug compared to 0.9% for parent compound[13]. If the rate of hydrolysis in bulk solution, DNA alkylation potential, and all other intracellular transport and trafficking processes are equal, it is reasonable to expect that more DNA adducts and crosslinks would be formed by the metabolite than the parent compound solely based on its bioavailability. Furthermore, clearance of small-molecule xenobiotics has been shown to depend on albumin concentration in sandwich-cultured rat hepatocytes[14]. This system is capable of modeling macroscopic plasma and extracellular transport processes that are absent or irrelevant in *in vitro* tissue culture studies, where the surface area to volume ratio of media to cells is significantly higher and the spatial configuration of cell-cell junctions is artificial.

Between administration and terminal action (either covalent binding to DNA or clearance), each member of the set of 11β derivatives will likely have a distinct distribution pathway controlled by plasma protein binding affinity, and the aggregate exposure to drug experienced by a tumor cell is necessarily the convolution of transport and activity. For example, it is reasonable to speculate that deschloroethyl-11β, after having shed a hydrophobic constituent, may demonstrate increased bioavailability yet contribute nothing to toxicity. In this case, counting radioactivity to quantify exposure at the compartment level is insufficient to distinguish carbon labels associated with active compounds from those associated with inactive metabolites. Mechanistically, it may be sufficient to consider only the subset of 11β species that still maintain two chlorine atoms, such that therapeutic effects attributable to the formation of DNA crosslinks can be parsed from those that arise through other mechanisms, such as protein hijacking or deactivation through covalent binding to functionally-critical nucleophilic residues[15], structural disruption of membranes through direct displacement of cholesterol or inhibition of cholesterol metabolism[6], or oxidative stress and dysregulation of bioenergetics provoked by redox cycling[16]. The multiplicity of pathways available to 11β between administration and covalent reaction with target macromolecules is outlined in Figure 4-8.

Hydrolysis of 11β in cell culture

The rate of disappearance of 11β-dichloro in media with cells ($t_{1/2}$ = 3.33 h) was superficially only marginally slower than what had been observed in media alone (Figure 2-11; $t_{1/2}$ = 3.03 h). This observation was not statistically significant, but the fact that the cellular compartment demonstrated concentrations of 11β on the same order of magnitude as the media compartment was suggestive of the presence of a hydrophobic sink, most likely the cell membranes. The modeled logD of 11β-dichloro is on the order of -5.0, suggesting that at equilibrium, a media:cell volume ratio of 100,000:1 would yield equal amounts of 11β-dichloro in each compartment. While the media fraction is not quite water, and the cellular fraction is not quite octanol, the assumption of ~100,000 cells per well and $(10\ \mu m)^3$ = 1 fL per cell gives a total cellular compartment volume in the system of 100 pL, which is 5×10^{-7} the volume of the 2 mL media layer. With these assumptions, a logD of -6.30 would result in the segregation of equivalent amounts of material—i.e., more than an order of magnitude away from what was observed.

Regardless of the precision of this calculation, it is reasonable to model the transport of 11β in this reduced system as shuttling between the following compartments: 1) bound to plasma protein, 2) free in plasma, 3) sequestered in cell membranes, 4) free in cytoplasm, and 5) covalently bound to cellular targets (Figure 4-8).

Subcellular distribution

Sequential separation and differential centrifugation of cells treated with various concentrations of 11β revealed interesting patterns of distribution within cellular compartments, most strikingly the high level of radioactivity detected in the putative mitochondrial DNA (mtDNA) fraction. While the methods used were not sufficient to derive a quantitative measure of DNA damage in terms of adducts per base pair, the design of such an experiment follows directly from this work. The combination of the inability of mitochondria to perform nucleotide excision repair[4], the hydrophobic-yet-cationic character of 11β facilitating mitochondrial uptake, and the natural trafficking of steroid hormones in and around the mitochondria suggests that covalent DNA damage in that organelle is not only likely to occur but also a probable contributor to the initiation of an apoptotic cascade.

Covalent binding to non-DNA targets

The failure to detect covalent adduction between nucleophilic residues of cytochrome c and 11β is almost certainly attributable to the experimental design, which preceded the quantitative assessment of the stability of 11β to hydrolysis discussed in Chapter 2. The 24-hour incubation time used by Williams et al. to study the presence and extent of protein binding between cytochrome c and reactive aldehydes formed from the hemolytic decomposition of polyunsaturated fatty acids[9] was ideal for the system for which it was designed but proved to be well beyond the timescale of 11β hydrolysis in aqueous systems. Furthermore, the covalent attack of 11β by buffer HEPES contributed to premature inactivation of the electrophile and raised questions about the use of HEPES in tissue culture media. It is yet unclear whether 11β-HEPES adducts form in media at a rate and to an extent sufficient for substantially detoxifying compound, or at least altering the effective exposure experienced by cells.

Quantitative structure-activity relationship of metabolites

As discussed in Chapter 3, solving exact structures of metabolites would require the processing of an amount of material greater than what is currently available, in addition to labor-intensive syntheses of putative metabolites for direct comparison, exhaustive purification schemes to facilitate nuclear magnetic resonance, or ion trap mass spectrometry, all of which were beyond the scope or resources of this work. However, the ability to narrow down the location of the modifications through triple quad mass spectrometry allows the modeling of the logP values of the potential compounds and the development of a preliminary quantitative structure-activity relationship. As expected, the most dramatic effects on the solubility of the molecule came from removal of chlorine or dechloroethylation. While it may be an artifact of the limitations of the modeling algorithm, it is interesting to note that the location of oxidation on the steroid ring had little influence on theoretical logP, but the addition of a hydroxyl group adjacent to a linker or mustard heteroatom strongly suggested increased hydrophilicity.

Future Directions

The therapeutic effects of 11β may extend beyond those of either androgen ablatives or non-specific toxicants, as the continued high expression of the androgen receptor in tumor cells having achieved androgen-independence should elicit greater toxicity in cells arising from prostate tumors than from healthy tissue, even after the failure of the conventional androgen blockade[17]. Cytotoxicants best achieve toxicity in dividing cells, including both rapidly-dividing tumor cells and healthy tissue. The damage to the latter is responsible for side effects that may be as serious to the health of the patient as the tumors themselves. Healthy tissue with intact nucleotide excision repair pathways should not sustain damage as persistent or extensive as that found in tumor tissue. Unlike drug design efforts that seek to target tumor cells specifically, 11β, if successful, would achieve systemic distribution and penetrate metastatic loci.

The presence or absence of estrogen receptor in ovarian cancer cells has been shown to have a strong influence[†] on the kinetics of the formation of adducts between DNA and E2-7α, a programmable genotoxicant synthesized[18] by the Essigmann Laboratory comprising an estradiol moiety connected to the aniline mustard warhead by the carbamate amine linker (Figure 1-5). Estrogen receptor, which demonstrates nuclear localization even in the absence of ligand[19], is likely to shield adducts from repair without influencing the rate of their formation. The androgen receptor, however, is localized to the cytoplasm in the absence of ligand, and must traverse a more complex path to reach not only its native function as a transcription factor but also the potentially toxic 11β-DNA adduct[20-23]. The degree to which 11β can cause AR translocation suggests that both the rate and extent of adduct formation may be enhanced through specific AR-mediated delivery of 11β from the cytoplasm to DNA.

Fully elucidating the mechanisms of toxicity of 11β observed against cells in culture and xenografts in the mouse model will require precise characterization of all of the pathways to covalent binding of cellular macromolecules. Preliminary attempts to assess the presence and extent of covalent adduction to cytochrome c were unsuccessful but provoked the posing of a far more fundamental question as to the stability of the mustard functional groups in aqueous systems. While metabolism studies comprised the

[†] Sreeja Gopal, unpublished data.

bulk of the work described in this report, revising the protein adduction efforts would be worthwhile, especially in the context of the possibility of covalent bonds to either albumin (or any plasma carrier protein) or the androgen receptor itself. One hypothesis worth exploring is that if covalent adduction to the androgen receptor occurs (via either the mustard electrophile or through a Michael addition to the conjugated 3-keto position of the steroid), residues that are in and around the active site would disproportionately participate in binding compared to those on the periphery of the molecule. Sequential incubations and fragmentations to optimize the protocol would be necessary upstream of mass spectrometry to analyze and deconvolve the data, but if successful, the cartography of adduction could be solved.

Finally, the lipophilic and cationic character of 11β makes it a prime candidate for passive diffusion into the mitochondria, where it would encounter DNA unprotected by histones and irreparable by the nucleotide excision repair (NER) machinery present in the nucleus. Mitochondrial DNA demonstrates great redundancy, with the 16 kilobase genome expressed in bundles localized to the inner membrane in copy numbers of 4–10 per mitochondrion, with 100–1000 mitochondria observed per cell[24]. The dynamics of mitochondrial DNA repair with respect to both machinery and temporal relation to replication are not sufficiently characterized to derive a hypothesis governing potential dysregulation by a bulky alkylating agent. Similarly, the regulation of mitochondrial fission, fusion, and replication does not seem to correlate with the cell cycle, except during segregation into daughter cells during mitosis[7,25-28]. Recombination may salvage mtDNA containing alkylation damage, but it is just as likely that damaged mtDNA copies would be degraded, with the overall expression level balanced by accelerated replication of undamaged copies. The high level of oxidation damage incurred by mtDNA due to respiration necessitates the constitutive expression of base excision repair proteins, so mechanisms for maintenance of mitochondrial genomic integrity do exist.

The degree to which cancer cells demonstrate different bioenergetics from healthy tissue, especially as a function of vascularization and nutrient availability, is reflected in the observation that cancer cells may generate all of the ATP they need through glycolysis. However, it is also understood that not all cells in a tumor are actively dividing, with those cells closest to blood vessels more likely to divide and progress to a

state of being able to infiltrate. In these more rapidly-dividing cells, it is unclear whether disruption of mitochondrial function caused by alkylation damage would be simply an energetic block[29] or an informational trigger of a cascade of programmed cell death. However, the absence of NER suggests that an administration pattern resulting in the accumulation of a lethal level of mtDNA damage while nuclear DNA (nDNA) adduct levels remain below a toxic threshold could be derived (Figure 4-9). Sequential small doses of 11β may create both mtDNA and nDNA adducts with measurable dose–response kinetics. Nuclear DNA would experience a peak adduction level and then demonstrates repair of adducts over time. Mitochondrial DNA, however, could experience persistent adduction with each dose resulting in a plateau at that level of damage. A subsequent dose would begin from that pre-existing level of damage, while nDNA would have been fully repaired in the time interval. As such, a threshold of mtDNA damage could be achieved before the triggering of the apoptotic cascade provoked by excessive nDNA damage or saturation of repair machinery. Increased persistence of mtDNA damage as compared to nDNA damage has been observed in the context of reactive oxygen species caused by mitochondrial oxidative phosphorylation[30].

Furthermore, increasing evidence of the activity of steroid receptors in and around the mitochondria, including the mitochondrial localization of estrogen receptor beta (ERβ)[31-38], suggests that the repair shielding and transcription factor hijacking mechanisms central to the hypothesis governing the design of these programmable genotoxicants may apply to mtDNA damage and repair as well as the nDNA originally targeted. If metabolic transformation of 11β includes aromatization of the A-ring, the resulting 3-hydroxy functionality could yield affinity for the estrogen receptor—11β already possesses two unsaturated carbon–carbon bonds conjugated to the 3-keto moiety, and, as such, could rearrange to an aromatic group without further oxidation. Competitive binding between modified steroids and estradiol has been shown to occur with lower IC_{50} values with ERβ than ERα[39], suggesting that the mitochondrial version of the receptor may be more permissive and therefore more likely to interact with 11β.

Given the electronic favorability of 11β entering the mitochondria, the potential for interaction between 11β (or its potential DNA adducts) and ERβ, and the likelihood that mitochondrial DNA damage caused by 11β would persist in the absence of

nucleotide excision repair, it is reasonable to consider the possibility that the apoptotic cascade observed *in vitro* could be provoked directly from mitochondrial dysregulation in addition to, or instead of, a series of nuclear events[7,8,25,29]. The high number of individual mitochondria in a cell and the high copy number of mtDNA molecules in an individual mitochondrion offer redundancy that protects the cell from a loss of mitochondrial function following irreparable alkylation damage. However, a probabilistic threshold could exist if there is either a minimum number of copies or a minimum fraction of the total copy number that must remain intact to preserve mitochondrial function, and treatment with 11β is sufficient to breach that threshold. As such, the extents and timescales of mitochondrial DNA damage and repair, as well as the ensuing dynamic changes in mitochondrial structure and function must be studied to assess the importance of the activity of 11β in this critical organelle.

Figure 4-1: 11β achieves more uniform biodistribution after intraperitoneal injection than gavage delivery

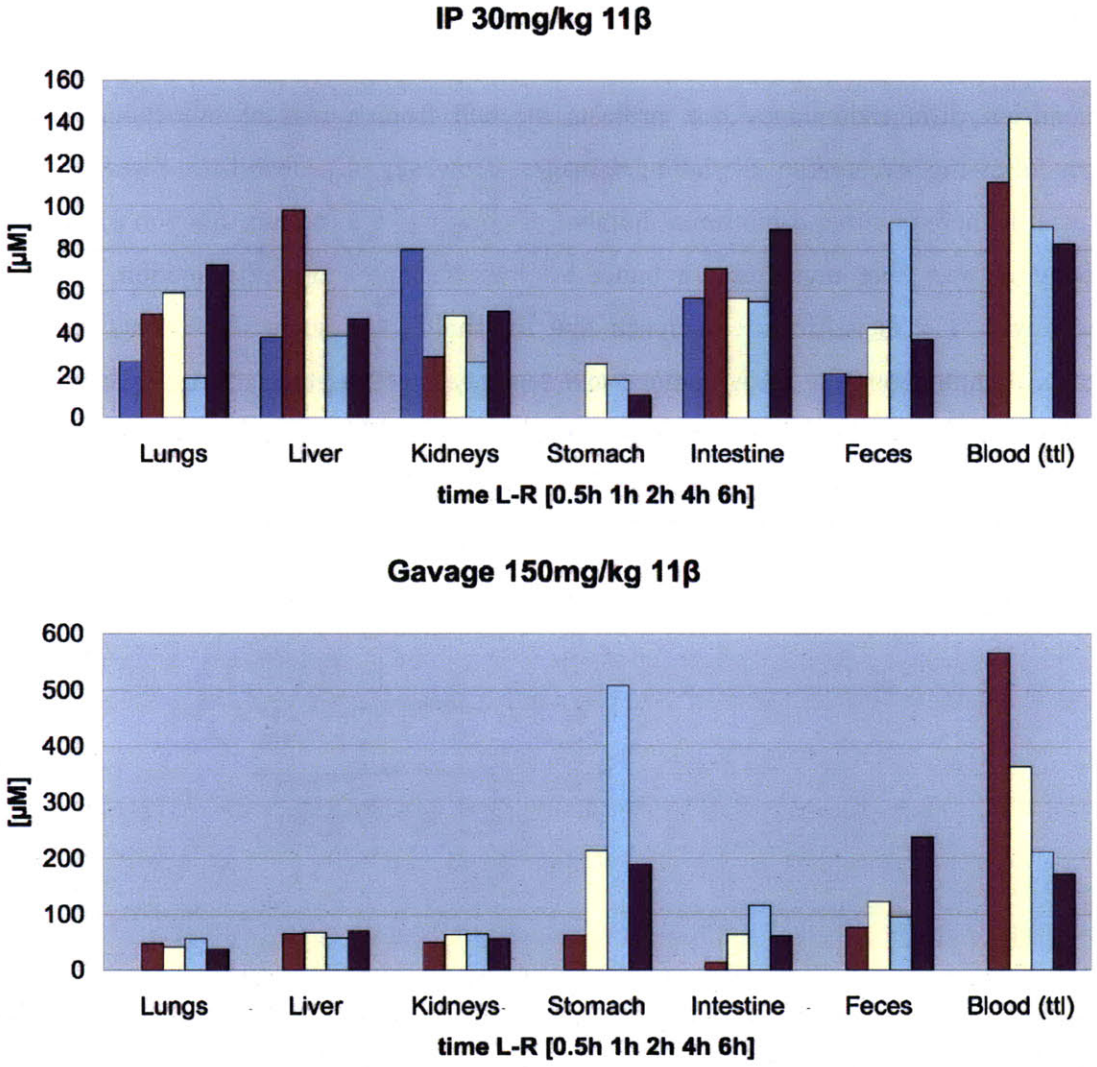

Figure 4-2: 11β is absorbed by blood cells following distribution into plasma

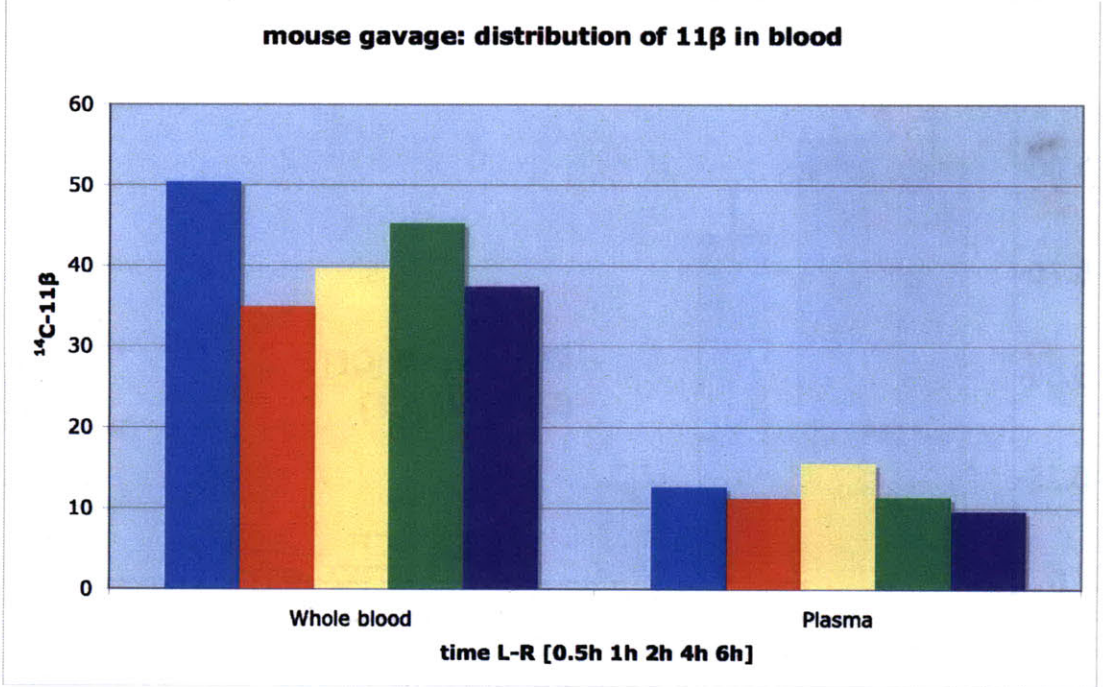

Approximately 75% of the radioactivity associated with 11β in blood was in the cellular pellet following centrifugation of sample collected with EDTA to avoid clotting.

Figure 4-3: Albumin and high chloride slowed 11β hydrolysis

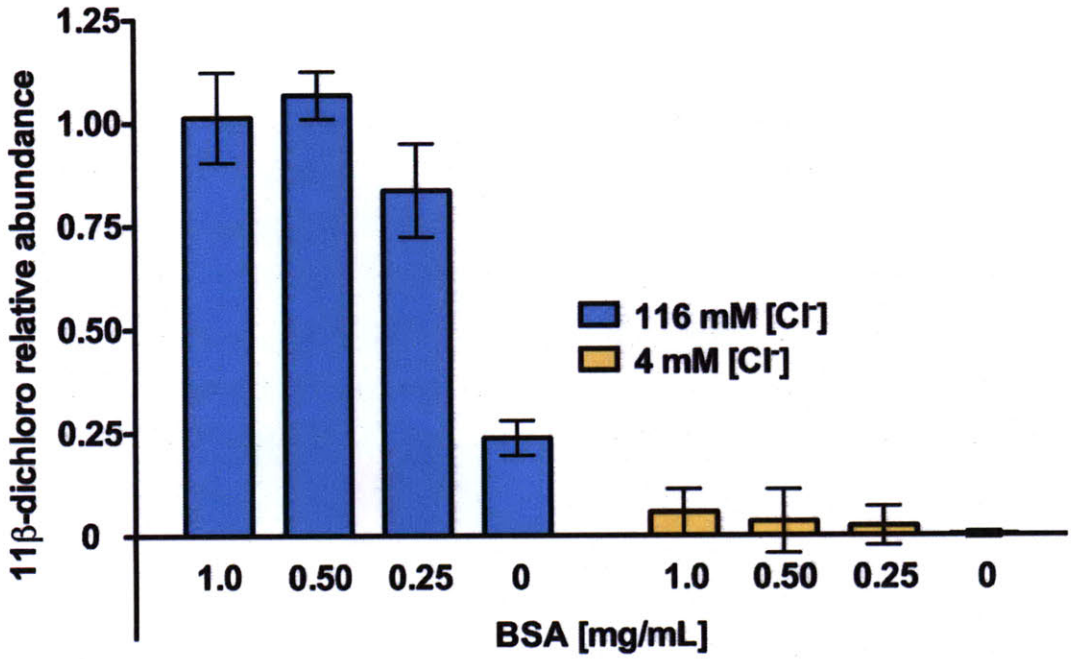

After two hours, the presence of 1 mg/mL bovine serum albumin protected 11β-dichloro from hydrolysis, showing four times the level of intact compound than the reaction with no protein. The reactions with plasma levels of chloride ion (116 mM) showed substantially more intact dichloro compound than those prepared with cytoplasmic levels (4 mM). The adsorption of 11β to plasma protein following administration has a significant influence on the bioavailability of the drug. All samples were performed in triplicate; error bars represent 95% confidence intervals.

Figure 4-4: Comparable levels of 11β were present in the media and cellular fractions of an in vitro incubation with PC3-AR1 cells

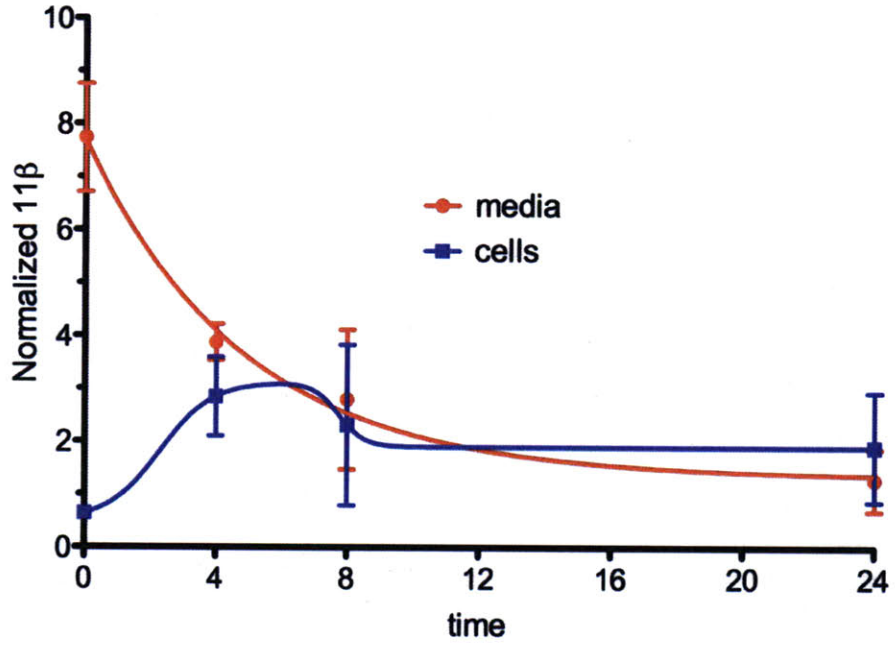

The rate of disappearance of 11β in the media compartment was comparable to that observed in hydrolysis in cell culture media. A significant amount of compound was taken up by cells, with equal partitioning between the two compartments achieved after six hours.

Figure 4-5: Sequential separation of system compartments following in vitro treatment of LNCaP cells with various doses of ^{14}C-11β

a) Media aspirated from wells contained activity proportional to the initial dose at time points up to six hours after initiation of treatment, indicating no depletion caused by cellular uptake.

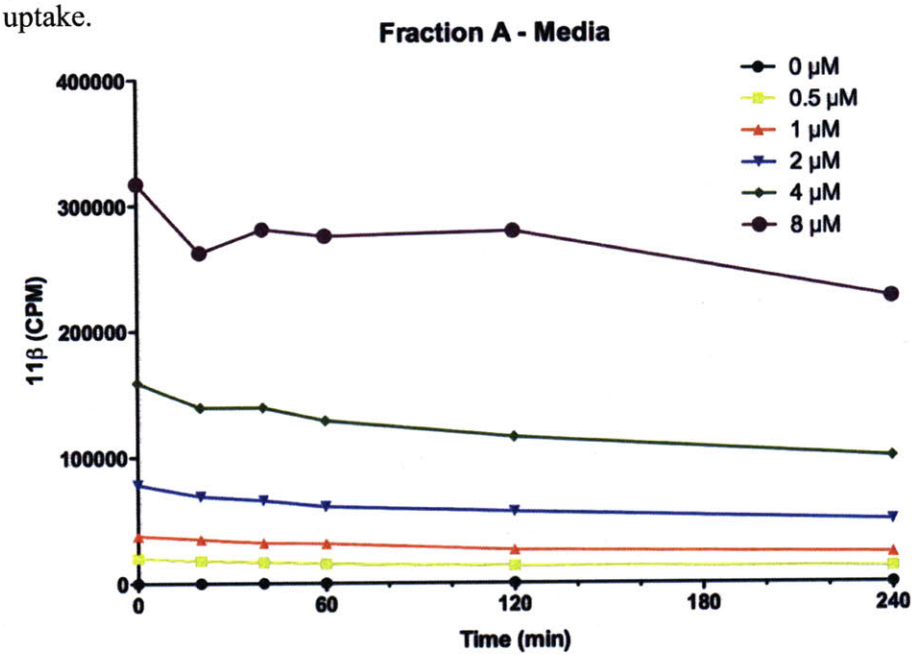

b) The supernatant after trypsinization possessed low activity and was roughly proportional to dose.

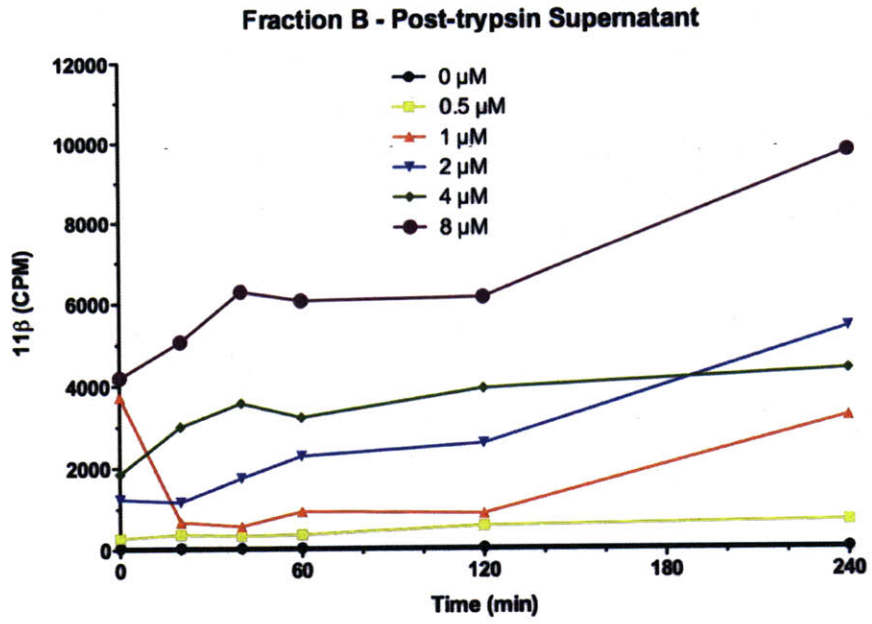

Figure 4-5: Sequential separation of system compartments following in vitro treatment of LNCaP cells with various doses of ^{14}C-11β

c) Whole cell lysate revealed levels of uptake of compound roughly proportional to dose and nearly-linear kinetics. After six hours, no more than 10% of the total radioactivity introduced into the system had diffused into cells.

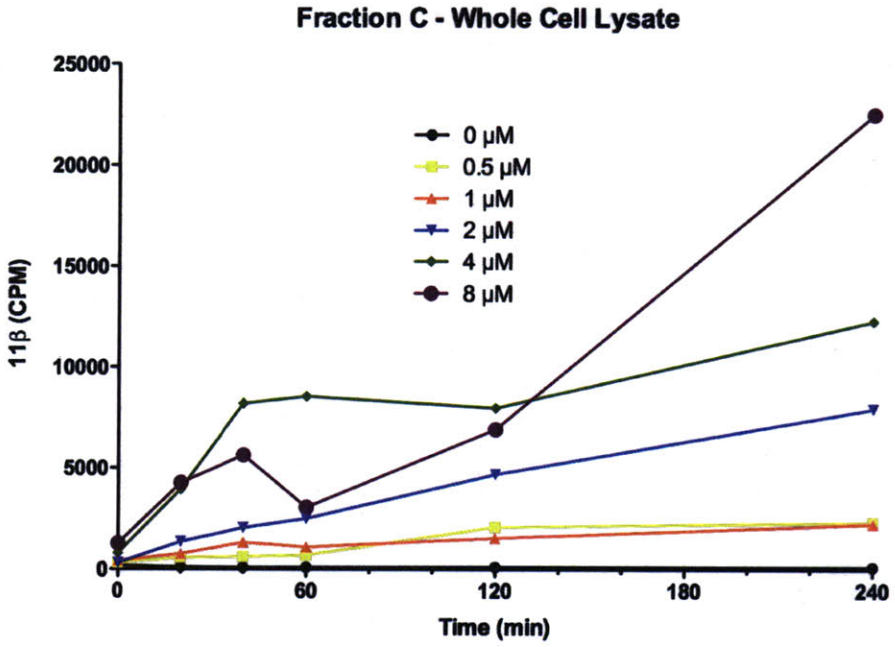

d) Washes of the plates post-trypsinization indicated measurable quantities of compound adsorbed to the plastic. However, it is curious that low doses (≤ 2 μM) leave negligible residue, while treatments in the dose ranges where toxicity is expected seemed to generate more debris, cellular or otherwise.

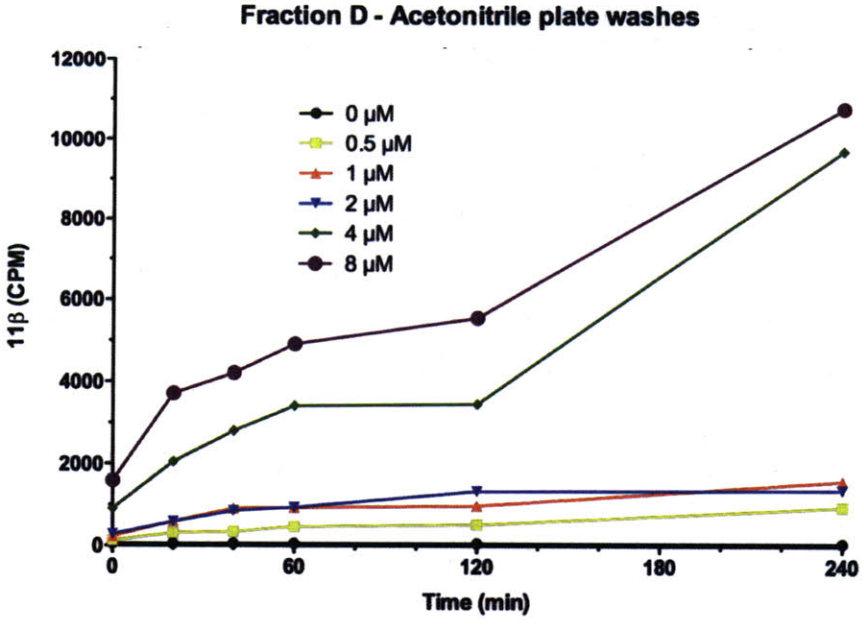

Figure 4-5: Sequential separation of system compartments following in vitro treatment of LNCaP cells with various doses of ^{14}C-11β

e) The organic fraction from the first extraction step of the post-nuclear supernatant showed some lingering activity that was most likely free compound; whether that represents 11β or some hydrolytic or metabolic derivative is unclear.

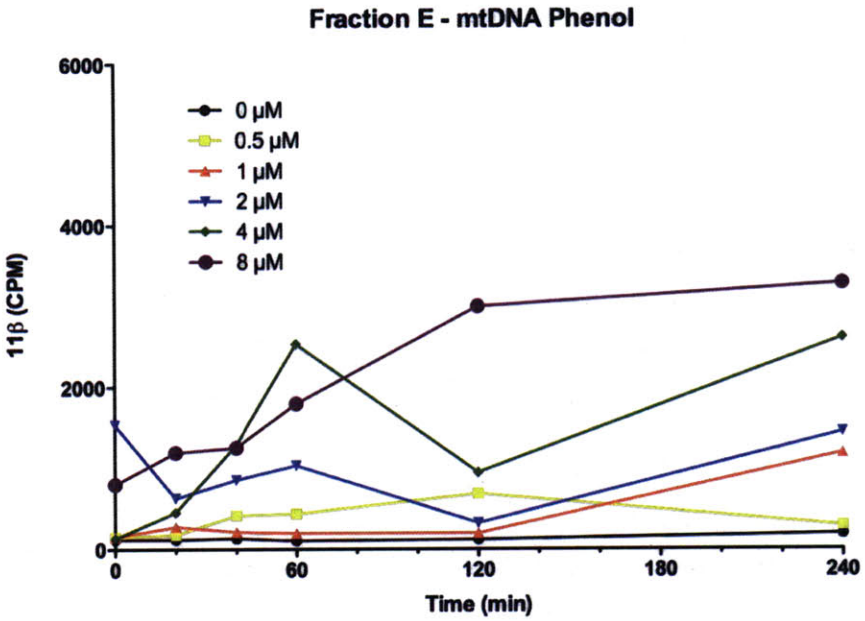

f) Similarly, activity left in the system after the pelleting of nuclei and heavy organelles seemed to increase with time and be proportional to initial dose.

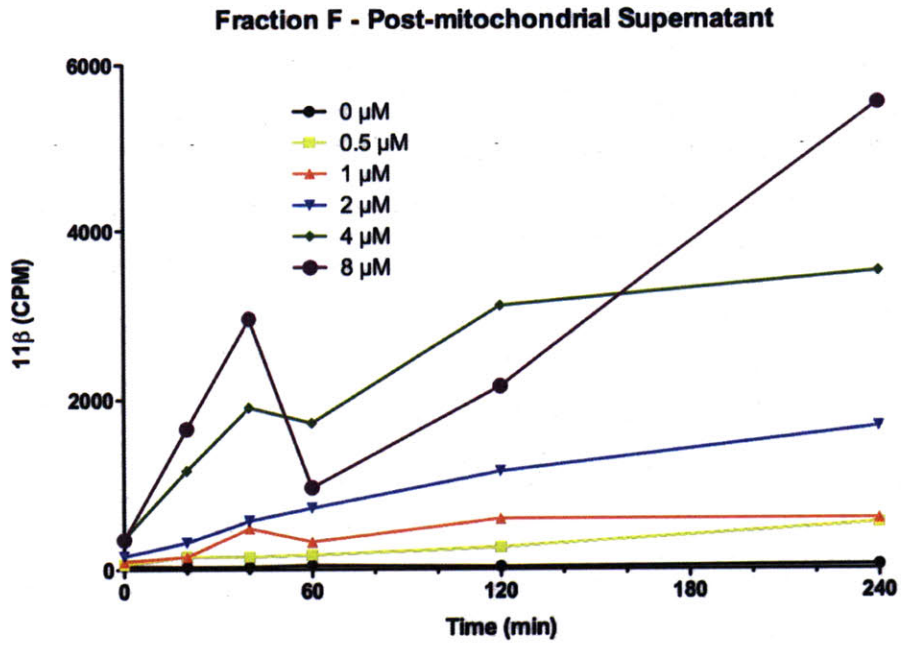

Figure 4-5: Sequential separation of system compartments following in vitro treatment of LNCaP cells with various doses of ^{14}C-11β
g) The levels of activity left in the nuclear fraction following the first extraction step were comparable to that seen in the mitochondrial DNA phenol phase.

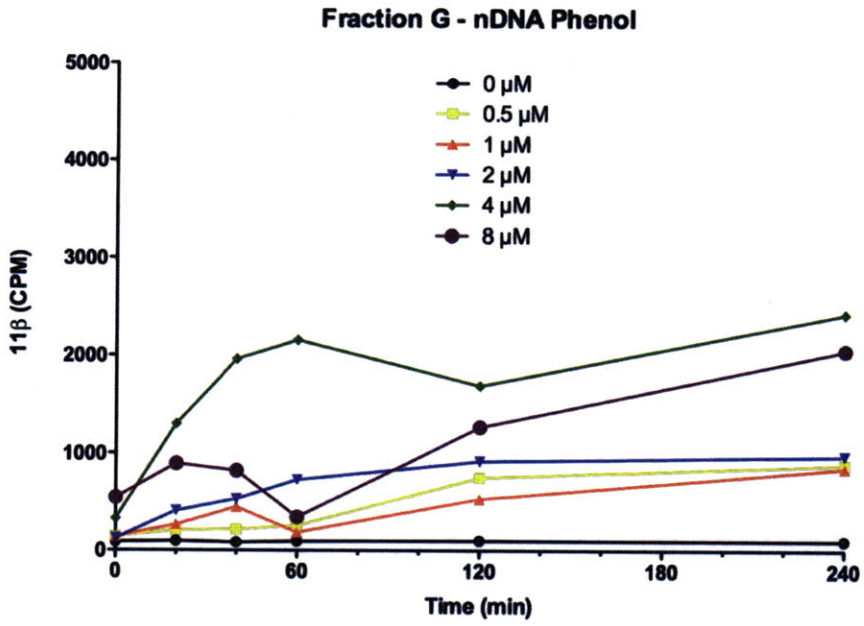

Figure 4-5: Sequential separation of system compartments following in vitro treatment of LNCaP cells with various doses of ^{14}C-11β

h) Activity associated with nuclear DNA was roughly proportional to dose except in the case of the 8μM treatment, which seemed to immediately permeate the system and form DNA adducts but then experienced a lag until later in the treatment.

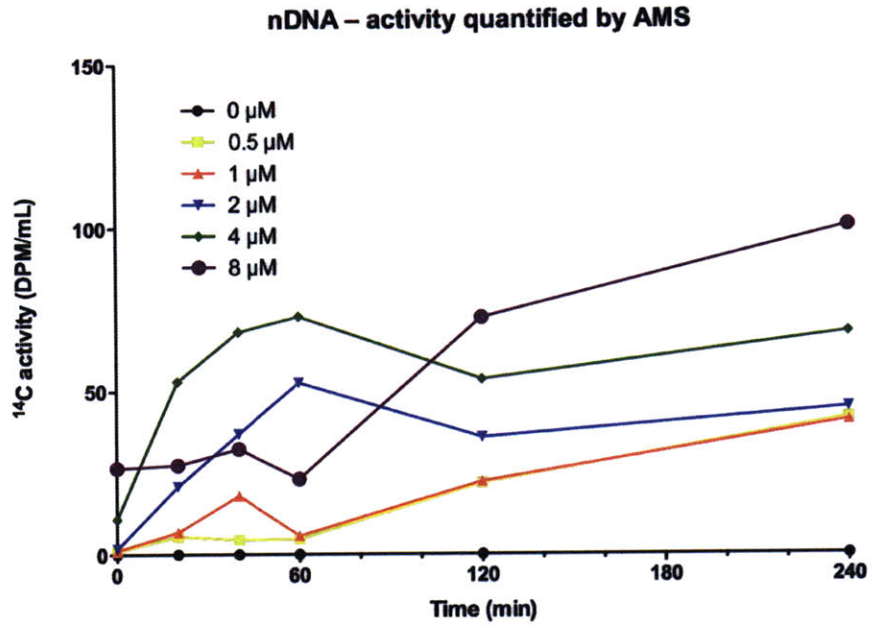

i) Interestingly, activity levels in the mitochondrial DNA fraction were on the same order of magnitude as those in nuclear DNA, which, since mitochondrial DNA comprises roughly 2% of all cellular DNA, and assuming that the yields of the respective extractions were comparable, suggests that significantly higher levels of DNA damage on a per-base-pair basis are occurred in mitochondria.

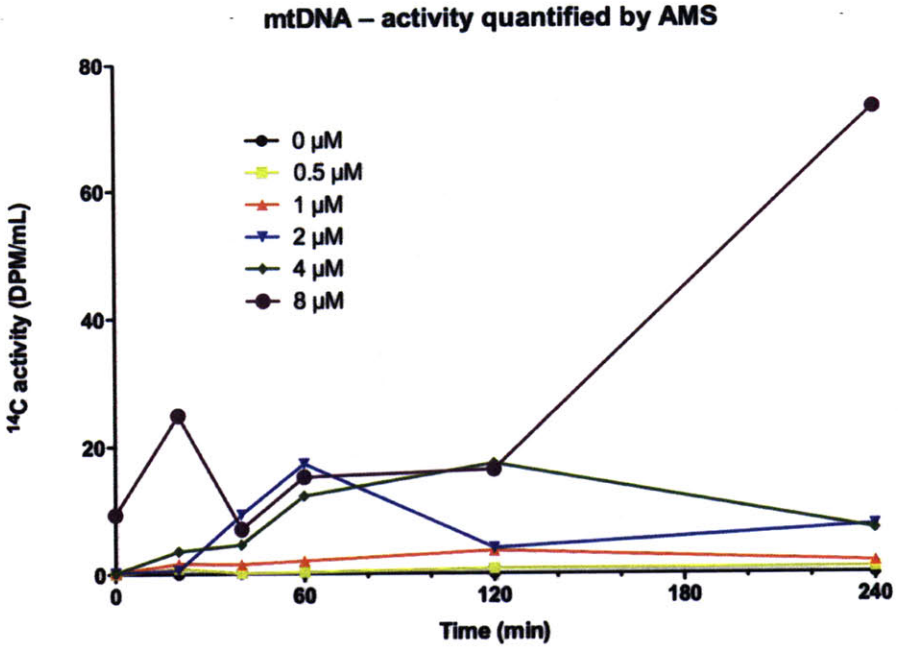

Figure 4-6: LC–ESI-TOF of cytochrome c/11β system
a) Cytochrome c charge envelope

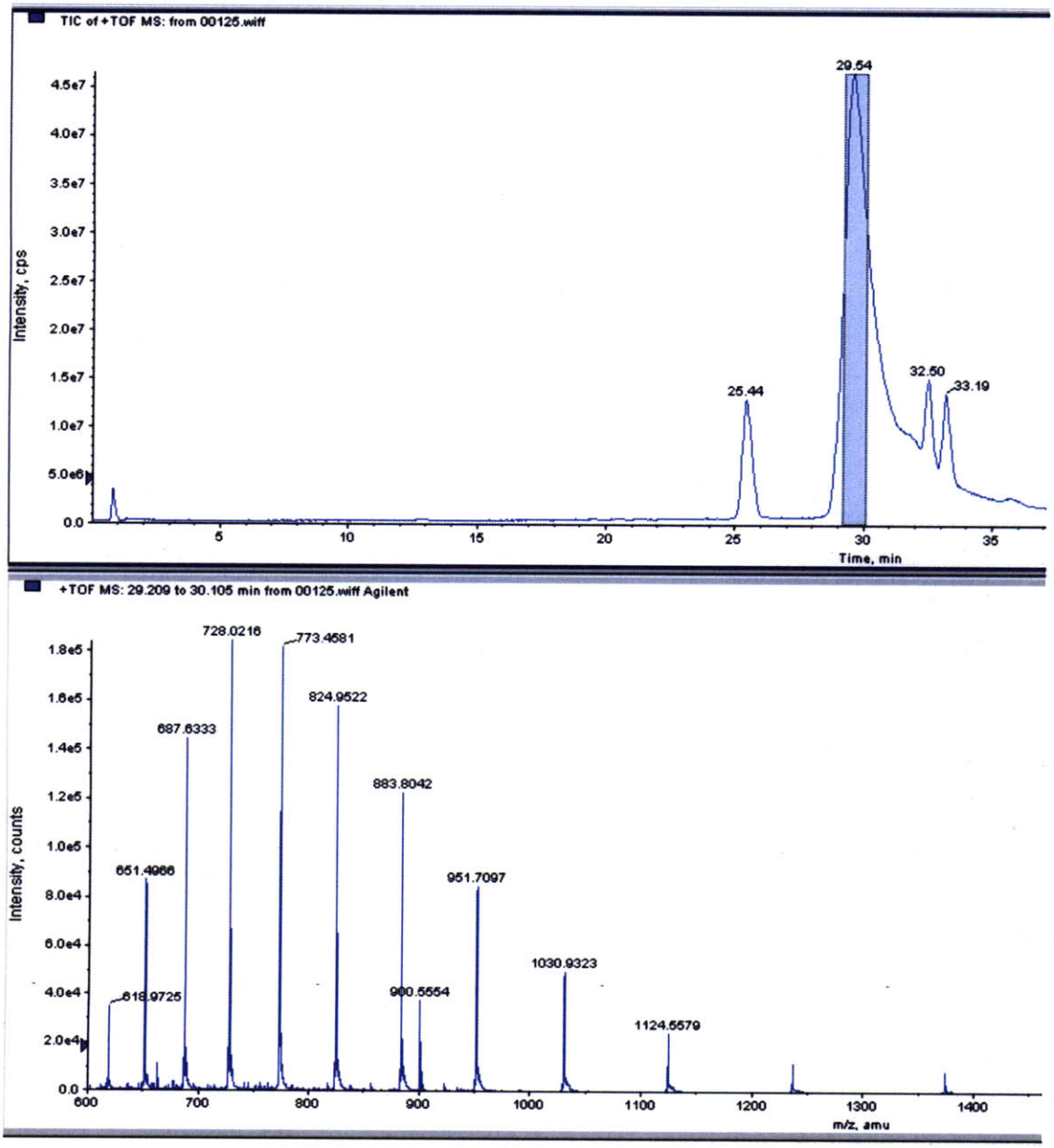

Incubation of 11β with cytochrome c yielded no apparent protein adducts. A single adduct would have appeared as a charge envelope that deconvolved to MW 13,001. The most abundant charge state observed at these conditions was the $[M+17]^{17+}$ peak at m/z 728, and absence of a signal at 766 confirmed the lack of these reaction conditions to allow covalent adducts to form.

Figure 4-6: LC–ESI-TOF of cytochrome c/11β system
b) HEPES reacts with 11β

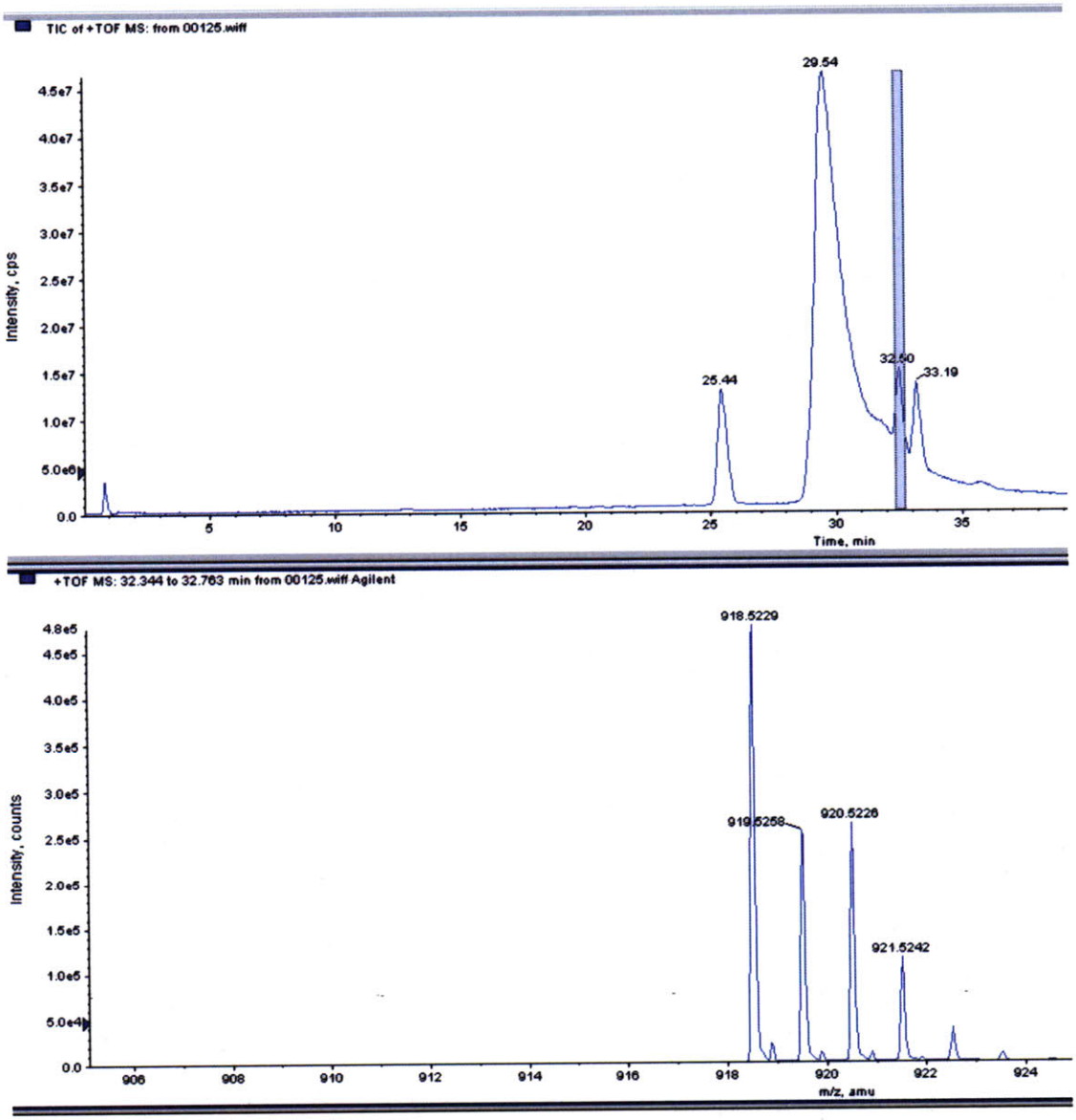

A species with m/z 918 and isotope character suggesting one chlorine atom was observed, consistent with the product of a reaction between 11β and HEPES. The displacement of chlorine (-35) and the subsequent attack by HEPES (+237) resulted in a net +202 change from parent 11β.

Figure 4-6: LC–ESI-TOF of cytochrome c/11β system
c) HEPES reacts with 11β

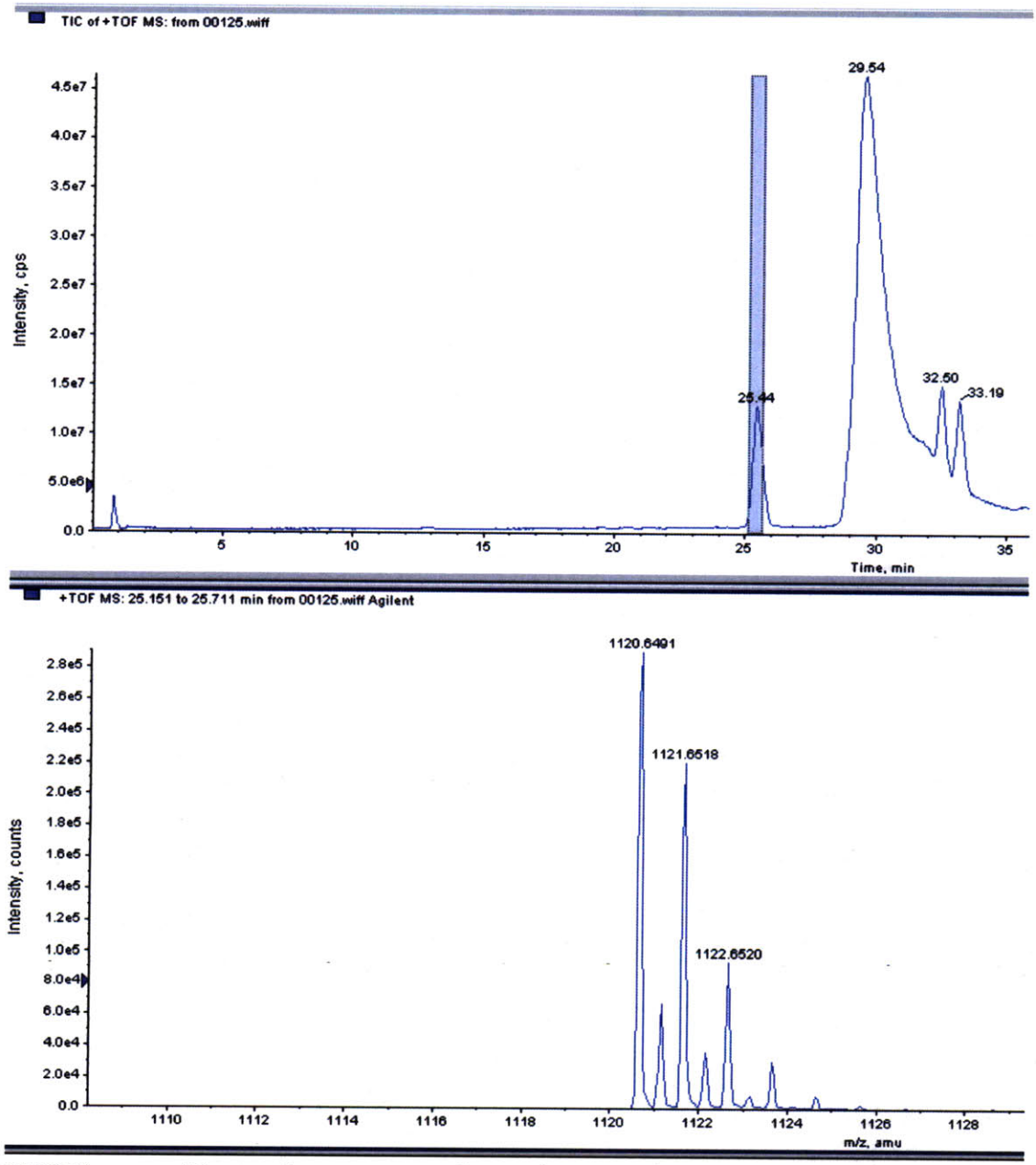

HEPES was able to form a second covalent species with 11β with m/z 1120 (716+202+202) and no chlorine isotope character.

Figure 4-7: QSAR modification analysis

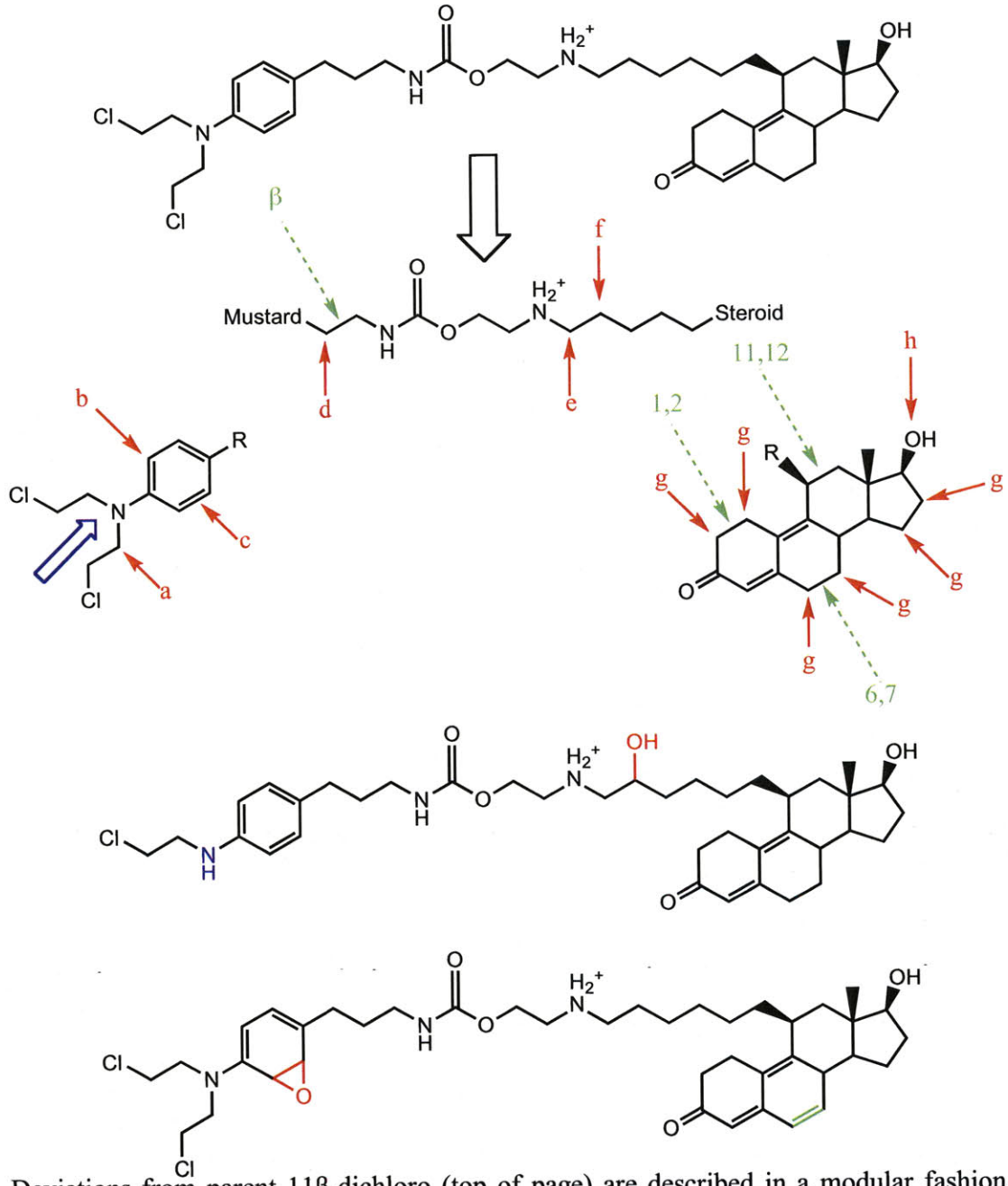

Deviations from parent 11β-dichloro (top of page) are described in a modular fashion. Red arrows and small letters indicate locations where addition of an oxygen atom (+16) was modeled. Green dashed arrows and numbers designate locations of oxidation to an alkene or keto group (-2). The blue solid arrow indicates an N-dealkylation. The two example product structures shown correspond a species with m/z 670 (top) with one mustard arm lost and hydroxylation at position f, β to the linker amine; and a species with m/z 730 (bottom) with oxidation at the 6–7 position of the steroid and epoxidation at position c, the aniline phenyl ring (bottom).

Figure 4-8: Plasma protein binding and subcellular distribution of 11β

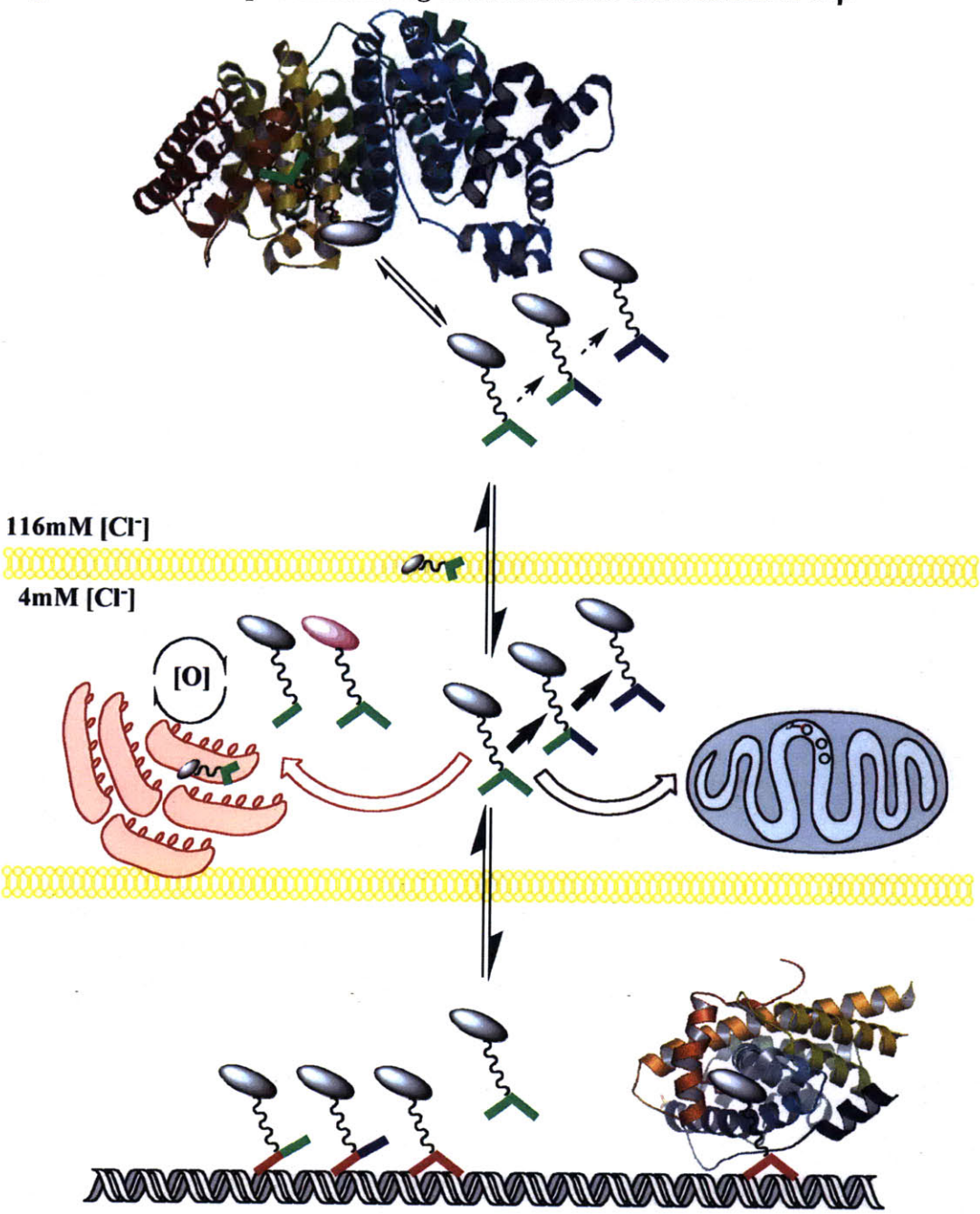

The pathways available to 11β between absorption into the blood stream and formation of nuclear DNA adducts and crosslinks includes, but is not limited to, equilibrium between free compound and plasma protein (albumin, shown), sequestration in lipophilic cell membranes, metabolism in endoplasmic reticulum, and diffusion into mitochondria. In either the nucleus or the mitochondria, DNA adducts may form. The relative rates of hydrolysis of parent compound are strongly dependent on chloride ion concentration, but metabolic transformations may also influence the dynamics of the compound.

Figure 4-9: Theoretical accumulation of damage in an NER-deficient compartment

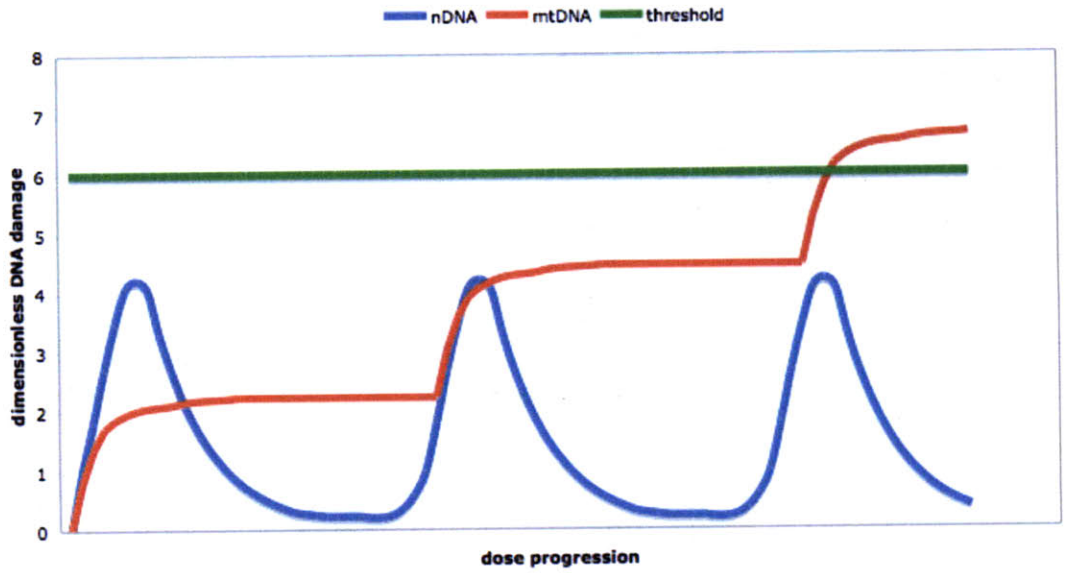

Repeated small doses of an alkylating agent should generate transient damage and repair patterns in the nuclear compartment. However, irreparable mitochondrial DNA damage may accumulate over the same time scale, reaching a threshold of toxicity and activating a program of cell death directly.

Table 4-1: Predicted milogP values for observed metabolites

m/z	Q1->Q3	logP[NH]	Δ716	logP[NH$_2^+$]	Δ+/0	mustard side modification	steroid side modification
748	374->398	7.158	-0.583	4.494	2.664	2,6-dihydroxyphenyl	
	374->414	7.142	-0.599	4.128	3.014	2-hydroxyphenyl	+O α to linker N
	374->398	6.792	-0.949	4.128	2.664	2-hydroxyphenyl, +O α to mustard N	
	374->414	6.776	-0.965	3.761	3.015	+O α to mustard N	+O α to linker N
	374->414	6.534	-1.207	3.870	2.664	2-hydroxyphenyl	+O on steroid
	374->414	6.346	-1.395	3.332	3.014	epoxide on phenyl	+O α to linker N
	374->414	6.299	-1.442	3.635	2.664	2-hydroxyphenyl	+O β to linker N
	374->398	6.287	-1.454	3.623	2.664	2-hydroxyphenyl, +O β to phenyl/carbamate N	
	374->414	6.271	-1.470	3.256	3.015	+O β to phenyl/carbamate N	+O α to linker N
	374->414	6.167	-1.574	3.503	2.664	+O α to mustard N	+O on steroid
	374->414	5.933	-1.808	3.269	2.664	+O α to mustard N	+O β to linker N
	374->398	5.920	-1.821	3.256	2.664	+O α to mustard N, +O β to phenyl/carbamate N	
	374->414	5.738	-2.003	3.074	2.664	epoxide on phenyl	+O on steroid
	374->414	5.662	-2.079	2.998	2.664	+O β to phenyl/carbamate N	+O on steroid
	374->414	5.504	-2.237	2.840	2.664	epoxide on phenyl	+O β to linker N
	374->414	5.428	-2.313	2.764	2.664	+O β to phenyl/carbamate N	+O β to linker N
	374->398	5.262	-2.479	2.598	2.664	+O α to mustard N on both arms	
732	366->398	7.449	-0.292	4.785	2.664	2-hydroxyphenyl	
	366->414	7.433	-0.308	4.419	3.014		+O α to linker N
	366->398	7.083	-0.658	4.419	2.664	+O α to mustard N	
	366->414	6.825	-0.916	4.161	2.664		+O on steroid
	366->398	6.654	-1.087	3.990	2.664	epoxide on phenyl	
	366->414	6.591	-1.150	3.927	2.664		+O β to linker N
	366->398	6.578	-1.163	3.914	2.664	+O β to the phenyl/carbamate N	
730	365->412	8.108	0.367	5.099	3.009		1=2, +O α to linker N
	365->412	7.505	-0.236	4.841	2.664		1=2, +O on steroid
	365->398	7.479	-0.262	4.815	2.664	2-hydroxyphenyl, unsaturated C=C conjugated to phenyl	
	365->412	7.271	-0.470	4.607	2.664		1=2, +O β to linker N
	365->412	7.248	-0.493	4.233	3.015		17-keto, +O α to linker N
	365->398	7.112	-0.629	4.448	2.664	+O α to mustard N, unsaturated C=C conjugated to phenyl	
	365->412	6.927	-0.814	3.913	3.014		6=7, +O α to linker N
	365->398	6.654	-1.087	3.990	2.664	epoxide on phenyl, unsaturated C=C conjugated to phenyl	
	365->412	6.640	-1.101	3.976	2.664		17-keto, +O on steroid
	365->412	6.405	-1.336	3.741	2.664		17-keto, +O β to linker N
	365->412	6.319	-1.422	3.655	2.664		6=7, +O on steroid
	365->398	6.147	-1.594	3.483	2.664	epoxide on phenyl	6=7
	365->412	6.084	-1.657	3.420	2.664		6=7, +O β to linker N
716	358->398	7.741	-	5.077	2.664		
714	357->398	8.351	0.610	5.757	2.594		1=2
	357->396	7.770	0.029	5.106	2.664	unsaturated C=C conjugated to phenyl	
	357->398	7.557	-0.184	4.893	2.664		11=12
	357->398	7.555	-0.186	4.891	2.664		17-keto
	357->398	7.234	-0.507	4.570	2.664		6=7
712	356->396	8.372	0.631	5.786	2.586		1=2
	356->394	8.239	0.498	5.606	2.633		1=2, 6=7
	356->394	8.213	0.472	5.573	2.640		11=12, 1=2
	356->394	8.211	0.470	5.571	2.640		17-keto, 1=2
	356->398	7.850	0.109	5.186	2.664		
	356->396	7.586	-0.155	4.922	2.664		11=12
	356->396	7.584	-0.157	4.920	2.664	unsaturated C=C conjugated to phenyl	17-keto
	356->394	7.557	-0.184	4.893	2.664		17-keto, 11=12
	356->394	7.533	-0.208	4.869	2.664		17-keto, 15=16
	356->396	7.264	-0.477	4.600	2.664		6=7
	356->394	7.051	-0.690	4.387	2.664		11=12, 6=7
	356->394	7.049	-0.692	4.385	2.664		17-keto, 6=7
698	349->398	6.503	-1.238	3.839	2.664	singly-hydrolyzed mustard	
680	340->398	5.265	-2.476	2.601	2.664	doubly-hydrolyzed mustard	
670	335->398	6.599	-1.142	3.935	2.664	-EtCl, phenyl OH	
	335->414	6.583	-1.158	3.568	3.015		+O β to linker N
	335->398	6.232	-1.509	3.568	2.664	-EtCl, +O α to mustard N	
	335->414	5.975	-1.766	3.311	2.664		+O on steroid
	335->398	5.803	-1.938	3.139	2.664	-EtCl, epoxide on phenyl	
	335->414	5.740	-2.001	3.076	2.664		+O α to linker N
	335->398	5.727	-2.014	3.063	2.664	-EtCl, +O β to phenyl/carbamate N	
654	327->398	6.890	-0.851	4.226	2.664	-EtCl	

Orange: parent 11β-dichloro. **Yellow:** single subtractive modifications. **Blue:** single additive modifications.
m/z: mass-to-charge ratio of monoisotopic +1 species. **Q1->Q3:** transition in triple quadrupole.
milogP[NH]: modeled partition coefficient with neutral linker amine. **Δ716:** change in milogP from 11β-dichloro.
milogP[NH$_2^+$]: modeled partition coefficient with positively charged linker amine. **Δ+/0:** difference in charged vs. neutral milogP.

Metabolic modifications to 11β resulted in modular changes to the milogP, with hydroxylation at the beta position between the carbamate nitrogen and the phenyl ring generating the highest increase in hydrophilicity without hydrolyzing a mustard chloroethyl arm. The balance between increasing bioavailability by lowering milogP and losing AR affinity through steroid ring modification would be one aspect of the next iteration of compound design.

References

1. Hillier, S.M. et al. DNA adducts formed by a novel antitumor agent 11beta-dichloro in vitro and in vivo. *Mol. Cancer Ther* **5**, 977-984(2006).
2. Marquis, J.C. et al. Disruption of gene expression and induction of apoptosis in prostate cancer cells by a DNA-damaging agent tethered to an androgen receptor ligand. *Chem. Biol* **12**, 779-787(2005).
3. Rink, S.M. et al. Synthesis and biological activity of DNA damaging agents that form decoy binding sites for the estrogen receptor. *Proc. Natl. Acad. Sci. U.S.A* **93**, 15063-15068(1996).
4. Clayton, D.A., Doda, J.N. & Friedberg, E.C. The absence of a pyrimidine dimer repair mechanism in mammalian mitochondria. *Proc. Natl. Acad. Sci. U.S.A* **71**, 2777-2781(1974).
5. Mannella, C.A. & Wang, Q. Permeability of the mitochondrial outer membrane to organic cations. *Biochim. Biophys. Acta* **981**, 363-366(1989).
6. Di Vizio, D., Solomon, K.R. & Freeman, M.R. Cholesterol and cholesterol-rich membranes in prostate cancer: an update. *Tumori* **94**, 633-639(2008).
7. Karbowski, M. & Youle, R.J. Dynamics of mitochondrial morphology in healthy cells and during apoptosis. *Cell Death Differ* **10**, 870-880(2003).
8. Youle, R.J. & Karbowski, M. Mitochondrial fission in apoptosis. *Nat. Rev. Mol. Cell Biol* **6**, 657-663(2005).
9. Williams, M.V., Wishnok, J.S. & Tannenbaum, S.R. Covalent adducts arising from the decomposition products of lipid hydroperoxides in the presence of cytochrome c. *Chem. Res. Toxicol* **20**, 767-775(2007).
10. Fang, H. et al. Study of 202 natural, synthetic, and environmental chemicals for binding to the androgen receptor. *Chem. Res. Toxicol* **16**, 1338-1358(2003).
11. Doumas, B.T. et al. A candidate reference method for determination of total protein in serum. I. Development and validation. *Clin. Chem* **27**, 1642-1650(1981).
12. Bhattacharya, A.A., Grüne, T. & Curry, S. Crystallographic analysis reveals common modes of binding of medium and long-chain fatty acids to human serum albumin. *J. Mol. Biol* **303**, 721-732(2000).
13. Lee, F.Y., Coe, P. & Workman, P. Pharmacokinetic basis for the comparative antitumour activity and toxicity of chlorambucil, phenylacetic acid mustard and beta, beta-difluorochlorambucil (CB 7103) in mice. *Cancer Chemother. Pharmacol* **17**, 21-29(1986).
14. Wolf, K.K. et al. Effect of Albumin on the Biliary Clearance of Compounds in Sandwich-Cultured Rat Hepatocytes. *Drug Metab Dispos* **36**, 2086-2092(2008).
15. Cai, J., Bhatnagar, A. & Pierce, W.M. Protein modification by acrolein: formation and stability of cysteine adducts. *Chem. Res. Toxicol* **22**, 708-716(2009).
16. Shu, Y., Johnson, B.M. & Yang, T.J. Role of biotransformation studies in minimizing metabolism-related liabilities in drug discovery. *AAPS J* **10**, 178-192(2008).
17. Scher, H.I. et al. Targeting the androgen receptor: improving outcomes for castration-resistant prostate cancer. *Endocr Relat Cancer* **11**, 459-476(2004).
18. Mitra, K. et al. A rationally designed genotoxin that selectively destroys estrogen receptor-positive breast cancer cells. *J Am Chem Soc* **124**, 1862-3(2002).

19. Welshons, W.V., Lieberman, M.E. & Gorski, J. Nuclear localization of unoccupied oestrogen receptors. *Nature* **307**, 747-749(1984).
20. Baulieu, E.E. & Jung, I. A prostatic cytosol receptor. *Biochem. Biophys. Res. Commun* **38**, 599-606(1970).
21. Jenster, G., Trapman, J. & Brinkmann, A.O. Nuclear import of the human androgen receptor. *Biochem J.* **293**, 761–768(1993).
22. Roy, A.K. et al. Androgen receptor: structural domains and functional dynamics after ligand-receptor interaction. *Ann N Y Acad Sci* **949**, 44-57(2001).
23. Tyagi, R.K. et al. Dynamics of Intracellular Movement and Nucleocytoplasmic Recycling of the Ligand-Activated Androgen Receptor in Living Cells. *Mol Endocrinol* **14**, 1162-1174(2000).
24. Jansen, R.P. Origin and persistence of the mitochondrial genome. *Hum. Reprod* **15 Suppl 2**, 1-10(2000).
25. Detmer, S.A. & Chan, D.C. Functions and dysfunctions of mitochondrial dynamics. *Nat. Rev. Mol. Cell Biol* **8**, 870-879(2007).
26. Chen, H. & Chan, D.C. Emerging functions of mammalian mitochondrial fusion and fission. *Hum. Mol. Genet* **14 Spec No. 2**, R283-289(2005).
27. Yaffe, M.P. The machinery of mitochondrial inheritance and behavior. *Science* **283**, 1493-1497(1999).
28. Chan, D.C. Mitochondrial fusion and fission in mammals. *Annu. Rev. Cell Dev. Biol* **22**, 79-99(2006).
29. Hammerman, P.S., Fox, C.J. & Thompson, C.B. Beginnings of a signal-transduction pathway for bioenergetic control of cell survival. *Trends Biochem. Sci* **29**, 586-592(2004).
30. Yakes, F.M. & Van Houten, B. Mitochondrial DNA damage is more extensive and persists longer than nuclear DNA damage in human cells following oxidative stress. *Proc. Natl. Acad. Sci. U.S.A* **94**, 514-519(1997).
31. Solakidi, S. et al. Estrogen receptors alpha and beta (ERalpha and ERbeta) and androgen receptor (AR) in human sperm: localization of ERbeta and AR in mitochondria of the midpiece. *Hum. Reprod* **20**, 3481-3487(2005).
32. Yang, S. et al. Mitochondrial localization of estrogen receptor beta. *Proc. Natl. Acad. Sci. U.S.A* **101**, 4130-4135(2004).
33. Cammarata, P.R. et al. Subcellular distribution of native estrogen receptor alpha and beta subtypes in cultured human lens epithelial cells. *Exp. Eye Res* **78**, 861-871(2004).
34. Yang, S. et al. Estrogen receptor beta as a mitochondrial vulnerability factor. *J. Biol. Chem* **284**, 9540-9548(2009).
35. Chen, J., Yager, J.D. & Russo, J. Regulation of mitochondrial respiratory chain structure and function by estrogens/estrogen receptors and potential physiological/pathophysiological implications. *Biochim. Biophys. Acta* **1746**, 1-17(2005).
36. Chen, J.Q. et al. Binding of MCF-7 cell mitochondrial proteins and recombinant human estrogen receptors alpha and beta to human mitochondrial DNA estrogen response elements. *J. Cell. Biochem* **93**, 358-373(2004).

37. Stettner, M. et al. The relevance of estrogen receptor-{beta} expression to the antiproliferative effects observed with histone deacetylase inhibitors and phytoestrogens in prostate cancer treatment. *Mol Cancer Ther* **6**, 2626-2633(2007).
38. Maggiolini, M. et al. Oestrogen receptor beta is required for androgen-stimulated proliferation of LNCaP prostate cancer cells. *J Mol Endocrinol* **32**, 777-91(2004).
39. Blizzard, T.A. et al. Androstene-3,5-dienes as ER-beta selective SERMs. *Bioorg. Med. Chem. Lett* **17**, 6295-6298(2007).

Charles I. Morton
cimiv@mit.edu
(617) 253-6207

Massachusetts Institute of Technology
Department of Biological Engineering
32 Vassar St. 56-686 • Cambridge, MA 02139

EDUCATION

Massachusetts Institute of Technology — Cambridge, MA
Department of Biological Engineering — *June, 2009*
Ph.D., Molecular and Systems Toxicology and Pharmacology
Advisor: Prof. John M. Essigmann
Thesis: Metabolic and Mechanistic Exploration of a Novel Programmable Genotoxicant against Prostate Cancer

Massachusetts Institute of Technology — Cambridge, MA
S.B. in Chemical Engineering, minor in Biomedical Engineering — *June, 1997*
Advisor: Prof. Karen Gleason
Minor Advisor: Prof. Linda Griffith

RESEARCH EXPERIENCE

MIT Department of Biological Engineering — Cambridge, MA
Advisor: Prof. John M. Essigmann — *2000-2009*
Research focused on the administration, metabolism, and mechanism of a novel agent designed to treat metastatic prostate cancer by forming covalent adducts with DNA and interacting with the androgen receptor

Arthur D. Little Corporation — Cambridge, MA
Technology and Product Development Division — *Research Analyst, 1998-2000*
Projects: Performance modeling of alternative energy technologies, including gas-to-liquid processing of oil field-associated natural gas into clean diesel, solid oxide fuel cell heat integration, and small-particle catalyst generation

Massachusetts Institute of Technology — Cambridge, MA
Department of Chemical Engineering — *Research Assistant, 1997*
Advisors: Prof. Robert Langer, Prof. Guillermo Ameer (Northwestern)
Project: Development and testing of an extracorporeal blood filtration device, allowing deheparinization of blood downstream of and in series with dialysis

Suntory Ltd.
Research and Technology Development Center — Yamazaki, Osaka, JAPAN
Katsura Brewery — Nagaokakyo, Kyoto, JAPAN
Advisor: Dr. Kenzo Nagami — *Research Assistant, Summer 1996*
Project: Assessment of the efficacy of various polymer membranes used to reject lactobacillus downstream of beer fermentation and yeast separation, testing of enzymatic additive processes in preventing membrane fouling from gluten accumulation

Massachusetts Institute of Technology — Cambridge, MA
Department of Chemical Engineering Undergraduate Research Lab — *Fall 1995*
Sponsor: Baxter Pharmaceuticals
Project: Construction and implementation of a small multi-compartment reactor for the testing of semipermeable membranes intended for immunoisolation of xenograft porcine islet cells in a developmental artificial pancreas

Rochem Corporation Torrance, CA
Advisor: David LaMonica *Research Assistant, Summer 1994*
Project: Development of reverse osmosis wastewater treatment devices for environmental cleanup. Responsibilities included bench-scale testing, fluid dynamics modeling, and performance evaluation through analysis of the physical and biochemical phenomena responsible for membrane fouling

INVITED TALKS

"*Metabolic and Mechanistic Exploration of Programmable Genotoxins*"
CCSB Interdisciplinary Seminar Series, February 21, 2008
Center of Cancer Systems Biology at Caritas St. Elizabeth's Medical Center
Tufts University School of Medicine, Boston, MA

TEACHING EXPERIENCE

Massachusetts Institute of Technology Cambridge, MA
Department of Biological Engineering *Fall 2001, Winter 2002*
BE.201 Molecular and Systems Toxicology *Teaching Assistant*

Massachusetts Institute of Technology Cambridge, MA
Department of Chemical Engineering
10.001 Introduction to Chemical Engineering *Teaching Assistant 1997-1998*
10.302 Transport Phenomena *Grader 1997*

Massachusetts Institute of Technology Cambridge, MA
Office of Minority Education *1994-1998*
7.012 Introductory Biology *Tutor*
8.01 Mechanics
8.02 Electricity & Magnetism
18.01 Calculus I
5.12 Organic Chemistry I
5.13 Organic Chemistry II
5.60 Thermodynamics and Kinetics
5.07 Biological Chemistry I
10.213 Chemical and Biological Engineering Thermodynamics
10.302 Transport Phenomena
10.32 Separation Processes

Massachusetts Institute of Technology Cambridge, MA
Department of Athletics, Physical Education, and Recreation
Women's Varsity Volleyball *Assistant Coach, 1999-Present*
Men's Varsity Volleyball *Assistant Coach, 1999-2002, 2004-Present*

SELECTED AWARDS

Norman Leventhal Presidential Fellow *2000*
Boulé Foundation Scholar *1993-1997*
Xerox Technical Minority Fellow *1994*

ACTIVITIES

MIT Biological Engineering Graduate Student Board
Toxicology Representative, 2002-2003
Undergraduate Curriculum Committee, 2004
Co-director, 2003-2004
Certified Mediator, 2004-2006

Big Brother Big Sister of Massachusetts Bay *Big Brother, 1998-2006*
MIT Varsity Volleyball *1995-1998, Captain 1998, MVP 1998*
MIT Undergraduate Administration *Class Vice President, 1995-1996*